A novel cascade controlling hematopoiesis and the inflammatory response in flies

Wael Bazzi

UNIVERSITÉ DE STRASBOURG

ÉCOLE DOCTORALE DES SCIENCES DE LA VIE ET DE LA SANTÉ
INSTITUT DE GÉNÉTIQUE ET DE BIOLOGIE MOLÉCULAIRE ET CELLULAIRE

THÈSE

présentée par :

Wael BAZZI

soutenue le : 18 Septembre 2017

pour obtenir le grade de : **Docteur de l'Université de Strasbourg**

Mention : Sciences de la Vie et de la Santé

Discipline/Spécialité : Génétique, Biologie Moléculaire et Cellulaire

Une nouvelle cascade régulant l'hématopoïèse et la réponse inflammatoire chez la drosophile

THÈSE dirigée par :

Mme. GIANGRANDE Angela — Directeur de recherche, IGBMC - Illkirch, France

RAPPORTEURS EXTERNES :

M. LÉOPOLD Pierre — Directeur de recherche, iBV - Nice, France

M. NAIT OUMESMAR Brahim — Directeur de recherche, ICM - Paris, France

EXAMINATEUR INTERNE :

M. FERRANDON Dominique — Directeur de recherche, IBMC - Strasbourg, France

"I have discovered in life that there are ways of getting almost anywhere you want to go, if you really want to go." - Langston Hughes

Acknowledgements

The participation and guidance of many people led my amazing PhD journey reach the desired accomplishment. A total of 4 years have passed filled with hard work, patience, determination and unforgettable memories, where I gained the best experience and excellent science at University of Strasbourg and IGBMC. First of all, I would like to express my sincere gratitude to my advisor Dr. Angela Giangrande for your continuous guidance, motivation and support during my PhD research work. Without your comments and advices, I would not have reached my target. I will always be thankful for your time and for believing in me as a young scientist.

Also, I would like to express my special appreciation to my jury members: Dr. Pierre Léopold, Dr. Brahim Nait Oumesmar and Dr. Dominique Ferrandon for accepting to read and judge my work. Your achievements in the research field have widened the scientific knowledge.

To my lab colleagues, I will never forget all the joyful moments behind the bench. To Dr. Pierre Cattenoz, thank you so much for all the support, assist and guidance all through my PhD. For me, you are a true brother and friend. To Mrs. Claude Delaporte, thank you so much for all the experimental help and dissections. Without your support, many experiments would not have been accomplished. Special thanks to Dr. Yoshihiro Yuasa for all the valuable comments on my manuscript and the continuous scientific discussions. I also thank Mrs. Céline Riet for being a great colleague and for helping me order materials and fly stocks. To Rosy and Ekin, thank you for keeping the good spirit in the lab. I also thank Mrs. Holy Dietreich for preparing fly medium. In addition, I would like to thank former lab members Dr. Tripti Gupta, Dr. Vasanthi Dasari, Giuseppe Aiello and Nicola Di Iacovo for being great friends.

To all my friends in France and Lebanon, thank you so much for standing by my side all through. During my stay in France, I gained not only friends, but brothers and sisters. To the “Dr. to be” Zeinab Wehbe, thank you for all the support and I wish you the best in your journey, you are a true friend. To Ali and Hamed Wehbe, thank you for the help in many tasks. Special thanks to Ms. Loulwa Reda, whom I consider a continuous positive vibe and a true supporter. To Dr. Hussein Hmadeh, you were and will always remain a brother.

Last but not least, no words can explain the amount of love I hold for my parents, to whom I dedicate this work. You were always encouraging with continuous inspiration to aim high and follow my dreams. I hope I made you proud. To my brother Jad, thank you for always being there for me, your support is priceless, I miss you so much. To Racha, I could not have imagined a better sister than you, thank you for being next to me in every step and for all your advices. Much love to you and Houssam, my new brother. To my nephew baby Sam, since your birth you became my continuous joy during my tough times. I wish you the best in life and I dedicate my work to you as well.

Also, I would like to thank “University of Strasbourg” and the “Fondation pour la Recherche Médicale en France (FRM)” for supporting my PhD studies.

List of contents

List of abbreviations

Abbreviation	Term
AML	Acute myeloid leukemia
AMP	Antimicrobial peptide
APC	Antigen-presenting cell
ATP	Adenosine triphosphate
Col	Collier
Crq	Croquemort
CZ	Cortical zone
DamID	DNA adenine methyltransferase identification
DBD	DNA-binding domain
DC	Dendritic cell
DD	Death domain
dMyD88	Myeloid differentiation primary-response protein 88
DN	Dominant negative
Dpias	Drosophila protein inhibitors of activated stats
DV	Dorsal vessel
E	Glutamic acid
ECM	Extracellular matrix
Edin	Elevated during infection
FERM	4-point-1, Erzin, Radixin, Moesin
FOG	Friend-of-GATA
G	Glycine
GBS	Gcm binding site
Gcm/Glide	Glial cell missing/Glial cell deficient
GH	Growth hormone
GOF	Gain-of-function
Hh	Hedgehog
Hop	Hopscotch
ICZ	Intermediate cortical zone
IFN	Interferon
IL	Interleukin
IMD	Immunodeficiency
IRAK	Interleukin-1 (IL-1) receptor-associated kinase
IRAKM	Interleukin-1 (IL-1) receptor-associated kinase M
IRF	Interferon-regulatory factor
JAK/STAT	Janus kinase/signal transducer and activator of transcription
JH	JAK homoloy
JNK	JUN N-terminal kinase
K	Lysine

KD	Knockdown
LG	Lymph gland
LOF	Loss-of-function
LPS	Lipopolysaccharides
LRR	Leucine-rich repeats
Lz	Lozenge
MAL	Myeloid differentiation primary-response protein 88 adaptor-like protein
MAPK	Mitogen-activated protein kinase
MyD88	Myeloid differentiation primary-response protein 88
MZ	Medullary zone
NF-κB	Nuclear factor-κB
NO	Nitric oxide
NOD2	Nucleotide-binding oligomerization domain-containing protein 2
PAMP	Pathogen-associated molecular pattern
PDGF	Platelet-derived growth factor
PGRP	Peptidoglycan recognition protein
Phe	Phenylalanine
PI3K	Phospatidylinositol 3-kinase
PIAS	Protein inhibitors of activated stats
PNS	Peripheral nervous system
PO	Phenoloxidase
PPO	Prophenoloxidase
PRR	Pattern recognition receptors
PSC	Posterior signaling center
PTH	Parathyroid hormone
PTP	Protein tyrosine phosphatase
PTP61F	Protein tyrosine phosphatase 61F
Pxn	Peroxidasin
RNAi	RNA interference
ROS	Reactive oxygen species
SAP	SAF-A/B, Acinus and PIAS
Ser	Serrate
Sn	Singed
SOCS	Suppressors of cytokine signaling
SOCS36E	Suppressors of cytokine signaling 36E
SPE	Spatzle-processing enzyme
Spn	Serine protease inhibitor
Spz	Spatzle
Srp	Serpent
STAT92E	Signal transducer and activator of transcription 92E
TIR	Toll/IL-1 receptor

TLR	Toll-like receptor
TOLLIP	Toll-interacting protein
TRAF	TNF receptor-associated factor
TRAM	TRIF-related adaptor molecule
TRIF	Toll/IL-1 receptor domain-containing adaptor protein inducing IFNβ
Tum-l	Tumorous lethal
UAS	Upstream activating sequence
Upd	Unpaired
Ush	U-shaped
Val	Valine
VEGF	Vascular endothelial growth factor
WBC	White blood cell
WntD	Wnt inhibitor of Dorsal
WT	Wild type

Résumé en Français

Introduction

Les cellules immunitaires qui sont produites en différentes vagues d'hématopoïèse sont essentielles pour monter une réponse immunitaire efficace. La réponse immunitaire a un rôle primordial dans la modulation de la progression des tumeurs. Les cascades inflammatoires telles que la cascade Toll et la cascade JAK/STAT sont connues pour réguler l'hématopoïèse. Les mutations de chacune d'entre elles sont associées à des défauts d'hématopoïèse et au développement de cancer du sang chez l'humain (CHEN *et al.* 2012; MAI *et al.* 2013). L'activation de TLR4 est liée à l'inhibition et à l'augmentation de fréquence de cancer (MAI *et al.* 2013), tandis que la voie JAK/STAT induit la croissance de divers types de cancers humains incluant les lymphomes et les cancers du côlon et gastrique. Enfin, la dérégulation de la voie JAK/STAT a été décrites dans plusieurs maladies hématologiques, notamment les maladies myéloïdes (FURQAN *et al.* 2013).

De la même manière que les facteurs de transcription clés contrôlant l'hématopoïèse, les voies de signalisation Toll et JAK/STAT sont fortement conservées dans l'évolution. Chez la drosophile, la voie Toll, activée par les bactéries à GRAM positif et les champignons, peut contrôler l'expression de centaines de protéines incluant des peptides antimicrobiens (AMP), des protéases, des cytokines et d'autres acteurs de la réponse inflammatoire (HETRU AND HOFFMANN 2009). Le récepteur Toll est activé par le ligand Spatzle (Spz). Ceci conduit à l'activation des facteurs NF-κB Dorsal et Dif qui migrent dans le noyau et induisent l'expression des gènes codant pour les AMP (HULTMARK 2003; VALANNE *et al.* 2011). La voie JAK/STAT répond à la liaison des cytokines tels que les Upds sur leurs récepteurs, ce qui active la kinase JAK. Ceci fait

suite à une cascade de phosphorylation ciblant STAT et le récepteur aux cytokines, ce qui conduit à la dimérisation de STAT et à sa translocation dans le noyau. Dans le noyau, STAT agit en tant que facteur de transcription (BINARI AND PERRIMON 1994; HARRISON *et al.* 1998; CHEN *et al.* 2012).

La sur-activation de la voie JAK/STAT ou de la voie Toll induit dans la larve de drosophile la formation de tumeurs du sang appelées tumeurs mélanotiques. Ces masses de cellules sont dues à la prolifération des hémocytes et à la présence d'hémocytes inflammés appelés lamellocytes. Ces lamellocytes s'agrègent et forment des tumeurs mélanisées noires dans la larve (SCHMID *et al.* 2014). Au cours de mon doctorat, j'ai caractérisé l'impact de Gcm, le seul facteur de transcription spécifique de la vague d'hématopoïèse embryonnaire (BERNARDONI *et al.* 1997), sur la réponse immunitaire innée et l'inflammation, en me concentrant sur les voies de signalisation JAK/STAT et Toll, *in vivo*, en utilisant le modèle simple de la drosophile. Mes données ont également permis de mettre en évidence un mode de signalisation entre les deux vagues d'hématopoïèses.

Objectifs

- Définir l'impact et le mode d'action du facteur de transcription spécifique des hémocytes embryonnaires, Gcm, sur les voies inflammatoires JAK/STAT et Toll et sur la formation des tumeurs mélanotiques.
- Caractériser la communication entre les hémocytes issues des différentes vagues d'hématopoïèse lors de la réponse inflammatoire. Ceci a été réalisé en définissant le rôle de Gcm dans le mécanisme de signalisation des hémocytes primitifs vers les hémocytes définitifs.

- Caractériser le transcriptome des hémocytes larvaires d'animaux présentant un fond génétique conduisant à la production de tumeurs mélanotiques et à un état inflammatoire.
- Explorer la conservation du rôle de Gcm sur l'inflammation au cours de l'évolution, en se concentrant sur l'interaction mGcm2-JAK/STAT.

Résultats

Gcm induit l'expression d'inhibiteurs des voies JAK/STAT et Toll

Un crible DamID, dont les résultats sont similaires à un crible ChIPseq, a permis d'identifier 1031 gènes ciblés directement par Gcm (CATTENOZ *et al.* 2016b). Parmi ces gènes, des inhibiteurs clés de la voie JAK/STAT (*Ptp61F, Socs36E, Socs44A, ken and barbie* (*ken*) et *Su(var)3-9*) et de la voie Toll (*cactus*) ont été trouvés, suggérant un rôle de Gcm sur l'inhibition des deux voies au niveau transcriptionnel. A la suite de cette constatation, j'ai étudié l'impact de Gcm sur l'activation de l'expression de ces inhibiteurs. J'ai également utilisé un système de cellule en culture et est prouvé que Gcm induit l'expression de *Ptp61F*, *Socs36E*, *Socs44A*, *Su(var)3-9* et *cactus* dans la lignée cellulaire de drosophile S2.

Gcm supprime les phénotypes de tumeurs mélanotiques induits par les voies JAK/STAT et Toll

A la suite de l'analyse *in vitro*, j'ai exploré l'interaction entre Gcm et les voies inflammatoires *in vivo* en utilisant le phénotype de tumeur mélanotique et en analysant l'hémolymphe (équivalent au sang). La mutation gain de fonction (GOF) $hop^{Tum\text{-}l}$ active de manière constitutive la seule kinase JAK présente chez la drosophile et provoque une sur-prolifération des hémocytes et la formation de tumeurs mélanotiques. Un phénotype similaire est

induit par la mutation GOF *Toll*^{10b} qui rend le récepteur Toll actif de manière constitutive. J'ai caractérisé l'impact de Gcm sur ces cascades en inhibant l'expression de Gcm avec un transgène *gcmRNAi* (*gcm KD*) dans les souches mutantes *hop*$^{Tum-l}$ ou *Toll*^{10b} et en analysant l'effet de ce transgène sur la formation de tumeurs mélanotiques. Le phénotype de tumeurs mélanotiques est plus marqué dans les animaux *hop*$^{Tum-l}$ et *Toll*^{10b} quand Gcm est inhibé (*hop*$^{Tum-l}$*/gcm>gcm KD* ou *Toll*^{10b}*/gcm>gcm KD*). Ces animaux présentent plus de tumeurs par animal (expressivité) et plus d'animaux avec des tumeurs (pénétrance). De plus, la surexpression de Gcm sauve les phénotypes tumoraux induits par *hop*$^{Tum-l}$*/gcm>gcm KD* et par *Toll*^{10b}*/gcm>gcm KD*.

Enfin, j'ai également montré que *Ptp61F* interfère avec le phénotype de tumeurs mélanotiques observé dans les animaux *hop*$^{Tum-l}$*/gcm>gcm KD* puisque sa surexpression sauve significativement le phénotype du double mutant. L'inhibition de chacun des trois inhibiteurs (*Ptp61F*, *Socs36E* et *Socs44A*) de la voie JAK/STAT et de Gcm dans un fond génétique *hop*$^{Tum-l}$ augmente le phénotype tumoral. De ce fait, Gcm régule la formation de tumeurs mélanotiques en induisant l'expression d'inhibiteurs des JAK/STAT.

Communication entre l'hématopoïèse primitive et définitive

Les tumeurs mélanotiques ont été décrites comme issues des hémocytes originaires de l'hématopoïèse définitive dans la larve. Comme Gcm est exprimé uniquement lors de l'hématopoïèse primitive dans l'embryon, nos observations indiquent une contribution des hémocytes embryonnaires et suggèrent une communication entre les deux vagues d'hématopoïèse. Afin de caractériser ce mode de communication, j'ai étudié comment les hémocytes embryonnaires envoient des signaux vers les hémocytes larvaires. J'ai découvert que JAK/STAT signaling induit l'expression de cytokines Upd2 et Upd3 dans les hémocytes

embryonnaires. Gcm inhibe la sécrétion des ces cytokines que ne peuvent pas activer la voie JAK/STAT. Les cytokines pro-inflammatoires sécrétées par les hémocytes embryonnaires peuvent induire la voie JAK/STAT de manière non-autonome dans les muscles somatiques et dans l'organe de l'hématopoïèse définitive, la glande lymphatique, pour activer l'hématopoïèse larvaire. Donc, Gcm supprime la voie JAK/STAT, qui active en temps normal l'expression des cytokines. Ces cytokines sont sécrétées et agissent de manière non-autonome.

Caractérisation du transcriptome des hémocytes mutants

J'ai réalisé une analyse transcriptomique sur les hémocytes circulants de larves $Toll^{10b}$ et de larves combinant $Toll^{10b}$ avec une mutation nulle de *gcm* ($gcm^{26}/+;Toll^{10b}/+$). La comparaison des doubles mutants avec les mutants simples a révélé un total de 472 gènes modulés par les deux mutations combinées. L'analyse Go-term a révélé que ces gènes sont notamment impliqués dans la mitochondrie avec les Go-term mitochondrie présentant l'enrichissement le plus fort avec les plus fortes p-values. Au total, 24 gènes codant pour des protéines mitochondriales ont été détectés, 19 sont surexprimé et 5 sous-exprimés dans le double mutant comparé aux contrôles (mutants simples). Le gène codant pour le récepteur de la voie JAK/STAT, dome, est spécifiquement induit dans le double mutant, suggérant que les deux voies inflammatoires communiquent entre elles durant la réponse inflammatoire. Pour conclure, les transcriptomes ont permis de mettre en lumière l'impact d'un facteur de transcription embryonnaire sur les mitochondries et la voie de signalisation Toll dans l'hématopoïèse post-embryonnaire. Ces données ouvrent également de nouvelles perspectives sur la caractérisation des liens entre Gcm, les mitochondries, et la formation des tumeurs mélanotiques.

Gcm inhibe la voie JAK/STAT dans une lignée leucémique humaine

Le génome des vertébrés contient deux orthologues de Gcm, *GCMa/GCM1* et *GCMb/GCM2*, qui n'ont jamais été associés à l'immunité. Pour débuter leur caractérisation chez les mammifères, j'ai transfecté un vecteur d'expression de GCM2 murin dans la lignée cellulaire immortalisée de leucémie myélogénique chronique K562. Dans cette lignée, la voie JAK/STAT est activée de manière constitutive. Suite à la transfection, j'ai analysé l'expression des inhibiteurs de la voie JAK/STAT : *SOCS1*, *SOCS3* et *PTPN2*. Le niveau d'expression de ces trois inhibiteurs augmente significativement, de manière similaire à mes observations chez la drosophile. De plus, j'ai pu observer une apoptose accrue dans les cellules transfectées, ce qui peut être comparé aux effets pro-apoptotiques des inhibiteurs pharmacologiques de JAK2 tel que l'AG490 sur les cellules cancéreuses colorectales (Du *et al.* 2012). Ensemble, ces données suggèrent un rôle conservé de Gcm au cours de l'évolution.

Conclusion

Mes travaux ont permis de caractériser Gcm comme un nouvel acteur inhibant la formation de tumeurs mélanotiques et régulant deux cascades inflammatoires. De plus, mes données dévoilent pour la première fois une interaction entre les deux vagues d'hématopoïèse, nécessaire pour monter une réponse inflammatoire efficace. Enfin, j'ai montré que Gcm régule des gènes codant pour des protéines mitochondriales dans les hémocytes circulants, et j'ai transposé mes découvertes chez les mammifères en montrant l'impact de GCM2 murin sur la voie JAK/STAT. Etant donnée la conservation au cours de l'évolution des mécanismes biologiques de base, je pense que mes travaux peuvent ouvrir de nouvelles perspectives sur les voies de régulation du système immunitaire des vertébrés. Sur le long terme, mes travaux

peuvent aider à comprendre les mécanismes physiopathologiques sous-jacents des maladies humaines liées au système immunitaire qui représentent un lourd fardeau pour notre société.

Matériels et méthodes

Pénétrance et expressivité des tumeurs mélanotiques

La pénétrance des tumeurs indique le pourcentage de larves au troisième stade qui portent une ou plus de tumeurs. Pour mesurer l'expressivité du phénotype tumoral, les tumeurs ont été classées en trois catégories selon leurs tailles : petite (S), moyenne (M) et large (L) (MULLER *et al.* 2005). Une tumeur est considéré comme large si elle couvre plus de la moitié de la distance entre les bords d'un segment, comme moyenne si la masse mélanotique couvre ¼ de la distance entre les bords d'un segment et comme petite si elle est inférieur au ¼ de la distance entre les bords d'un segment. L'expressivité a été déterminée en calculant le pourcentage de tumeurs petites, moyennes et grandes mesurées dans chaque animal. Les p-values sont estimées en utilisant le test du Khi Deux pour la comparaison de fréquences entre deux populations.

Comptage d'hémocytes

Dix larves au stade L3 ont été nettoyées dans une solution de Ringer (pH 7.3-7.4) contenant 0.12g/L de CaCl2, 0.105g/L de KCl et 2.25g/L de NaCl, puis séchées et saignées dans 50 µL de milieu Schneider complémenté avec 10% de sérum de veau fœtale (FCS), 0.5% de pénicilline, 0.5% de streptomycine (PS), et quelques cristaux de N-phenylthiourée ≥98% (PTU) (Sigma-Aldrich (P7629)) pour prévenir la mélanisation des hémocytes (LERNER AND FITZPATRICK 1950) dans une plaque de microtitration à fond incurvé de 96 puits. Pour la collecte d'hémocytes circulants, l'hémolymphe est laissée s'est écouler passivement de la larve

et le volume total a été transféré sur un hémocytomètre, où le nombre total de cellules a été compté, multiplié par le volume original (50 µL), et le nombre moyen d'hémocytes par larve a été calculé comme décrit par (KACSOH AND SCHLENKE 2012). Pour les hémocytes sessiles, l'hémolymphe contenant les hémocytes circulants a été transféré dans un premier puit, puis les hémocytes sessiles ont été grattés de la carcasse dans un deuxième puit comme décrit par (PETRAKI *et al.* 2015) et comptés comme les hémocytes circulants. Chaque comptage a été réalisé au moins trois fois. Les p-values ont été estimées après analyse de variance en utilisant le test de Student bilatéral.

Summary

Introduction

Immune cells originating from different hematopoietic waves coexist in the organisms and mount efficient immune responses. These responses have pivotal roles in modulating tumor progression. Inflammatory cascades, such as the JAK/STAT and the Toll pathways are also known to regulate hematopoiesis and mutations in either of them are associated with defects in hematopoiesis and blood cancers in humans (CHEN *et al.* 2012; MAI *et al.* 2013). TLR-4 activation has been linked to both cancer inhibition and growth (MAI *et al.* 2013). On the other hand, the JAK/STAT pathway promotes the growth of diverse types of human cancers including lymphoma, colon and gastric cancers. Finally, dysregulation in JAK/STAT signaling has been described in many hematological malignancies, especially myeloid disorders (FURQAN *et al.* 2013).

Like the key transcription factors controlling hematopoiesis, the JAK/STAT and the Toll signaling pathways are highly conserved in evolution. In *Drosophila*, the Toll pathway activated by Gram-positive bacteria and fungi controls the expression of hundreds of proteins including antimicrobial peptides (AMPs), proteases, cytokines and others leading to an inflammatory response (HETRU AND HOFFMANN 2009). The Toll receptor is activated by the binding of the ligand Spatzle (Spz) to the receptor, leading to the activation of the NF-κB factors Dorsal and/or Dif, which translocate to the nucleus and drive the expression of AMP encoding genes (HULTMARK 2003; VALANNE *et al.* 2011).

The JAK/STAT pathway responds to the binding of cytokines like Upds to their receptors, which activates the JAK kinase. A cascade of phosphorylations targeting STAT and

the receptor leads to STAT dimerization and translocation into the nucleus, where it acts as a transcription factor (BINARI AND PERRIMON 1994; HARRISON *et al.* 1998; CHEN *et al.* 2012).

The over-activation of either the JAK/STAT or the Toll pathway triggers the formation of blood tumors in *Drosophila* larvae also called "melanotic tumors". These masses of cells are due to hemocyte proliferation and to the presence of hemocytes in an inflammatory state, named lamellocytes, which aggregate and form black melanized tumors in larvae (SCHMID *et al.* 2014). For my PhD, I proposed to decipher the impact of Gcm, the only known transcription factor specific to embryonic hematopoiesis (BERNARDONI *et al.* 1997), on the innate immune response and on inflammation, by focusing on the JAK/STAT and Toll signaling cascades *in vivo* using the simple *Drosophila* model.

Objectives

- To define the impact and mode of action of the transcription factor Gcm specific to embryonic hemocytes, on the JAK/STAT and the Toll inflammatory pathways and on the formation of melanotic tumors.
- To characterize the communication of distinct hematopoietic waves during the inflammatory response, by defining the role of Gcm in the signaling mechanism from the embryonic wave to the larval definitive wave.
- To characterize the molecular landscape of hemocytes in genetic backgrounds that lead to melanotic tumors and to an inflammatory state.
- To explore a possible conserved role of Gcm genes in evolution, by focusing on mGcm2 - JAK/STAT interaction.

Results

Gcm induces the expression of the inhibitors of the JAK/STAT and of the Toll pathways

A DamID genome-wide screen, a variant of the ChIP-chip approach, identified 1031 potential direct targets for Gcm (CATTENOZ *et al.* 2016b). Among them are key inhibitors of the JAK/STAT pathway (*Ptp61F*, *Socs36E*, *Socs44A*, *ken and barbie* (*ken*) and *Su(var)3-9*), and of the Toll cascade (*cactus*), which suggested an inhibitory role of Gcm on both pathways at the transcriptional level. Hence, I asked whether Gcm regulates the inflammatory cascades by inducing the expression of their inhibitors. First, I validated this hypothesis in a cell culture system and found that transfected Gcm induces the endogenous expression of *Ptp61F*, *Socs36E*, *Socs44A*, *Su(var)3-9* and *cactus* in the S2 *Drosophila* cell line.

Gcm suppresses the JAK/STAT and Toll induced blood tumor phenotypes

Next, I explored the genetic interactions *in vivo*, using the melanotic tumor phenotypic readout. The $hop^{Tum\text{-}l}$ gain-of-function (*GOF*) mutation constitutively activates the only JAK kinase present in flies and triggers the over-proliferation of hemocytes and the formation of melanotic tumors. A similar phenotype is induced by the $Toll^{10b}$ mutation, which renders the Toll receptor constitutively active. Thus, I asked whether Gcm counteracts the phenotypes induced by these inflammatory cascades. I down-regulated *gcm* expression using a *gcmRNAi* (*gcm* knockdown or *KD*) line and studied the effect on the formation of melanotic tumors in combination with mutations over-activating either cascade. The melanotic phenotypes are stronger in $hop^{Tum\text{-}l}$ and $Toll^{10b}$ animals upon *gcm KD* ($hop^{Tum\text{-}l}$*/gcm>gcm KD*) or ($Toll^{10b}$*/gcm>gcm KD*) in terms of penetrance and expressivity of tumors. Interestingly, over-

expressing *gcm* rescues both the $hop^{Tum\text{-}l}$*/gcm>gcm KD* and the $Toll^{10b}$*/gcm>gcm KD* phenotypes.

Moreover, I showed that *Ptp61F* interferes with the melanotic tumor phenotype observed in the $hop^{Tum\text{-}l}$*/gcm>gcm KD* animals, as its over-expression significantly alleviates the double mutant phenotype. Also, down-regulating separately the three JAK/STAT inhibitors and *gcm* in a $hop^{Tum\text{-}l}$ background further increases the melanotic phenotype. Thus, *gcm* impacts tumor development by inducing the expression of the inhibitors of the JAK/STAT cascade.

Communication between primitive and definitive hematopoiesis

Melanotic tumors are thought to originate from the larval, definitive hematopoiesis. Since Gcm is only expressed in the embryonic, primitive hematopoiesis, our findings suggest a contribution from embryonic hemocytes, and sheds light onto the communication between the hematopoietic waves. To get a mechanistic insight on this communication, I asked how does embryonic hematopoiesis signal to larval hematopoiesis and found that Gcm inhibits the secretion of the proinflammatory cytokines Upd2 and Upd3 from embryonic hemocytes, where JAK/STAT acts cell-autonomously to activate their expression. The proinflammatory cytokines secreted by embryonic hemocytes can induce the JAK/STAT pathway non-autonomously in the somatic muscles and the definitive hematopoietic organ, the lymph gland to activate larval hematopoiesis. Therefore, Gcm suppresses the JAK/STAT pathway, which normally activates the expression of proinflammatory cytokines that are secreted and act non-autonomously.

Characterizing the transcriptional landscape of mutant hemocytes

I performed a transcriptome analysis on *Toll*^{10b} circulating hemocytes and upon combining the inflammatory state with a *gcm* null mutation (*gcm*^{26}/+;*Toll*^{10b}/+). The comparison of double mutants with single mutants revealed a total of 472 differentially expressed genes. Interestingly, Go-term analysis highlighted the mitochondria with the highest fold enrichment and the most significant p-values. In total, a list of 24 genes was obtained, where 19 genes were up-regulated and 5 genes were down-regulated as compared to the controls. Interestingly, the JAK/STAT receptor encoding gene *dome* (BINA *et al.* 2010) was specifically induced in double mutants, suggesting cross-talking between cascades during an inflammatory state. Thus, our transcriptome data sheds light onto the impact of an embryonic transcription factor on mitochondria and Toll signaling. This also opens novel perspectives onto investigating a possible link between Gcm, mitochondria, and melanotic tumor formation.

Gcm inhibits the JAK/STAT pathway in a human leukemia cell line

Vertebrate genomes contain two genes, *GCMa/GCM1* and *GCMb/GCM2*, which have never been associated with immunity or cancer. To start elucidating their role in mammals, I transfected a mouse *GCM2* expression vector in the human immortalized chronic myelogenous leukemia cell line K562, where the JAK/STAT cascade is constitutively active, followed by assessing the expression levels of JAK/STAT inhibitors *SOCS1*, *SOCS3* and *PTPN2*. Interestingly, the transcript levels of all three inhibitors increase significantly, paralleling the data I obtained in flies. In addition, GCM2 expression induces the apoptosis of K562 cells as pharmacological JAK2 inhibitor like AG490 in colorectal cancer cells (DU *et al.* 2012), highlighting a possible conserved role of the Gcm genes in evolution.

Conclusions

My work has spotted Gcm as a new player in inhibiting melanotic tumor formation and regulating both the JAK/STAT and the Toll inflammatory cascades. In addition, my data describes for the first time the interaction occurring between the primitive and the definitive hematopoietic waves and necessary to trigger an appropriate inflammatory response. In line with this, I show that Gcm impacts the molecular landscape of genes associated with mitochondria in circulating hemocytes. Moreover, I transpose my findings to vertebrates by showing the impact of a GCM murine gene onto the JAK/STAT pathway. Given the evolutionary conservation of the basic biological processes, I believe that my work will shed light on the immune response in higher organisms as well. In the long term, this may help understanding the physio-pathological mechanisms underlying human diseases linked to JAK/STAT dysregulation, which represent a heavy burden to our societies.

1. INTRODUCTION

Introducing inflammation

Inflammation is the first immune response to tissue damage or to microbial infection. This process allows destroying the infectious agent and healing of the damaged tissue, and usually the inflammatory response lasts for a short term. However, prolonged inflammation can lead to further tissue destruction, organ failure and mortality (GRANGER AND SENCHENKOVA 2010). Diseases such as atherosclerosis, diabetes, cancer and Alzheimer are directly linked to excessive inflammatory responses and research nowadays focuses on understanding the mechanisms regulating these responses (MEDZHITOV 2008; LIBBY *et al.* 2009; ZEYDA AND STULNIG 2009; QUERFURTH AND LAFERLA 2010).

Many signals form a regulatory network that coordinates the inflammatory response and understanding them is essential to dissect the process of inflammation. These signals are classified into inducers, sensors and mediators, where the latter initiates the inflammatory response by activating specific effectors that in turn alter the functional state of the tissue. Thus, the function of this network is to provide suitable conditions for the tissue to adapt to infections and to augment efficient inflammatory responses (**Figure 1**) (MEDZHITOV 2008).

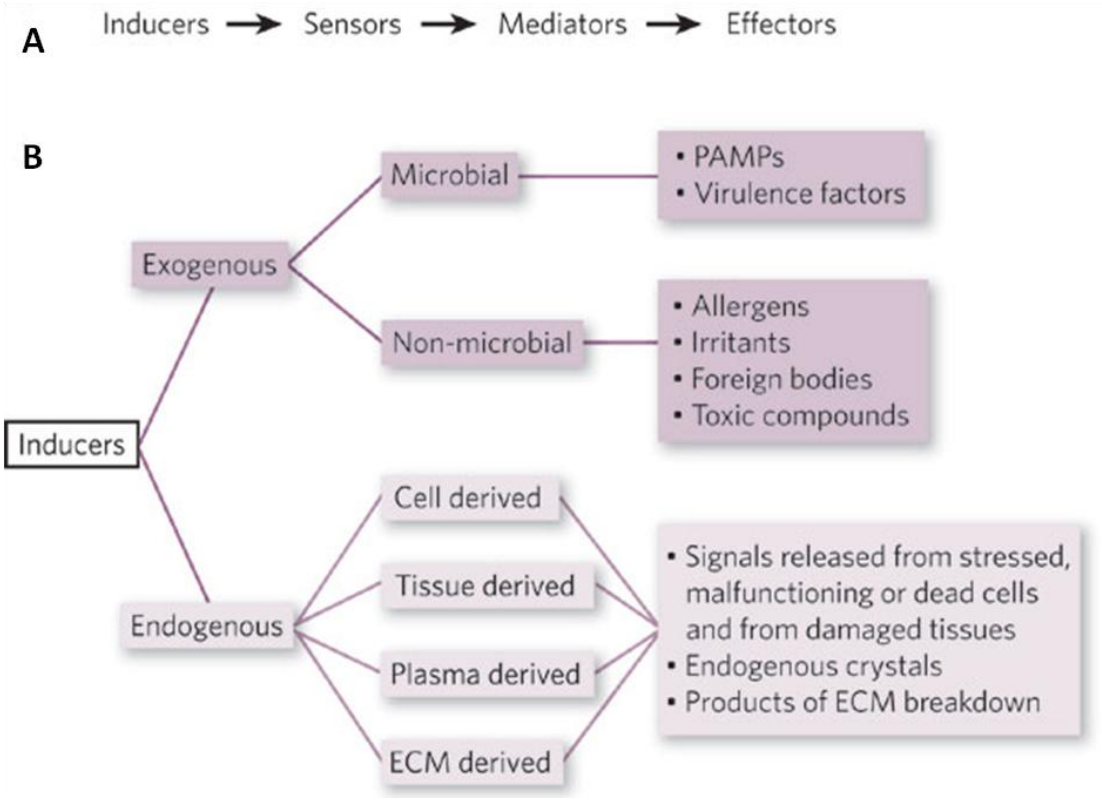

Figure 1: The signals regulating the inflammatory response. (**A**) An inflammatory response consists of inducers, sensors, mediators and effectors. (**B**) Inducers of inflammation are classified as exogenous or endogenous. ECM: extracellular matrix; PAMP: pathogen-associated molecular pattern. Modified from (MEDZHITOV 2008).

The coordination between inflammation and cancer goes back to 1863. At that time, Virchow hypothesized that cancers originated at sites of chronic inflammation, leading to enhanced proliferation (VIRCHOW 1881; VIRCHOW 1989; BALKWILL AND MANTOVANI 2001; COUSSENS AND WERB 2002). To understand this link, it is important to elucidate how inflammation contributes to the physiological processes, such as wound healing and infections. Upon injury, chemotactic factors direct the migration of white blood cells (WBCs) like leukocytes (neutrophils, monocytes and eosinophils) to the damaged site, followed by the recruitment of macrophages, fibroblasts and endothelial cells. These players coordinate to provide the suitable microenvironment for tissue repair (COUSSENS AND WERB 2002). Many

cancers and malignancies arise from inflammatory regions, where statistical analysis reveals that more than 15% of cancers are due to infectious agents (1.2 million cases per year) (KUPER *et al.* 2000; COUSSENS AND WERB 2002). In brief, leukocytes and other phagocytic cells lead to DNA damage in proliferating cells upon the generation of reactive oxygen species (ROS) that are initially produced to combat the infections. The continuous DNA damage/ROS production leads to tumor development (MAEDA AND AKAIKE 1998).

Drosophila melanogaster harbors an open circulatory system, which makes its immune cells an ideal signaling tool for inducing inflammatory responses upon infections and tissue damages. The available genetic tools applied to a simple genome make *Drosophila* a popular system for studying the mechanism of cancer development. Moreover, genes associated with human leukemia and inflammation are being transformed into *Drosophila* and therapeutic drugs are under trial (WANG *et al.* 2014b).

Chapter I

How is inflammation triggered?

Many studies have now elucidated the trigger of the inflammatory response (MEDZHITOV 2008; ROCK AND KONO 2008; GRANGER AND SENCHENKOVA 2010). Inflammation is triggered by the release of cytokines from injured cells that are recognized by cellular receptors, leading to the production of proinflammatory mediators that are in turn responsible for inducing an inflammatory response (ROCK AND KONO 2008). The detailed responses and cascades involved in inflammation are discussed below in both mammals and *Drosophila*.

Inflammation in mammals

Innate immunity is the first line of defense upon infection and plays a key role in triggering an inflammatory response (MEDZHITOV AND JANEWAY 2000), whereas adaptive immunity interferes at a later phase to eliminate the pathogen and create an immunological memory. Many types of cells contribute to the innate immune response, such as the phagocytic cells and antigen-presenting cells (APCs) like granulocytes, macrophages and dendritic cells (DCs) (IWASAKI AND MEDZHITOV 2004). Upon infection, pathogen-associated molecular patterns (PAMPs) are recognized by pattern recognition receptors (PRRs) like the Toll-like receptors family (TLRs) (IWASAKI AND MEDZHITOV 2004; AKIRA *et al.* 2006). Following PAMPs recognition, PRRs located on immune cells or intracellularly send signals to activate a vast number of downstream signaling pathways like, kinases and transcription factors that ultimately lead to proinflammatory and antimicrobial responses (AKIRA AND TAKEDA 2004; MOGENSEN 2009). The outcome of a PRR-induced signaling pathway is the production of cytokines, cell-

adhesion molecules and immunoreceptors that coordinate to augment an immune response (AKIRA *et al.* 2006; MOGENSEN 2009). Two major signaling cascades involved in inducing an inflammatory response are the Janus kinase/signal transducer and activator of transcription (JAK/STAT) and the Toll-like receptors (TLRs) signaling cascades (RAWLINGS *et al.* 2004; LIEW *et al.* 2005a; KAPLAN 2013). Both pathways are discussed below.

JAK/STAT signaling cascade in mammals

The JAK/STAT pathway is a key signaling cascade that induces many downstream targets during development and plays role in maintaining the homeostasis in mammals and flies. It is required for many cellular events, such as cell proliferation, cell differentiation, cell migration and apoptosis that are crucial for hematopoiesis, immune response induction, mammary glands development, adipogenesis and many other events (RAWLINGS *et al.* 2004; KAPLAN 2013). When JAK/STAT signaling is malfunctioning due to mutations, many processes are altered leading to a wide spectrum of inflammatory diseases and many types of blood cancers, such as leukemia (RAWLINGS *et al.* 2004; VAINCHENKER AND CONSTANTINESCU 2013).

The complexity of the JAK/STAT network is demonstrated by the presence of more than 50 ligands that are capable of inducing the cascade, such as erythropoietin, growth hormones (GHs), interferons (IFNs - IFN-α, β, γ) and interleukins (ILs - IL-2, IL-4, IL-7, IL-9, IL-13, IL-15, IL-21 etc.) (RAWLINGS *et al.* 2004; KAPLAN 2013; VILLARINO *et al.* 2015). In addition, 4 Janus kinases (JAKs) (JAK1, JAK2, JAK3, TYK2) and 7 Signal transducers and activators of transcription (STATs) (STAT1, STAT2, STAT3, STAT4, STAT5a, STAT5b, STAT6) are involved in the signaling transduction process (LEVY AND DARNELL 2002; VILLARINO *et al.* 2015). Upon ligand binding to the cytokine transmembrane receptor, intracellular JAKs are

brought in close proximity allowing a conformational change that frees their kinase domain from the inhibitory domain (**Figure 3**). This allows the two JAK molecules to transphosphorylate each other, a step necessary to activate their kinase domains (**Figure 2**) (BROOKS *et al.* 2014; VILLARINO *et al.* 2015). Following this, activated JAKs phosphorylate their downstream targets STATs, which are dormant transcription factors located in the cytoplasm. All 7 STATs are phoshporylated on a conserved tyrosine residue next to the C-terminus. When 2 subunits of STAT are phosphorylated, they hetero- or homodimerize upon interaction with a conserved SH2 domain (SRC homology 2), leading to their nuclear translocation, where they activate or repress the transcription of target genes (**Figure 2**) (RAWLINGS *et al.* 2004; KAPLAN 2013; VILLARINO *et al.* 2015).

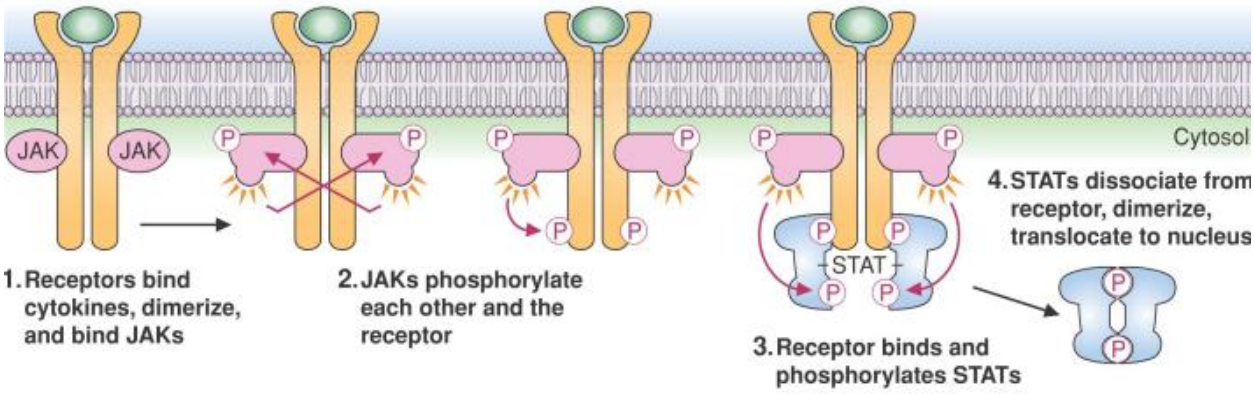

Figure 2: Schematic of the JAK/STAT signaling cascade. 1- Cytokine binds the receptor, leading to receptor dimerization 2- JAKs phosphorylate each other and the receptor to get activated. 3- STATs bind to the receptor and get phosphorylated by JAKs. 4- STATs dissociate from the receptor, dimerize and translocate to the nucleus.

The JAK/STAT cascade is regulated by three major inhibitors that exert their roles at different levels: Suppressors of cytokine signaling (SOCS), Protein inhibitors of activated stats (PIAS) and Protein tyrosine phosphatases (PTPs) (GREENHALGH AND HILTON 2001; RAWLINGS *et al.* 2004). PTPs are considered the simplest in their mode of inhibition. For example, SHP-1

(encoded by the mouse *motheaten* gene), contains two SH2 domains that can bind and dephosphorylate the phoshphorylated JAKs or the phosphorylated receptors thus, inhibiting their activity (RAWLINGS *et al.* 2004). The SOCS family of proteins includes at least 8 members that harbor an SH2 domain and a SOCS-box (40 homologous amino acids) at the C-terminus. SOCS1 and SOCS3 also contain an inhibitory kinase domain at the N-terminus. This family exerts its inhibitory function on the JAK/STAT pathway via a negative feedback loop, where activated STAT induces the transcription of *SOCS* genes, and the subsequent protein product binds the phosphorylated JAKs and their receptors to repress the cascade in two main ways: Either they inhibit the kinase activity of the phosphorylated JAKs or they block STAT from binding to the receptor. In addition, SOCS proteins play roles as ubiquitin ligases and induce proteosomal degradation (RAWLINGS *et al.* 2004; THOMAS *et al.* 2015). The PIAS family of proteins includes 4 members (PIAS1, PIAS2, PIAS3 and PIASy). They all contain a Zn-binding RING-finger domain in the central region and a SAF-A/B, Acinus and PIAS (SAP) motif at the N-terminus domain, which plays role in binding to dimerized STAT and sequesters it hence preventing nuclear translocation (RAWLINGS *et al.* 2004; THOMAS *et al.* 2015).

JAK/STAT cascade activating mutations are associated with many types of cancer and hematopoietic defect, however the underlying mechanisms are poorly understood. Studies revealed that activating mutations in the SH2 domain of STAT3 are associated with large granular lymphocytic leukemia in 40% of the patients (THOMAS *et al.* 2015) and *STAT5A* and *STAT5B* loci mutations are linked to prostate cancers (HADDAD *et al.* 2013). In addition, gain-of-function (*GOF*) mutations in JAKs are associated with a constitutively active JAK/STAT pathway and hematological malignancies (NIELSEN *et al.* 2011; THOMAS *et al.* 2015; PENCIK *et al.* 2016). For example, *JAK2* mutations are reported in many patients with myeloproliferative

neoplasms, such as thrombocythemia, myelofibrosis and polycythemia vera (JONES *et al.* 2005; LEVINE *et al.* 2005; KILADJIAN 2012). Each JAK harbors an active tyrosine domain (JAK homology 1 (JH1)), a catalytic pseudokinase domain (JAK homology 2 (JH2)), an SH2 domain and an amino terminal domain FERM (4-point-1, Erzin, Radixin, Moesin) (MCLORNAN *et al.* 2006) (**Figure 3**). An amino acid substitution mutation from Valine (Val) to Phenylalanine (Phe, F) at position 617 within the pseudokinase domain (*JAK2* V617F) induces a conformational change in the protein structure that leads to constitutive kinase activity (**Figure 3**). This is an acquired somatic mutation that appears in the majority of patients with myeloproliferative cancer (myeloproliferative neoplasms), 100% of patients with polycythemia vera, and 50% of patients with essential thrombocytosis and primary myelofibrosis (BAXTER *et al.* 2005; LEVINE *et al.* 2005; SCOTT *et al.* 2005). In conclusion, all these examples highlight strong correlations between cancer and JAK/STAT signaling.

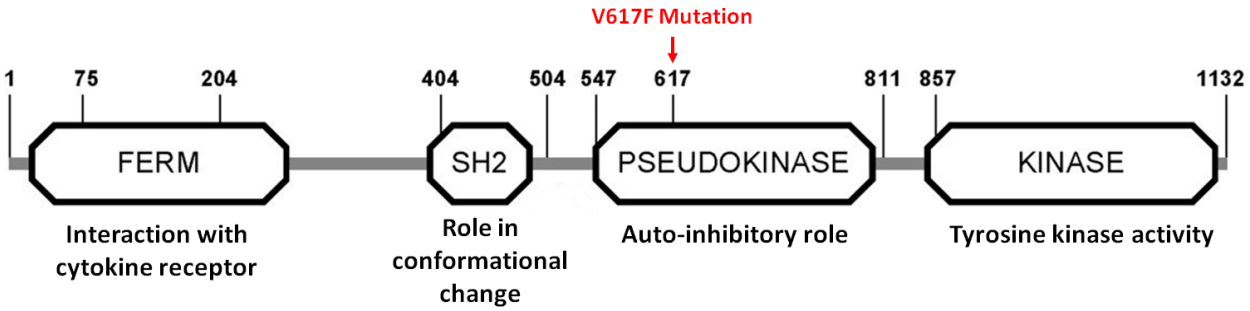

Figure 3: Schematic of the JAK2 domains indicating the approximate location of the V617F mutation. FERM domain plays role in cytokine-receptor interactions; SH2 domain plays role in inducing a conformational change; Pseudokinase domain has a JAK2 auto-inhibitory role; Kinase domain has a tyrosine kinase activity, where it phosphorylates downstream molecules; Note in red the V617F mutation within the pseudokinase domain. Modified from (PIETRA *et al.* 2008).

Toll signaling cascade in mammals

Microbes are sheltered by molecular patterns that are shared by many pathogens. For example, Lipopolysaccharides (LPS) surround Gram-negative bacteria while Lipoteichoic acids surround Gram-positive bacteria. Lipoproteins are characteristics of parasites and glycolipids of mycobacteria. The variety of molecular patterns within pathogens highlights the importance of harboring a wide range of cellular receptors. For example, PRRs can recognize PAMPs while other receptors like Toll can either directly interact with PAMPs or with an intermediate PAMP-binding molecule (MEDZHITOV AND JANEWAY 2000). TLRs are major regulators of immune responses upon infections. Interestingly, the development of the mammalian innate immunity is highly related to the involvement of the Toll protein in *Drosophila* (BRIGHTBILL AND MODLIN 2000; MEDZHITOV AND JANEWAY 2000; O'NEILL *et al.* 2013), which will be thoroughly discussed later.

The mammalian TLR family of proteins includes 13 members (TLR1 to TLR13), although TLR12 and 13 are not present in humans (ROCK *et al.* 1998; BRIGHTBILL AND MODLIN 2000; MAHLA *et al.* 2013). Interestingly, TLRs 1-5 are considered the direct homologs of the *Drosophila* Toll protein (ROCK *et al.* 1998). The structure of TLRs includes leucine-rich repeats (LRRs) in the extracellular domain and a cytoplasmic domain homologous to IL-1 receptor (TIR) (**Figure 4**) (KOPP AND MEDZHITOV 1999). The variations that appear in the extracellular domains help in PAMPs recognition and provide specificity for the immune response (MCDOWELL *et al.* 1998).

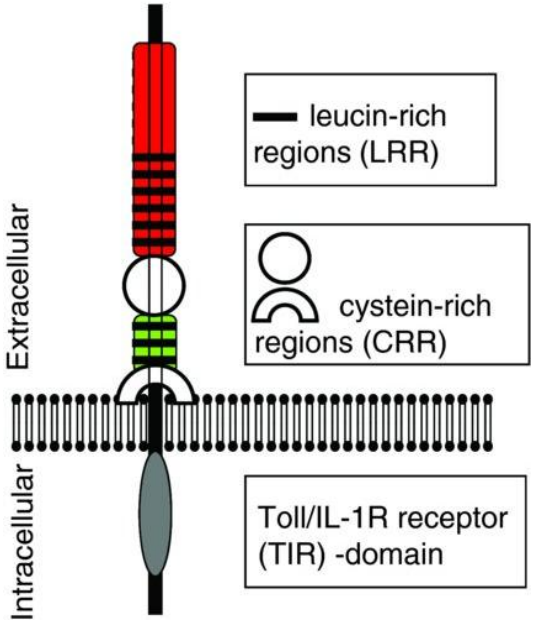

Figure 4: Schematic of the Toll-like receptor. The extracellular domains of all TLRs contain leucine-rich repeats (LRR) in addition to one or two cysteine-rich regions (CRR). The intracellular domain of a TLR is similar to the cytoplasmic region of the IL-1-receptor ("Toll/IL-1 receptor" domain, TIR). Modified from (ROTH AND BLATTEIS 2014).

TLRs 1, 2, 4, 6 and 11 are located within the plasma membrane and mainly recognize Gram-negative bacteria through LPS recognition, whereas TLRs 3, 7, 8, 9 and 13 are located within the endosomes and mainly recognize nucleic acids. Viral and bacterial DNA can be sensed by TLR9. TLR5 can recognize microbial flagellin. Interestingly, TLR4 is present in both the plasma membrane and in endosomes, highlighting it as a major receptor for transducing downstream signals (**Figure 5**) (HEMMI *et al.* 2000; PETER *et al.* 2009; KAWAI AND AKIRA 2010).

TLR signaling is initiated upon ligand binding, leading to receptor dimerization. The intracellular TIR domain then binds to the coupled TIR domain-containing adaptor proteins, such as the combined myeloid differentiation primary-response protein 88 (MyD88) and the MyD88-adaptor-like protein (MAL), or the coupled TIR domain-containing adaptor protein inducing IFNβ (TRIF) and the TRIF-related adaptor molecule (TRAM). These bindings induce downstream signaling via interactions between IL-1R-associated kinases (IRAKs) and the adaptor molecules TNF receptor-associated factors (TRAFs), resulting in the activation of mitogen-activated protein kinases (MAPKs), JUN N-terminal kinases (JNKs) and p38 proteins

(**Figure 5**). Following this, kinases phosphorylate and activate downstream transcription factors, such as the nuclear factor-κB (NF-κB) and the interferon-regulatory factors (IRFs) that in turn induce the expression of a wide spectrum of proinflammatory cytokines and type 1 interferons (IFNs) (**Figure 5**) (O'NEILL *et al.* 2013).

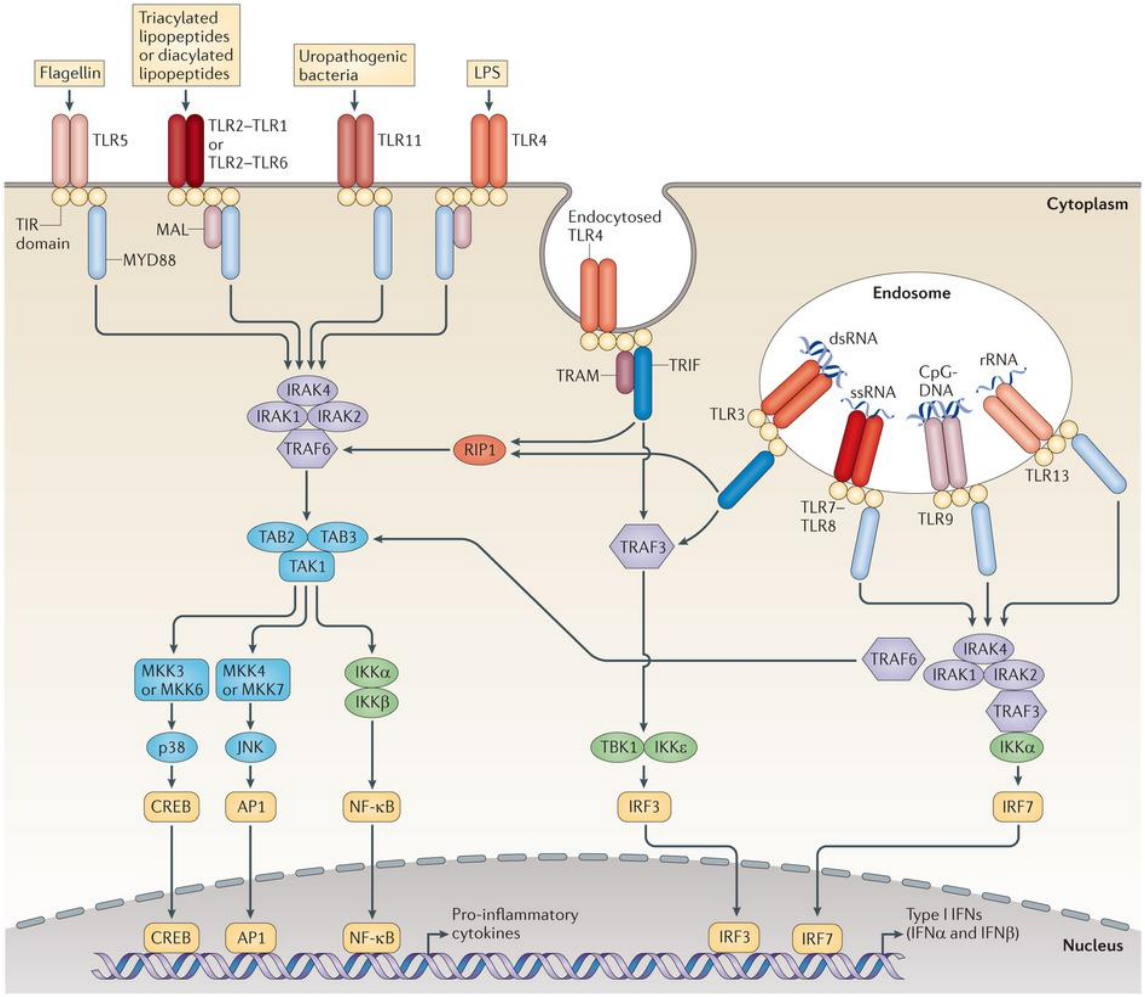

Figure 5: The mammalian TLR signaling pathways. Schematic of the mammalian Toll-like receptors (TLRs) signaling cascade. Modified from (O'NEILL *et al.* 2013).

The TLR signaling cascade is tightly regulated to maintain an immune balance within the body. In normal conditions, regulation is mainly achieved by down-regulating the transcription and translation of TLR genes, in addition to inducing the degradation of the corresponding

proteins (COLOTTA *et al.* 1994; LIEW *et al.* 2005b). Upon infection, soluble TLRs are produced in the blood and tissues to serve as regulators, where they act as "trap" receptors that prevent direct interactions between the cellular TLRs and the ligands. Intracellular TLR signaling regulators include many factors such as: the short form of MyD88 (MyD88s), which antagonizes MyD88 activity. Interleukin-1 (IL-1) receptor-associated kinase M (IRAKM), suppressor of cytokine signaling 1 (SOCS1) and Toll-interacting protein (TOLLIP) inhibit IRAK by targeting different phosphorylation steps of the cascade. Moreover, the nucleotide-binding oligomerization domain-containing protein 2 (NOD2) inhibits NF-κB activity. Phospatidylinositol 3-kinase (PI3K) inhibits TLR responses in an unclear mechanism (LIEW *et al.* 2005b).

Similar to the JAK/STAT cascade, Toll signaling has been linked to many types of cancer. Studies revealed that *Helicobacter pylori* and viral hepatitis infections are associated with gastric and liver cancers, respectively and inflammatory Bowel's disease is linked to colorectal cancer (XU *et al.* 2013; ROGLER 2014; WANG *et al.* 2014a). In all cases, an increased activity of TLR4 was documented and interestingly, its silencing declined tumor progression in colorectal metastasis (EARL *et al.* 2009). In addition, constitutive expression of TLR4 is also linked to breast cancer (WOLSKA *et al.* 2009; OBLAK AND JERALA 2011; YANG *et al.* 2013), where the migration, invasion, survival and proliferation of cancerous cells are augmented upon triggering a TLR4-NF-κB inflammatory situation (IKEBE *et al.* 2009; KELSH AND MCKEOWN-LONGO 2013; YUAN *et al.* 2013). Thus, Toll signaling cascade and mainly TLR4 were linked to both cancer growth and inhibition, depending on the microenvironment and the metastatic phase present.

***Drosophila*: a model for inflammation**

Many biological, cellular and molecular mechanisms are highly conserved between *Drosophila* and mammals. For example, the RUNT and Notch signaling cascades that are conserved in evolution play role in *Drosophila* hematopoiesis and are associated with tumors development in humans (GEISSLER AND ZACH 2012; HARVEY *et al.* 2013). Interestingly, *Drosophila* harbors a primitive, but efficient circulatory system with three types of immune cells or hemocytes that act as sensors to elicit an immune response. They function during various developmental stages, morphogenesis and in response to environmental stimuli like tissue damage. Also, they share common characteristics with the mammalian blood cells (HARTENSTEIN 2006; WANG *et al.* 2014b). The most prominent type of hemocytes in *Drosophila* is provided by the plasmatocytes (size; <20μm), which constitute more than 95% of the whole population. Plasmatocytes resemble mammalian macrophages and are involved in phagocytosis of foreign bodies, microbial organisms and apoptotic cells when recruited to infection sites (**Figure 6**) (TEPASS *et al.* 1994; FRANC *et al.* 1999; ELROD-ERICKSON *et al.* 2000; WANG *et al.* 2014b). The second cell type is provided by the crystal cells that constitute 5% of the total hemocytes. They are larger than plasmatocytes in size (>20μm) and their wound healing role is comparable to that of platelets in mammals (VLISIDOU AND WOOD 2015). Crystal cells harbor paracrystalline inclusions in their cytoplasm, which gives them their name. These inclusions contain zymogens, such as prophenoloxidases (PPOs) that are involved in the melanization process, after being cleaved into the phenoloxidase (PO) active form, upon activating a serine protease signaling cascade, which ultimately leads to melanin production (JIRAVANICHPAISAL *et al.* 2009; WANG *et al.* 2014b). Melanin is essential to prevent hemolymph leakiness (equivalent to blood in mammals) at the wounded site, to immobilize the pathogen and to promote healing

(**Figure 6**). The last cell type is constituted by the lamellocytes that are equivalent to granulocytes in mammals. They are flat, adhesive and the largest hemocytes in terms of size (>40µm in diameter) (LANOT *et al.* 2001; WANG *et al.* 2014b; VLISIDOU AND WOOD 2015). They are absent in normal conditions; however, upon infections they differentiate from plasmatocytes after the activation of many signaling events including JAK/STAT (**Figure 6**). They play role in encapsulating large bodies like parasitoid eggs that plasmatocytes cannot engulf (SORRENTINO *et al.* 2002; LEE *et al.* 2009). In addition, they are capable of melanizing foreign bodies with the help of the crystal cells (KRZEMIEN *et al.* 2010). The development of the hemocytes and the factors involved are discussed later.

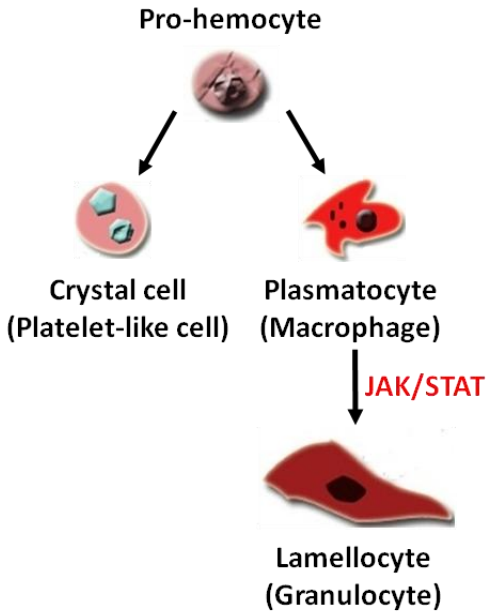

Figure 6: Schematic of the hemocytes in *Drosophila*. A prohemocyte can give rise to crystal cells and plasmatocytes. Lamellocytes differentiate from plasmatocytes upon infections or constitutive activation of JAK/STAT signaling cascade. Equivalent mammalian cells are in parenthesis. Modified from (WANG *et al.* 2014b)

During an immune challenge, three humoral responses can occur in the hemolymph to combat the pathogen. First, rapid killing of the microbe can be achieved upon antimicrobial peptides (AMPs) released into circulation, mainly from the hemocytes and the fat body. Second, hydrogen peroxide (H_2O_2) or nitric oxide (NO) production during the melanization process,

serve as direct chemical tools for pathogen killing. Finally, immobilizing the pathogen upon melanin release is an important event to facilitate the encapsulation mechanism (LEMAITRE AND HOFFMANN 2007; KOUNATIDIS AND LIGOXYGAKIS 2012).

Organs in *Drosophila* involved in innate immunity mainly include the fat body, somatic muscles and lymph gland (discussed later). The fat body in *Drosophila* is equivalent to the liver in humans. It plays role in storing energy, nutrient sensing and in inducing innate immune responses (AGAISSE AND PERRIMON 2004). Upon infections, it is considered the primary source of AMPs production after the activation of inflammatory cascades, such as the JAK/STAT and Toll pathways, in response to proinflammatory signals released by the plasmatocytes (DUSHAY AND ELDON 1998; AGAISSE AND PERRIMON 2004). Interestingly, it was recently shown that infections can also activate the somatic muscles that contribute to the systemic immune response. Plasmatocytes send proinflammatory signals to induce the JAK/STAT cascade in the somatic muscles, which in turn signals to the definitive hematopoietic organ, the lymph gland to induce the differentiation and production of lamellocytes (YANG *et al.* 2015). Other inflammatory cascades involved in innate immune responses include the Jun N-terminal kinase (JNK) and the immunodeficiency (IMD) cascades that are also activated upon bacterial and fungal infections and lead to the production of AMPs (LEMAITRE *et al.* 1995a; ROSETTO *et al.* 1995). The JAK/STAT and Toll signaling cascades are discussed below.

JAK/STAT signaling cascade in *Drosophila*

The JAK/STAT pathway in *Drosophila* is highly conserved throughout evolution and is present with complete core components that are simpler as compared to mammals, and sufficient to induce downstream targets and regulate many biological processes (ARBOUZOVA AND ZEIDLER 2006). It plays role in maintaining the homeostasis in the body through its involvement in regulating many cellular processes, such as cell proliferation, differentiation and migration, in addition to its involvement in apoptosis, organogenesis, axon development, hematopoiesis and immune responses (O'SHEA *et al.* 2002; HOMBRIA AND SOTILLOS 2013).

Drosophila JAK/STAT pathway has two transmembrane receptors (Dome) and its distant structural homolog and JAK/STAT inhibitor (*latran/eye transformer* (*et*), CG14225), one JAK tyrosine kinase (Hopscotch), and one STAT transcription factor (STAT92E). In addition, three ligands called Unpaired (Upd or os); Unpaired 2 (Upd2) and Unpaired 3 (Upd3) that are related to the mammalian Leptin family of ligands are capable of inducing the cascade (BINARI AND PERRIMON 1994; YAN *et al.* 1996; HARRISON *et al.* 1998; BROWN *et al.* 2001; LANGER *et al.* 2004; KALLIO *et al.* 2010; MAKKI *et al.* 2010). Following Upd binding, the dimerization of the receptor (Dome) induces a downstream signaling transduction cascade, which stimulates the two receptor associated JAK kinases (Hopscotch) to transphosphorylate each other and the cytoplasmic tail of Dome, providing docking sites for the dormant cytoplasmic transcription factor STAT92E. When two subunits of STAT92E are phosphorylated, they dimerize and translocate to the nucleus to bind palindromic target sites and induce gene expression (**Figure 7**) (HOU *et al.* 1996; YAN *et al.* 1996; BROWN *et al.* 2001; CHEN *et al.* 2002).

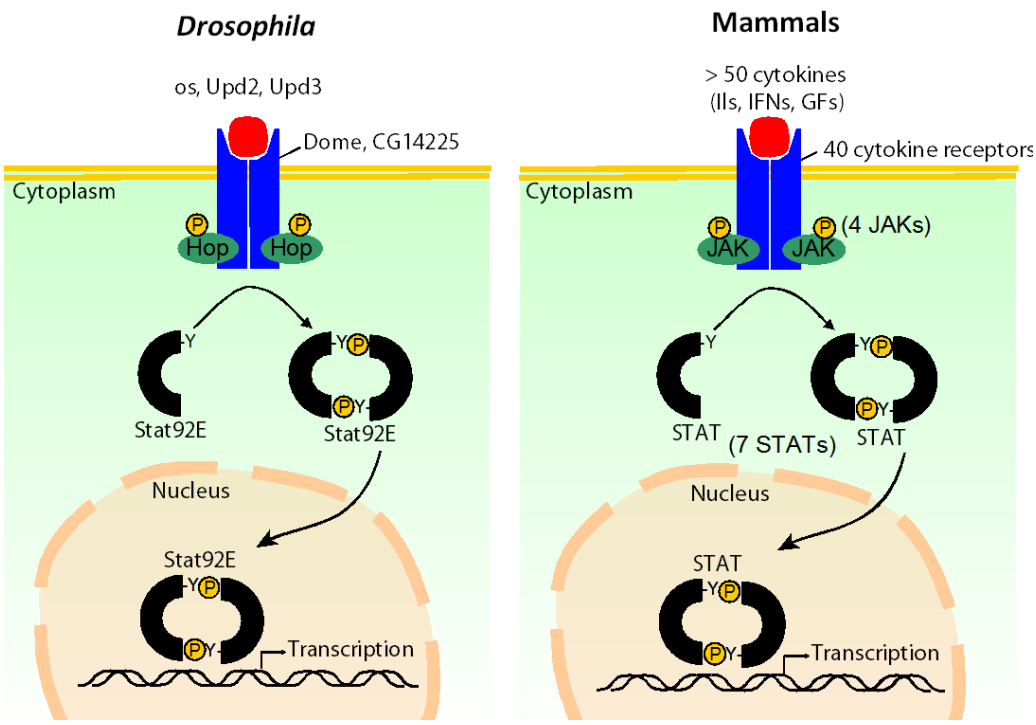

Figure 7: Schematic of the JAK/STAT signaling cascade in *Drosophila* (right) and mammals (left). The JAK/STAT cascade is highly conserved throughout evolution and is less complex in *Drosophila*. The ligands (os, Upd2 and Upd3) bind the receptor (Dome) and induce a series of phosphorylation events, leading to the activation of (STAT92E) and thus, activating the transcription of target genes.

Like in mammals, the JAK/STAT cascade is highly regulated by three major inhibitors: Suppressor of cytokine signaling 36E (SOCS36E), drosophila Protein inhibitor of activated stat (dPIAS) and Protein tyrosine phosphatase 61F (PTP61F). The best-characterized family is the *Socs* family of genes, where three *Socs*-like genes were identified in *Drosophila*: *Socs16D*, *Socs36E* and *Soscs44A*. All three harbor an SH2 domain and a SOCS-box at the C-terminus. 29.7% similarity is present between SOCS36E and SOC5 in mammals. SOCS44A and SOCS16D are similar to SOCS6 and SOCS7, respectively. SOCS36E and SOCS44A exert their inhibitory function by competing with STAT92E for binding to Hopscotch catalytic domain. Interestingly, SOCS36E is both a JAK/STAT inhibitor and a STAT92E direct target gene, whereas SOCS44A is capable of repressing the JAK/STAT pathway in some tissues, but is not a

direct target (CALLUS AND MATHEY-PREVOT 2002; BAEG *et al.* 2005; MULLER *et al.* 2005; KARSTEN *et al.* 2006). SOCS16D precise function is still not clear (**Figure 8**).

The second inhibitor dPIAS was documented as a repressor of the JAK/STAT pathway, upon a series of experiments showing that a decrease in dPIAS expression is accompanied by an increase in JAK/STAT reporter *in vivo*, and its increased expression leads to a decrease in JAK/STAT activity (BETZ *et al.* 2001; MULLER *et al.* 2005). dPIAS regulates the JAK/STAT pathway by targeting STAT92E for degradation via SUMOylation (**Figure 8**) (KOTAJA *et al.* 2002).

PTP61F is the homolog of the mammalian (PTPB1). It was initially described as a JAK/STAT regulator in two genome-wide RNAi screens (BAEG *et al.* 2005; MULLER *et al.* 2005). PTP61F exerts its inhibitory role by dephosphorylating Hopscotch and STAT92E. Also, it was suggested that PTP61F can directly bind and dephosphorylate STAT92E (MULLER *et al.* 2005). Moreover, some studies highlighted that *Ptp61F* might also be a direct JAK/STAT target (**Figure 8**) (BAEG *et al.* 2005).

Other indirect JAK/STAT inhibitors include *ken and barbie* (*ken*) and *Su(var)3-9*. The *ken* gene encodes a DNA-binding protein harboring three zinc finger domain and an N-terminal BTB/POZ domain commonly present in transcriptional repressors (homolog of human *B-cell lymphoma 6* (*BCL6*)) (ARBOUZOVA AND ZEIDLER 2006). Interestingly, the binding domain of Ken overlaps half the palindromic STAT92E binding site. Luciferase reporter assays in cell lines revealed that Ken acts as a repressor of the JAK/STAT pathway (ARBOUZOVA AND ZEIDLER 2006). *Su(var)3-9* induces the methylation of Histone3 at amino acid 9 Lysine (K) and Heterochromatin Protein 1 (HP1), which induces heterochromatin formation. Removal of one

copy of these loci induces JAK/STAT activation, suggesting a link between JAK/STAT and heterochromatin formation (BINA *et al.* 2010).

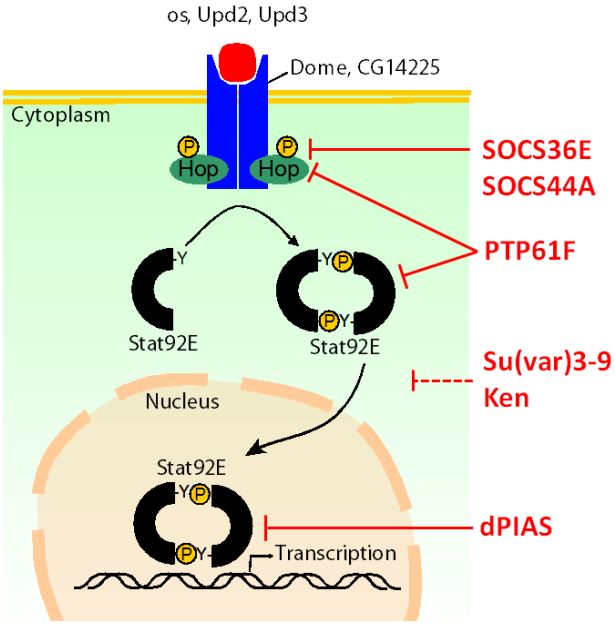

Figure 8: Schematic of the JAK/STAT signaling cascade inhibitors in *Drosophila*. SOCS36E and SOCS44A inhibit the transphosphorylation of Hopscotch and compete with STAT92E to bind the Hopscotch catalytic domain. PTP61F dephosphorylates Hopscotch and STAT92E. dPIAS inhibits the activated STAT92E from binding to its target genes and thus, shuts down gene expression. Ken and Su(var)3-9 indirectly inhibit JAK/STAT signaling.

JAK/STAT dysregulation is associated with several tumorous models in *Drosophila*, such as epithelial and hematopoietic tumors. The combination of JAK/STAT simplicity and the availability of a wide range of genetic tools increased the popularity of *Drosophila* as a model for tumorigenesis. Similar to *JAK2* V617F mutation, two dominant *GOF* mutations within Hopscotch induce hematopoietic defects and the formation of blood melanotic tumors (discussed below). The first is termed $hop^{Tum\text{-}l}$, where "*Tum-l*" stands for "*Tumorous lethal*" and is due to amino acid substitution from Glycine (G) to Glutamic acid (E) at position 341 (G341E) in the JH4 domain (**Figure 9**). The second mutation termed hop^{T42} is similar to $hop^{Tum\text{-}l}$ in terms of blood melanotic tumors production, but is due to amino acid substitution from Glutamic acid (E) to Lysine (K) at position 695 (E695K) in the JH2 domain (**Figure 9**) (HANRATTY AND DEAROLF 1993; HARRISON ET AL. 1995; LUO ET AL. 1995; LUO ET AL. 1997). Importantly, Hopscotch in

Drosophila is highly similar to JAK1 and 2 in mammals (CHEN ET AL. 2002), with one catalytic and one pseudokinase domains, an SH2 and FERM domains (**Figure 9**).

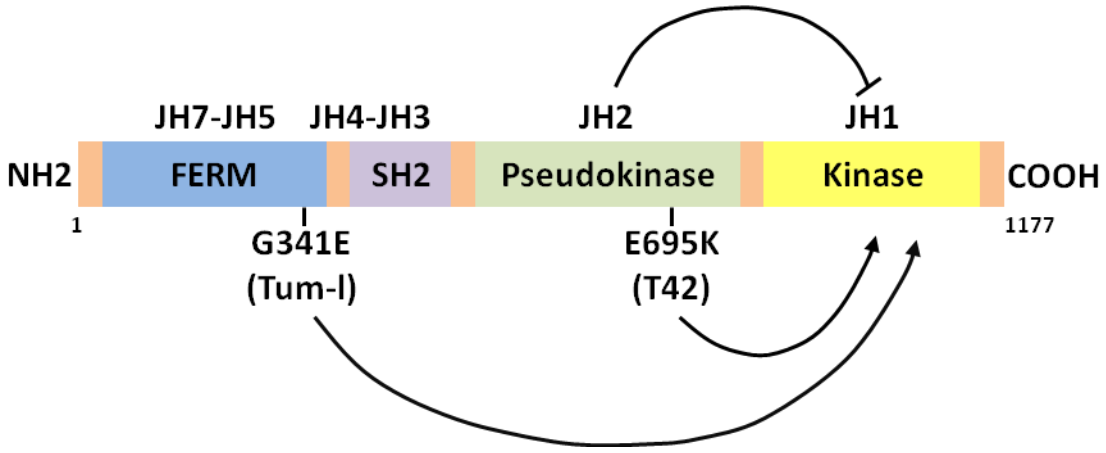

Figure 9: Schematic of the Hopscotch domain structure in *Drosophila*. Hopscotch contains a catalytic tyrosine kinase domain (JH1, yellow), a pseudokinase domain (JH2, green), an SH2 domain (magenta) and a FERM domain (blue) that mediates in cytokine-receptor interactions. In normal conditions, the JH2 domain regulates the activation of the kinase domain, JH1. The E695K (*T42*) or G341E (*Tum-l*) mutations lead to constitutive activation of JH1. Modified from (AMOYEL *et al.* 2014).

The constitutive activation of the JAK/STAT pathway due to $hop^{Tum\text{-}l}$ or hop^{T42} mutations induces over-proliferation of hemocytes (SILVERS AND HANRATTY 1984; LUO *et al.* 1995; LANOT *et al.* 2001). These mutations mimic the *JAK2* V617F mutation in humans that induces a conformational change in the protein structure and leads to constitutive JAK/STAT activity. Interestingly, the lamellocytes reach approximately 70% the total population in both $hop^{Tum\text{-}l}$ and hop^{T42} mutations (AMOYEL *et al.* 2014). When lamellocytes trans-differentiate from plasmatocytes, they induce auto encapsulation, aggregation of cells and the formation of black melanotic tumors (LUO *et al.* 2002) (**Figure 10**).

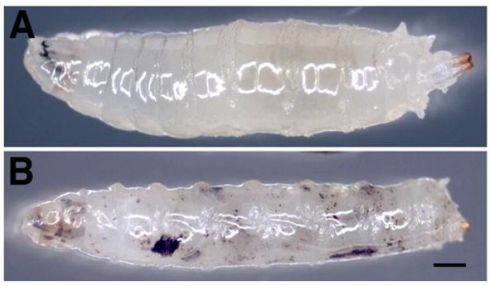

Figure 10: JAK/STAT constitutive activation results in cellular over-proliferation. (**A**) WT 3rd instar larva (stage during *Drosophila* life cycle). (**B**) 3rd instar larva carrying a $hop^{Tum\text{-}l}$ mutation leads to over-proliferation of lamellocytes that aggregate and form black melanized tumors (dark masses); scale bar: 50µm. Modified from (ARBOUZOVA AND ZEIDLER 2006).

Toll signaling cascade in *Drosophila*

Due to the high similarity of innate immunity between *Drosophila* and mammals, the Toll signaling pathway initially discovered in *Drosophila* has become a reference for investigating innate immune responses (NUSSLEIN-VOLHARD AND WIESCHAUS 1980; BELVIN AND ANDERSON 1996; ZAMBON *et al.* 2005). Studies on the Toll cascade go back to 1995, when Toll (Toll1) was described as an activator of immunity in a *Drosophila* cell line, before being identified in mammals (LEMAITRE *et al.* 1995b; ROSETTO *et al.* 1995). This pathway is mainly involved in *Drosophila* in cellular defense mechanisms against pathogens. For example, upon infections by a Gram-positive bacteria or fungi, the Toll pathway is activated leading to the production of AMPs, such as the antibacterial peptide Defensin or the antifungal peptide Drosomycin (AGGARWAL AND SILVERMAN 2008; HETRU AND HOFFMANN 2009). In addition, parasitic wasp infection activates several inflammatory cascades including the Toll pathway, however its contribution to the defense mechanisms against wasps is limited (YANG AND HULTMARK 2016). Yet, it induces an increase in the total number of plasmatocytes and lamellocytes. Interestingly, Toll signaling was also shown to play roles in regulating hemocytes density and proliferation (ZETTERVALL *et al.* 2004; VALANNE *et al.* 2011).

Nine Toll receptors were identified in *Drosophila* (Toll1 to Toll9) (TAUSZIG *et al.* 2000). Toll (Toll1) along with Toll5 and Toll9 play major roles in augmenting an immune response, where all three can induce *Drosomycin* expression (LUO *et al.* 2001; OOI *et al.* 2002). Moreover, all 9 Toll receptors share an ectodomain with LRR repeats and cystein flanking motifs (**Figure 11**), except for Toll9, which harbors only one cystein motif, a structure similar to TLRs in mammals. Like in vertebrates, *Drosophila* Toll receptors have a cytosolic TIR domain that plays role in interacting and activating downstream molecules (**Figure 11**) (TAUSZIG *et al.* 2000; IMLER AND HOFFMANN 2001; VALANNE *et al.* 2011).

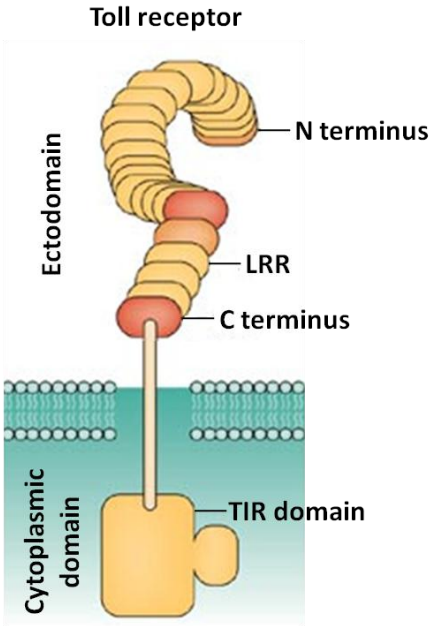

Figure 11: Schematic of the Toll receptor in *Drosophila*. The Toll receptor has an extracellular ectodomain and an intracellular cytoplasmic domain. Two LRR repeats are present in the extracellular domain. TIR domain is present in the intracellular region. Modified from (GAY *et al.* 2006).

Upon infections by Gram-positive bacteria or fungi, a series of proteolytic cleavages by Spatzle-processing enzyme (SPE) leads to the activation of the Toll receptor ligand Spatzle (Spz). These cleavages are essential to induce a conformational change in Spz and expose its binding domains to the Toll receptor (JANG *et al.* 2006; ARNOT *et al.* 2010; VALANNE *et al.* 2011). Following Spz binding, the adaptor protein dMyD88 binds the TIR domain of the receptor. This induces the recruitment of Tube and the kinase Pelle, to form a dMyD88-Tube-Pelle heterotrimeric complex

in the intracellular region via death domain (DD) interactions (**Figure 12**). Pelle, which has a kinase activity, phosphorylates the downstream IκB factor Cactus, leading to its dissociation from the NF-κB transcription factors Dorsal (in case of bacterial infection) and/or Dif (in case of fungal infection), allowing their translocation to the nucleus (**Figure 12**) (SUN *et al.* 2002; MONCRIEFFE *et al.* 2008; VALANNE *et al.* 2011). In normal conditions, Cactus binds Dorsal and/or Dif, preventing their nuclear translocation. When it is phosphorylated by Pelle at two different N-terminal motifs, it is directed for degradation (FERNANDEZ *et al.* 2001).

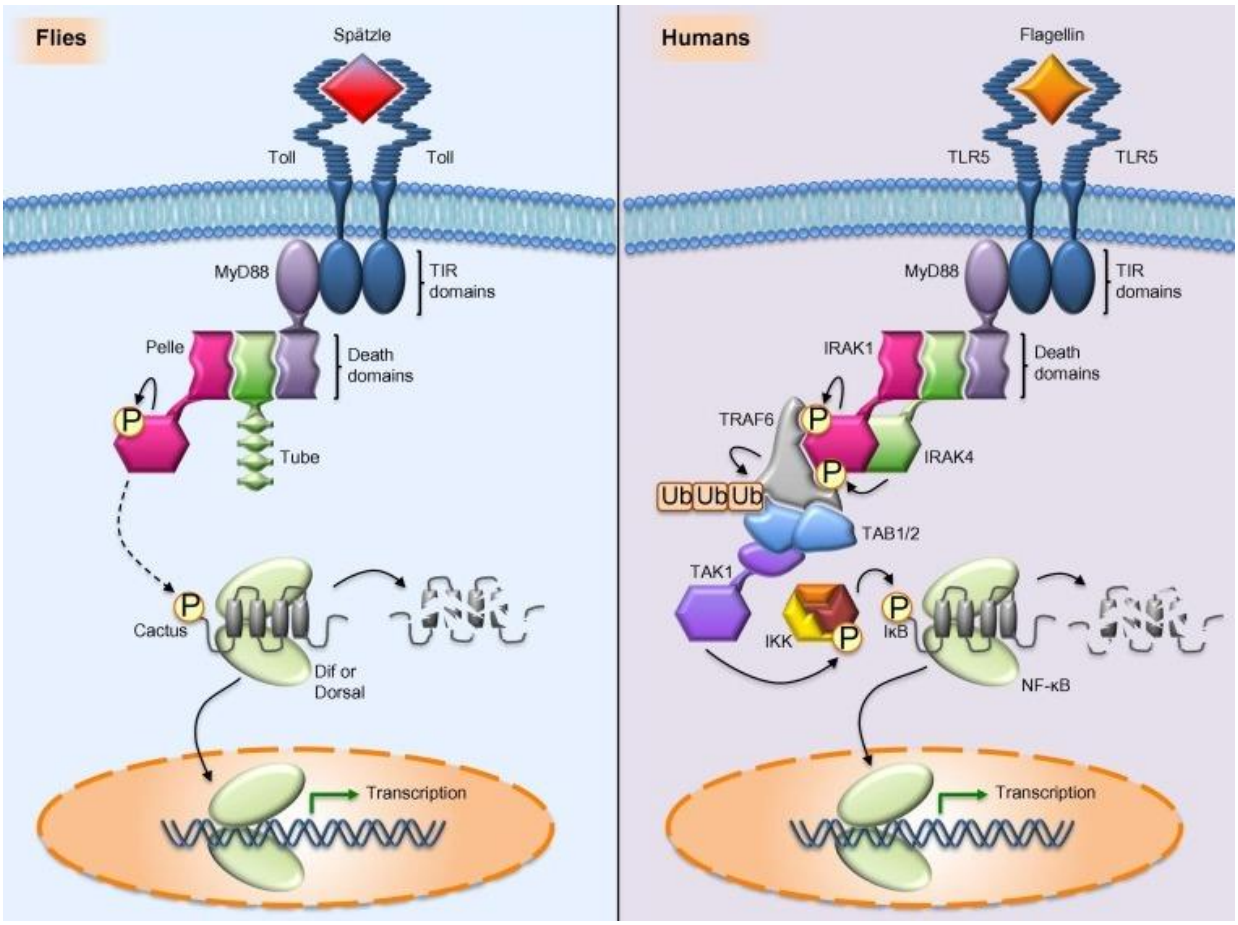

Figure 12: Comparison of the Toll signaling cascade in flies and humans. The Toll cascade is highly conserved in evolution and is simpler in *Drosophila*. The core components and the homologous orthologs between *Drosophila* and humans have the same color code. Modified from (LINDSAY AND WASSERMAN 2014).

Like in mammals, Toll signaling in *Drosophila* is robustly regulated to prevent a constitutively active cascade and over-proliferation of hemocytes. Cactus is a major negative regulator of the Toll cascade that inhibits the constitutive activation of downstream transcription factors (VALANNE *et al.* 2011). Moreover, the Serpin family of proteins, such as Spn77Ba and Spn27A are serine protease inhibitors that repress a protease-phenoloxidase (PO) cascade and ultimately melanin synthesis, which in turn prevents melanization in normal conditions. These proteases indirectly regulate the Toll cascade by preventing excess melanin production by lamellocytes, which are also produced upon Toll cascade activation (TANG *et al.* 2008).

Similar to the JAK/STAT pathway, dysregulations within the Toll cascade are associated with melanotic tumors development. For example, loss-of-function (*LOF*) mutation within *cactus*, *GOF* point mutation within the *Toll* receptor gene named $Toll^{10b}$, or continuous expression of *dorsal* cause a constitutively active form of the NF-κB transcription factor Dorsal and over-proliferation of lamellocytes. This ultimately leads to aggregation of cells and the formation of melanotic tumors, which are mainly present in the hemolymph (LEMAITRE *et al.* 1995b; MINAKHINA AND STEWARD 2006; VALANNE *et al.* 2011). Furthermore, studies documented that Spn77Ba disturbance induces tracheal melanization, due to the constitutive expression of the antifungal encoding gene *Drosomycin* (TANG *et al.* 2008).

Chapter II

Development of immune cells in *Drosophila*

Immune cells play major roles in killing foreign pathogens and endogenous abnormal cells, which makes them indispensible for survival. In mammals, a complex network of innate and adaptive immune responses is present. In *Drosophila* the existence of only innate immunity and three types of hemocytes makes our understanding to the development of immune responses simpler. In addition, the common characteristics of *Drosophila* hemocytes and their mammalian counterparts further justify the importance of investigating immunity in flies (HARTENSTEIN 2006; WANG *et al.* 2014b). In the following section, I will describe the development and differentiation of immune cells in *Drosophila* in the primitive and definitive hematopoietic waves.

Primitive vs. definitive hematopoiesis

In *Drosophila* and vertebrates, immune cells originating from different hematopoietic waves coexist in the organism and are necessary for mounting efficient immune responses. Interestingly, many similarities at the level of immune cells development are present between *Drosophila* and vertebrates. These common features are highlighted through the conservation of signaling cascades and transcription factors controlling proliferation, differentiation and specific cell lineage commitment (EVANS *et al.* 2003). In *Drosophila*, primitive hematopoiesis occurs during embryonic development, where hemocytes arise from the procephalic mesoderm and disperse within the embryo, and then in the larva, where they migrate as circulating blood cells or organize in sessile patches to become resident hemocytes (**Figure 13**) (TEPASS *et al.* 1994;

EVANS *et al.* 2003; WOOD AND MARTIN 2017). The sessile/resident hemocytes constitute the majority of the immune cells in the larval stages, where they get attached to the cuticular epidermis and only mobilize into circulation upon infections (LANOT *et al.* 2001; KURUCZ *et al.* 2007; MAKHIJANI *et al.* 2011) (**Figure 13**). The peripheral nervous system (PNS) provides a suitable environment for the maintenance of sessile hemocyte population (MAKHIJANI *et al.* 2011). Primitive hematopoiesis in *Drosophila* is equivalent to its mammalian counterpart, which occurs during embryogenesis in the yolk sac and gives rise to primitive large erythroblasts (PALIS *et al.* 2010; BARON 2013). Embryonic development in *Drosophila* and vertebrates is isolated and protected from the surrounding environment, preventing any infection in normal conditions until hatching (*Drosophila*) or birth (vertebrates). Therefore, to increase protection levels after embryonic development, a second hematopoietic wave is required in both cases to produce huge populations of immune cells (EVANS *et al.* 2003).

The second wave (definitive hematopoiesis) in *Drosophila* gets active during the larval stage in a specific organ called the lymph gland (discussed below), which is formed during embryogenesis and grows and proliferate until the pupal stage (metamorphosis stage), where it histolyses at 8-10hrs before pupa formation and releases its hemocytes into circulation to populate the adult (**Figure 13**) (RUGENDORFF *et al.* 1994; EVANS *et al.* 2003). This wave is equivalent to the mammalian hematopoiesis occurring during the late fetal stages in the bone marrow and the fetal liver to give rise to lymphoid, myeloid and erythroid lineages (TAVIAN AND PEAULT 2005; MIKKOLA AND ORKIN 2006). Interestingly, it was believed that no hematopoiesis occurs in *Drosophila* adults; however, it was recently proposed that active hematopoietic hubs located within the dorsal abdominal hemocyte cluster, is capable of proliferating and can react to bacterial infections (GHOSH *et al.* 2015).

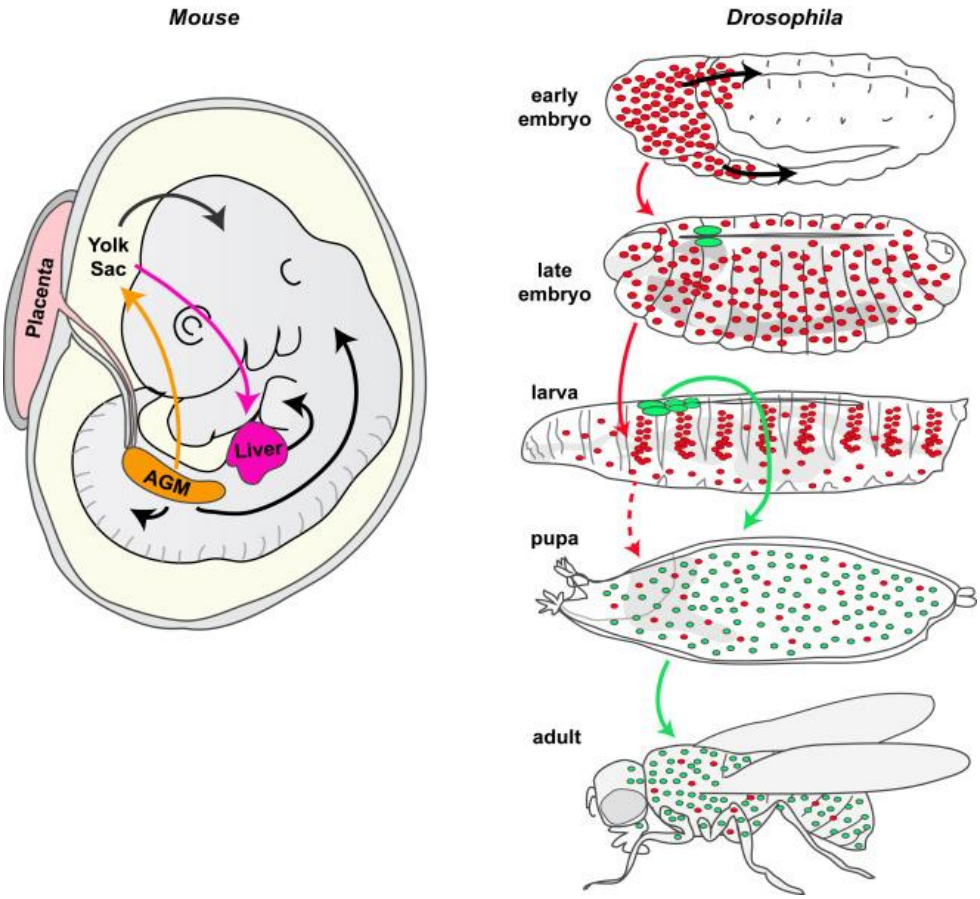

Figure 13: Hematopoiesis in mammals and *Drosophila*. A schematic of a mouse embryo (left), showing the migration of macrophage progenitors (arrows) derived from the yolk sac and the aorta-gonad-mesonephros (AGM) towards their ultimate destinations in tissues. In *Drosophila* (right), primitive hematopoiesis gives rise to embryonic hemocytes (macrophages) that migrate within the embryo and populate the larva as circulating cells, or in organized patches called sessile hemocytes (resident cells). Definitive hematopoiesis occurs in the lymph gland (green), where hemocytes are released at the onset of metamorphosis (pupal stage). Modified from (WOOD AND MARTIN 2017).

Lymph gland structure

The lymph gland is made up of a pair of anterior primary lobes that start forming during late embryonic stages (20 precursor cells/lobe), and a number of secondary and tertiary lobes that are produced during the larval life along the sides of the dorsal vessel (DV) (**Figure 14**). The primary lobes are made up of three distinct regions: the medullary zone (MZ), which contains

tightly packed hematopoietic progenitor cells; the petal shaped cortical zone (CZ), with differentiating and loosely packed cells; and the posterior signaling center (PSC), that serves as a hematopoietic niche and plays role in maintaining the balance between the prohemocytes in the MZ and the differentiating hemocytes in the CZ (**Figure 14**). The secondary lobes represent the pool of immature prohemocytes (LEBESTKY *et al.* 2003; JUNG *et al.* 2005; KRZEMIEN *et al.* 2007; TAN *et al.* 2012). During the mid-3rd instar, MZ cells become dormant while CZ cells continue proliferating until the onset of metamorphosis. At this stage, CZ cells are named intermediate progenitors as they are still proliferating and differentiating (JUNG *et al.* 2005; KRZEMIEN *et al.* 2010). By late 3rd instar, CZ cells become fully differentiated, allowing their release into circulation at the onset of metamorphosis as plasmatocytes and crystal cells. Upon infections or mutations, such as *hop*$^{Tum\text{-}l}$ or *Toll*^{10b}, the number of proliferating cells, the total number of plasmatocytes and lamellocytes increases and the lymph gland histolyses before pupariation (RIZKI AND RIZKI 1992; SORRENTINO *et al.* 2002; KURUCZ *et al.* 2007). The transcription factors required in the differentiation of immune cells in *Drosophila* are discussed below.

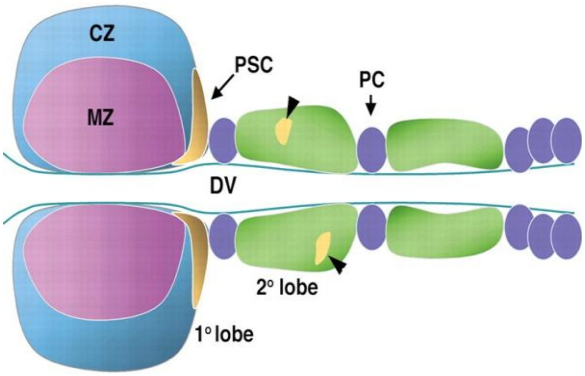

Figure 14: Schematic of the 3rd instar lymph gland. The lymph gland is located along the sides of the dorsal vessel. Lobes are separated by pericardial cells (PC). Primary lobes constitute 3 zones: (1) cortical zone (CZ) with differentiating cells; (2) medullary zone (MZ), with progenitor cells lacking differentiation markers; (3) posterior signaling center (PSC), which serves as a hematopoietic niche. Secondary lobes are reservoirs for immature hemocytes except for random regions of maturation (arrowheads). Modified from (JUNG *et al.* 2005).

Factors involved in immune cells differentiation in *Drosophila*

During the embryonic life, the hemocyte anlagen is first detected at embryonic stage 5 upon the expression of Serpent (Srp), a GATA transcription factor involved in hematopoiesis in the procephalic mesoderm region (TEPASS *et al.* 1994; REHORN *et al.* 1996; EVANS *et al.* 2003). The last division of cells occurs at stage 12, and by the end of embryogenesis prohemocytes differentiate into plasmatocytes or crystal cells (TEPASS *et al.* 1994; LEBESTKY *et al.* 2000). While plasmatocytes disperse within the embryo upon maturation, crystal cells remain confined near the procephalic mesoderm. In total, embryonic hematopoiesis gives rise to approximately 700 plasmatocytes and 36 crystal cells (TEPASS *et al.* 1994). While the procephalic mesoderm gives rise to primitive hematopoiesis, the cardiogenic mesoderm gives rise to the site of definitive hematopoiesis, the lymph gland (**Figure 15**) (HOLZ *et al.* 2003), where approximately 20 precursor cells attach to the sides of the dorsal vessel and express Srp, and start differentiating during the 2nd instar larval stage, when they form the different lobes (LEBESTKY *et al.* 2000). Proliferation of prohemocytes in both the procephalic mesoderm and the cardiogenic mesoderm is under strict control, where four rounds of divisions occur at precise times (TEPASS *et al.* 1994; EVANS *et al.* 2003; HOLZ *et al.* 2003).

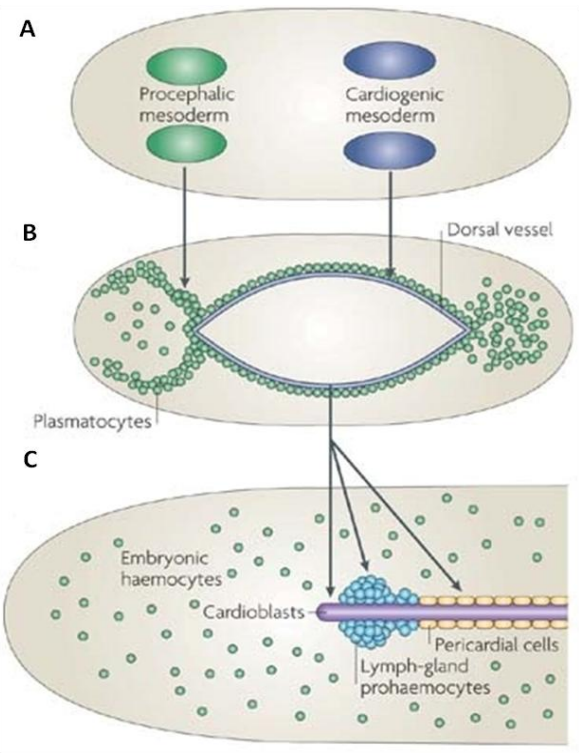

Figure 15: Hemocyte development in *Drosophila* embryo. (**A**) Embryonic hemocytes are derived from the procephalic mesoderm (green). Lymph-gland precursors arise from the cardiogenic mesoderm (blue). (**B**) Plasmatocytes (green) proliferate and migrate within the embryo along the dorsal vessel (blue). (**C**) Cardiogenic mesoderm cells differentiate to form pericardial cells (yellow), cardioblasts (purple) and lymph-gland cells (light blue). Modified from (WOOD AND JACINTO 2007).

Serpent (Srp) and U-Shaped (Ush)

Srp is a zinc finger GATA transcription factor that plays key roles in favoring cells towards the hemocyte fate, after its early expression in the hemocyte analgen. Other GATA transcription factors are also present in *Drosophila*, such as *pannier*, *grain*, *dGATA-D*, and *dGATA-E*. However, Srp is the major factor directly required in hematopoiesis (LEBESTKY *et al.* 2000; PATIENT AND MCGHEE 2002; EVANS *et al.* 2003). In addition to its hematopoietic role, Srp is required in many developmental programs and proliferative mechanisms. In the embryo, its expression in the procephalic mesoderm at embryonic stage 5 directly precedes prohemocyte

differentiation (**Figure 16**). In lymph gland progenitors, Srp expression is delayed, due to the absence of differentiation capacities and the fact that the generation of these cells is downstream to many signaling inputs. However, after Srp expression in lymph gland precursor cells, extensive proliferation is maintained until the 2nd instar larval stage, when the process of hemocyte differentiation is initiated upon Lozenge (Lz) expression (see below) (EVANS *et al.* 2003). Two protein isoforms of Srp are present that arise from alternative splicing of *srp* transcripts, where SrpNC contains two zinc fingers, while SrpC harbors one zinc finger domain (WALTZER *et al.* 2002). The former can interact with the Friend-of-GATA (FOG) homolog U-shaped (Ush) (TEVOSIAN *et al.* 1999; WALTZER *et al.* 2002). Both isoforms are capable of inducing the differentiation of prohemocytes into plasmatocytes or crystal cells.

Ush belongs to the FOG family of proteins that play role in controlling the function of GATA transcription factors (CHANG *et al.* 2002). Ush expression is initiated at embryonic stage 8 and interacts with Srp to repress the crystal cell fate (**Figure 16**). *LOF* mutations in *ush* and miss-expression of Ush protein in the prohemocytes result in an increase and a decrease in the total number of crystal cells, respectively (FOSSETT *et al.* 2001). As Ush antagonizes the crystal cell fate, its expression is sustained in plasmatocytes (FOSSETT *et al.* 2001).

Lozenge (Lz)

Lz belongs to the RUNX family of transcription factors. It has 71% homology in its RUNT domain with the human AML-1/RUNX-1, which is associated with acute myeloid leukemia (DAGA *et al.* 1996; EVANS *et al.* 2003). In *Drosophila*, Lz plays key roles in crystal cells differentiation (**Figure 16**). Its expression appears in the procephalic mesoderm at embryonic stage 10, when crystal cell development is initiated (LEBESTKY *et al.* 2000). At that

stage, Lz is expressed in approximately 18 Srp positive prohemocytes marking them as crystal cell progenitors. By the end of stage 17, fully differentiated crystal cells remain fixed near the procephalic mesoderm although, they scatter in circulation during larval stages (LEBESTKY *et al.* 2000). In the lymph gland, the differentiation of crystal cells starts upon the expression of Lz during the 2nd instar larval stage, where it is restricted to few cells in the primary lobes. By late 3rd instar stages, more crystal cell precursors are present within the primary lobes and few are detected in the secondary lobes (LEBESTKY *et al.* 2000). Mature crystal cells in circulation and lymph gland maintain Lz expression (EVANS *et al.* 2003). Studies revealed that co-expression of Lz and Srp during embryonic stages induces the development of large populations of crystal cells. In addition, co-expression of Lz and SrpNC represses Ush, further confirming that the latter inhibits the crystal cell fate (FOSSETT *et al.* 2003).

Glial cell missing/Glial cell deficient (Gcm/Glide)

Glide/Gcm, (for the sake of simplicity Gcm in the rest of the text) and its homolog Gcm2 are zinc finger transcription factors initially discovered for their role in the nervous system, where they determine the glial cell fate (HOSOYA *et al.* 1995; JONES *et al.* 1995; VINCENT *et al.* 1996; KAMMERER AND GIANGRANDE 2001). Gcm is expressed early and transiently during embryogenesis and is considered the master regulator gene for glial cell development. Removal of *gcm* converts glia into neurons, while ectopic expression of *gcm* leads to an excess of glial cells at the expense of neurons (VAN DE BOR AND GIANGRANDE 2002; CATTENOZ AND GIANGRANDE 2013).

Interestingly, Gcm and Gcm2 are also required in plasmatocyte differentiation (BERNARDONI *et al.* 1997; LEBESTKY *et al.* 2000). As for glial cells, the major role is played by

Gcm as Gcm2 displays a weak and delayed expression compared to Gcm. The two genes are 27kb apart; they share *cis*-regulatory elements and are capable of self and cross-regulation (KAMMERER AND GIANGRANDE 2001). During blood cell development in *Drosophila*, Gcm/Gcm2 expression is first observed in plasmatocyte precursors at embryonic stage 5, just after Srp expression (**Figure 16**). By stages 10 and 11, Gcm/Gcm2 expression co-localizes with that of other plasmatocytes markers, such as Peroxidasin (Pxn) and Croquemort (Crq) (BERNARDONI *et al.* 1997; ALFONSO AND JONES 2002; EVANS *et al.* 2003). Gcm expression is transient and its transcripts are no longer detected after embryonic stage 11 or in fully differentiated plasmatocytes (EVANS *et al.* 2003). Embryos mutant for *gcm* show a stronger phenotype as compared to *gcm2* mutant embryos and this is demonstrated by decreased number of plasmatocytes (BERNARDONI *et al.* 1997; ALFONSO AND JONES 2002). Interestingly, a stronger decrease in plasmatocyte number accompanied with abnormal morphology, migratory defects and loss of Crq expression is observed when both *gcm* genes are mutated (ALFONSO AND JONES 2002). The reduction is also associated with an increase in crystal cell numbers in *gcm* mutant embryos only, as the absence of *gcm2* does not significantly affect their development (BATAILLE *et al.* 2005). Interestingly, Gcm can induce plasmatocyte markers when expressed ectopically in crystal cell progenitors (LEBESTKY *et al.* 2000; EVANS *et al.* 2003).

In mammals, two Gcm homologs *GCMa/GCM1* and *GCMb/GCM2* were indentified. *Drosophila* and mammalian Gcm proteins have a conserved DNA-binding domain (DBD) "(A/G)CCCGCAT" (AKIYAMA *et al.* 1996; WEGNER AND RIETHMACHER 2001). *GCMa/GCM1* is involved in placental development, where it is expressed in the mouse placental trophoblast cells from embryonic day 7.5 (E7.5) until (E17.5) (ALTSHULLER *et al.* 1996; BASYUK *et al.* 1999; NAIT-OUMESMAR *et al.* 2000). *GCMa/GCM1* mutations lead to placental failure due to the

absence of a functional labyrinth for nutrients exchange (SCHREIBER *et al.* 2000; MAO *et al.* 2012). *GCMb/GCM2* is involved in parathyroid gland development and its mutation is associated with hypothyroidism, due to the decrease in parathyroid hormone (PTH) production (KIM *et al.* 1998; GORDON *et al.* 2001). So far, no involvement in mammalian hematopoiesis was described for the Gcm proteins.

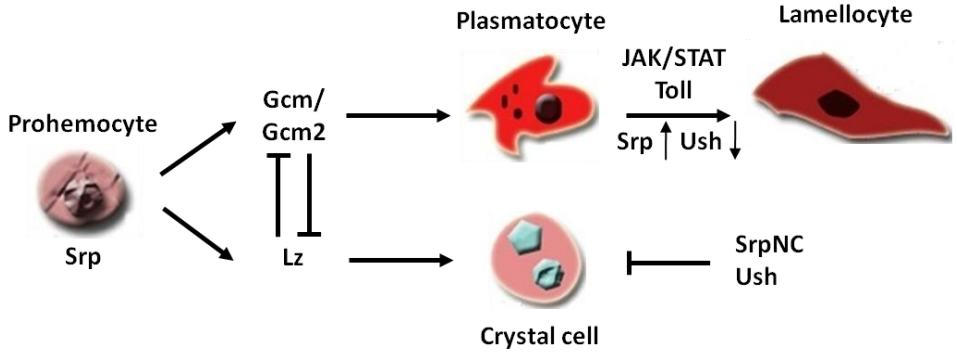

Figure 16: The transcriptional network involved in hemocyte differentiation. First, prohemocytes express the GATA transcription factor Srp. Later, Gcm and Gcm2 are expressed in Srp positive cells, which induce the expression of plasmatocytes markers, such as Pxn and Crq. However, a small subset of cells expresses the RUNX transcription factor Lz, which antagonizes Gcm, to favor the crystal cell fate lineage. The friend-of-GATA (FOG) transcription factor Ush interacts with SrpNC to repress the crystal cell fate. Upon infections, lamellocytes production is induced. Lineage tracing experiments reveal the trans-differentiation of plasmatocytes into lamellocytes upon up-regulating Srp and down-regulating Ush to repress the plasmatocyte fate. In addition, an increase in the total number of lamellocytes is induced upon activating the JAK/STAT and Toll cascades. Modified from (WANG *et al.* 2014b)

Other cascades and hematopoiesis

In addition to JAK/STAT and Toll signaling pathways, Notch, Hedgehog (Hh), and Wnt/Wingless (Wnt/Wg) cascades are also involved in regulating hematopoiesis and the prohemocyte fate (MANDAL *et al.* 2007; OWUSU-ANSAH AND BANERJEE 2009; SINENKO *et al.* 2010; WANG *et al.* 2014b). At the level of the lymph gland, the PSC plays role in maintaining the balance between the undifferentiated cells in the MZ and the differentiating hemocytes in the

CZ. For that, PSC cells extend filopodial projections named cytonemes into the MZ that provide local Hh signal to sustain the MZ prohemocytes undifferentiated and promote their maintenance (**Figure 17**) (MANDAL *et al.* 2007).

Moreover, Notch signaling plays key roles in lineage specifications. Absence of Notch inhibits the expression of Lz in the procephalic mesoderm and thus, the crystal cell fate (LEBESTKY *et al.* 2003). Two ligands (Serrate (Ser) and Delta) are capable of inducing the Notch pathway, however, only Ser functions during hematopoiesis. In the lymph gland, Ser is mainly expressed in the PSC region, where Notch signaling is essential for crystal cell differentiation (LEBESTKY *et al.* 2003). In addition, Notch signaling is essential in the same compartment to maintain normal concentrations of Collier (Col), the ortholog of Early B Cell Factor in mammals. The presence of Col identifies the PSC region and activates the JAK/STAT pathway to maintain the undifferentiated prohemocytes in the MZ, similar to the role of Hh signaling in the same compartment (**Figure 17**) (KRZEMIEN *et al.* 2007; OYALLON *et al.* 2016).

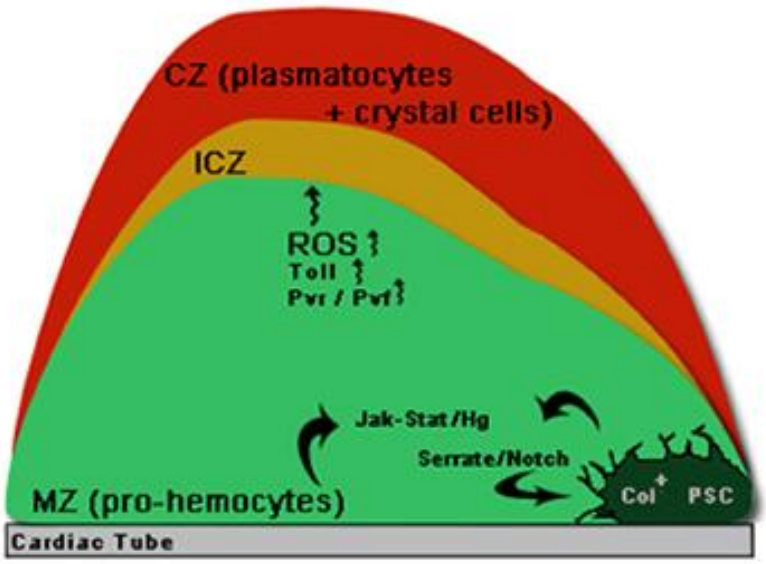

Figure 17: The signaling cascades in larval hemocytes development in the lymph gland. In addition to the MZ, CZ and PSC, a small region called the "Intermediate Cortical Zone" (ICZ) contains intermediate phase hemocytes, defined by the expression both prohemocyte and differentiating hemocyte markers. Prohemocytes fate is maintained through communication between PSC cells and the MZ by filopodia extensions. The JAK/STAT and Hh cascades maintain undifferentiated prohemcoytes in the MZ. Moreover, Col expression is regulated by Notch signaling and this process identifies the PSC. The Toll pathway is involved in the proliferation of prohemocytes, where increased concentrations of ROS induce plasmatocytes differentiation. The receptor tyrokinase (Pvr) is the homolog of the vertebrate Platelet-derived growth factor (PDGF) and Vascular endothelial growth factor (VEGF) receptors. Pvf or PDGF- and VEGF-related factor is the ligand. When Pvr/Pvf signaling is up-regulated, plasmatocytes differentiation is induced. Modified from (WANG *et al.* 2014b).

Chapter III

Gcm and inflammation

The Gcm gene in *Drosophila* is necessary in glial cells differentiation (HOSOYA *et al.* 1995; JONES *et al.* 1995; VINCENT *et al.* 1996; KAMMERER AND GIANGRANDE 2001), embryonic plasmatocyte (BERNARDONI *et al.* 1997; ALFONSO AND JONES 2002) and in tendon cells (SOUSTELLE *et al.* 2004; LANEVE *et al.* 2013). The link between Gcm and inflammation has been suggested by a previous study in the lab (JACQUES *et al.* 2009), where Gcm was shown by yeast two-hybrid assay to interact biochemically with the JAK/STAT regulator dPIAS. This raised an important question as to whether Gcm is necessary to control the inflammatory response. To that purpose, my main aim during my PhD work was to address the role of the embryonic hemocyte specific factor Gcm in the context of inflammation and melanotic tumors formation.

A dominant negative Gcm mutation induces melanotic tumors

Mutations within *dpias*, which is normally required in hematopoiesis regulation, were previously reported to induce melanotic tumors due to STAT92E constitutive activation (**Figure 18**) (BETZ *et al.* 2001; HARI *et al.* 2001). Moreover, conditional expression of gcm^{DN} construct using a Srp driver expressed in all organs involved in hematopoiesis and in innate immunity, such as the lymph gland (LANOT *et al.* 2001), fat body (CHERRY AND SILVERMAN 2006; LEMAITRE AND HOFFMANN 2007) and hemocytes (CROZATIER *et al.* 2004), induces melanotic tumors in 100% of 3rd instar larvae, delayed developmental processes and death at pupal stage (JACQUES *et al.* 2009), a phenotype similar to what is seen in *dpias* mutant animals (**Figure 18**). This suggested a novel anti-inflammatory role for Gcm (JACQUES *et al.* 2009). However, at that

time, the only available tool to address the role of Gcm in inflammation was by using a *gcm*^{DN} mutant construct as no efficient *gcmRNAi* line was available. Fortunately, the availability of efficient tools now prompted me to investigate the role of Gcm in inflammation and elucidate the molecular landscape controlling inflammatory responses.

Figure 18: *gcm* or *dpias* mutations induce melanotic tumors. (**A**) Melanotic tumors in *dpias* mutant 3rd instar larva. (**B**) Melanotic tumors in 3rd instar larva upon conditional expression of *gcm*^{DN} using Srp driver. To overcome the embryonic lethality induced by *gcm* mutation, *gcm*^{DN} was expressed at the larval stage. Modified from (JACQUES *et al.* 2009).

Gcm DamID screen

The fact that Gcm acts as a cofactor for dPIAS, the inhibitor of JAK/STAT cascade, prompted us to further investigate the presence of other Gcm-JAK/STAT interactions. To that purpose and due to the absence of an efficient antibody against Gcm (POPKOVA *et al.* 2012; LANEVE *et al.* 2013), the DNA adenine methyltransferase identification (DamID) approach was used to determine the Gcm binding sites in the *Drosophila* genome (CATTENOZ *et al.* 2016b). DamID is an antibody independent method allowing the identification of loci bound by transcription factors (VAN STEENSEL AND HENIKOFF 2000; VAN STEENSEL *et al.* 2001). The principle of this technique is based on fusing the bacterial Dam methylase with the protein of interest, leading to genomic adenine methylation near the protein's binding sites. By performing this approach, a total of 1031 Gcm direct targets were identified. Many of these targets include genes that had not been associated with Gcm as well as Notch, the Hh, the JAK/STAT and the

Toll cascades (CATTENOZ *et al.* 2016b), which are all involved in regulating hematopoiesis in *Drosophila* (MANDAL *et al.* 2007; OWUSU-ANSAH AND BANERJEE 2009; SINENKO *et al.* 2010; VALANNE *et al.* 2011; HOMBRIA AND SOTILLOS 2013; WANG *et al.* 2014b).

The Gcm DamID screen analysis identified direct interactions with key inhibitors of the JAK/STAT pathway (*Ptp61F*, *Socs36E*, *Socs44A*, *ken* and *Su(var)3-9*), and of the Toll cascade (*cactus*) (CATTENOZ *et al.* 2016b). This suggests that the embryonic hematopoietic transcription factor Gcm may play inhibitory roles onto the JAK/STAT and Toll inflammatory cascades involved in inducing an immune response. Moreover, this aspect might further elucidate the link between Gcm and inflammation and whether distinct hematopoietic waves communicate.

Based on this, during my PhD thesis I proposed to decipher the impact of Gcm on the innate immune response and inflammation, by focusing on the JAK/STAT and Toll signaling cascades *in vivo* using the simple *Drosophila* model. The aims that I have addressed are the following:

- To define the impact and mode of action of the embryonic specific hemocyte transcription factor Gcm, on the JAK/STAT and the Toll inflammatory pathways and on the formation of melanotic tumors.
- To characterize the communication of distinct hematopoietic waves during the inflammatory response, by defining the role of Gcm in the signaling mechanism from the embryonic wave to the larval definitive wave.
- To characterize the molecular landscape of hemocytes in genetic backgrounds that lead to melanotic tumors and to an inflammatory state.
- To explore a possible conserved role of Gcm genes in evolution, by focusing on mGcm2 - JAK/STAT interaction.

Chapter IV

The *Drosophila* toolbox

This section introduces the *Drosophila* life cycle and the *Gal4-UAS* system, where the latter represents the main genetic tool I used to perform crosses, and to manipulate gene expression (gain-of-function or (GOF) and knockdown or (KD)).

***Drosophila* life cycle**

The *Drosophila* life cycle takes around 10-12 days at 25°C from egg laying to the adult stage. After fertilization, the female lays embryos on culture media containing yeast, apple juice and necessary nutrients. The embryonic stage remains for approximately 24hrs, followed by egg hatching into larva. The larval phase lasts for 4 days and includes three consecutive larval stages. To undergo metamorphosis, the larva chooses a dry place for pupation, and the animal stays as pupae for approximately 4 days. During that time, the adult becomes visible through the pupal case until it hatches (**Figure 19**).

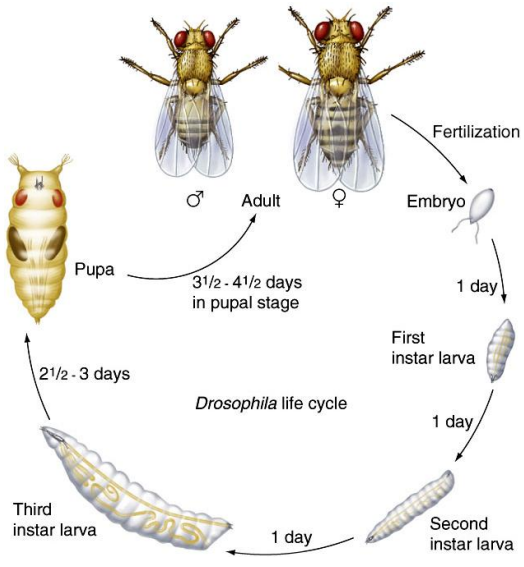

Figure 19: The *Drosophila* life cycle. After fertilization, the *Drosophila* female lays its embryos. The egg hatches into a larva after 24hrs. The larval stage lasts for 4 days before pupation, which in turn lasts for 4 additional days, before giving rise to an adult *Drosophila*.

***Gal4-UAS* system**

The *Gal4-UAS* system is a powerful tool that provides targeted expression/silencing of any gene of interest in a wide variety of tissues and in cell specific patterns (FISCHER *et al.* 1988; BRAND AND PERRIMON 1993). It can be used to investigate regulatory interactions during development. The Gal4 protein can induce the transcription of target genes in *Drosophila*, mammals and plants that have been fused to Gal4 binding sites (FISCHER *et al.* 1988; WEBSTER *et al.* 1988; ORNITZ *et al.* 1991; BRAND AND PERRIMON 1993).

To induce/silence the expression of a target gene (gene X), the yeast transcriptional activator Gal4 protein binds to its target Upstream Activating Sequence (UAS) and activates transcription (BRAND AND PERRIMON 1993). This allows the expression of (gene X) in a tissue specific manner, upon crossing "*UAS-gene-X-RNAi*" or "*UAS-geneX*" lines to transgenic flies expressing the Gal4 protein in a cell-specific manner (**Figure 20**).

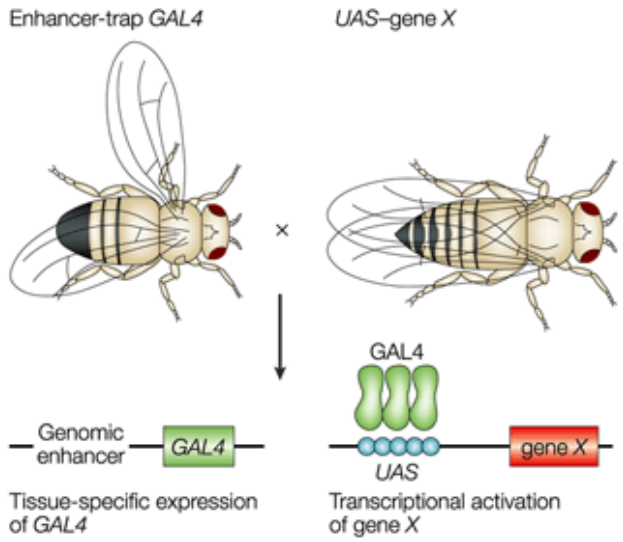

Figure 20: Tissue specific expression using the *Gal4-UAS* system. Crossing a specific *Gal4* driver line with a *UAS* reporter line allows the expression of (gene X) in a tissue specific manner. The Gal4 protein binds the UAS sequence and induces the transcription of (gene X). Modified from (ST JOHNSTON 2002).

2. MATERIALS AND METHODS

Materials and Methods

Fly strains and genetics

The *Drosophila Gal4-UAS* system was used to produce fly stocks and induce conditional expression of target genes, where the Gal4 protein binds the UAS sequence and activates transcription (see above) (BRAND AND PERRIMON 1993). All flies were raised on standard media at 25°C. The following list of fly stocks was used during my PhD.

Genotypes	Abbreviation	Origin	Remarks
w^{1118}	WT	Bloomington #5905	
hop^{Tum-l}/*FM7c*	hop^{Tum-l}	Bloomington #8492	point mutation that constitutively activates the JAK/STAT pathway
UAS-hop^{Tum-l}*/CyO,twilacZ*	*UAS-*hop^{Tum-l}	(HARRISON *et al.* 1995)	reporter line for hop^{Tum-l} over-expression
$Toll^{10b}$*/Ser,TM3*	$Toll^{10b}$	Bloomington #30914	*GOF* point mutation that constitutively activates the *Toll* receptor gene
gcmGal4,UAS-mCD8GFP/CyO,Tb	*gcm>GFP*	(SOUSTELLE AND GIANGRANDE 2007)	driver specific to embryonic hemocytes and glia, *gcm* hypomorphic mutation
UAS-gcmRNAi	*gcm KD*	Bloomington #31519	dsRNA line for *gcm* down-regulation
UAS-gcmF18A	*gcm GOF*	(BERNARDONI *et al.* 1997)	reporter line for *gcm* over-expression
gcm^{26}*/CyOactinGFP*	gcm^{26}	(VINCENT *et al.* 1996)	null *gcm* mutation
Df(2L)132/CyOactinGFP	*Df132*	(KAMMERER AND GIANGRANDE 2001)	large deletion including the *gcm* and *gcm2*

			loci
upd2$^{\Delta}$		Bloomington #55727	4.7 kb deletion
upd3$^{\Delta}$		Bloomington #55728	imprecise excision
UAS-upd2RNAi	*upd2 KD*	Bloomington #33988	dsRNA line for *upd2* down-regulation
UAS-upd3RNAi	*upd3 KD*	Bloomington #32859	dsRNA line for *upd3* down-regulation
UAS-upd2/CyO	*upd2 GOF*	(JIANG *et al.* 2009)	reporter line for *upd2* over-expression
UAS-upd3/CyO	*upd3 GOF*	(JIANG *et al.* 2009)	reporter line for *upd3* over-expression
UAS-Ptp61FRNAi	*Ptp61F KD*	Bloomington #32426	dsRNA reporter line for *Ptp61F* down-regulation
UAS-Socs36ERNAi	*Socs36E KD*	Bloomington #35036	dsRNA reporter line for *Socs36E* down-regulation
UAS-Socs44ARNAi	*Socs44A KD*	Bloomington #42830	dsRNA reporter line for *Socs44A* down-regulation
UAS-Ptp61Fa/CyO	*Ptp61Fa GOF* (cytoplasmic)	(MULLER *et al.* 2005)	reporter line to over-express the cytoplasmic splicing isoforms
UAS-Ptp61Fc/TM3	*Ptp61Fc GOF* (nuclear)	(MULLER *et al.* 2005)	reporter line to over-express the nuclear splicing isoforms
gcmGal4,UAS-mCD8GFP,repoGal80/CyO	*repoGal80, gcm>*	(CATTENOZ *et al.* 2016b)	*gcm* driver not expressed in glia, hypomorphic mutation
snGal4		(ZANET *et al.* 2012)	*singed* driver, specific to embryonic hemocytes
srp(hemo)Gal4		(BRUCKNER *et al.* 2004)	*serpent* driver specific to embryonic hemocytes

DotGal4		Bloomington #67608	*Dorothy* driver specifically expressed in embryonic and larval lymph gland
lzGal4,UAS-mCD8GFP	*lz>GFP*	Bloomington #6314	*lozenge* driver expressed in crystal cells
10xStat92E-GFP		Bloomington #26198	reporter line for STAT activity, 10 Stat92E binding sites driving GFP expression
UAS-FLP;;Ubi-p63E(FRT.STOP)Stinger	*Gtrace*	Bloomington #28282	This line allows the analysis of lineage-traced expression of Gal4 drivers

*Bloomington: Bloomington Drosophila Stock Center at Indiana University (BDSC).

Penetrance and expressivity of melanotic tumors

Tumor penetrance was determined by assessing the percentage of 3rd instar larvae carrying one or more tumors. To assess the expressivity of the phenotype, tumors were classified into three categories according to their size: Small (S), Medium (M) and Large (L) (MULLER *et al.* 2005). A tumor was considered as large when the melanotic spot covered ½ the distance between the borders of a segment. We considered a tumor as medium tumor when the melanotic mass covered ¼ the distance between the borders of a segment and as small when it is less than ¼ the distance between the borders of a segment. The expressivity of the melanotic tumor phenotype was then determined by calculating the percentage of small, medium and large tumors counted in each genotype. The p-values were estimated using the chi-squared test for frequency comparisons between two populations (see also section on statistics).

Hemocyte counting

Ten 3rd instar larvae were washed in Ringer's solution (pH 7.3-7.4) containing 0.12g/L of CaCl2, 0.105g/L KCl, and 2.25g/L NaCl, then dried, and bled in a 96 well U-shaped microtiter plate containing 50µL of Schneider medium complemented with 10% Fetal Calf Serum (FCS), 0.5% penicillin, 0.5% streptomycin (PS), and few crystals of N-phenylthiourea ≥98% (PTU) (Sigma-Aldrich (P7629)) to prevent hemocyte melanization (LERNER AND FITZPATRICK 1950). For circulating hemocyte collection, the hemolymph was gently allowed to exit, and the total volume was transferred onto a haemocytometer, where the total number of cells were counted, multiplied by the original volume (50µL), and the average number of hemocytes per larva was calculated as described in (KACSOH AND SCHLENKE 2012). For sessile hemocyte collection, the hemolymph containing the circulating hemocytes was transferred to a first well, while sessile hemocytes were scraped and/or jabbed off the carcass in a second well as described in (PETRAKI *et al.* 2015) and counted as above. Each counting was carried out at least in triplicates. The p-values were estimated after variance analysis using bilateral student test (see statistics section).

Hemocyte immunolabeling

Ten 3rd instar larvae were treated as stated above and bled in a 96 well U-shaped microtiter plate containing 200µL of Schneider medium. Circulating and sessile hemocytes were collected as indicated above and transferred onto a slide using the Cyto-Tek® 4325 Centrifuge (Miles Scientific). Samples were then marked by Dako Pen (Dako (Code S2002)) to introduce a hydrophobic medium around the transferred material, fixed for 10min in 4% paraformaldehyde/PBS at room temperature (RT), incubated with blocking reagent (Roche) for 1hr at RT, incubated overnight at 4°C with primary antibodies diluted in blocking reagent,

washed three times for 10min with PTX (PBS, 0.3% triton-x100), incubated for 2hrs with secondary antibodies, washed two times for 10min with PTX, incubated for 20min with DAPI to label nuclei (Sigma-Aldrich) (diluted to 10^{-3} g/L in blocking reagent), and then mounted in Vectashield® (Vector Laboratories). The slides were analyzed by confocal microscopy (see section below for confocal imaging). The following combination of primary antibodies was used to determine the fraction of lamellocytes: rabbit anti-Serpent (1/1000) (Trébuchet, unpublished results) was used to immunolabel hemocytes. Serpent is expressed in all hemocyte precursors and is required for the development of plasmatocytes and crystal cells (LEBESTKY *et al.* 2003). Mouse anti-L4 (1/30) was kindly provided by I. Ando, L4 is an early lamellocyte marker expressed after immune stimulation (HONTI *et al.* 2010). The fraction of lamellocytes was determined by counting the number of L4/DAPI positive cells out of the total population of hemocytes present in six confocal fields of vision at 40X magnification and based on Z-series projections. The following combination of primary antibodies was used to determine the fraction of dividing blood cells: rabbit anti-PH3 (1/1000) (Upstate biotechnology #06-570), to assess the mitotic activity, and mouse anti-Hemese (1/30) (kindly provided by I. Ando), which recognizes a glycosylated transmembrane protein belonging to the sialophorin protein family and expressed in all larval hemocytes (KURUCZ *et al.* 2003). The fraction of dividing cells was determined by counting the number of PH3/Hemese/DAPI positive cells out of the total population of hemocytes, as above. The following combination of primary antibodies was used to determine the fraction of crystal cells: rabbit anti-Serpent (1/1000) and chicken anti-GFP (1/500) (abcam #13970), directed against the membrane GFP signal in *lzGal4,UAS-mCD8GFP* driver expressed in crystal cells. The fraction of crystal cells was determined by counting the number of GFP/Srp/DAPI positive cells out of the total population of hemocytes, as above. Secondary

antibodies were: donkey anti-rabbit coupled with Cy3 (1/600) (Jackson #711-165-152), donkey anti-mouse coupled with Cy3 (1/600) (Jackson #715-165-151), goat anti-mouse coupled with FITC (1/400) (Jackson #115-095-166), goat anti-mouse coupled with Alexa Fluor 647 (1/400) (Jackson #115-175-100) and goat anti-rabbit coupled with Alexa Fluor 647 (1/400) (Jackson #711-175-144). Each immunolabeling was carried out on three independent trials. The p-values were estimated after variance analysis using bilateral student test (see below).

Lymph gland immunolabeling

Lymph glands from 3rd instar wandering larvae (6hrs before pupation) were dissected in Ringer's solution (pH 7.3-7.4), fixed for 10min in 4% paraformaldehyde/PBS at RT, incubated with blocking reagent for 1hr at RT, incubated overnight at 4°C with primary antibodies, washed three times for 10min with PTX, incubated for 2hrs with secondary antibodies, washed two times for 10min with PTX, incubated for 20min with DAPI and then mounted on slides in Vectashield®. The slides were analyzed by confocal microscopy (see below). The primary antibody was the mouse anti-L4 (1/30). The secondary antibody was the goat anti-mouse coupled with FITC (1/400) (Jackson #115-095-166). The percentage of precociously histolysed and lamellocyte expressing lymph glands was assessed. Semi-quantitative analysis on L4 expressing lymph glands was performed by measuring GFP intensity using Fiji (SCHINDELIN *et al.* 2012); the same correction was applied to all conditions. Note that in genotypes carrying the $hop^{Tum\text{-}l}$ and $Toll^{10b}$ systemic mutations most lymph glands lose their integrity and display only part of the primary and/or secondary lobes because the tissue undergoes precocious histolysis.

Embryo immunolabeling

Drosophila embryos from overnight egg laying at 25°C on apple agar plates were collected, treated and immunolabeled as described in (VINCENT *et al.* 1996). They were dechorionated in bleach, rinsed in water then fixed in 50% heptane/50% PEM-formaldehyde for 25min. Next, they were devitellinized in methanol and heptane for 1min followed by treatment with PTX and incubation in blocking reagent for 1hr at RT. Then, embryos were incubated overnight at 4°C with primary antibodies, washed three times for 10min with PTX, incubated for 2hrs with secondary antibodies, washed two times for 10min with PTX, incubated for 20min with DAPI and then mounted on slides in Vectashield®. The slides were analyzed by confocal microscopy (see section below). The following combination of primary antibodies was used to label crystal cells: rabbit anti-PPO1 (1/100) was kindly provided by WJ. Lee. PPOs are essential enzymes in the melanization process, where PPO1 is crystal cell specific marker (NAM *et al.* 2012; BINGGELI *et al.* 2014). Chicken anti-GFP (1/500) (abcam #13970) was used to select for right genotype embryos based on *CyOactinGFP* expression. Rabbit anti-RFP (1/500) (abcam #62341) was directed against the RFP signal driven by *lzGal4* driver expressed in crystal cells. Secondary antibodies used were: donkey anti-rabbit coupled with Cy3 (1/600) (Jackson #711-165-152) and donkey anti-chicken coupled with FITC (1/400) (Jackson #703-095-155).

Transfection and qPCR in *Drosophila* S2 cells

Six million *Drosophila* S2 cells were plated per well in a 6-well plate with 1.5mL of Schneider medium + 10% FCS + 0.5% PS. Transfections were carried out 12hrs after plating using the Effectene Transfection Reagent (Qiagen) as described in (CATTENOZ *et al.* 2016b).

These transfection assays were used to assess the transactivation potential of a) Gcm and b) $hop^{Tum\text{-}1}$.

a) To determine the role of Gcm in inducing *Ptp61F*, *Socs36E*, *Socs44A*, *upd2*, *upd3* and *cactus* expression, 2µg of *pPac-gcm* expression vector (MILLER et al. 1998) was transfected together with 1µg of *4.3kb repo-GFP* (*repoGFP)* (LANEVE et al. 2013): Gcm induces the expression of its target gene *repo* through the regulatory sequences contained in this fragment, hence the co-transfection of the two plasmids leads to the expression of GFP, allowing us to recognize and sort the transfected cells (LANEVE *et al.* 2013). Co-transfection of 2µg of *pPac-gal4* driver plasmid and 1µg of *pUAS-GFP* reporter plasmid was performed as a negative control.

b) To determine the role of $hop^{Tum\text{-}l}$ in inducing *upd2* and *upd3* expression, 0.5µg of *pPac-gal4* plasmid, 0.5µg of *pUAS-GFP* and 0.5µg of *pUAS-*$hop^{Tum\text{-}l}$ reporters were co-transfected (HARRISON *et al.* 1995). Co-transfection of 0.5µg of *pPac-gal4* driver plasmid and 0.5µg of *pUAS-GFP*, and 0.5µg of *pUAS-Empty* (empty backbone vector) was performed as a negative control.

For the transfection assays, each combination of plasmids was mixed in 90µL of EC buffer and 8µL of enhancer per µg of plasmid followed by 5min incubation at RT. 25µL of Effectene was then added and the mix was incubated at RT for 20min. Then, 500µL of Schneider medium + 10% FCS + 0.5% PS was added to the mix followed by spreading it on the cells. Plates were then incubated at 25°C for 48hrs followed by sorting on a BD FACSAria, according to GFP or RFP expression to obtain more than 80% of transfected cells in the sample (CATTENOZ *et al.* 2016b). RNA was then extracted using TRI reagent (Sigma-Aldrich), 1µg was treated by DNAse1 (RNAse-free) (Thermo Fisher Scientific) and reverse transcribed with Superscript II (Invitrogen). Quantitative PCR (qPCR) assays were performed on a lightcycler LC480 (Roche)

with SYBR master (Roche) on the equivalent of 5ng of reverse transcribed RNA with the primer pairs targeting *Ptp61F*, *Socs36E*, *Socs44A*, *upd2*, *upd3* and *cactus* listed below. Each PCR was carried out in triplicates on at least three independent replicates. The quantity of each transcript was normalized to the levels of transcripts of two different housekeeping genes, *Glyceraldehyde-3-phosphate-dehydrogenase-1* (*Gapdh1*) and *Actin-5c* (*Act5c*). The p-values were estimated after comparing control to transfected cells using bilateral student test (see below).

Assessment of *gcm* RNAi's efficiency in *Drosophila* S2 cells

Six million S2 cells were transfected as described above with 0.25µg *pPac-gal4* driver, 0.25µg of *pUAS-gcm* expression vector, 0.25µg of *4.3kb repo-GFP* (*repoGFP*) (LANEVE *et al.* 2013), 0.25µg of *pUAS-RFP* reporter and 0.25µg *of pUAS-gcmRNAi* vector (Vienna Drosophila Resource Center (VDRC) #dna1452, used to build the *UAS-gcmRNAi* strain Bloomington #31519). Gcm induces the expression of its target gene *repo* through the regulatory sequences contained in this fragment, hence the co-transfection of the two plasmids leads to the expression of GFP, allowing us to recognize and sort the transfected cells. Gal4 induces the expression of *gcm*, *RFP* and *gcmRNAi*. *pUAS-gcm* vector contains the target sequences of *UAS-gcmRNAi* construct. The controls were S2 cells transfected with the same set of plasmids except for *pUAS-gcm* or *pUAS-gcmRNAi* that were replaced by *pUAS-Empty* vector. The levels of GFP and RFP were analyzed 48hrs after transfection using FACSCalibur. The GFP levels were measured in RFP positive cells. The p-values were estimated after comparing control to transfected cells using bilateral student test (see below).

Transfection and qPCR in leukemia K562 cells

The K562 human immortalized chronic myelogenous leukemia cell line, which harbors the Philadelphia translocation and displays a constitutively active JAK/STAT cascade (DE GROOT *et al.* 1999; LIN *et al.* 2000) was used to assess the impact of mGcm2 on JAK/STAT over-activation. Two million K562 cells were plated per well in a 6-well plate with 1.5mL of Roswell Park Memorial Institute medium (RPM1) complemented with 10% FCS, 40µg/mL Gentamicin (Gen), 2mM Glutamine (Glu). Transfection was carried out 12hrs after plating using the Lipofectamine® 2000 Transfection Reagent (Thermo Fisher Scientific). To determine the impact of mGcm2 on *PTPN2*, *SOCS1*, *SOCS3*, *BCL2* and *BCL2L1* expression, 2.5µg of *pCIG* plasmid expressing mouse *Gcm2* (*pCIG-mGcm2*) (SOUSTELLE *et al.* 2007) were used in transfection assays; 2.5µg of *pCIG* plasmid were transfected in negative control wells (*pCIG-Empty*). *pCIG* is a mammalian expression vector harboring a CMV promoter and a nuclear GFP. Each plasmid was mixed with 250µL of RPMI medium + 10% FCS + 40µg/mL Gen + 2mM Glu and incubated at RT for 15min. In parallel, 14µL of Lipofectamine were mixed with 250µL of RPMI medium + 10% FCS + 40µg/mL (Gen) + 2mM (Glu) and incubated at RT for 15min as well. Then, the Lipofectamine/RPMI medium was mixed with the plasmid/RPMI medium and incubated at RT for 15min. Next, the total volume (500µL) was spread on the cells which were in turn incubated in a 37°C (5% CO_2) incubator. Cells were then sorted on a BD FACSAria 48hrs after transfection, according to GFP expression. RNA was then extracted and Quantitative PCR (qPCR) assays were performed on a lightcycler LC480 as stated above with the primer pairs targeting *PTPN2*, *SOCS1*, *SOCS3*, *BCL2* and *BCL2L1* listed below. Each PCR was carried out in triplicates on at least three independent replicates. The quantity of each transcript was normalized to the quantity of two different housekeeping genes *Glyceraldehyde-3-phosphate-*

dehydrogenase (*GAPDH*) and *Actin-Beta* (*ACTNB*). The p-values were estimated after comparing control to transfected cells using bilateral student test (see below).

Apoptotic assay in K562 cells

K562 leukemic cells are immortalized, proliferating cells that harbor the Philadelphia translocation and display a constitutively active JAK/STAT cascade (DE GROOT *et al.* 1999; LIN *et al.* 2000). Pharmacological JAK2 inhibitor AG490 is known to induce apoptosis of cancerous cells (DU *et al.* 2012). To that purpose, we assessed the impact of mGcm2 on the profile of apoptosis upon transfection. We used the Amaxa® Cell Line Nucleofector® Kit V (Lonza) to obtain approximately 80% of transfected cells in the sample. One million K562 cells were counted and centrifuged at 200xg for 10min at RT. The supernatant was discarded and the pellet was resuspended with 100µL of RT Nucleofector® solution. 2.5µg of (*pCIG-Empty*) or 2.5µg of (*pCIG-mGcm2*) were mixed with the resuspended pellet. Then, the cell/DNA suspension was transferred into a certified cuvette and electroporation was performed relying on the T-16 program for Nucleofector® I Device (Lonza). Next, 500µL of RT RPMI medium + 10% FCS + 40µg/mL Gen + 2mM Glu was immediately added to the cuvette and gently spread into a 6-well plate containing 3mL of RT RPMI medium + 10% FCS + 40µg/mL Gen + 2mM Glu. Plates were then incubated at 37°C (5% CO_2). Apoptosis of was measured 72hrs after transfection (HE *et al.* 2003). 500µL of cell suspension were analyzed using the BD FACSCalibur. K562 cell survival and apoptosis were determined by calculating the ratio of GFP+/GFP- cells and GFP+/TB+ cells, after adding 200µL of 0.4% Trypan blue (TB) (Sigma-Aldrich) as a quencher (SRIVASTAVA *et al.* 2011). The quantification was carried out in three independent trials. The p-

values were estimated after comparing control to transfected cells using bilateral student test (see below).

Larval hemocyte RNA extraction and qPCR

Thirty 3rd instar larvae were bled in a 96 well U-shaped microtiter plate containing 200µL of Schneider medium to collect circulating hemocytes as stated above. Cells were centrifuged at 3000rpm for 10min at 4°C. RNA was then extracted using TRI reagent and Quantitative PCR (qPCR) assays were performed on a lightcycler LC480 as stated above with the primer pairs listed below targeting plasmatocytes markers (STOFANKO *et al.* 2010): *crq*, *Hml*, *lectin-24A*, *eater*, *He* and *NimC1*; lamellocyte markers: *Filamin-240 (cher)*, *α-PS4 (ItgaPS4)*, *α-PS5 (ItgaPS5)*, *mys*, *βInt-v (Itgbn)*, *Tep1*, *Tep4* and *PPO3*; crystal cell markers: *lz*, *hnt (peb)* and *PPO1*; proinflammatory cytokines: *upd2* and *upd3*. Each PCR was carried out in triplicates on at least three independent replicates. The p-values were estimated after comparing control to transfected cells using bilateral student test (see below).

Crystal cell quantification on larval cuticle

Six 3rd instar larvae were washed in 1X PBS and heated at 70°C for 10min in 500µL of 1X PBS. This procedure leads to the activation of PPOs within the crystal cells and as a result, these cells appear as black superficial spots on the larval cuticle (RIZKI *et al.* 1980; BINGGELI *et al.* 2014). 3rd instar larval lateral view images were taken under the fluorescent macroscope (Leica, Z16 APO) to cover parts of the dorsal and ventral sides, and superficial crystal cells were counted as described in (BRETSCHER *et al.* 2015). The p-values were estimated after variance analysis using bilateral student test (see below).

JAK/STAT reporter activity in larval somatic muscles

Activation of the JAK/STAT pathway was observed in the somatic muscles using the *10xStat92E-GFP* reporter as indicated in (YANG *et al.* 2015). The larvae were frozen and mounted between two slides in water. The images of the larvae were taken at the fluorescent macroscope (Leica, Z16 APO) using 10X magnification and 500ms of exposure time. The contrast and luminosity of each image were adjusted using Fiji (SCHINDELIN *et al.* 2012); the same correction was applied to all conditions.

LPS treatment in *Drosophila* S2 cells

Six million *Drosophila* S2 cells were plated per well in a 6-well plate with 1.5mL of Schneider medium + 10% FCS + 0.5% PS. Transfections were carried out 12hrs after plating using the Effectene Transfection Reagent (Qiagen) as described in (CATTENOZ *et al.* 2016b). To determine the impact of LPS on *gcm* expression, 0.5µg *p6kb-gcm-gal4* driver plasmid (FLICI *et al.* 2014), 0.5µg *pPac-lacZ* and 0.5µg *pPac-gcm* expression vectors (MILLER et al. 1998) were co-transfected. The *p6kb-gcm-gal4* plasmid harbors the 6kb *gcm* promoter sequence fused to *Gal4* gene (*gcm* reporter) (FLICI *et al.* 2014) that is bound by Gcm and allows for Gcm dependent gene expression. Co-transfection of 0.5µg *p6kb-gcm-gal4* driver plasmid, 0.5µg *pPac-lacZ*, and 0.5µg *pPac-Empty* was performed as a negative control.

Each combination of plasmids was mixed in 90µL of EC buffer and 8µL of enhancer per µg of plasmid followed by 5min incubation at RT. 25µL of Effectene was then added and the mix was incubated at RT for 20min. Then, 500µL of Schneider medium + 10% FCS + 0.5% PS was added to the mix followed by spreading it on the cells. Plates were then incubated at 25°C for 24hrs. Next, 10µg/mL of LPS from *Escherichia coli* (InvivoGen, O111:B4) was added onto the

wells for 3hrs as indicated in (SILVERMAN *et al.* 2000; PARK *et al.* 2004). LPS contains bacterial peptidoglycan that activates several cascades, such as the IMD, JNK and Toll pathways (SLUSS *et al.* 1996; LEULIER *et al.* 2003). RNA was then extracted using TRI reagent and treated by DNAse1 (RNAse-free) and reverse transcribed with Superscript II. Quantitative PCR (qPCR) assays were performed on a lightcycler LC480 with SYBR master on the equivalent of 5ng of reverse transcribed RNA with the primer pairs targeting *AttacinB*, *Gal4* and *lacZ* genes listed below. *AttacinB* is an AMP encoding gene induced upon LPS treatment and was used as readout for LPS efficiency (PARK *et al.* 2004). Each PCR was carried out in triplicates on at least three independent replicates. The quantity of *AttacinB* was normalized to the levels of transcripts of two different housekeeping genes, *Glyceraldehyde-3-phosphate-dehydrogenase-1* (*Gapdh1*) and *Actin-5c* (*Act5c*). *gcm* reporter expression levels (*6kb-gcm-gal4*) were determined by normalizing *Gal4* expression levels to *lacZ* (*Gal4*/*lacZ*). The p-values were estimated after comparing control to transfected cells using bilateral student test (see below).

Embryo RNA extraction and qPCR

Drosophila Toll^{10b} flies were crossed with WT flies and *Toll*^{10b}/+ embryos of stages (5-7) were collected from apple agar plates and treated as described in (VINCENT *et al.* 1996). Embryos were dechorionated in bleach, rinsed in water and grinded with a pestle in TRI reagent. RNA was extracted and Quantitative PCR (qPCR) assays were performed on a lightcycler LC480 as stated above with primer pairs targeting *gcm* listed below. Each PCR was carried out in triplicates on at least three independent replicates. The quantity of each transcript was normalized to the levels of transcripts of two different housekeeping genes, *Glyceraldehyde-3-phosphate-dehydrogenase-1*

(*Gapdh1*) and *Actin-5c* (*Act5c*). The p-values were estimated after comparing control to transfected cells using bilateral student test (see below).

Transcriptome analysis

One hundred 3rd instar larvae were bled in a 96 well U-shaped microtiter plate containing 200µL of Schneider medium to collect circulating hemocytes from double mutants gcm^{26}/+;$Toll^{10b}$/+ and single mutants (gcm^{26}/+) ($Toll^{10b}$/+) as stated above. This was done in triplicates. Then, cells were centrifuged at 3000rpm for 10min at 4°C. RNA was then extracted using TRI reagent and Quantitative PCR (qPCR) assays were performed on a lightcycler LC480 to assess enrichment of hemocytes with primer pairs targeting *serpent* listed below. RNA was then analyzed by high throughput sequencing at IGBMC deep sequencing platform, to characterize the molecular landscape of hemocytes in different mutant backgrounds. Gene ontology (Go-term) analysis was performed using the Functional Annotation Bioinformatics Microarray Analysis (DAVID) software (https://david.ncifcrf.gov). Heatmaps were prepared using "R Software - Version 3.2.1".

Wasp survival and encapsulation assays

Wasp parasitization by *Leptopilina boulardi* is commonly used to study the immune response of *Drosophila* larvae (SMALL *et al.* 2012; VANHA-AHO *et al.* 2015; KARI *et al.* 2016). The wasp survival and encapsulation assays were conducted as described in (VANHA-AHO *et al.* 2015; KARI *et al.* 2016) with some modifications.

For the wasp survival, 100 1st instar *Drosophila* larvae (24hrs after egg laying) of the indicated genotypes were transferred into a fresh vial at 25°C. At 2nd instar stage (48hrs after egg laying),

20 couples of *L. boulardi* were added into the vial for infestation for 2hrs, then removed. Following this, the number of wasps hatching from each vial was counted to estimate the percentage of lethality (number of wasps/number of *Drosophila* larvae), which allows us to determine whether the larvae mounted an effective immune response against the wasp egg. This is represented by the number of wasp adults hatching.

For the encapsulation assay, *Drosophila* of the indicated genotypes were allowed to lay eggs for 12hrs at 25°C. The vials containing the embryos were then transferred to 29°C until 2nd instar stage (48hrs). The *Drosophila* larvae were then exposed to 10 couples of *L. boulardi* for 2hrs at 25°C and after parasitization the vials were incubated at 29°C until 3rd instar stage. Wandering larvae were dissected to assess the level of melanization of the wasp larvae: total encapsulation (dead larvae completely melanized), partial encapsulation (living larvae, with some melanization), no encapsulation (living larvae, no melanization). Only *Drosophila* larvae containing a single wasp larva were analyzed.

DamID peaks

The DNA adenine methyltransferase identification (DamID) is an antibody independent method allowing the identification of loci bound by transcription factors (VAN STEENSEL AND HENIKOFF 2000; VAN STEENSEL *et al.* 2001). Using this approach, Gcm binding sites in the *Drosophila* genome were recently determined (CATTENOZ *et al.* 2016b). The peaks indicating Gcm binding onto the *Ptp61F*, *Socs36E*, *Socs44A* and *cactus* loci are represented using the University of California Santa Cruz (UCSC) Genome Browser (https://genome.ucsc.edu).

Statistical analysis

The chi-squared test for frequency comparisons between two populations was used to estimate the p-values between percentages of tumors in 3rd instar larvae and the expressivity of melanotic tumors in various genotypes tested, where bilateral student test is not applicable. Variance analysis using bilateral student tests for unpaired samples was used to estimate the p-values in hemocyte counting, hemocyte immunolabeling and qPCR assays; in each case, at least three independent trials were performed. In all analyses, "ns" stands for not significant, for p-value >0.05; "*" for p-value < 0.05; "**" for p-value < 0.01; "***" for p-value < 0.001.

Confocal imaging

Leica SP5 inverted-based microscope equipped with 20, 40 and 63X objectives was used to obtain confocal images. GFP/FITC was excited at 488nm; the emission filters 498-551 were used to collect the signal. Cy3 was excited at 568nm; emission filters 648-701 were used to collect the signal, and Cy5 was excited at 633nm; emission signal was collected at 729-800nm. A step size between 0.2 and 2µm was used to collect the Z-series of images, which were then treated with Fiji (SCHINDELIN *et al.* 2012) to obtain fluorescent images with maximum Z-projections. In all images the intensity of the signals was set to the same threshold in order to compare the different genotypes.

List of primers

Species	Gene	Forward	Reverse
Drosophila	*Gapdh1*	CCCAATGTCTCCGTTGTGGA	TGGGTGTCGCTGAAGAAGTC
Drosophila	*Act5c*	GCCAGCAGTCGTCTAATCCA	GACCATCACACCCTGGTGAC
Drosophila	*Ptp61F*	GAAACTGCCCCACGTCAAAC	CTTAAGGAATGCGTTCGGCG
Drosophila	*Socs36E*	GTGTCCAACACCAGCTACGA	GAGACCCGTATGTTGACCCC

Drosophila	*Socs44A*	CACTCCAAAATGAGCCACGG	GAGTGGAACCAGCCCTTCTT
Drosophila	*cactus*	AAAGCGGTCAGTTCCCTGAG	AGTTGGCCAGATCCTCGTTG
Drosophila	*upd2*	ACCCTGGAGTACGGCAATCT	CTGATCCTTGCGGAACTTGT
Drosophila	*upd3*	CCACAGTGAGCACCAAGACT	CAGGTCCCAGTGCAACTTGA
Drosophila	*crq*	GCGATCATCGAAGCGGGAAG	GCATTAGCTTCTGATGGCTC
Drosophila	*Hml*	CCGATGATGACGACGAGGAT	GATGTTGAAGCTAATGTGGC
Drosophila	*lectin-24A*	CAATGCCTACAGCCAGGATT	AGGCTAGGTGACCTCCCATT
Drosophila	*eater*	CGTCTGTCAATGCCTGACGG	AGACACCTTCCAGCTTCGTG
Drosophila	*He*	GGCGGAGCAGTTCACACTAA	AGTTGGAGATGGACGGTTGC
Drosophila	*NimC1*	TCCAATGCCTTTGGGTGTGT	GGTGCGGTATTTTGTCTGCC
Drosophila	*Filamin-240 (cher)*	CGGATCAGTACGAGGAGAAC	GATCGATGGTCTTCAGGTGC
Drosophila	*α-PS4 (ItgaPS4)*	ACACCGACTCCTTGACCATC	TGAGCACGTTGGTTAGCTTG
Drosophila	*α-PS5 (ItgaPS5)*	ACTTCGGTTACTCCGTGGTG	GCACCCACGTCATAGGAATC
Drosophila	*Mys*	GATCACGGTACATGCGAGTG	GTACCATGACCGGAGCAGAT
Drosophila	*βInt-v (Itgbn)*	CTCGCCGGCAACTACTTAAC	GGACAGCCTGATCACTGGTT
Drosophila	*Tep1*	CTGAAGTCTCAGTCAGCCTGACTGGACCTT	CGTAATCGCCTTCTGTTAGCTTCGGAATGT
Drosophila	*Tep4*	GTCAATGTCCATCTGGACTC	GAAGTCCTTGAGATCCATGG
Drosophila	*PPO3*	AGAGCGTGGCGGTGTACGCCAGGGATCGCG	CTTGGGGAAGTAGCCCTCGGCAATTGGTTC
Drosophila	*lz*	CTCCAACTCCATCAGCATCT	CCAATCCGAGTCCGAGTCCG
Drosophila	*hnt (peb)*	TTTCAACGGGAACCAAGCCT	AGCATTTTTCCAACGGCTAGTT
Drosophila	*PPO1*	GATACTCGCGCGCTACAATG	GGTTATTCGTGCTGGACAGG
Drosophila	*gcm*	GAGAGATCTTATCCCGATCCCCTAGC	CTACTACTACAGCAATACGGG
Drosophila	*serpent*	CTTTCCTGCTCCAACTGCCA	TCGCTCTTCGTTCCTTTCGG
Drosophila	*AttacinB*	CACAACTGGCGGAACTTTGG	CCATGTCCGTTGATGTGGGA
Drosophila	*Gal4*	GGGCACATCTGACAGAAGTG	CATGTCAAGGTCTTCTCGAGG
Drosophila	*lacZ*	TGTGCCGAAATGGTCCATCA	GTATCGCCAAAATCACCGCC
Human	*GAPDH*	GAGAAGGCTGGGGCTCATTT	AGTGATGGCATGGACTGTGG
Human	*ACTNB*	ATGATGATATCGCCGCGCTC	TCGATGGGGTACTTCAGGGT
Human	*PTPN2*	TGATCACAGTCGTGTTAAACTGC	GCTGCCAAACCATAAGCCAG
Human	*SOCS1*	AGAGCTTCGACTGCCTCTTC	AATCTGGAAGGGGAAGGAGC
Human	*SOCS3*	GTGGCCACTCTTCAGCATCT	CCCCAGAGCTACAGGACTCT
Human	*BCL2*	GGGAGGATTGTGGCCTTCTT	GGGCCAAACTGAGCAGAGTC
Human	*BCL2L1*	ATTGGTGAGTCGGATCGCAG	CGACTGAAGAGTGAGCCCAG

3. RESULTS

Chapter I

The fact that the Gcm DamID screen analysis identified direct interactions with key inhibitors of the JAK/STAT pathway (*Ptp61F*, *Socs36E*, *Socs44A*, *ken and barbie* (*ken*) et *Su(var)3-9*), suggest that the embryonic hematopoietic transcription factor Gcm may play inhibitory roles onto the JAK/STAT inflammatory cascade involved in inducing an immune response upon infections. Moreover, the presence of two distinct hematopoietic waves in *Drosophila* and the expression of Gcm specifically in the primitive wave strongly suggest that both waves interact during an immune response. My work tested these two hypotheses.

The following manuscript entitled: "A transcription factor specific to embryonic hematopoiesis modulates the inflammatory response and larval hematopoiesis in *Drosophila*", addresses the role of Gcm in regulating the JAK/STAT inflammatory cascade and proinflammatory signals that control larval definitive hematopoiesis, highlighting communication between hematopoietic waves. We show that Gcm inhibits the melanotic phenotype induced by JAK/STAT over-activation and the secretion of the proinflammatory cytokines Upd2 and Upd3 from embryonic hemocytes. Our data describes for the first time the interaction occurring between hematopoietic waves during an immune response and show that a developmental pathway regulates the competence to respond to inflammation. Also, we transpose our findings to vertebrates and demonstrate that Gcm inhibits the JAK/STAT pathway in a human leukemia cell line and induces their apoptosis, shedding light onto a possible conserved role of Gcm in evolution.

Title: A transcription factor specific to embryonic hematopoiesis modulates the inflammatory response and larval hematopoiesis in *Drosophila*

Authors: Wael Bazzi [1]†, Pierre B. Cattenoz [1]†, Claude Delaporte [1], Vasanthi Dasari [1], Angela Giangrande [1*]

Short title: The hematopoietic waves interact in *Drosophila*

Affiliations:

[1] Institut de Génétique et de Biologie Moléculaire et Cellulaire, IGBMC/CNRS/INSERM/UDS, BP 10142, 67404 ILLKIRCH, CU de Strasbourg, France.

† These authors contributed equally to this work.

* Correspondence to: Angela Giangrande: angela@igbmc.fr

Abstract:

In vertebrates and *Drosophila*, immune cells originating from different hematopoietic waves coexist in the organism, raising the possibility that mounting an appropriate immune response requires the interaction between distinct waves. Here we report a mechanism that controls the immune response in *Drosophila* and involves the communication between the embryonic wave occurring in the procephalic mesoderm and the larval hematopoietic wave occurring in the lymph gland. The developmental transcription factor Gcm specific to embryonic hematopoiesis affects the transduction of acute and chronic inflammatory signals that control larval hematopoiesis. Our data highlight the importance of hematopoietic wave communication in the immune response and show that a developmental pathway regulates the competence to respond to inflammation.

Main Text:

The immune response depends on a layered system built upon complex developmental processes (*1*). In flies, inter-organ communication between the lymph gland niche and the vascular system ensures proper self-renewal and differentiation during the second hematopoietic wave (*2*). Moreover, interaction between the lymph gland and the fat body, the nervous system and the muscles is necessary for the systemic response (*3-5*). We therefore asked whether, in addition to interactions between organs and tissues of different nature, communication between the different hematopoietic waves of the immune system also controls the immune response. Fly embryonic hematopoiesis generates plasmatocytes and crystal cells that represent 95% and 5% of the hemocyte population, respectively. Crystal cells remain close to the proventriculus and control melanization, plasmatocytes are professional macrophages that populate the whole animal. Plasmatocytes are dynamic cells that shuttle between the hemolymph (circulating

hemocytes) (*6, 7*) and a subpithelium compartment they transiently attach to (called resident or sessile hemocytes). The second hematopoietic tissue, the lymph gland, disintegrates and produces plasmatocytes and crystal cells that are released into the organism by the end of the larval life. Embryonic and larval hemocytes coexist throughout development and in the adult (*8, 9*). Genetic mutations as the one that constitutively activates the Jak/Stat pathway or immune challenges such as wasp infestation trigger an inflammatory response that involves embryonic and larval hematopoiesis. Hemocyte aggregates called 'melanotic tumors' form due to precocious lymph gland histolysis, hemocyte proliferation and massive appearance of lamellocytes, hemocytes in an inflammatory state that differentiate from plasmatocytes of embryonic and larval origins. To start addressing the role of wave interactions, we focused on the only known transcription factor specific to the embryonic hemocytes, Glide/Gcm (Gcm throughout the manuscript) (**Fig. S1**) (*10-15*), and assessed the specific impact of embryonic hematopoiesis on the immune response and on larval hematopoiesis.

A genome-wide DamID screen identifying the direct targets of Gcm suggested an inhibitory role on the Jak/Stat pathway at the transcriptional level (*16*). We identified the genes of the pathway directly targeted by Gcm and selected three, based on their role in hematopoiesis: Ptp61F, Socs36E and Socs44A (*17*) (**Figs. 1A, S2A-C**). Ptp61F inhibits the Jak/Stat pathway by de-phosphorylating the only Jak present in flies (called Hop) and the transcription factor Stat92E (*17-19*). Socs36E and Socs44A belong to the suppressor of cytokine signaling family that suppresses Jak/Stat activation by competing with Stat for binding to the Jak catalytic domain (*20, 21*). In line with the DamID data, transfecting S2 *Drosophila* cells with a *gcm* expression vector (*pPac-gcm*) increases the endogenous levels of *Ptp61F*, *Socs36E* and *Socs44A* transcripts (**Fig. 1B**).

Since Gcm is specifically expressed in the embryonic hemocytes we assessed whether inhibiting the Jak/Stat pathway only in those cells affects the immune response. The constitutive activation of the pathway ($hop^{Tum\text{-}l}$ mutation) induces the formation of melanotic tumors in 36% of the larvae (**Fig. 1C, see materials and methods**). $hop^{Tum\text{-}l}$ animals in which the expression of any of the three inhibitors is silenced only in embryonic hemocytes (*gcmGal4* or *gcm>* driver) show a strong enhancement of the tumor penetrance (> 90%, **Fig. 1C**).

In line with these findings, reducing Gcm expression enhances the $hop^{Tum\text{-}l}$ phenotype strongly (**Figs. 1C**, **S3, S4**). This is also observed upon crossing a *gcm KD* reporter (*UAS-gcmRNAi/+*) with a *gcmGal4* driver inactive in glia (*repoGal80,gcm>*), the other main territory of Gcm expression, with other, independent, embryonic-specific hemocyte drivers (*srp(hemo)>* and *sn>*) or upon using the lethal gcm^{26} mutation in heterozygous conditions (**Figs. 1C, S4**). Tumor expressivity measured by tumor size also increases upon silencing Gcm expression in $hop^{Tum\text{-}l}$ animals (*14*) (**Figs. 1D,E, S5**). In addition, Gcm over-expression (*gcm Gain of Function* or *GOF*) rescues the $hop^{Tum\text{-}l}$ mediated phenotype (**Fig. 1C**). Gcm acts as a

suppressor of the inflammatory response rather than as a tumor suppressor since the number of circulating hemocytes cells increases more than 5.5-fold in *hop*$^{Tum\text{-}l}$ compared to wild-type animals, but only moderately in *hop*$^{Tum\text{-}l}$*; gcm KD* compared to *hop*$^{Tum\text{-}l}$ animals (1.1-fold), mostly due to an increase of lamellocytes' number (**Fig. 1F**). Gcm seems to have a regulatory role, since silencing its expression in an otherwise wild-type background triggers the formation of few lamellocytes but no tumors (**Figs. 1C, S6, see materials and methods**). Accordingly, *gcm KD* hemocytes show an intermediate phenotype characterized by the expression of most plasmatocyte but also some lamellocyte markers (**Figs. 1C, S7**). The crystal cell population increases moderately in *gcm* null embryos, as shown in (*13*), but not in *gcm KD* larvae (**Figs. S7, S8, see materials and methods**).

Ptp61F represents a major Gcm target in the regulation of the Jak/Stat pathway as its over-expression rescues the exacerbated phenotype observed in the *hop*$^{Tum\text{-}l}$/+;*gcm KD* larvae (**Fig. 1C**). Finally and most strikingly, Gcm affects the Jak/Stat-mediated lymph gland phenotype (**Fig. 2**): the penetrance of precocious histolysis and the presence of lamellocytes observed in *hop*$^{Tum\text{-}l}$/+ larvae are rescued in *hop*$^{Tum\text{-}l}$/+ larvae in which Gcm is over-expressed (*hop*$^{Tum\text{-}l}$/+;*gcm GOF*) while they seem enhanced in *hop*$^{Tum\text{-}l}$/+;*gcm KD* larvae (although the penetrance of the *hop*$^{Tum\text{-}l}$/+ phenotypes is already high).

In sum, Gcm counteracts the inflammatory response induced by over-activation of the Jak/Stat pathway by inducing the expression of inhibitors of that pathway. This is the first direct evidence that a transcription factor controlling the first hematopoietic wave affects the second wave.

We then asked how do the embryonic hemocytes signal to the lymph gland. Prime candidates are the proinflammatory cytokines of the Upd family since their expression is induced in cells of both hematopoietic waves by wasp infestation or septic injury (*4*, *22*) and their mutations prevent the encapsulation of the wasp egg by the fly hemocytes (*23*). In line with these data, we found that *hop*$^{Tum\text{-}l}$ animals that are heterozygous for *upd2* and *upd3* display a reduced penetrance of the melanotic tumor phenotype (**Fig. S9A, see materials and methods**). Importantly, specific Upd2 or Upd3 over-expression in the embryonic hemocytes (*upd2 GOF* and *upd3 GOF*) is sufficient to induce lymph gland precocious histolysis as well as melanotic tumor formation (**Fig. 3A,D**). In addition, while the *hop*$^{Tum\text{-}l}$ lymph glands lose their integrity and contain lamellocytes, down-regulating *upd2* or *upd3* in *hop*$^{Tum\text{-}l}$ embryonic hemocytes rescues those phenotypes, as many lymph glands are intact and none display lamellocytes (**Fig. 3A-C**). Thus, cytokine expression solely in the embryonic hemocytes is sufficient to trigger an inflammatory response.

We next speculated that the inhibitory role of Gcm on the Jak/Stat pathway involves Upd2 and Upd3. We found that knocking down Gcm expression in larvae that over-express Upd2 or Upd3 in the embryonic hemocytes enhances the tumor phenotype due to *upd2/3 GOF* (**Fig. 3D**). Furthermore, Gcm inhibits the expression of *upd2* and *upd3*, as their transcript levels increase upon silencing Gcm in hemocytes (**Fig.**

3E,F). In addition, transfecting a *gcm* expression vector lowers the expression of the two cytokines in S2 cells (**Fig. 3G**). Most importantly, Upd2 and Upd3 are epistatic to Gcm *in vivo* since down-regulating their expression in $hop^{Tum\text{-}l}$ and even in $hop^{Tum\text{-}l}$*/+;gcm>gcm KD* animals almost abolishes the formation of tumors (**Fig. 3H, see materials and methods**). Finally, transfecting a $hop^{Tum\text{-}l}$ expression vector strongly induces the expression of *upd2* and *upd3* (**Fig. 3G**) and these two loci contain STAT binding sites (**Fig. S9B,C**). Of note, the tumor phenotype is induced by Upd2 or Upd3 over-expression but not by Gcm silencing, suggesting that threshold levels of the inflammatory pathway may be required for the melanotic tumors to form. Accordingly, the number of circulating hemocytes is higher in larvae over-expressing Upd2 or Upd3 compared to those observed in *gcm KD* animals (**Fig. S9D**), and so are the levels of the cytokine transcripts (**Fig. 3E-F'**). Finally, silencing Gcm in animals that over-express either cytokine has a moderate effect on the number of circulating hemocytes, further supporting the view that Gcm does not act as a tumor suppressor (**Fig. S9D**). In sum, Gcm suppresses the Jak/Stat pathway, which normally activates the expression of proinflammatory cytokines that are secreted and act non-autonomously.

Following this, we asked whether the constitutive activation of the Jak/Stat pathway within the first hematopoietic wave is also sufficient to trigger tumor formation and lymph gland defects. Larvae carrying the *UAS-*$hop^{Tum\text{-}l}$ transgene and drivers specific to the embryonic hemocytes do display tumors, abnormal hematopoiesis and precocious lymph gland histolysis (**Figs. 4, S10A, see materials and methods**). The penetrance of the tumors is similar to that seen in $hop^{Tum\text{-}l}$ larvae (**Fig. 4A, see materials and methods**), in which the Jak/Stat pathway is constitutively active, however, the overall phenotype is weaker: the tumors are smaller and only 28% lymph glands are histolysed (vs. 88.8% in $hop^{Tum\text{-}l}$ animals), none of which contains lamellocytes (**Fig. 4D**). Interestingly, Jak/Stat activation in the first hematopoietic wave, much like wasp infestation, is sufficient to activate the Jak/Stat pathway in the somatic muscles (as measured by the 10xStat92E-GFP reporter, **Fig**. **4G-I**), which Hultmark and collaborators recently showed to control wasp egg encapsulation (*4*). To further characterize the role of Jak/Stat activation during the first wave, we took into account both resident and circulating hemocyte populations and found that their total number (**Fig. 4E**) as well as that of the dividing cells are significantly lower (5.1% vs. 12.5%) and the percentage of lamellocytes tends to decrease (**Fig. 4F**) compared to what observed upon systemic activation. To highlight the cell autonomous requirements of the Jak/Stat pathway we also analysed the resident and the circulating populations separately (**Fig. S10B-D**). Conditional and systemic activation of the Jak/Stat pathway induces lamellocyte markers in a high fraction of hemocytes and triggers proliferation in both compartments, however, conditional activation does not trigger hemocyte mobilization (**Fig. S10B**), a key process in the inflammatory response. In addition, the percentage of

resident lamellocytes and the rate of proliferation tend to be lower upon conditional activation (**Fig. S10C,D**).

Similar to what observed in *hop^{Tum-l}; gcm KD* animals (**Figs. 1-3**), reducing Gcm expression in *gcm>hop^{Tum-l}* animals enhances the phenotype induced by conditional Jak/Stat activation (**Fig. 4A-F**). The tumour penetrance and expressivity increase and the lymph glands are always precociously histolysed. These phenotypes are not associated with an increase of the total hemocyte number but with their enhanced mobilization from the resident compartment (+ 411 hemocytes in circulation). This perfectly matches with the finding that *eater* expression decreases in *gcm KD* hemocytes (**Fig. S7A**), since it has been shown that *eater* is required for the attachment of hemocytes to the sessile compartment and that the decreases of its expression is linked to the production of lamellocytes (*24*). Finally, silencing the Gcm target and Jak/Stat inhibitor *Ptp61F* in the embryonic hemocytes also triggers tumor formation (**Fig. S11**). Overall, our results demonstrate that a molecular cascade specific to the first hematopoietic wave controls the second wave and the inflammatory response. Gcm inhibits the Jak/Stat pathway and hence the secretion of the Upd2 and Upd3 inflammatory cytokines from the embryonic hemocytes (**Fig. 4J**). How general are these anti-inflammatory effects awaits further investigation, however, first data show that *gcm KD* does not only enhance the response to the chronic inflammatory state induced by a genetically mutated background. *gcm KD* also mount an enhanced response to an acute challenge such as wasp infestation, where mutant larvae show a higher rate of wasp egg encapsulation compared to control larvae, hence allowing fewer wasp eggs to develop and fewer adults wasps to hatch (**Fig. 4K,L, see materials and methods**). Since *gcm* is no longer expressed by the time of infestation (nor is its expression induced by infestation or by Jak/Stat activation) (**Fig. S12**), this transcription factor acts by finely tuning the development of immune cells so as to prevent their inappropriate activation: when Gcm is silenced, hemocytes are primed to an inflammatory state. Finally, one of the two murine Gcm orthologs, mGcm2 (*25*), negatively regulates the Jak/Stat pathway in a human leukemia cell line in which that pathway is over-activated (**Fig. S13, see materials and methods**), calling for a possible conserved role of the Gcm genes in evolution.

References and Notes:

1. M. Letourneau *et al.*, Drosophila hematopoiesis under normal conditions and in response to immune stress. *FEBS Lett* **590**, 4034-4051 (2016).
2. I. Morin-Poulard *et al.*, Vascular control of the Drosophila haematopoietic microenvironment by Slit/Robo signalling. *Nat Commun* **7**, 11634 (2016).
3. L. M. Vanha-aho *et al.*, Edin Expression in the Fat Body Is Required in the Defense Against Parasitic Wasps in Drosophila melanogaster. *Plos Pathogens* **11**, (2015).
4. H. Yang, J. Kronhamn, J. O. Ekstrom, G. G. Korkut, D. Hultmark, JAK/STAT signaling in Drosophila muscles controls the cellular immune response against parasitoid infection. *EMBO Rep* **16**, 1664-1672 (2015).
5. J. Shim *et al.*, Olfactory control of blood progenitor maintenance. *Cell* **155**, 1141-1153 (2013).

6. K. S. Gold, K. Bruckner, Drosophila as a model for the two myeloid blood cell systems in vertebrates. *Exp Hematol* **42**, 717-727 (2014).
7. M. Stofanko, S. Y. Kwon, P. Badenhorst, A misexpression screen to identify regulators of Drosophila larval hemocyte development. *Genetics* **180**, 253-267 (2008).
8. A. Holz, B. Bossinger, T. Strasser, W. Janning, R. Klapper, The two origins of hemocytes in Drosophila. *Development* **130**, 4955-4962 (2003).
9. S. Ghosh, A. Singh, S. Mandal, L. Mandal, Active hematopoietic hubs in Drosophila adults generate hemocytes and contribute to immune response. *Developmental cell* **33**, 478-488 (2015).
10. R. Bernardoni, V. Vivancos, A. Giangrande, glide/gcm is expressed and required in the scavenger cell lineage. *Developmental biology* **191**, 118-130 (1997).
11. T. Lebestky, T. Chang, V. Hartenstein, U. Banerjee, Specification of Drosophila hematopoietic lineage by conserved transcription factors. *Science* **288**, 146-149 (2000).
12. T. B. Alfonso, B. W. Jones, gcm2 promotes glial cell differentiation and is required with glial cells missing for macrophage development in Drosophila. *Developmental biology* **248**, 369-383 (2002).
13. L. Bataille, B. Auge, G. Ferjoux, M. Haenlin, L. Waltzer, Resolving embryonic blood cell fate choice in Drosophila: interplay of GCM and RUNX factors. *Development* **132**, 4635-4644 (2005).
14. A. Avet-Rochex *et al.*, An in vivo RNA interference screen identifies gene networks controlling Drosophila melanogaster blood cell homeostasis. *BMC Dev Biol* **10**, 65 (2010).
15. A. Zaidman-Remy, J. C. Regan, A. S. Brandao, A. Jacinto, The Drosophila larva as a tool to study gut-associated macrophages: PI3K regulates a discrete hemocyte population at the proventriculus. *Developmental and Comparative Immunology* **36**, 638-647 (2012).
16. P. B. Cattenoz *et al.*, Functional Conservation of the Glide/Gcm Regulatory Network Controlling Glia, Hemocyte, and Tendon Cell Differentiation in Drosophila. *Genetics* **202**, 191-219 (2016).
17. P. Muller, D. Kuttenkeuler, V. Gesellchen, M. P. Zeidler, M. Boutros, Identification of JAK/STAT signalling components by genome-wide RNA interference. *Nature* **436**, 871-875 (2005).
18. G. H. Baeg, R. Zhou, N. Perrimon, Genome-wide RNAi analysis of JAK/STAT signaling components in Drosophila. *Genes Dev* **19**, 1861-1870 (2005).
19. A. V. Villarino, Y. Kanno, J. J. O'Shea, Mechanisms and consequences of Jak-STAT signaling in the immune system. *Nat Immunol* **18**, 374-384 (2017).
20. T. Naka *et al.*, Structure and function of a new STAT-induced STAT inhibitor. *Nature* **387**, 924-929 (1997).
21. H. Yasukawa *et al.*, The JAK-binding protein JAB inhibits Janus tyrosine kinase activity through binding in the activation loop. *Embo Journal* **18**, 1309-1320 (1999).
22. H. Agaisse, U. M. Petersen, M. Boutros, B. Mathey-Prevot, N. Perrimon, Signaling role of hemocytes in Drosophila JAK/STAT-dependent response to septic injury. *Developmental cell* **5**, 441-450 (2003).
23. R. Makki *et al.*, A short receptor downregulates JAK/STAT signalling to control the Drosophila cellular immune response. *PLoS Biol* **8**, e1000441 (2010).
24. I. Anderl *et al.*, Transdifferentiation and Proliferation in Two Distinct Hemocyte Lineages in Drosophila melanogaster Larvae after Wasp Infection. *PLoS Pathog* **12**, e1005746 (2016).
25. S. Hashemolhosseini, M. Wegner, Impacts of a new transcription factor family: mammalian GCM proteins in health and disease. *The Journal of cell biology* **166**, 765-768 (2004).
26. D. A. Harrison, R. Binari, T. S. Nahreini, M. Gilman, N. Perrimon, Activation of a Drosophila Janus kinase (JAK) causes hematopoietic neoplasia and developmental defects. *The EMBO journal* **14**, 2857-2865 (1995).
27. L. Soustelle, A. Giangrande, Novel gcm-dependent lineages in the postembryonic nervous system of Drosophila melanogaster. *Developmental dynamics : an official publication of the American Association of Anatomists* **236**, 2101-2108 (2007).
28. S. Vincent, J. L. Vonesch, A. Giangrande, Glide directs glial fate commitment and cell fate switch between neurones and glia. *Development* **122**, 131-139 (1996).
29. H. Jiang *et al.*, Cytokine/Jak/Stat signaling mediates regeneration and homeostasis in the Drosophila midgut. *Cell* **137**, 1343-1355 (2009).
30. J. Zanet *et al.*, Fascin promotes filopodia formation independent of its role in actin bundling. *The Journal of cell biology* **197**, 477-486 (2012).
31. K. Bruckner *et al.*, The PDGF/VEGF receptor controls blood cell survival in Drosophila. *Developmental cell* **7**, 73-84 (2004).

32. S. McLaughlin, J. E. Dixon, Alternative splicing gives rise to a nuclear protein tyrosine phosphatase in Drosophila. *J Biol Chem* **268**, 6839-6842 (1993).
33. A. B. Lerner, T. B. Fitzpatrick, Biochemistry of melanin formation. *Physiol Rev* **30**, 91-126 (1950).
34. B. Z. Kacsoh, T. A. Schlenke, High hemocyte load is associated with increased resistance against parasitoids in Drosophila suzukii, a relative of D. melanogaster. *PLoS One* **7**, e34721 (2012).
35. S. Petraki, B. Alexander, K. Bruckner, Assaying Blood Cell Populations of the Drosophila melanogaster Larva. *J Vis Exp*, (2015).
36. T. Lebestky, S. H. Jung, U. Banerjee, A Serrate-expressing signaling center controls Drosophila hematopoiesis. *Genes Dev* **17**, 348-353 (2003).
37. V. Honti *et al.*, Cell lineage tracing reveals the plasticity of the hemocyte lineages and of the hematopoietic compartments in Drosophila melanogaster. *Mol Immunol* **47**, 1997-2004 (2010).
38. E. Kurucz *et al.*, Hemese, a hemocyte-specific transmembrane protein, affects the cellular immune response in Drosophila. *Proc Natl Acad Sci U S A* **100**, 2622-2627 (2003).
39. O. Binggeli, C. Neyen, M. Poidevin, B. Lemaitre, Prophenoloxidase activation is required for survival to microbial infections in Drosophila. *PLoS Pathog* **10**, e1004067 (2014).
40. T. M. Rizki, R. M. Rizki, E. H. Grell, A mutant affecting the crystal cells inDrosophila melanogaster. *Wilhelm Roux's archives of developmental biology* **188**, 91-99 (1980).
41. A. J. Bretscher *et al.*, The Nimrod transmembrane receptor Eater is required for hemocyte attachment to the sessile compartment in Drosophila melanogaster. *Biol Open* **4**, 355-363 (2015).
42. A. A. Miller, R. Bernardoni, A. Giangrande, Positive autoregulation of the glial promoting factor glide/gcm. *The EMBO journal* **17**, 6316-6326 (1998).
43. P. Laneve *et al.*, The Gcm/Glide molecular and cellular pathway: new actors and new lineages. *Developmental biology* **375**, 65-78 (2013).
44. R. P. de Groot, J. A. Raaijmakers, J. W. Lammers, R. Jove, L. Koenderman, STAT5 activation by BCR-Abl contributes to transformation of K562 leukemia cells. *Blood* **94**, 1108-1112 (1999).
45. T. S. Lin, S. Mahajan, D. A. Frank, STAT signaling in the pathogenesis and treatment of leukemias. *Oncogene* **19**, 2496-2504 (2000).
46. L. Soustelle *et al.*, Neurogenic role of Gcm transcription factors is conserved in chicken spinal cord. *Development* **134**, 625-634 (2007).
47. R. He *et al.*, Inhibition of K562 leukemia angiogenesis and growth by expression of antisense vascular endothelial growth factor (VEGF) sequence. *Cancer Gene Ther* **10**, 879-886 (2003).
48. G. K. Srivastava *et al.*, Trypan Blue staining method for quenching the autofluorescence of RPE cells for improving protein expression analysis. *Exp Eye Res* **93**, 956-962 (2011).
49. M. Stofanko, S. Y. Kwon, P. Badenhorst, Lineage tracing of lamellocytes demonstrates Drosophila macrophage plasticity. *PLoS One* **5**, e14051 (2010).
50. H. J. Nam, I. H. Jang, H. You, K. A. Lee, W. J. Lee, Genetic evidence of a redox-dependent systemic wound response via Hayan protease-phenoloxidase system in Drosophila. *The EMBO journal* **31**, 1253-1265 (2012).
51. J. Schindelin *et al.*, Fiji: an open-source platform for biological-image analysis. *Nature methods* **9**, 676-682 (2012).
52. C. Small, I. Paddibhatla, R. Rajwani, S. Govind, An introduction to parasitic wasps of Drosophila and the antiparasite immune response. *J Vis Exp*, e3347 (2012).
53. B. Kari *et al.*, The raspberry Gene Is Involved in the Regulation of the Cellular Immune Response in Drosophila melanogaster. *Plos One* **11**, (2016).
54. B. van Steensel, S. Henikoff, Identification of in vivo DNA targets of chromatin proteins using tethered dam methyltransferase. *Nat Biotechnol* **18**, 424-428 (2000).
55. B. van Steensel, J. Delrow, S. Henikoff, Chromatin profiling using targeted DNA adenine methyltransferase. *Nat Genet* **27**, 304-308 (2001).
56. D. A. Kimbrell, C. Hice, C. Bolduc, K. Kleinhesselink, K. Beckingham, The Dorothy enhancer has Tinman binding sites and drives hopscotch-induced tumor formation. *Genesis* **34**, 23-28 (2002).
57. C. J. Evans *et al.*, G-TRACE: rapid Gal4-based cell lineage analysis in Drosophila. *Nature methods* **6**, 603-605 (2009).
58. C. Chotard, W. Leung, I. Salecker, glial cells missing and gcm2 cell autonomously regulate both glial and neuronal development in the visual system of Drosophila. *Neuron* **48**, 237-251 (2005).
59. D. Osman *et al.*, A Drosophila model identifies calpains as modulators of the human leukemogenic fusion protein AML1-ETO. *Proc Natl Acad Sci U S A* **106**, 12043-12048 (2009).

60. L. Waltzer, G. Ferjoux, L. Bataille, M. Haenlin, Cooperation between the GATA and RUNX factors Serpent and Lozenge during Drosophila hematopoiesis. *Embo Journal* **22**, 6516-6525 (2003).
61. R. Yan, S. Small, C. Desplan, C. R. Dearolf, J. E. Darnell, Jr., Identification of a Stat gene that functions in Drosophila development. *Cell* **84**, 421-430 (1996).

Acknowledgments:

We thank Y. Yuasa, R. Sakr, E. Sonmez, A. Bogomolova and the Imaging Center of the IGBMC for technical assistance and Y. Yuasa for critical reading of the manuscript. We thank I. Ando and WJ. Lee for providing us with antibodies and K. Bruckner, M. Crozatier, BA. Edgar, M. Meister, N. Perrimon and MP. Zeidler for providing us with fly stocks. In addition, stocks obtained from the Bloomington Drosophila Stock Center (NIH P40OD018537) as well as antibodies obtained from the Developmental Studies Hybridoma Bank were used in this study. This work was supported by INSERM, CNRS, UDS, Ligue Régionale contre le Cancer, Hôpital de Strasbourg, ARC and ANR grants. P. Cattenoz was funded by the ANR and by the ARSEP, W. Bazzi by the USIAS and by the FRM (FDT20160435111), V. Dasari by COFUND. The IGBMC was also supported by a French state fund through the ANR labex.

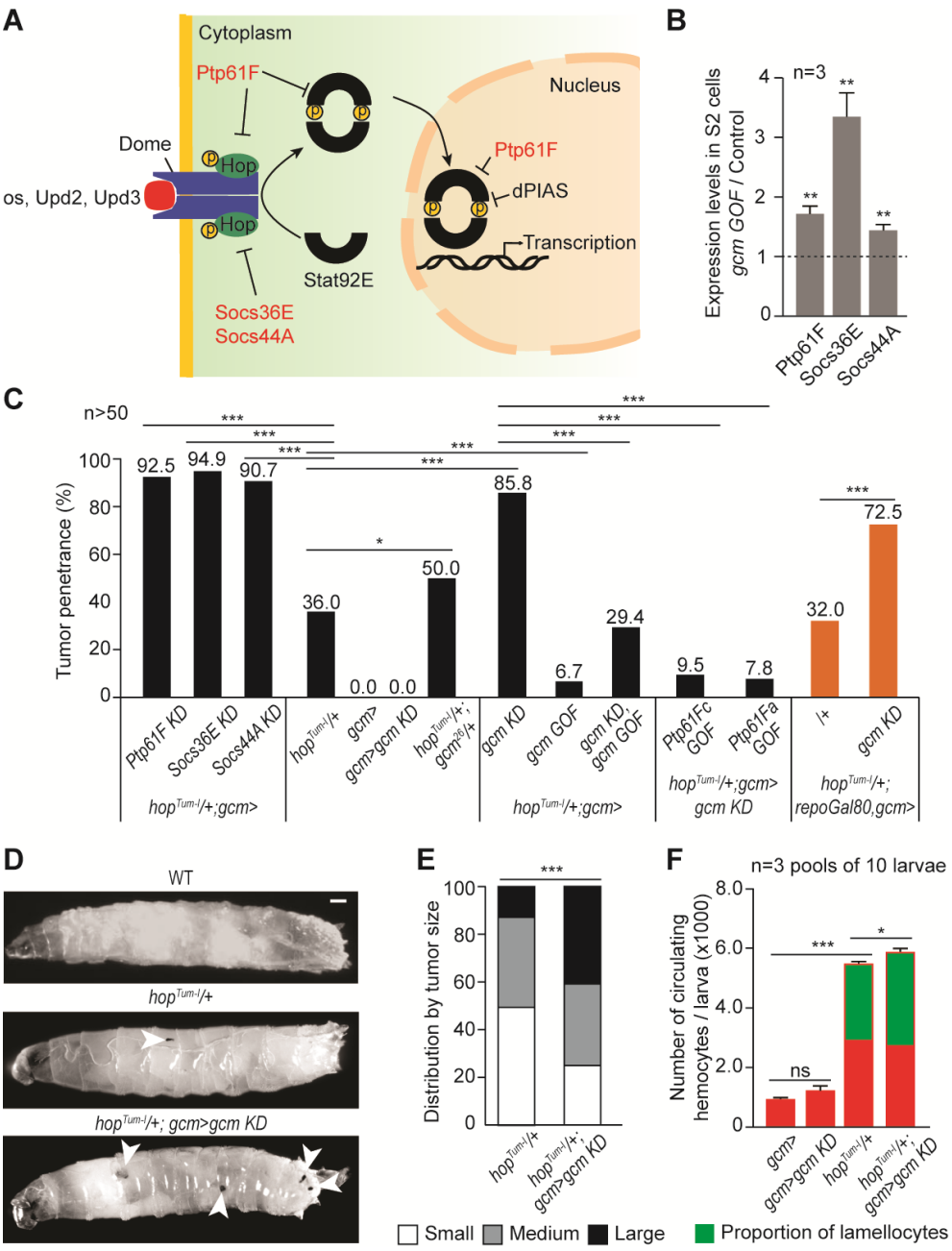

Fig. 1. Gcm induces the expression of Jak/Stat inhibitors and hinders Jak/Stat-mediated melanotic tumor formation. (**A**) Jak/Stat pathway: Gcm direct targets in red. (**B**) Relative expression levels of Jak/Stat inhibitors in S2 cells transfected with a *pPac-gcm* expression plasmid (3 independent assays). (**C**) Penetrance of melanotic tumors. (n>50). (**D**) 3rd instar larvae of the indicated genotypes. Arrowheads indicate melanotic tumors. (**E**) Phenotype expressivity assessed as tumor size (n>40). (**F**) Total number of circulating hemocytes and lamellocyte contribution (n=3, using 10 larvae/replicate). In all figures, **p*<0.0.5, ***p*<0.01; ****p*<0.001, ns: not significant; scale bar: 50µm.

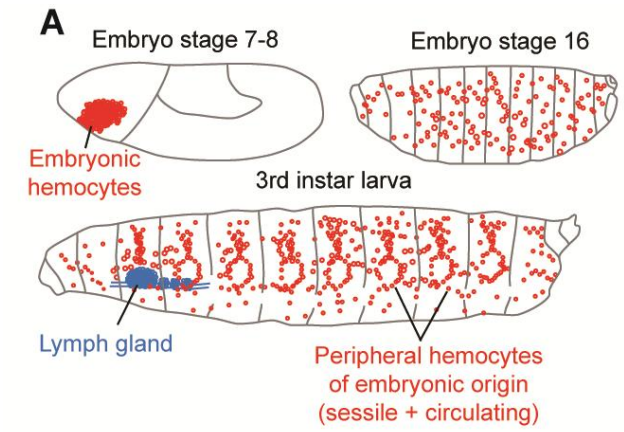

B

	Precocious histolysis	Lamellocyte marker
gcm>	0/13 (0%)	0/13 (0%)
hop^{Tum-l}/+	8/9 (88.8%)	8/9 (88.8%)
hop^{Tum-l}/+;gcm> gcm KD	14/15 (93.3%)	15/15 (100%)
hop^{Tum-l}/+;gcm> gcm GOF	2/9 (22.2%)	1/9 (11.1%)

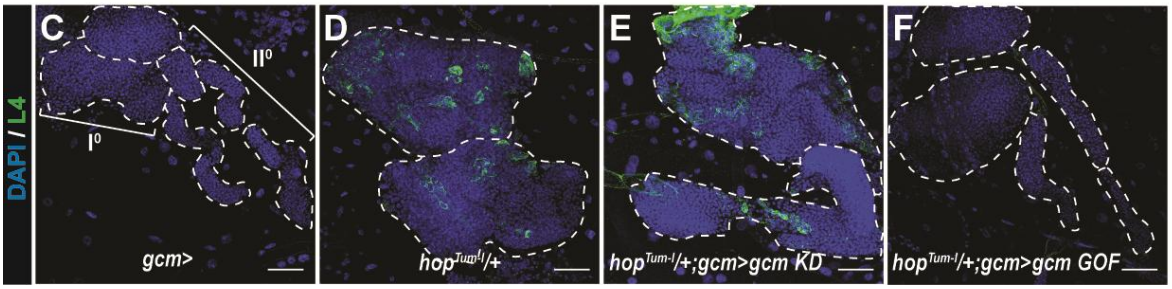

Fig. 2. Embryonic hemocytes signal to the lymph gland. (**A**) Embryonic hemocytes (red) in early and late embryo and in 3rd instar larva. The lymph gland (blue) histolyses at the larva to pupa transition. (**B**) Number and percentage of lymph glands showing precocious histolysis and lamellocyte labeling (L4 marker, green), DAPI is in blue. (**C**-**F**) Lymph glands are indicated by hatched lines. (**C**) Control lymph gland (*gcm>*): I° and II° indicate primary and secondary lobes, respectively. (**D**,**E**) show hypertrophic glands, lack of lobes and L4 expression. (**F**) rescue of the phenotype.

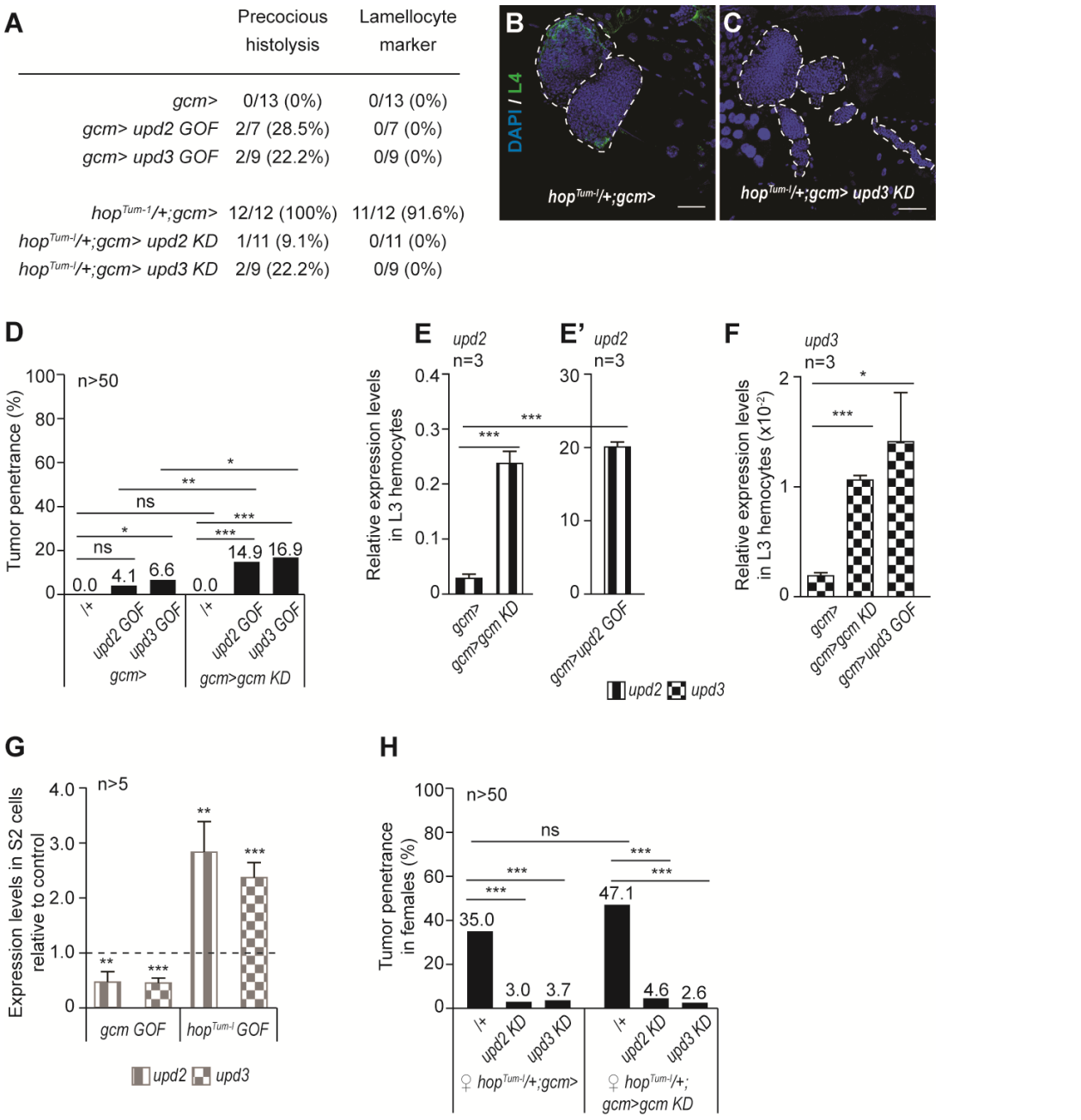

Fig. 3. Embryonic hemocytes signal through Upd2 and Upd3. (**A**) Lymph gland phenotypes. (**B**,**C**) Lymph gland immunolabeling as in Fig. 2C-F. (**D**) Tumor penetrance. (**E-F**) *upd2* and *upd3* expression levels increase in *gcm>gcm KD* (**E**, first two columns from the left in **F**) and even further in *gcm>gcm KD upd2/3 GOF* 3rd instar larval hemocytes (**E',** column three in **F**). Note the different scale between (E) and (E'). (**G**) *upd2* and *upd3* expression levels in S2 cells upon transfection with *pPac-gcm* or *pUAS-hop*$^{Tum-l}$ expression vectors, compared to control levels shown by the dashed line (transfection of an empty expression vector) (n>5). (**H**) Tumor penetrance in 3rd instar female larvae.

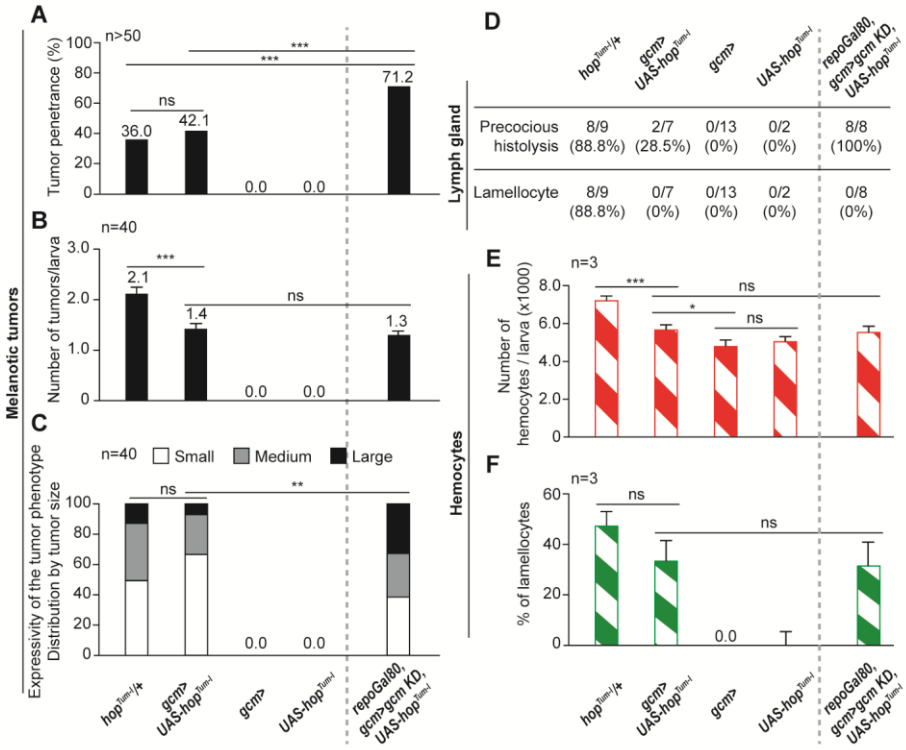
A
n>50
Tumor penetrance (%)
36.0
42.1
0.0
0.0
71.2
ns
***
***
B
n=40
Number of tumors/larva
2.1
1.4
0.0
0.0
1.3
***
ns
C
n=40
Small
Medium
Large
Expressivity of the tumor phenotype
Distribution by tumor size
ns
**
0.0
0.0
Melanotic tumors
Hemocytes
Lymph gland
hopTum-l/+
gcm> UAS-hopTum-l
gcm>
UAS-hopTum-l
repoGal80, gcm>gcm KD, UAS-hopTum-l
D
Precocious histolysis
8/9 (88.8%)
2/7 (28.5%)
0/13 (0%)
0/2 (0%)
8/8 (100%)
Lamellocyte
8/9 (88.8%)
0/7 (0%)
0/13 (0%)
0/2 (0%)
0/8 (0%)
E
n=3
Number of hemocytes / larva (x1000)
***
*
ns
ns
F
n=3
% of lamellocytes
ns
ns
0.0
G
10xStat92E-GFP
GFP
H
srp(hemo)>hopTum-l; 10xStat92E-GFP
I
10xStat92E-GFP (infested)

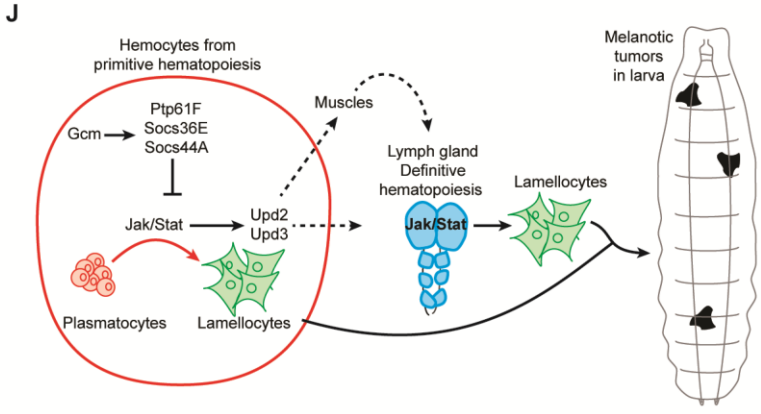
J
Hemocytes from primitive hematopoiesis
Gcm
Ptp61F
Socs36E
Socs44A
Jak/Stat
Upd2
Upd3
Muscles
Lymph gland
Definitive hematopoiesis
Jak/Stat
Lamellocytes
Plasmatocytes
Lamellocytes
Melanotic tumors in larva

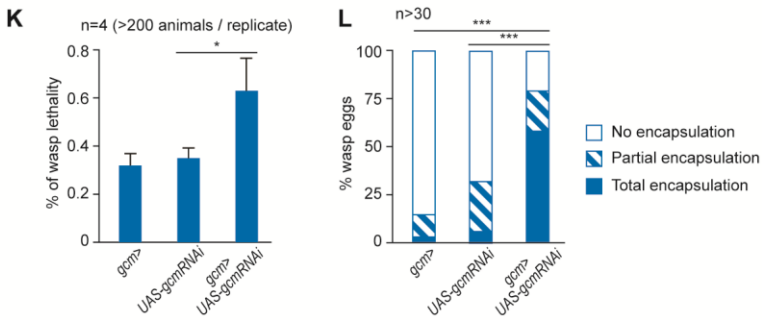
K
n=4 (>200 animals / replicate)
% of wasp lethality
*
gcm>
UAS-gcmRNAi
gcm> UAS-gcmRNAi
L
n>30
% wasp eggs
***
***
No encapsulation
Partial encapsulation
Total encapsulation

Fig. 4. Inflammatory response upon Jak/Stat constitutive activation in embryonic hemocytes or upon wasp infestation. (**A**) Tumor penetrance. (**B**-**C**) Phenotype expressivity assessed as number of tumors/larva (**B**) and tumor size (**C**) (n=40). (**D**) Precocious lymph glands histolysis and lamellocyte labeling, note the 100% histolysis in *repoGal80,gcm>gcm KD, UAS-hop*$^{Tum\text{-}l}$. (**E**) Total number of hemocytes (circulating + sessile) (n=3). (**F**) Percentage of lamellocytes in circulating and sessile compartments as above (n=3). (**G-I**) *10XStat92E-GFP* reporter intensity in somatic muscles. (**J**) Schematic of Gcm regulatory role. (**K**) Lethality of the parasitic wasp after infestation of *Drosophila* larvae (n=4) (>200 animals). (**L**) Histogram representing the percentage of total, partial and no wasp egg encapsulation (n>30).

Supplementary Materials:

Materials and Methods

Figures S1-S13

Authors contributions

References (*26-61*)

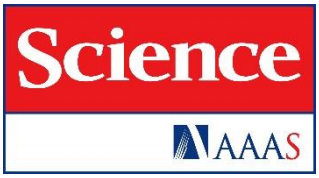

Supplementary Materials for

A transcription factor specific to embryonic hematopoiesis modulates the inflammatory response and larval hematopoiesis in *Drosophila*

Authors: Wael Bazzi [1]†, Pierre B. Cattenoz [1]†, Claude Delaporte [1], Vasanthi Dasari [1], Angela Giangrande [1*]

Affiliations:

[1] Institut de Génétique et de Biologie Moléculaire et Cellulaire, IGBMC/CNRS/INSERM/UDS, BP 10142, 67404 ILLKIRCH, CU de Strasbourg, France.

† These authors contributed equally to this work.

* Correspondence to: Angela Giangrande : angela@igbmc.fr.

This PDF file includes:

Materials and Methods

Figs. S1 to S13

Materials and Methods:

Fly strains and genetics

Flies were raised on standard media at 25°C. The following stocks were used:

Genotypes	Abbreviation	Origin	Remarks
w^{1118}	WT	Bloomington #5905	
$hop^{Tum-l}/FM7c$	hop^{Tum-l}	Bloomington #8492	point mutation that constitutively activates the Jak/Stat pathway
UAS-hop^{Tum-l}*/CyO,twilacZ*	*UAS-*hop^{Tum-l}	(*26*)	reporter line for hop^{Tum-l} over-expression
gcmGal4,UAS-mCD8GFP/CyO,Tb	*gcm>GFP*	(*27*)	driver specific to embryonic hemocytes and glia, *gcm* hypomorphic mutation
UAS-gcmRNAi	*gcm KD*	Bloomington #31519	dsRNA reporter line for *gcm* down-regulation
UAS-gcmF18A	*gcm GOF*	(*10*)	reporter line for *gcm* over-expression
gcm^{26}*/CyOactinGFP*	gcm^{26}	(*28*)	null *gcm* mutation
$upd2^{\Delta}$		Bloomington #55727	4.7 kb deletion
$upd3^{\Delta}$		Bloomington #55728	imprecise excision
UAS-upd2RNAi	*upd2 KD*	Bloomington #33988	dsRNA reporter line for *upd2* down-regulation
UAS-upd3RNAi	*upd3 KD*	Bloomington #32859	dsRNA reporter line for *upd3* down-regulation
UAS-upd2/CyO	*upd2 GOF*	(*29*)	reporter line for *upd2* over-expression
UAS-upd3/CyO	*upd3 GOF*	(*29*)	reporter line for *upd3* over-expression
UAS-Ptp61FRNAi	*Ptp61F KD*	Bloomington #32426	dsRNA reporter line for *Ptp61F* down-regulation
UAS-Socs36ERNAi	*Socs36E KD*	Bloomington #35036	dsRNA reporter line for *Socs36E* down-regulation
UAS-Socs44ARNAi	*Socs44A KD*	Bloomington #42830	dsRNA reporter line for *Socs44A* down-regulation
UAS-Ptp61Fa/CyO	*Ptp61Fa GOF* (cytoplasmic)	(*17*)	reporter line to over-express the cytoplasmic splicing isoform
UAS-Ptp61Fc/TM3	*Ptp61Fc GOF* (nuclear)	(*17*)	reporter line to over-express the nuclear splicing isoform
gcmGal4,UAS-mCD8GFP,repoGal80/CyO	*repoGal80,gcm>*	(*16*)	*gcm* driver not expressed in glia, hypomorphic mutation

snGal4		(*30*)	*singed* driver, specific to embryonic hemocytes
srp(hemo)Gal4		(*31*)	*serpent* driver specific to embryonic hemocytes
DotGal4		Bloomington #67608	*Dorothy* driver specifically expressed in embryonic and larval lymph gland
lzGal4,UAS-mCD8GFP	*lz>GFP*	Bloomington #6314	*lozenge* driver expressed in crystal cells
10xStat92E-GFP		Bloomington #26198	reporter line for STAT activity, 10 Stat92E binding sites driving GFP expression
UAS-FLP;;Ubi-p63E(FRT.STOP)Stinger	*gtrace*	Bloomington #28282	This line allows the analysis of lineage-traced expression of Gal4 drivers

Crosses' protocols

Fig. 1C: to assess the impact of JAK/STAT inhibitors on melanotic tumor formation, *Ptp61F*, *Socs36E* and *Socs44A* were silenced using *gcmGal4* in $hop^{Tum\text{-}l}$ mutant animals (columns 1, 2 and 3). $hop^{Tum\text{-}l}$/+ animals were generated by crossing $hop^{Tum\text{-}l}$ homozygous females with w^{1118} males (column 4). To assess the impact of Gcm on melanotic tumor formation we used either the null mutation gcm^{26} or *gcmGal4,UAS-mCD8GFP/CyO;UAS-gcmRNAi* (*gcm>gcm KD*) animals that were crossed with $hop^{Tum\text{-}l}$ females (columns 7 and 8). To confirm that the observed phenotypes arise from defects in the hemocytes, $hop^{Tum\text{-}l}$ females were crossed with *repoGal80,gcmGal4* that induces transcription in embryonic hemocytes but not in glia, the other main territory of Gcm expression (columns 13 and 14). Rescue experiments of the $hop^{Tum\text{-}l}$ phenotype were performed by over-expressing *gcm* (*gcm GOF*) or *Ptp61F* (*Ptp61F GOF*). For the latter, two splicing isoforms of the carboxyl terminal of the Ptp61F protein were used, the cytoplasmic isoform (*Ptp61Fa GOF*) and the nuclear isoform (*Ptp61Fc GOF*) (*32*) (columns 9, 10, 11 and 12).

Fig. 3H: rescue experiments of the $hop^{Tum\text{-}l}$ phenotype were performed by silencing *upd2* or *upd3* using *gcmGal4* in $hop^{Tum\text{-}l}$ mutant animals. To be consistent with the data in **Fig. S9A**, we analyzed only female larvae.

Fig. 4A-F: *UAS-*$hop^{Tum\text{-}l}$*/CyOactinGFP* females were crossed with *gcmGal4,UAS-mCD8GFP/CyO,Tb*. To assess the role of *gcm*, *UAS-*$hop^{Tum\text{-}l}$*/CyOactinGFP* females were crossed with *gcmGal4/CyO;UAS-gcmRNAi/+* males, however, the viability of *gcmGal4/UAS-*$hop^{Tum\text{-}l}$*;UAS-gcmRNAi/+* larvae, which all show tumors (100% penetrance), is very low (n=13). To avoid the issue of lethality generated by the wide expression of the driver, *UAS-*$hop^{Tum\text{-}l}$*/CyOactinGFP* females were

crossed with *gcmGal4,UAS-mCD8GFP,repoGal80/CyO,Tb;UAS-gcmRNAi* males to generate or *gcmGal4,repoGal80/UAS-hop^{Tum-l};UAS-gcmRNAi/+* animals. These larvae still show a significantly higher tumor penetrance than that observed in *gcmGal4,repoGal80/UAS-hop^{Tum-l}* animals (45.3%), see **Fig. S10A**.

Fig. 4K,L: to assess the impact of *gcm KD* on wasp encapsulation, we crossed *gcmGal4* or *UAS-gcmRNAi* or *gcmGal4,UAS-mCD8GFP/CyO,Tb;UAS-gcmRNAi* animals with *w^{1118}* to generate *gcmGal4/+*, *UAS-gcmRNAi/+*and *gcmGal4,UAS-mCD8GFP/+;UAS-gcmRNAi/+* respectively.

Fig. S6A-C''': to check the impact of the *gcm* mutation on lamellocyte formation, *gcmGal4,UAS-mCD8GFP/CyO,Tb;UAS-gcmRNAi* females were crossed with *UAS-gcmRNAi* males and *gcmGal4,UAS-mCD8GFP/CyO,Tb* females were crossed with *w^{1118}* males. Both crosses were set at 25°C for 24hrs. The tubes containing embryos were then shifted to 29°C until 3rd instar larval stage to enhance the phenotype.

Fig. S8E-G: to check the impact of the *gcm* mutation on crystal cells' formation, *lzGal4,UAS-mCD8GFP* females were crossed with males of one of the following genotypes: *w^{1118}*, the null mutation *gcm^{26}*, *gcmGal4,UAS-mCD8GFP/CyO,Tb* or *gcmGal4,UAS-mCD8GFP/CyO;UAS-gcmRNAi* (*gcm>gcm KD*).

Fig. S8J,K': to assess the impact of the *gcm* mutation on crystal cells' formation in embryos, *lzGal4,UAS-mCD8GFP* females were first crossed with males *gcm^{26},UAS-RFP/CyOactinGFP*. Males *lzGal4,UAS-mCD8GFP;gcm^{26},UAS-RFP/+* were then crossed with females *gcm^{26},UAS-RFP/CyOactinGFP*.

Fig. S9A: to assess melanotic tumor penetrance in double mutant animals, we only analyzed female larvae, as *hop*, *upd2* and *upd3* are all located on the 1st chromosome.

Fig. S10A: we crossed *srp(hemo)Gal4*, *snGal4* and *repoGal80,gcmGal4* animals with *UAS-hop^{Tum-l}/CyOactinGFP* animals to confirm the phenotype obtained using the *gcm* driver.

Penetrance and expressivity of melanotic tumors

Tumor penetrance was determined by assessing the percentage of 3rd instar larvae carrying one or more tumors. To assess the expressivity of the phenotype, we classified the tumors into three categories according to their size: Small (S), Medium (M) and Large (L) (*17*). A tumor was considered as small when a tiny melanotic mass was documented, see left panel of **Fig. S5A**. We considered a tumor as medium, when the melanotic mass covered ¼ the distance between the borders of a segment, see the middle panel of **Fig. S5B**. A tumor was considered as large when the melanotic spot covered ½ the distance between the borders of a segment, see the right panel of **Fig. S5C**. The expressivity of the melanotic tumor phenotype was then determined by calculating the percentage of small, medium and large tumors counted in each genotype, and this was represented in bar graphs in **Figs. 1E** and **4C**. The p-

values were estimated using the chi-squared test for frequency comparisons between two populations (see also section on statistics).

Hemocyte counting

Ten 3rd instar larvae were washed in Ringer's solution (pH 7.3-7.4) containing 0.12g/L of $CaCl_2$, 0.105g/L KCl, and 2.25g/L NaCl, then dried, and bled in a 96-well U-shaped microtiter plate containing 50µL of Schneider medium complemented with 10% Fetal Calf Serum (FCS), 0.5% penicillin, 0.5% streptomycin (PS), and few crystals of N-phenylthiourea ≥98% (PTU) (Sigma-Aldrich (P7629)) to prevent hemocyte melanization (*33*). For circulating hemocyte collection, the hemolymph was gently allowed to exit, and the total volume was transferred onto a haemocytometer, where the total number of cells were counted, multiplied by the original volume (50µL) and the average number of hemocytes per larva was calculated as described in (*34*). For sessile hemocyte collection, the hemolymph containing the circulating hemocytes was transferred to a first well, while sessile hemocytes were scraped and/or jabbed off the carcass in a second well as described in (*35*) and counted as above. Each counting was carried out at least in triplicates. The p-values were estimated after variance analysis using bilateral student test (see statistics section).

Hemocyte immunolabeling

Ten 3rd instar larvae were treated as stated above and bled in a 96-well U-shaped microtiter plate containing 200µL of Schneider medium. Circulating and sessile hemocytes were collected as indicated above and transferred onto a slide using the Cyto-Tek® 4325 Centrifuge (Miles Scientific). Samples were then marked by Dako Pen (Dako (Code S2002)) to introduce a hydrophobic medium around the transferred material, fixed for 10min in 4% paraformaldehyde/PBS at room temperature (RT), incubated with blocking reagent (Roche) for 1hr at RT, incubated overnight at 4°C with primary antibodies diluted in blocking reagent, washed three times for 10min with PTX (PBS, 0.3% triton-x100), incubated for 2hrs with secondary antibodies, washed two times for 10min with PTX, incubated for 20min with DAPI to label nuclei (Sigma-Aldrich) (diluted to 10^{-3} g/L in blocking reagent), and then mounted in Vectashield® (Vector Laboratories). The slides were analyzed by confocal microscopy (see section below on confocal imaging). The following combination of primary antibodies was used to determine the fraction of lamellocytes: rabbit anti-Serpent (1/1000) (Trébuchet, unpublished results) was used to immunolabel hemocytes. Serpent is expressed in all hemocyte precursors and is required for the development of plasmatocytes and crystal cells (*36*). Mouse anti-L4 (1/30) was kindly provided by I. Ando, L4 is an early lamellocyte marker expressed after immune stimulation (*37*). The fraction of lamellocytes was determined by counting the number of L4/DAPI positive cells out of the total population of hemocytes

present in six confocal fields of vision at 40X magnification and based on Z-series projections. The following combination of primary antibodies was used to determine the fraction of dividing blood cells: rabbit anti-PH3 (1/1000) (Upstate biotechnology #06-570), to assess the mitotic activity, and mouse anti-Hemese (1/30), kindly provided by I. Ando, which recognizes a glycosylated transmembrane protein belonging to the sialophorin protein family and expressed in all larval hemocytes (*38*). The fraction of dividing cells was determined by counting the number of PH3/Hemese/DAPI positive cells out of the total population of hemocytes, as above. The following combination of primary antibodies was used to determine the fraction of crystal cells: rabbit anti-Serpent (1/1000) and chicken anti-GFP (1/500) (abcam #13970), directed against the membrane GFP signal in *lzGal4,UAS-mCD8GFP* driver expressed in crystal cells. The fraction of crystal cells was determined by counting the number of GFP/Srp/DAPI positive cells out of the total population of hemocytes, as above. Secondary antibodies were: donkey anti-rabbit coupled with Cy3 (1/600) (Jackson #711-165-152), donkey anti-mouse coupled with Cy3 (1/600) (Jackson #715-165-151), goat anti-mouse coupled with FITC (1/400) (Jackson #115-095-166), goat anti-mouse coupled with Alexa Fluor 647 (1/400) (Jackson #115-175-100) and goat anti-rabbit coupled with Alexa Fluor 647 (1/400) (Jackson #711-175-144). Each immunolabeling was carried out on three independent trials. The p-values were estimated after variance analysis using bilateral student test (see below).

Crystal cell quantification on larval cuticle

Six 3rd instar larvae were washed in 1X PBS and heated at 70°C for 10min in 500µL of 1X PBS. This procedure leads to the activation of prophenoloxidases (PPOs) within the crystal cells and as a result, these cells appear as black superficial spots on the larval cuticle (*39*, *40*). 3rd instar larval lateral view images were taken under the fluorescent macroscope (Leica, Z16 APO) to cover parts of the dorsal and ventral sides, and superficial crystal cells were counted as described in (*41*). The p-values were estimated after variance analysis using bilateral student test (see below).

Transfection and qPCR in *Drosophila* S2 cells

Six million *Drosophila* S2 cells were plated per well in a 6-well plate with 1.5mL of Schneider medium + 10% FCS + 0.5% PS. Transfections were carried out 12hrs after plating, using the Effectene Transfection Reagent (Qiagen) as described in (*16*). These transfection assays were used to assess the transactivation potential of a) Gcm and b) Hop^{Tum-1}.

a) To determine the role of Gcm in inducing *Ptp61F*, *Socs36E*, *Socs44A*, *upd2* and *upd3* expression, 2µg of *pPac-gcm* expression vector (*42*) was transfected together with 1µg of *4.3kb repo-GFP* (*repoGFP*) (*43*): Gcm induces the expression of its target gene *repo* and drives the expression of GFP,

allowing us to recognize and sort the transfected cells (*43*). Co-transfection of 2µg of *pPac-gal4* driver plasmid and 1µg of *pUAS-GFP* reporter plasmid was performed as a negative control. These results are presented in **Figs. 1B, 3G.**

b) To determine the role of $hop^{Tum\text{-}l}$ in inducing *upd2* and *upd3* expression, 0.5µg of *pPac-gal4* plasmid, 0.5µg of *pUAS-GFP* and 0.5µg of *pUAS-*$hop^{Tum\text{-}l}$ reporters were co-transfected (*26*). Co-transfection of 0.5µg of *pPac-gal4* driver plasmid and 0.5µg of *pUAS-GFP*, and 0.5µg of *pUAS-Empty* was performed as a negative control. These results are presented in **Fig. 3G**.

For the transfection assays, each combination of plasmids was mixed in 90µL of EC buffer and 8µL of enhancer per µg of plasmid followed by 5min incubation at RT. 25µL of Effectene was then added and the mix was incubated at RT for 20min. Then, 500µL of Schneider medium + 10% FCS + 0.5% PS was added to the mix followed by spreading it on the cells. Plates were then incubated at 25°C for 48hrs followed by sorting on a BD FACSAria, according to GFP or RFP expression to obtain more than 80% of transfected cells in the sample (*16*). RNA was then extracted using TRI reagent (Sigma-Aldrich), 1µg was treated by DNAse1 (RNAse-free) (Thermo Fisher Scientific) and reverse transcribed with Superscript II (Invitrogen). Quantitative PCR (qPCR) assays were performed on a lightcycler LC480 (Roche) with SYBR master (Roche) on the equivalent of 5ng of reverse transcribed RNA with the primer pairs targeting *Ptp61F*, *Socs36E*, *Socs44A*, *upd2* and *upd3* listed below. Each PCR was carried out in at least three independent replicates. The quantity of each transcript was normalized to the levels of transcripts of two different housekeeping genes, *Glyceraldehyde-3-phosphate-dehydrogenase-1* (*Gapdh1*) and *Actin-5c* (*Act5c*). The p-values were estimated after comparing control to transfected cells using bilateral student test (see below).

Assessment of *gcm* RNAi efficiency in *Drosophila* S2 cells

Six million S2 cells were transfected as described above with 0.25µg *pPac-gal4* driver, 0.25µg of *pUAS-gcm* expression vector, 0.25µg of *4.3kb repo-GFP* (*repoGFP*) (*43*), 0.25µg of *pUAS-RFP* reporter and 0.25µg of *pUAS-gcmRNAi* vector (Vienna Drosophila Resource Center (VDRC) #dna1452, used to build the *UAS-gcmRNAi* strain Bloomington #31519). The controls were S2 cells transfected with the same set of plasmids except for *pUAS-gcm* or *pUAS-gcmRNAi* that were replaced by *pUAS-Empty* vector. The levels of GFP and RFP were analyzed 48hrs after transfection using FACSCalibur. The GFP levels were measured in RFP positive cells and plotted as histogram in **Fig. S3**.

Transfection and qPCR in leukemia K562 cells

The K562 human immortalized chronic myelogenous leukemia cell line, which harbors the Philadelphia translocation and displays a constitutively active Jak/Stat cascade (*44, 45*) was used to assess

the impact of mGcm2 on Jak/Stat over-activation. Two million K562 cells were plated per well in a 6-well plate with 1.5mL of Roswell Park Memorial Institute medium (RPM1) complemented with 10% FCS, 40µg/mL Gentamicin (Gen), 2mM Glutamine (Glu). Transfection was carried out 12hrs after plating using the Lipofectamine® 2000 Transfection Reagent (Thermo Fisher Scientific). To determine the impact of mGcm2 on *PTPN2*, *SOCS1*, *SOCS3*, *BCL2* and *BCL2L1* expression, 2.5µg of *pCIG* plasmid expressing mouse *Gcm2* (*pCIG-mGcm2*) (*46*) were used in transfection assays; 2.5µg of *pCIG* plasmid were transfected in negative control wells (*pCIG-Empty*). *pCIG* is a mammalian expression vector harboring a CMV promoter and a nuclear GFP.

Each plasmid was mixed with 250µL of RPMI medium + 10% FCS + 40µg/mL Gen + 2mM Glu and incubated at RT for 15min. In parallel, 14µL of Lipofectamine were mixed with 250µL of RPMI medium + 10% FCS + 40µg/mL (Gen) + 2mM (Glu) and incubated at RT for 15min as well. Then, the Lipofectamine/RPMI medium was mixed with the plasmid/RPMI medium and incubated at RT for 15min. Next, the total volume (500µL) was spread on the cells which were then incubated at 37°C (5% CO_2). Cells were then sorted on a BD FACSAria 48hrs after transfection, according to GFP expression. RNA was then extracted and Quantitative PCR (qPCR) assays were performed on a lightcycler LC480 as stated above with the primer pairs targeting *PTPN2*, *SOCS1*, *SOCS3*, *BCL2* and *BCL2L1* listed below. Each PCR was carried out in triplicates on at least three independent replicates. The quantity of each transcript was normalized to the quantity of two different housekeeping genes *Glyceraldehyde-3-phosphate-dehydrogenase* (*GAPDH*) and *Actin-Beta* (*ACTNB*). These results are presented in **Fig. S13A**. The p-values were estimated after comparing control to transfected cells using bilateral student test (see below).

Apoptotic assay in K562 cells

Our data shows that mGcm2 induces the expression of Jak/Stat inhibitors and reduces the expression of anti-apoptotic encoding genes in K562 cells (**Fig. S13A**). Since K562 leukemic cells are immortalized, proliferating cells (*44*, *45*), we assessed the impact of mGcm2 on the profile of apoptosis upon transfection. We used the Amaxa® Cell Line Nucleofector® Kit V (Lonza) to obtain approximately 80% of transfected cells in the sample. One million K562 cells were counted and centrifuged at 200xg for 10min at RT. The supernatant was discarded and the pellet was resuspended with 100µL of RT Nucleofector® solution. 2.5µg of (*pCIG-Empty*) or 2.5µg of (*pCIG-mGcm2*) were mixed with the resuspended pellet. Then, the cell/DNA suspension was transferred into a certified cuvette and electroporation was performed relying on the T-16 program for Nucleofector® I Device (Lonza). Next, 500µL of RT RPMI medium + 10% FCS + 40µg/mL Gen + 2mM Glu was immediately added to the cuvette and gently spread into a 6-well plate containing 3mL of RT RPMI medium + 10% FCS +

40µg/mL Gen + 2mM Glu. Plates were then incubated at 37°C (5% CO_2). Apoptosis was measured 72hrs after transfection (*47*). 500µL of cell suspension were analyzed using the BD FACSCalibur. K562 cell survival and apoptosis were determined by calculating the ratio of GFP+/GFP- cells and GFP+/TB+ cells, after adding 200µL of 0.4% Trypan blue (TB) (Sigma-Aldrich) as a quencher (*48*). The quantification was carried out in three independent trials. These results are presented in **Fig. S13B,C**. The p-values were estimated after comparing control to transfected cells using bilateral student test (see below).

Larval hemocyte RNA extraction and qPCR

Thirty 3rd instar larvae were bled in a 96-well U-shaped microtiter plate containing 200µL of Schneider medium to collect circulating hemocytes as stated above. Cells were centrifuged at 3000rpm for 10min at 4°C. RNA was then extracted using TRI reagent and Quantitative PCR (qPCR) assays were performed on a lightcycler LC480 as stated above with the primer pairs listed below targeting plasmatocytes markers (*49*): *crq*, *Hml*, *lectin-24A*, *eater*, *He* and *NimC1*; lamellocyte markers: *Filamin-240 (cher)*, *α-PS4 (ItgaPS4)*, *α-PS5 (ItgaPS5)*, *mys*, *βInt-v (Itgbn)*, *Tep1*, *Tep4* and *PPO3*; crystal cell markers: *lz*, *hnt (peb)* and *PPO1*; pro-inflammatory cytokines: *upd2* and *upd3*. Each PCR was carried out in triplicates in at least three independent replicates. The p-values were estimated after comparing control to transfected cells using bilateral student test (see below).

Lymph gland immunolabeling

Lymph glands from 3rd instar wandering larvae (6hrs before pupation) were dissected in Ringer's solution (pH 7.3-7.4), fixed for 10min in 4% paraformaldehyde/PBS at RT, incubated with blocking reagent for 1hr at RT, incubated overnight at 4°C with primary antibodies, washed three times for 10min with PTX, incubated for 2hrs with secondary antibodies, washed two times for 10min with PTX, incubated for 20min with DAPI and then mounted on slides in Vectashield®. The slides were analyzed by confocal microscopy (see below). The primary antibody was the mouse anti-L4 (1/30). The secondary antibody was the goat anti-mouse coupled with FITC (1/400) (Jackson #115-095-166). The percentage of precociously histolysed and lamellocyte expressing lymph glands was assessed. Note that in genotypes carrying the $hop^{Tum\text{-}l}$ systemic mutation most lymph glands lose their integrity and display only part of the primary and/or secondary lobes because the tissue undergoes precocious histolysis.

Embryo immunolabeling

Drosophila embryos from overnight egg laying at 25°C on apple agar plates were collected, treated and immunolabeled as described in (*28*). They were dechorionated in bleach, rinsed in water then fixed in 50% heptane/50% PEM-formaldehyde for 25min. Next, they were devitellinized in methanol and heptane

for 1min followed by treatment with PTX and incubation in blocking reagent for 1hr at RT. Then, embryos were incubated overnight at 4°C with primary antibodies, washed three times for 10min with PTX, incubated for 2hrs with secondary antibodies, washed two times for 10min with PTX, incubated for 20min with DAPI and then mounted on slides in Vectashield®. The slides were analyzed by confocal microscopy (see section below). The following combination of primary antibodies was used to label crystal cells: rabbit anti-PPO1 (1/100) was kindly provided by WJ. Lee. PPOs are essential enzymes in the melanization process, where PPO1 is crystal cell specific marker (*39, 50*). Chicken anti-GFP (1/500) (abcam #13970) was used to select for right genotype embryos based on *CyOactinGFP* expression. Rabbit anti-RFP (1/500) (abcam #62341) was directed against the RFP signal driven by *lzGal4* driver expressed in crystal cells. Secondary antibodies used were: donkey anti-rabbit coupled with Cy3 (1/600) (Jackson #711-165-152) and donkey anti-chicken coupled with FITC (1/400) (Jackson #703-095-155). These results are presented in **Fig. S8H-K'**.

Jak/Stat reporter activity in larval somatic muscles

Activation of the Jak/Stat pathway was observed in the muscles using the *10xStat92E-GFP* reporter as indicated in (*4*). The larvae were frozen and mounted between two slides in water. The images of the larvae were taken at the fluorescent macroscope (Leica, Z16 APO) using 10X magnification and 500ms of exposure time. The contrast and luminosity of each image were adjusted using Fiji (*51*); the same correction was applied to all conditions presented in **Fig. 4G-I**.

Wasp survival and encapsulation assays

Wasp parasitization by *L. Boulardi* is commonly used to study the immune response of *Drosophila (3, 4, 52, 53)*. The wasp lays eggs in the *Drosophila* larva, which induces a strong systemic inflammatory cascade that leads to the differentiation of plasmatocytes into lamellocytes and to the encapsulation of the wasp egg *(52)*. The wasp survival and encapsulation assays were conducted as described in *(3, 53)* with some modifications.

For wasp survival, 100 1st instar *Drosophila* larvae (24hrs after egg laying) of the indicated genotypes were transferred into a fresh vial at 25°C. At 2nd instar stage (48hrs after egg laying), 20 couples of *L. boulardi* were added into the vial for infestation for 2hrs, then removed. Following this, the number of wasps hatching from each vial was counted to estimate the % of lethality (1-wasps/*Drosophila* larvae) and plotted in **Fig. 4K**.

For the encapsulation assay, *Drosophila* of the indicated genotypes were allowed to lay eggs for 12hrs at 25°C. The vials containing the embryos were then transferred to 29°C until the 2nd instar stage (48hrs). The *Drosophila* larvae were then exposed to 10 couples of *L. boulardi* for 2hrs at 25°C and after

parasitization the vials were incubated at 29°C until the 3rd instar stage. Wandering larvae were dissected to assess the level of melanization of the wasp larvae: total encapsulation (dead wasp larvae completely melanized), partial encapsulation (living larvae, with some melanization), no encapsulation (living larvae, no melanization). Only *Drosophila* larvae containing a single wasp larva were analyzed and plotted in **Fig. 4L**.

DamID peaks

The DNA adenine methyltransferase identification (DamID) is an antibody independent method allowing the identification of loci bound by transcription factors (*54*, *55*). Using this approach, the Gcm binding sites in the *Drosophila* genome were recently determined (*16*). The peaks indicating Gcm binding onto the *Ptp61F*, *Socs36E* and *Socs44A* loci are represented in **Fig. S2** using the University of California Santa Cruz (UCSC) Genome Browser (https://genome.ucsc.edu).

Statistical analysis

The chi-squared test for frequency comparisons between two populations was used to estimate the p-values between percentages of tumors in 3rd instar larvae and the expressivity of melanotic tumors in various genotypes tested, where bilateral student test is not applicable. Variance analysis using bilateral student tests for unpaired samples was used to estimate the p-values in hemocyte counting, hemocyte immunolabeling and qPCR assays; in each case, at least three independent trials were performed. In all analyses, "ns" stands for not significant, for p-value >0.05; "*" for p-value < 0.05; "**" for p-value < 0.01; "***" for p-value < 0.001.

Confocal imaging

Leica SP5 inverted-based microscope equipped with 20, 40 and 63X objectives was used to obtain confocal images. GFP/FITC was excited at 488nm; the emission filters 498-551 were used to collect the signal. Cy3 was excited at 568nm; emission filters 648-701 were used to collect the signal, and Cy5 was excited at 633nm; emission signal was collected at 729-800nm. A step size between 0.2 and 2µm was used to collect the Z-series of images, which were then treated with Fiji (*51*) to obtain fluorescent images using maximum Z-projections. In all images, the intensity of the signals was set to the same threshold in order to compare the different genotypes.

List of primers

Species	Gene	Forward	Reverse
Drosophila	*Gapdh1*	CCCAATGTCTCCGTTGTGGA	TGGGTGTCGCTGAAGAAGTC

Drosophila	*Act5c*	GCCAGCAGTCGTCTAATCCA	GACCATCACACCCTGGTGAC
Drosophila	*Ptp61F*	GAAACTGCCCCACGTCAAAC	CTTAAGGAATGCGTTCGGCG
Drosophila	*Socs36E*	GTGTCCAACACCAGCTACGA	GAGACCCGTATGTTGACCCC
Drosophila	*Socs44A*	CACTCCAAAATGAGCCACGG	GAGTGGAACCAGCCCTTCTT
Drosophila	*upd2*	ACCCTGGAGTACGGCAATCT	CTGATCCTTGCGGAACTTGT
Drosophila	*upd3*	CCACAGTGAGCACCAAGACT	CAGGTCCCAGTGCAACTTGA
Drosophila	*crq*	GCGATCATCGAAGCGGGAAG	GCATTAGCTTCTGATGGCTC
Drosophila	*Hml*	CCGATGATGACGACGAGGAT	GATGTTGAAGCTAATGTGGC
Drosophila	*lectin-24A*	CAATGCCTACAGCCAGGATT	AGGCTAGGTGACCTCCCATT
Drosophila	*eater*	CGTCTGTCAATGCCTGACGG	AGACACCTTCCAGCTTCGTG
Drosophila	*He*	GGCGGAGCAGTTCACACTAA	AGTTGGAGATGGACGGTTGC
Drosophila	*NimC1*	TCCAATGCCTTTGGGTGTGT	GGTGCGGTATTTTGTCTGCC
Drosophila	*Filamin-240 (cher)*	CGGATCAGTACGAGGAGAAC	GATCGATGGTCTTCAGGTGC
Drosophila	*α-PS4 (ItgaPS4)*	ACACCGACTCCTTGACCATC	TGAGCACGTTGGTTAGCTTG
Drosophila	*α-PS5 (ItgaPS5)*	ACTTCGGTTACTCCGTGGTG	GCACCCACGTCATAGGAATC
Drosophila	*mys*	GATCACGGTACATGCGAGTG	GTACCATGACCGGAGCAGAT
Drosophila	*βInt-ν (Itgbn)*	CTCGCCGGCAACTACTTAAC	GGACAGCCTGATCACTGGTT
Drosophila	*Tep1*	CTGAAGTCTCAGTCAGCCTGACTGGACCTT	CGTAATCGCCTTCTGTTAGCTTCGGAATGT
Drosophila	*Tep4*	GTCAATGTCCATCTGGACTC	GAAGTCCTTGAGATCCATGG
Drosophila	*PPO3*	AGAGCGTGGCGGTGTACGCCAGGGATCGCG	CTTGGGGAAGTAGCCCTCGGCAATTGGTTC
Drosophila	*lz*	CTCCAACTCCATCAGCATCT	CCAATCCGAGTCCGAGTCCG
Drosophila	*hnt (peb)*	TTTCAACGGGAACCAAGCCT	AGCATTTTTCCAACGGCTAGTT
Drosophila	*PPO1*	GATACTCGCGCGCTACAATG	GGTTATTCGTGCTGGACAGG
Human	*GAPDH*	GAGAAGGCTGGGGCTCATTT	AGTGATGGCATGGACTGTGG
Human	*ACTNB*	ATGATGATATCGCCGCGCTC	TCGATGGGGTACTTCAGGGT
Human	*PTPN2*	TGATCACAGTCGTGTTAAACTGC	GCTGCCAAACCATAAGCCAG
Human	*SOCS1*	AGAGCTTCGACTGCCTCTTC	AATCTGGAAGGGGAAGGAGC
Human	*SOCS3*	GTGGCCACTCTTCAGCATCT	CCCCAGAGCTACAGGACTCT
Human	*BCL2*	GGGAGGATTGTGGCCTTCTT	GGGCCAAACTGAGCAGAGTC
Human	*BCL2L1*	ATTGGTGAGTCGGATCGCAG	CGACTGAAGAGTGAGCCCAG

Fig. S1

Fig. S1. Gcm is not expressed in the second hematopoietic wave. Control lineage tracing in the lymph gland using the *Dot>gtrace* line (*56*) (**A,A'**). Lineage tracing in the lymph gland using *gcm>gtrace* (**B,B'**) and *hop*$^{Tum\text{-}l}$*;gcm>gtrace* lines (**C,C'**). The gtrace construct allows the constitutive expression of GFP as soon as the driver (here *Dot>* or *gcm>*) is expressed in the cell. Thus, the GFP signal indicates cells that have expressed the driver during development and/or are still expressing it (*57*). DAPI in blue and gtrace in white, maximum Z-projections. Note the expression of Dot in all the cells of the lymph gland (**A,A'**) and the absence of Gcm expression (**B,B'**) even upon constitutive Jak/Stat activation (**C,C'**). (**D-D'''**) Control lineage tracing showing Gcm expression in the larval nervous system. In this case, the *gcm>gtrace,UAS-RFP* construct makes it possible to specifically identify the cells currently expressing Gcm as RFP positive. Gcm is expressed many cell lineages (mostly glia, gtrace signal) and in the lamina neurons (RFP signal) (*58*).

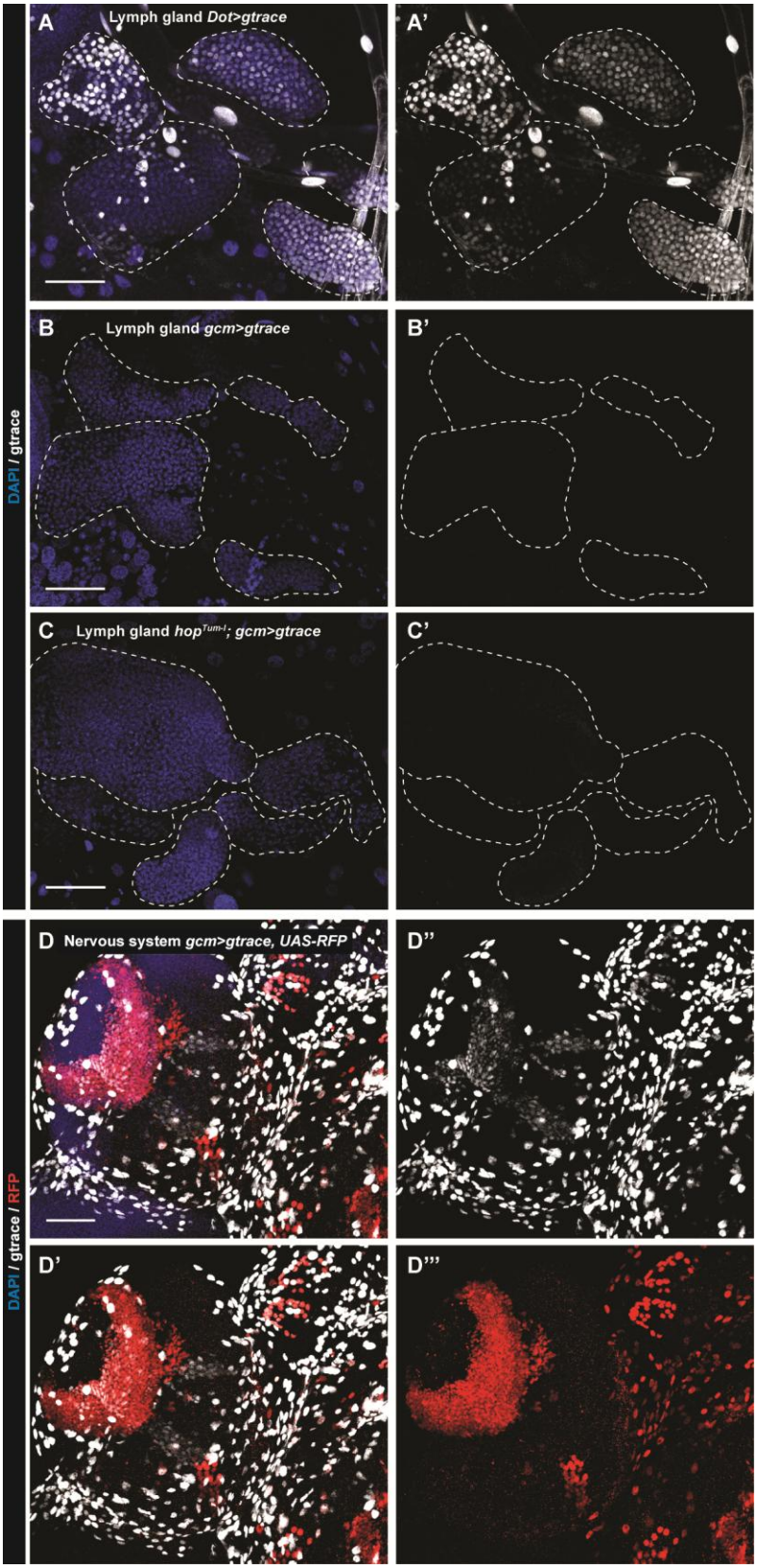

Fig. S2

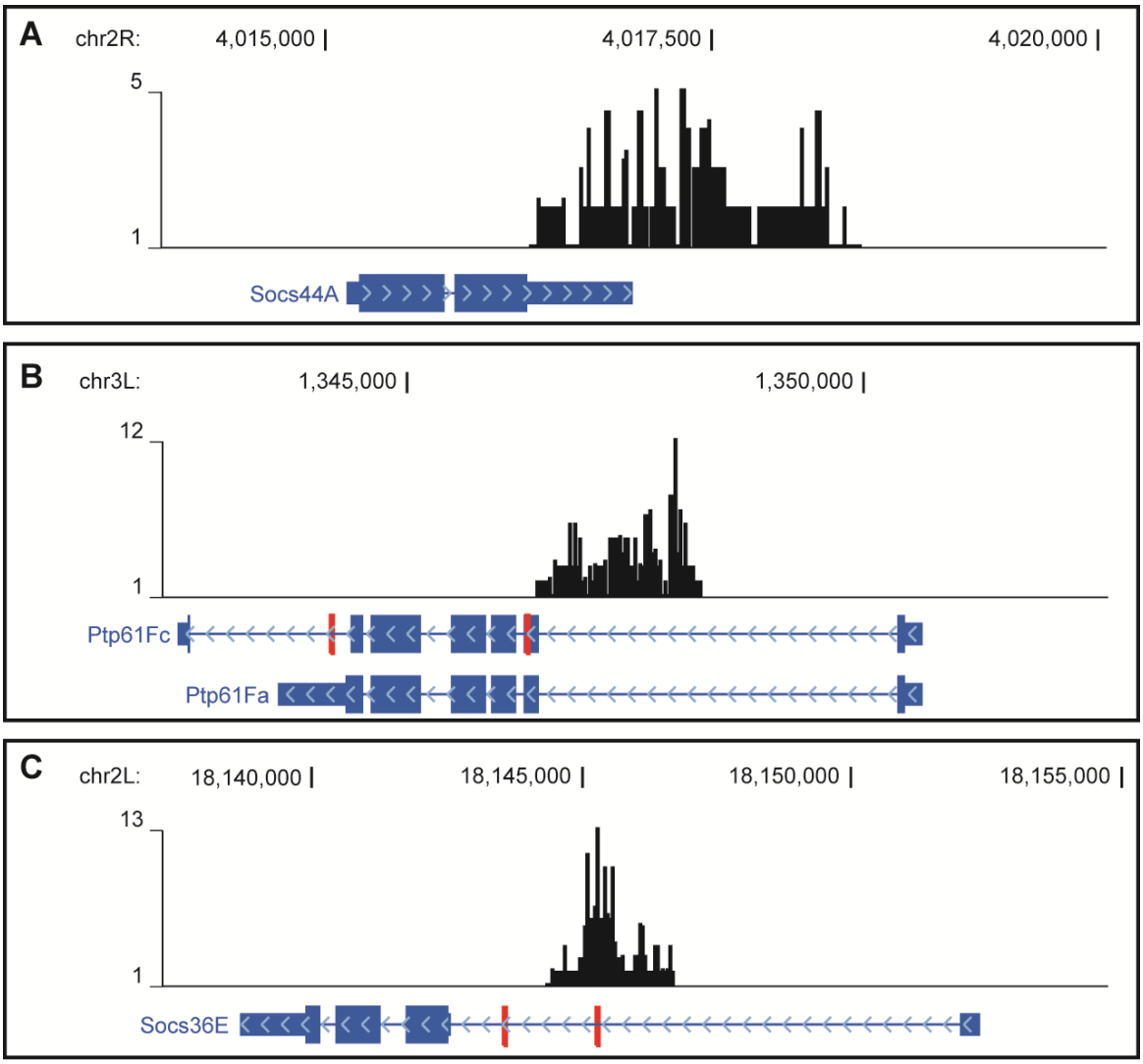

Fig. S2. Gcm induces Jak/Stat inhibitors at the transcriptional level. (**A-C**) Loci containing DamID peaks (black), Gcm binding sites (GBSs, in red), blue arrows within the loci indicate the direction of transcription, histograms above the locus show a region of 1kb on each side of a DamID peak scoring a FDR < 0.001, genomic coordinates of the loci are indicated above the histograms: *Socs44A* (**A**), *Ptp61Fa* (cytoplasmic) and *Ptp61Fc* (nuclear) obtained upon alternative splicing at the 3' carboxyl terminal of Ptp61F (**B**) and *Socs36E* (**C**).

Fig. S3

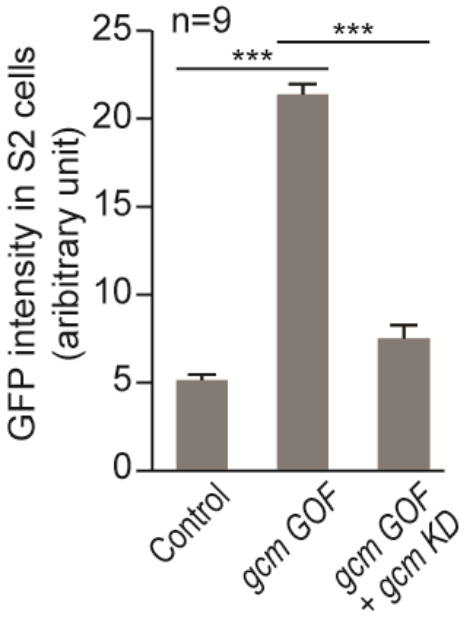

Fig. S3. Efficiency of the *gcm RNAi* construct. *gcm RNAi* efficiency in S2 cells detected by GFP intensity in *gcm GOF* and *gcm KD* as compared to controls (n=9). GFP signal measured upon transfection with *pUAS-gcm* and *repo-GFP* plasmids (column 2) or *pUAS-gcm*, *pUAS-gcmRNAi* and *repo-GFP* plasmids (column 3) respectively. *repo-GFP* represents the reporter for Gcm activity (*43*).

Fig. S4

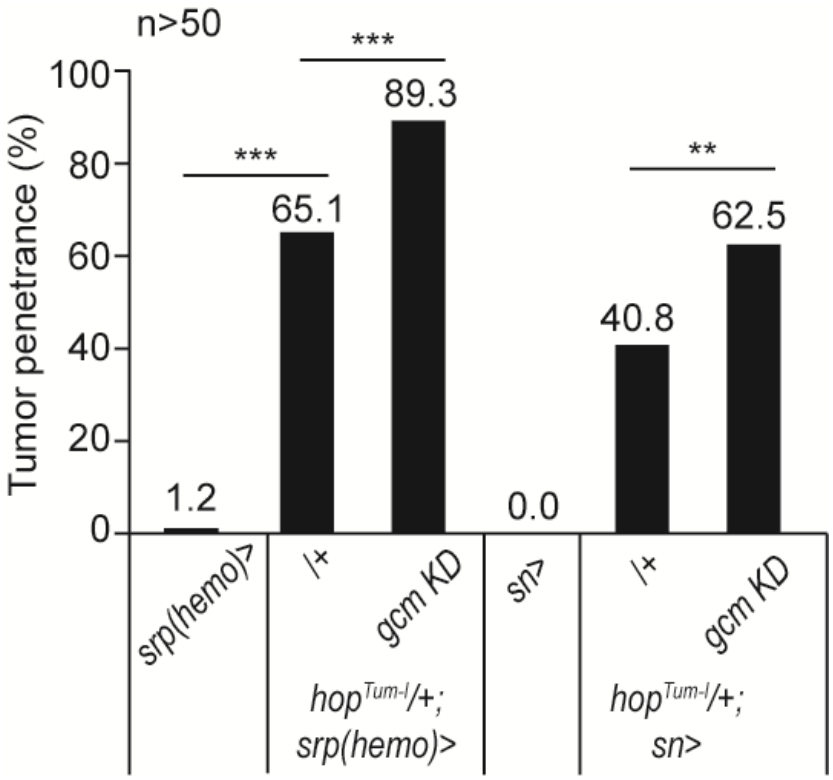

Fig. S4. Gcm inhibits Jak/Stat-mediated melanotic tumor formation. Tumor penetrance in *hop*$^{Tum\text{-}l}$*/+;srp(hemo)* larvae (column two) and *hop*$^{Tum\text{-}l}$*/+;snGal4/+* (column five), or upon *gcm KD* (columns three and six) as compared to controls (n>50).

Fig. S5

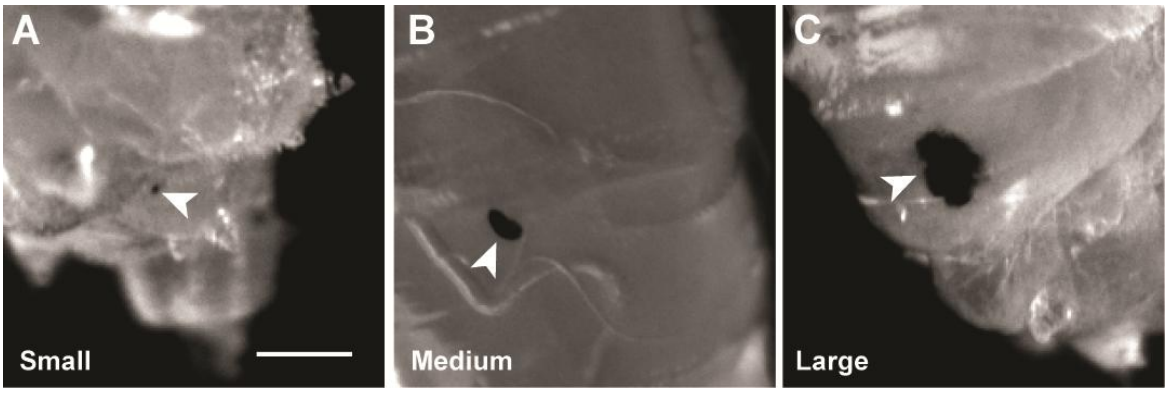

Fig. S5. Sizes of melanotic tumors. Melanotic tumors of different size (arrowheads). See material and methods for quantitative assessment.

Fig. S6

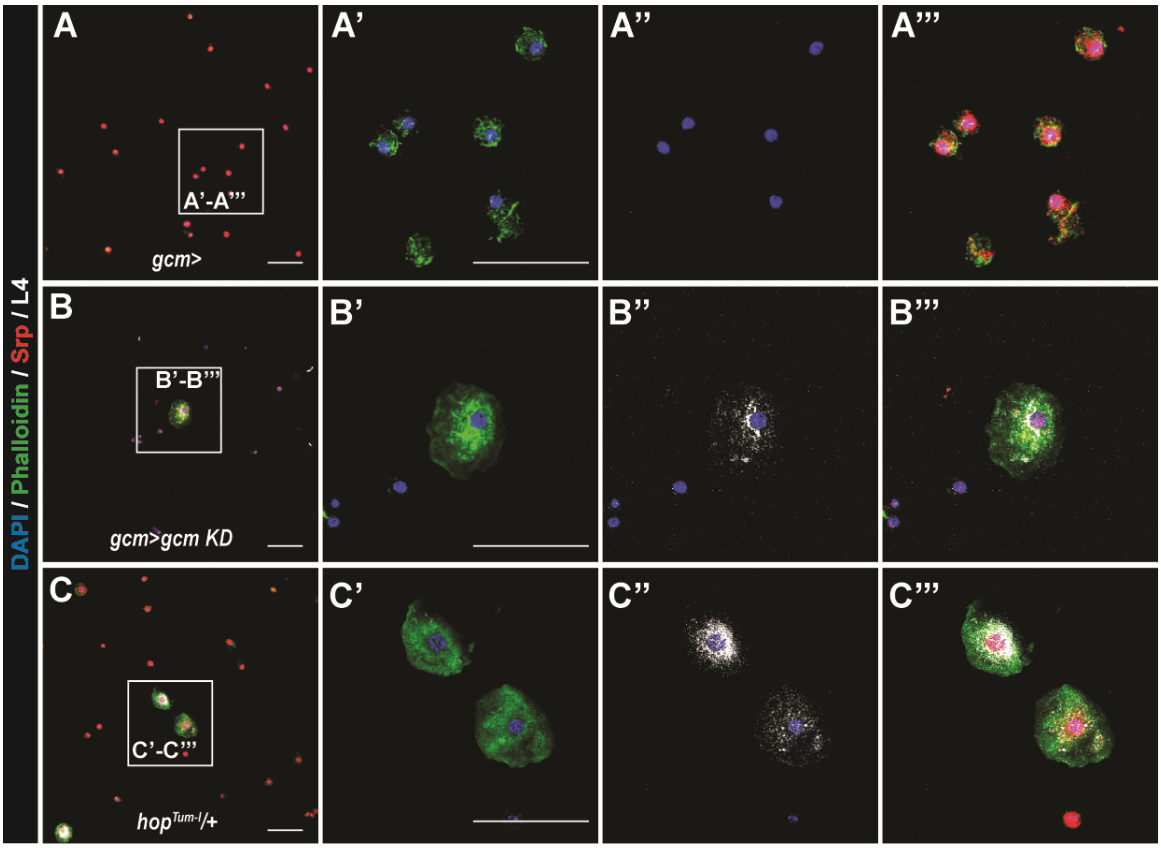

Fig. S6. *gcm KD* animals display lamellocytes. (**A-C'''**) Immunolabeling of hemocytes in the mentioned genotypes (DAPI in blue, Phalloidin in green, Srp in red, lamellocyte marker L4 in white). In all fluorescent confocal images, maximum Z-projections are presented. First panels on the left (**A, B, C**) are low magnification, the selected area (white square) are magnified in the next panels: (**A', B', C'**) show the merge of DAPI and Phalloidin, (**A'', B'', C'')** the merge between DAPI and L4 and (**A''', B''', C'''**) the merge of all markers.

Fig. S7

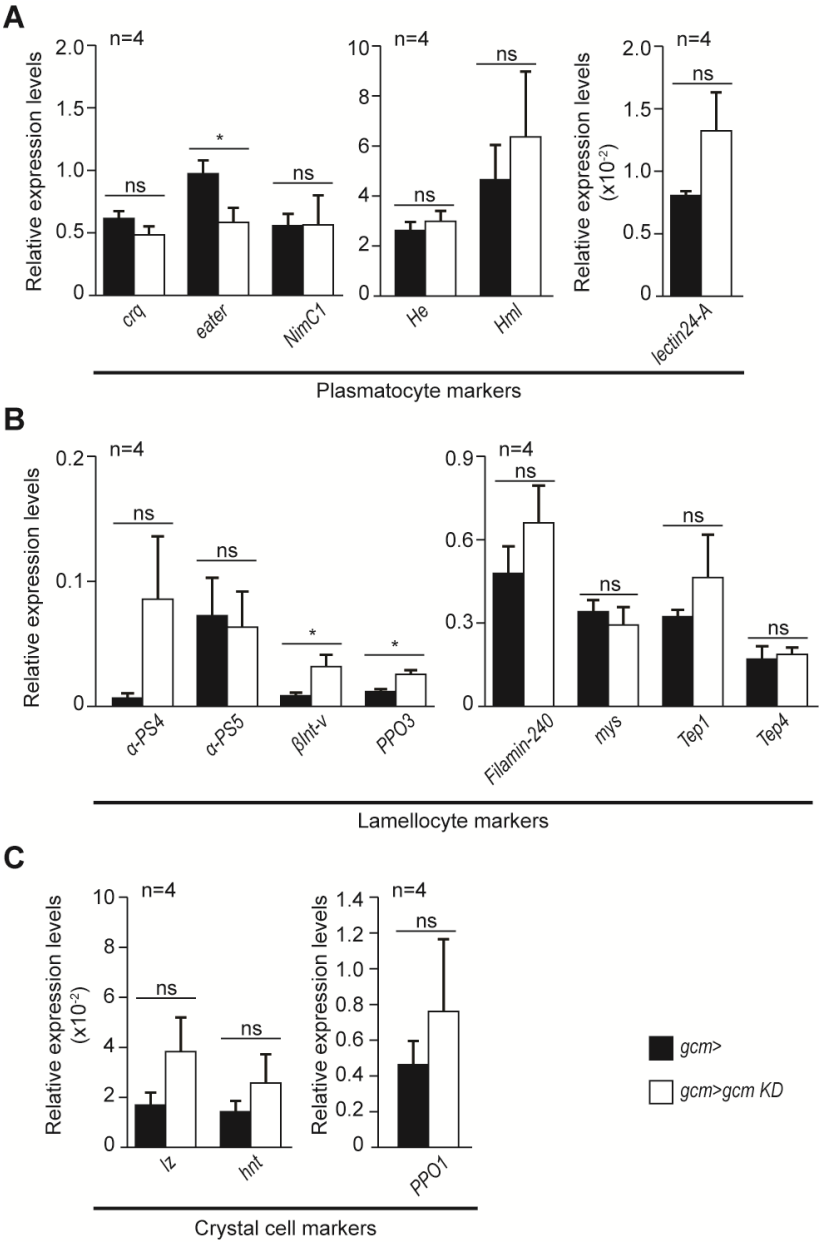

Fig. S7. *gcm KD* hemocytes show altered expression of subsets of plasmatocyte and lamellocyte markers but not crystal cell markers. (**A-C**) Relative levels of expression of plasmatocyte (**A**), lamellocyte (**B**) and crystal cell (**C**) markers in hemocytes from *gcm>* and *gcm>gcm KD* larvae measured by qPCR and normalized to two housekeeping genes (n=4). Note that some markers of plasmatocytes and lamellocytes varies upon *gcm KD* whereas the crystal cells markers are not impacted.

Fig. S8

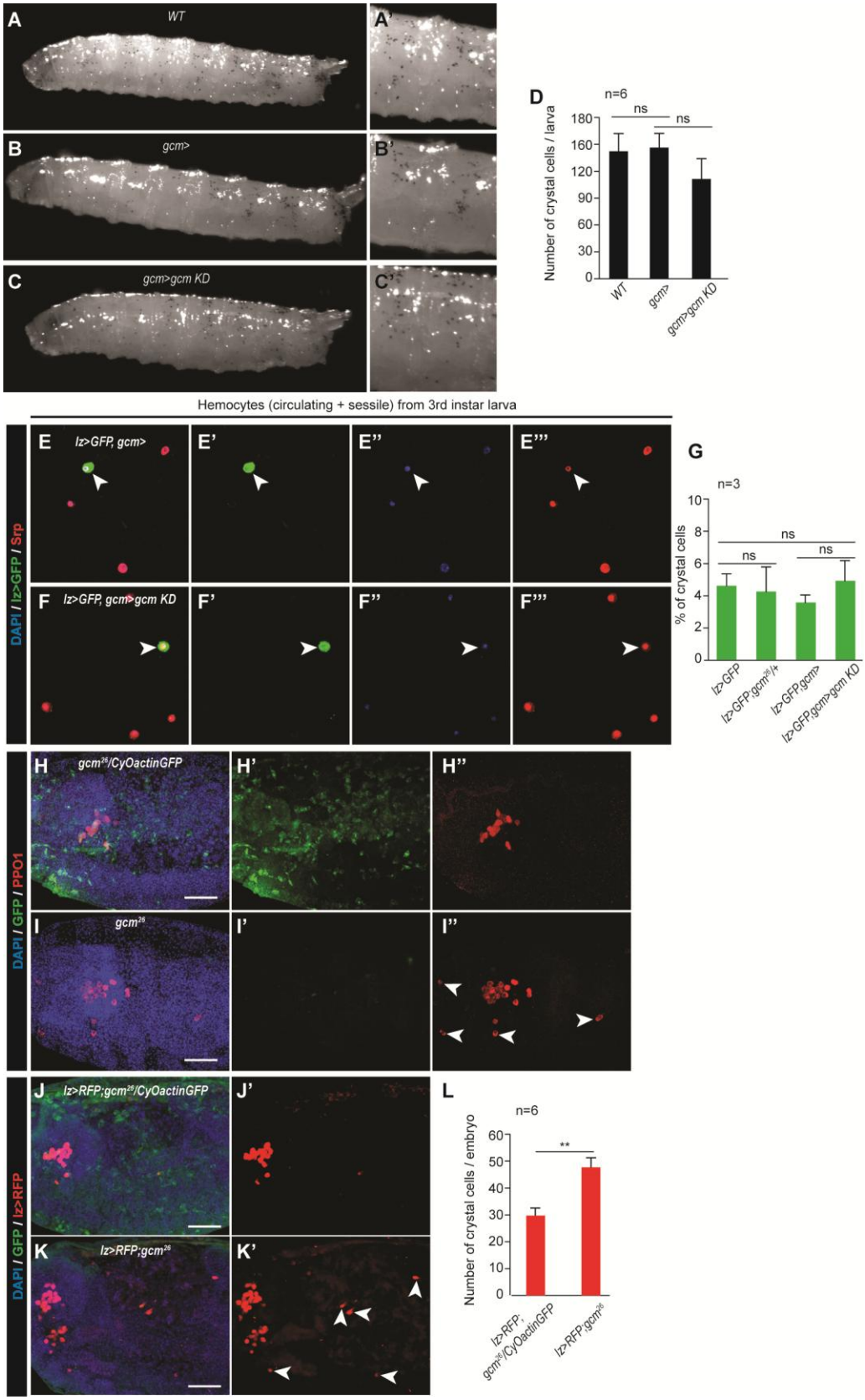
A
WT
A'
B
gcm>
B'
C
gcm>gcm KD
C'
D
n=6
ns
ns
Number of crystal cells / larva
180
160
120
90
60
30
0
WT
gcm>
gcm>gcm KD
Hemocytes (circulating + sessile) from 3rd instar larva
DAPI / lz>GFP / Srp
E
lz>GFP, gcm>
E'
E''
E'''
F
lz>GFP, gcm>gcm KD
F'
F''
F'''
G
n=3
ns
ns
ns
% of crystal cells
10
8
6
4
2
0
lz>GFP
lz>GFP;gcm26/+
lz>GFP;gcm>
lz>GFP;gcm>gcm KD
DAPI / GFP / PPO1
H
gcm26/CyOactinGFP
H'
H''
I
gcm26
I'
I''
DAPI / GFP / lz>RFP
J
lz>RFP;gcm26/CyOactinGFP
J'
K
lz>RFP;gcm26
K'
L
n=6
**
Number of crystal cells / embryo
60
50
40
30
20
10
0
lz>RFP; gcm26/CyOactinGFP
lz>RFP;gcm26

Fig. S8. Crystal cell phenotype in mutant *gcm* embryos and larvae. (**A-C'**) Crystal cells visualized in 3rd instar larvae after heat treatment at 70°C for 10min. (**D**) Average number of crystal cells/larva in *WT*, *gcm>* and *gcm>gcm KD* animals (n=6). (**E-F'''**) Immunolabeling of hemocytes in *lz>GFP, gcm>* and *lz>GFP, gcm>gcm KD* larvae (DAPI in blue, *lz>GFP* in green, Srp in red). (**G**) Average percentage of crystal cells in circulating and sessile compartments in the mentioned genotypes, using the *lz>GFP* driver specific to crystal cells (*59, 60*) (n=3). (**H-I''**) Immunolabeling of gcm^{26}*/CyOactinGFP* (**H,H''**) and gcm^{26} homozygous embryos (**I,I''**) (DAPI in blue, GFP in green, PPO1 crystal cell marker in red). (**H,I**) show merge of the three channels and the subsequent panels show GFP and PPO1 alone. (**J-K'**) Immunolabeling of *lz>RFP,*gcm^{26}*/CyOactinGFP* (**J,J'**) and *lz>RFP,*gcm^{26} embryos (**I,I'**) (DAPI in blue, GFP in green, RFP in red). (**J,K**) show merge of the three channels, (**J',K'**) show RFP labeling alone. (**L**) Number of crystal cells counted in stage 13 *lz>RFP,*gcm^{26}*/CyOactinGFP* and *lz>RFP,*gcm^{26} embryos. Note that in the mutant background crystal cell labeling is also observed at ectopic positions, scattered along the embryo (white arrowheads in **I''** and **K'**) and the total number of crystal cells increases compared to that observed in heterozygous embryos, in agreement with previous data (*13*).

Fig. S9

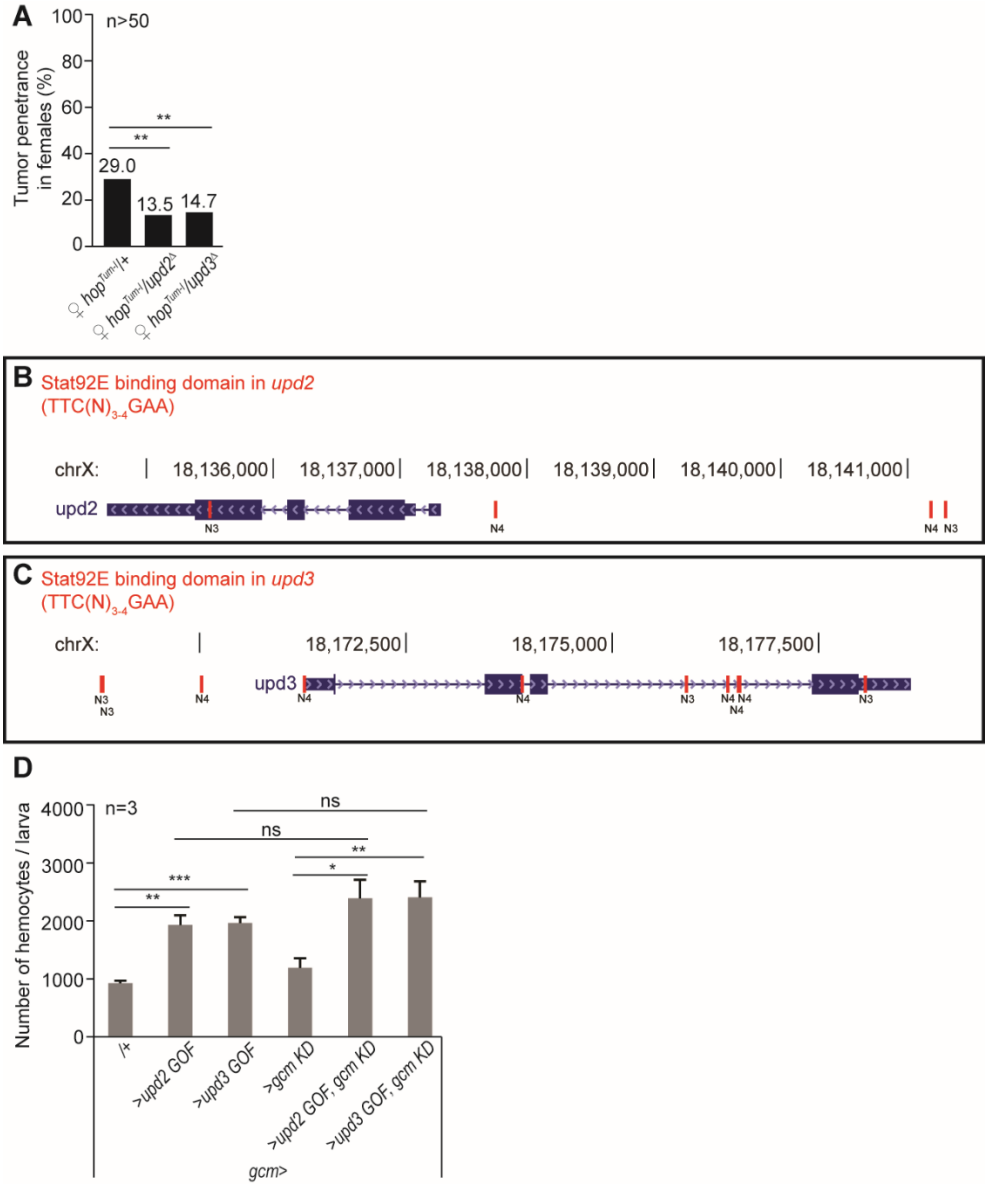

Fig. S9. Interaction between Jak/Stat pathway, Gcm and *upd2*/*upd3* cytokines. (**A**) Tumor penetrance in double heterozygous female larvae $hop^{Tum\text{-}l}/upd2^{\Delta}$ and $hop^{Tum\text{-}l}/upd3^{\Delta}$. (**B,C**) Canonical Stat92E binding sites ($TTC(N)_{3\text{-}4}GAA$) (*61*) at *upd2* and *upd3* loci (in red), symbols as in Fig. S1. (**D**) Total number of circulating hemocytes in the indicated genotypes (n=3).

Fig. S10

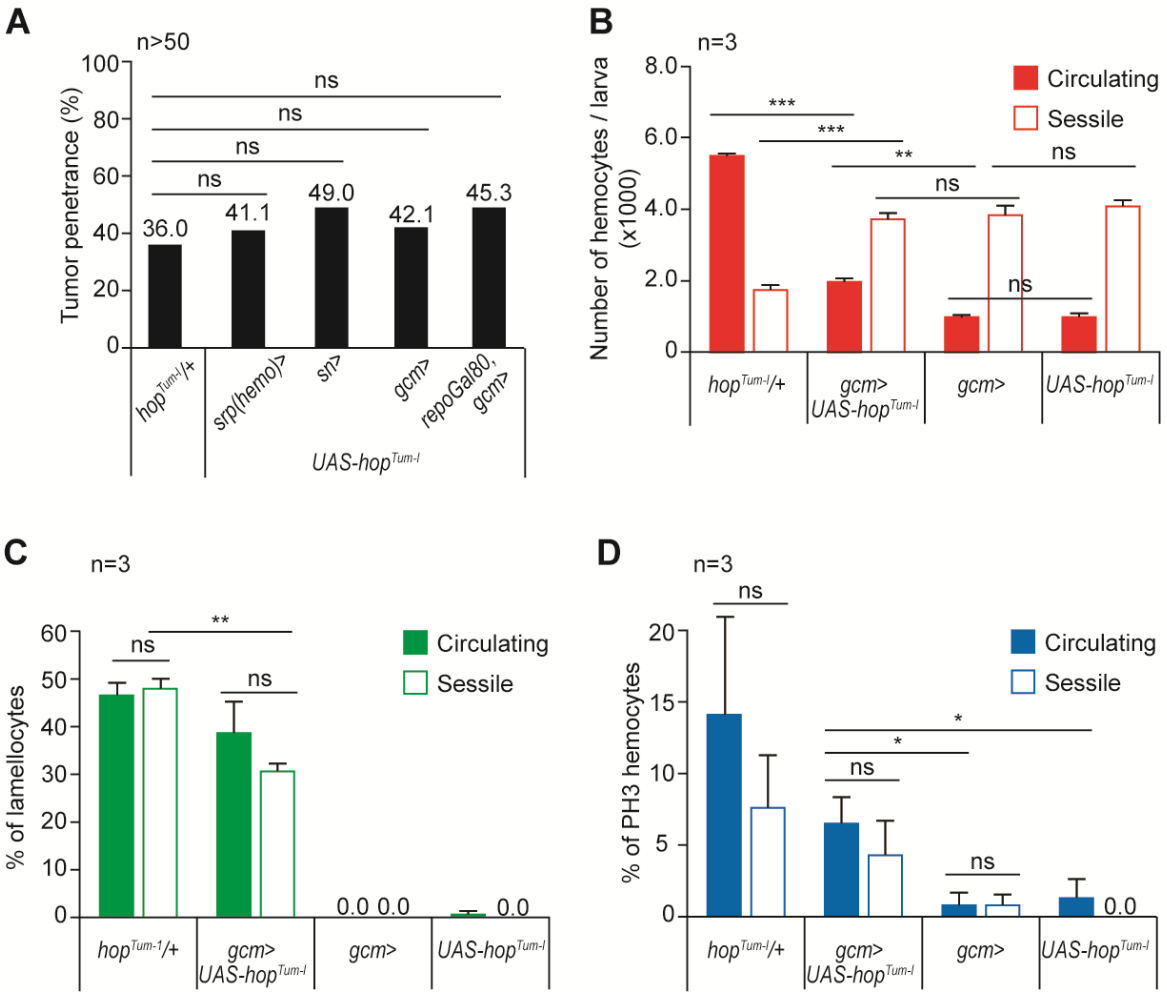

Fig. S10. Jak/Stat pathway in the embryonic hemocytes induces the formation of melanotic tumors in larvae. (**A**) Tumor penetrance in conditional *hop*$^{Tum\text{-}l}$ mutation (*UAS-hop*$^{Tum\text{-}l}$) using *srpHemo>*, *sn>*, *gcm>* and *repoGal80,gcm>* drivers as compared to *hop*$^{Tum\text{-}l}$/+ (n>50). (**B**) Total number of hemocytes in circulating and sessile compartments in systemic and conditional *hop*$^{Tum\text{-}l}$ mutations as compared to controls (n=3). (**C**) Percentage of lamellocytes in circulating and sessile compartments in the mentioned genotypes (n=3). (**D**) Fraction of PH3 positive (dividing) cells in circulating and sessile compartment in the same genotypes (n=3).

Fig. S11

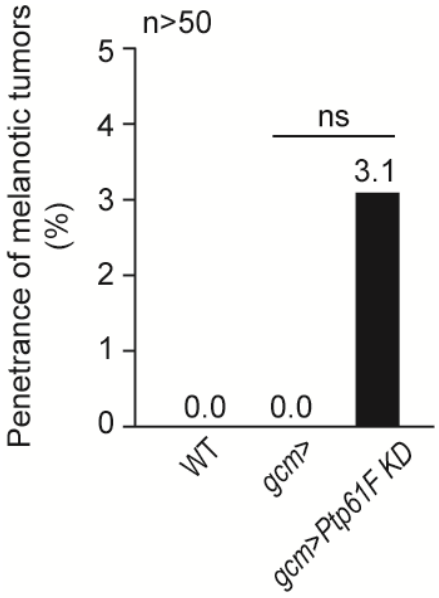

Fig. S11. Silencing Jak/Stat inhibitor *Ptp61F* induces melanotic tumors. Penetrance of melanotic tumors in *gcmGal4>Ptp61F KD* as compared to controls (n>50).

Fig. S12

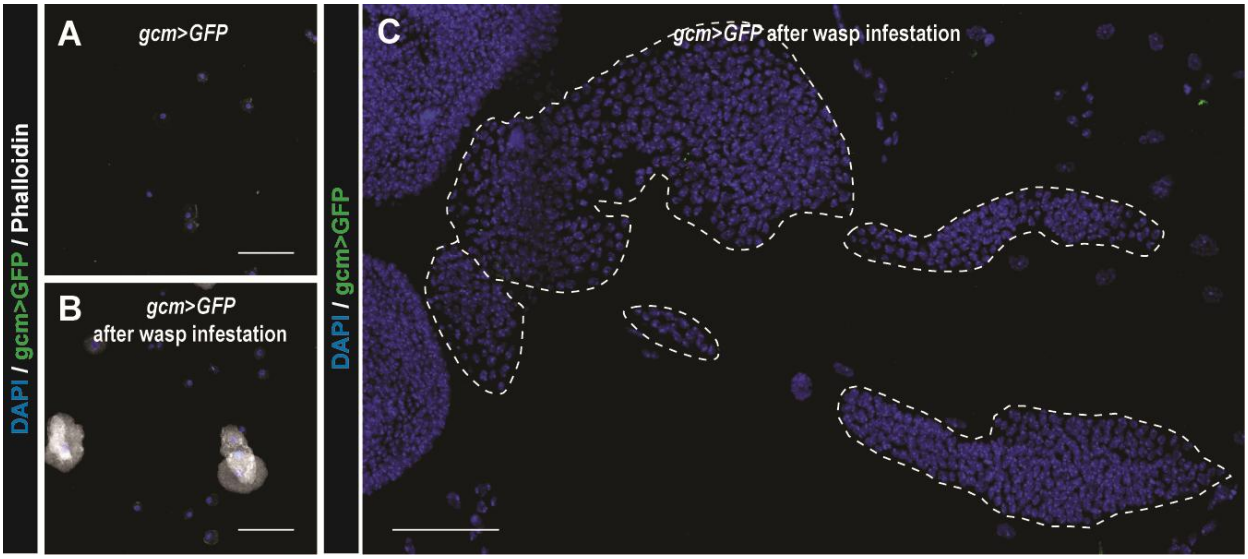

Fig. S12. Gcm is not induced in circulating hemocytes and lymph gland of 3rd instar larva upon wasp infestation. Immunolabeling of hemocytes from 3rd instar larvae *gcm>GFP* without (**A**) or after wasp infestation (**B**). (DAPI in blue, *gcm>GFP* in green and phalloidin in gray). (**C**) Immunolabeling of the lymph gland from 3rd instar larva *gcm>GFP* after wasp infestation. (DAPI in blue, *gcm>GFP* in green).

Fig. S13

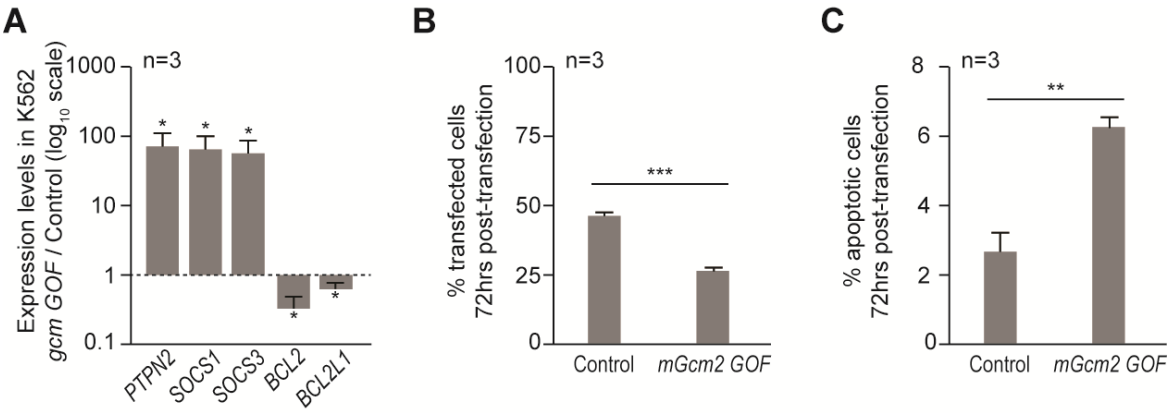

Fig. S13. Gcm induces Jak/Stat inhibitors and apoptosis in a human leukemia cell line K562. The K562 cell line, which harbors the Philadelphia translocation that renders a constitutively active Jak/Stat cascade, was used to assess the impact of mGcm2 on Jak/Stat over-activation. K562 are immortalized proliferating leukemic cells (*44, 45*). To that purpose, we first measured the expression levels of Jak/Stat inhibitors and anti-apoptotic encoding genes upon *pCIG-mGcm2* transfection. Next, we assessed the impact of mGcm2 on the survival and apoptosis of K562 cells. (**A**) Relative expression levels of Jak/Stat inhibitors *PTPN2*, *SOCS1* and *SOCS3* (first three columns) and anti-apoptotic encoding genes *BCL2* and *BCL2L2* (columns four and five) upon *pCIG-mGcm2* transfection (3 independent assays). (**B,C**) Percentage of K562 GFP positive cells and apoptotic cells 72hrs post transfection with *pCIG-mGcm2* (3 independent assays).

Authors contributions:

A.G., W.B. and P.B.C. conceived and designed the experiments. P.B.C., C.D., V.D. and W.B. performed the experiments. A.G., W.B. and P.B.C. analyzed the data and wrote the paper.

Conclusions

In this study, we demonstrate that Gcm is essential to set up the inflammatory machinery in the embryonic plasmatocytes. *gcm KD* during embryonic hemocytes development leads to the production of plasmatocytes that respond much more strongly to inflammatory cues. This is due, partially at least, to the dysregulation of the inhibitors of the JAK/STAT pathways PTP61F, SOCS36E and SOCS44A. In addition, we show that the embryonic plasmatocytes represent major mediators of the inflammatory response by transducing inflammatory signals to the organ of definitive hematopoiesis (i.e. the lymph gland) and to the somatic muscles. The activation of the JAK/STAT pathway in the primitive hemocytes leads to the secretion of proinflammatory cytokines (i.e. Upd2 and Upd3) that activate the JAK/STAT pathway in the somatic muscles and induce the histolysis of the lymph gland. Gcm expression counteracts this process. Our data indicate that Gcm regulates the mobilization of the sessile hemocytes during inflammation as *gcm KD* leads to the increase of the number of hemocytes in circulation and to the decrease of the number of sessile hemocytes. Finally, the inhibitory role of Gcm on the JAK/STAT pathway seems to be conserved in mammals. The over-expression of mGcm2 in mammalian cells in which JAK/STAT is activated leads to the expression of the JAK/STAT inhibitors PTPN2, SOCS1 and SOCS3, and to the apoptosis of the cells.

Given the known impact of immune responses in cancer development, future investigations are required to characterize the precise role of Gcm in inhibiting melanotic tumor formation and as a player involved in controlling the competence to respond to inflammation. This will further elucidate the communication between distinct hematopoietic waves during immune responses. In addition, focusing on the murine Gcm orthologs will possibly reveal conserved immune function and highlight on immune responses in higher organisms.

Chapter II

A novel role of Gcm in *Drosophila* Toll mediated inflammatory response

The Gcm DamID screen highlighted direct interaction with the Toll cascade major inhibitor *cactus*. This prompted me to assess whether Gcm has a regulatory role on the Toll inflammatory pathway and on the formation of melanotic tumors driven by over-activation of that pathway. I show here the inhibitory function of Gcm on the Toll mediated inflammatory response. I also characterized the interaction between Gcm and Toll signaling by assessing the molecular landscape of circulating hemocytes carrying the *gcm* mutation and a mutation over-activating the *Toll* receptor. Interestingly, high throughput sequencing analyses identified genes associated with mitochondria biology as a significant class of modified transcripts, which opens a novel perspective for understanding the molecular bases of melanotic tumor formation induced by Toll over-activation.

Introduction

The Toll signaling cascade initially discovered in *Drosophila* is highly conserved throughout evolution and is considered a model for studying innate immunity (refer to "Introduction") (NUSSLEIN-VOLHARD AND WIESCHAUS 1980; BELVIN AND ANDERSON 1996; ZAMBON *et al.* 2005). The efficiency of an immune response against infections relies on a complex network of events and inter-organ signaling cascades, which are not fully understood. Toll signaling is mainly activated upon infections by Gram-positive bacteria or fungi, leading to the binding of the activated form of the ligand Spatzle (Spz) to the Toll receptor and the recruitment of the adaptor protein dMyD88, in addition to Tube and Pelle in the cytosolic

domain (**Figure 21A**). This is followed by the phosphorylation of the IκB factor Cactus by Pelle, and its dissociation from the NF-κB transcription factors Dorsal/Dif, which allows their translocation to the nucleus to bind and activate the transcription of AMP encoding genes. The N-terminal motif phosphorylated form of Cactus is then directed for degradation (**Figure 21A**) (FERNANDEZ *et al.* 2001; SUN *et al.* 2002; MONCRIEFFE *et al.* 2008; VALANNE *et al.* 2011). A *GOF* mutation within the *Toll* receptor gene, named $Toll^{10b}$ leads to a constitutively active Toll cascade, over-proliferation of plasmatocytes and lamellocyte differentiation (LEMAITRE *et al.* 1995b). This induces auto encapsulation, aggregation of cells and the formation of melanotic tumors in 3rd instar larvae (LUO *et al.* 2002).

The Gcm DamID screen analysis (refer to "Introduction") suggested direct interaction with the Toll cascade major inhibitor *cactus*, calling for an inhibitory role of Gcm onto the Toll pathway at the transcriptional level (**Figure 21B**) (CATTENOZ *et al.* 2016b).

To define the impact of the embryonic transcription factor Gcm on Toll signaling and to understand the interaction between hematopoietic waves, I focused on the mode of action of Gcm on melanotic tumor formation and inflammatory responses induced by the Toll cascade. Also, I performed high throughput sequencing to analyze the molecular landscape of circulating hemocytes, upon combining *gcm* and $Toll^{10b}$ mutant backgrounds.

Results

Gcm inhibits Toll-mediated melanotic tumor formation

Transfection of a *gcm* expression vector (*pPac-gcm*) in the embryonic S2 *Drosophila* cell line induces an increase in the endogenous levels of *cactus* transcripts (**Figure 21C**), which validates the DamID data and spots Gcm as a transcriptional regulator of *cactus*.

Similar to the *in vivo* approach used to study the interaction between Gcm and the JAK/STAT pathway, I asked whether Gcm counteracts the immune response induced by the Toll cascade. For that, I assessed the penetrance of melanotic tumors in $Toll^{10b}$/+ 3rd instar larvae and upon knocking down *gcm* (*gcm KD*) using the embryonic-specific hemocyte driver *gcmGal4* (SOUSTELLE AND GIANGRANDE 2007). Interestingly, *gcm KD* significantly enhances the penetrance of tumors (from 22.2% to 40%) (**Figure 21D, columns one to four from the left**) and over-expressing *gcm* (*gcm GOF*) rescues the $Toll^{10b}$*/gcm>gcm KD* tumor penetrance (**Figure 21D, column five**). I further confirmed the $Toll^{10b}$*/gcm>gcm KD* phenotype by using a second embryonic-specific hemocyte driver *srp(hemo)Gal4* (BRUCKNER *et al.* 2004) (**Figure 22, columns one to three**).

As a second approach, we tested the interaction by using a *gcm* mutation. Since the total lack of Gcm leads to embryonic lethality, we used null *gcm* mutations in heterozygous condition. Combining the $Toll^{10b}$ mutation with the gcm^{26} mutation, which harbors a deletion covering all transcribed sequences (VINCENT *et al.* 1996), or with the *Df132*, a large deletion that removes both *gcm* and *gcm2* loci (KAMMERER AND GIANGRANDE 2001), also significantly increases the penetrance of tumors (to 75.5% and 60%, respectively) (**Figure 21D, columns six and seven and Figure 22, columns four and five**). Furthermore, phenotype expressivity assessed in terms

of melanotic tumor size increases in both *Toll^{10b}/gcm>gcm KD* and *gcm^{26}/+;Toll^{10b}/+* as compared to what observed in *Toll^{10b}/+* larvae (**Figure 21E**). This data strongly reveals that Gcm suppresses the formation of melanotic tumors mediated by systemic and constitutive activation of the Toll pathway.

To further characterize the obtained phenotypes, I counted the total number of circulating hemocytes and estimated the relative percentages and absolute number of lamellocytes. In *Toll^{10b}/+*, the total number of hemocytes increases by more than 3x as compared to that observed in control larvae (**Figure 21F, columns one to four and Figure 21G, first four rows, column two**). In *Toll^{10b}/gcm>gcm KD* and *gcm^{26}/+;Toll^{10b}/+* larvae, this number further increases, but only moderately (1.2x more than in *Toll^{10b}/+* larvae) (**Figure 21F, columns four to six and Figure 21G, bottom three rows, column two**). This suggests that, as for the interaction between Gcm and the proinflammatory JAK/STAT pathway, Gcm acts as a suppressor of the inflammatory response rather than as a tumor suppressor. The percentage of lamellocytes does not change significantly between *Toll^{10b}/+* and *Toll^{10b}/gcm>gcm KD*, and the respective absolute number of lamellocytes only increases by approximately +236 circulating lamellocytes in the double mutants (1159.0 lamellocytes in *Toll^{10b}/+* to 1395.3 in *Toll^{10b}/gcm>gcm KD*) (**Figure 21F, columns four and five (black panels) and Figure 21G, rows four and five, column three**). This reveals that the moderate increase in the total number of hemocytes is mainly due to plasmatocytes. Interestingly, a stronger phenotype was observed in *gcm^{26}/+;Toll^{10b}/+*, where the lamellocyte percentage represents 50% the total number of hemocytes, and the corresponding absolute number significantly increases by approximately +1000 lamellocytes as compared to what observed in *Toll^{10b}/+* animals (1159.0 lamellocytes in *Toll^{10b}/+* to 2255.5 in *gcm^{26}/+;Toll^{10b}/+*) (**Figure 21F, columns four and six (black panels) and Figure 21G, rows**

four and six, column three), revealing that in *gcm*^{26}*/+;Toll*^{10b}*/+* the main increase in circulating hemocytes is due to lamellocytes.

This data reveals slight differences in the pools of plasmatocytes and lamellocytes between in *Toll*^{10b}*/gcm>gcm KD* and *gcm*^{26}*/+;Toll*^{10b}*/+*, however the increase in the total number of hemocytes in circulation is similar, which further confirms the anti-inflammatory role of Gcm.

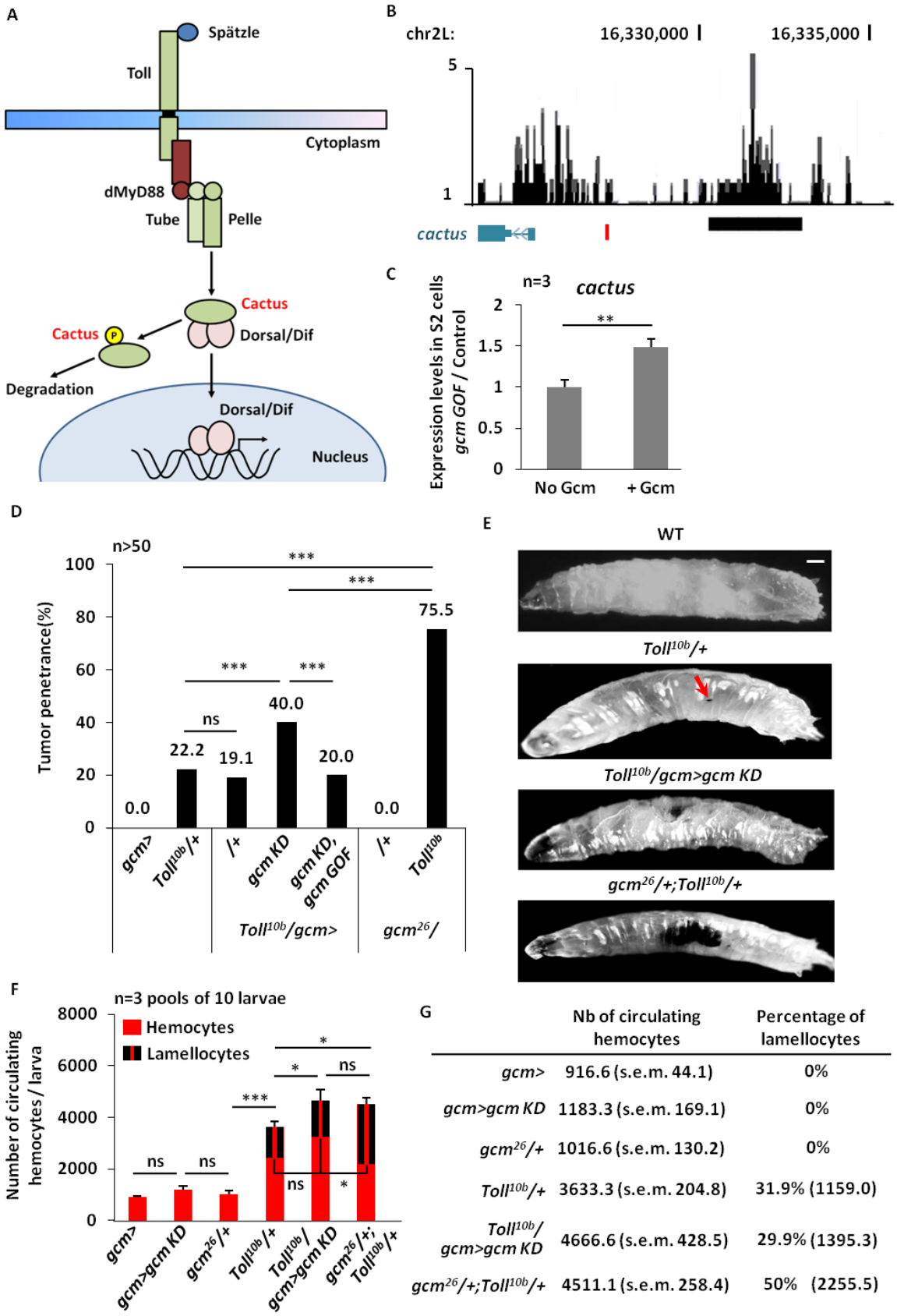

G

	Nb of circulating hemocytes	Percentage of lamellocytes
gcm>	916.6 (s.e.m. 44.1)	0%
gcm>gcm KD	1183.3 (s.e.m. 169.1)	0%
gcm^{26}/+	1016.6 (s.e.m. 130.2)	0%
Toll^{10b}/+	3633.3 (s.e.m. 204.8)	31.9% (1159.0)
Toll^{10b}/ gcm>gcm KD	4666.6 (s.e.m. 428.5)	29.9% (1395.3)
gcm^{26}/+;Toll^{10b}/+	4511.1 (s.e.m. 258.4)	50% (2255.5)

Figure 21: Gcm induces *cactus* and inhibits Toll-mediated melanotic tumors in 3rd instar larvae. (**A**) Schematics of the Toll signaling cascade, direct Gcm target in red. (**B**) *cactus* locus containing DamID peak (black), Gcm binding site (GBS, in red), blue arrows indicate the direction of transcription, histograms above the locus show a region of 1kb on each side of the DamID peak, genomic coordinates of *cactus* locus are indicated above the histogram. (**C**) Relative expression levels of *cactus* in S2 cells upon transfection with *pPac-gcm* (3 independent assays). (**D**) Tumor penetrance in $Toll^{10b}$/+ larvae (column 2), upon *gcm KD* (column 4), upon *gcm GOF* (column 5), in combination with gcm^{26} (column 7) and as compared to controls. In all tumor penetrance assays, we analyzed more than 50 larvae. (**E**) Melanotic tumors in $Toll^{10b}$/+, $Toll^{10b}$/*gcm>gcm KD* and gcm^{26}/+;$Toll^{10b}$/+ larvae. (**F,G**) Total number of circulating hemocytes and percentage of lamellocytes in $Toll^{10b}$/+, $Toll^{10b}$/*gcm>gcm KD*, and gcm^{26}/+;$Toll^{10b}$/+ larvae as compared to controls (3 independent assays); Estimated absolute numbers of lamellocytes indicated in parenthesis in column three of panel G; Note that for hemocyte counting experiments, each assay relies on bleeding 10 larvae/genotype. **P*<0.0.5, ***P*<0.01; ****P*<0.001, ns: not significant; scale bar: 50µm.

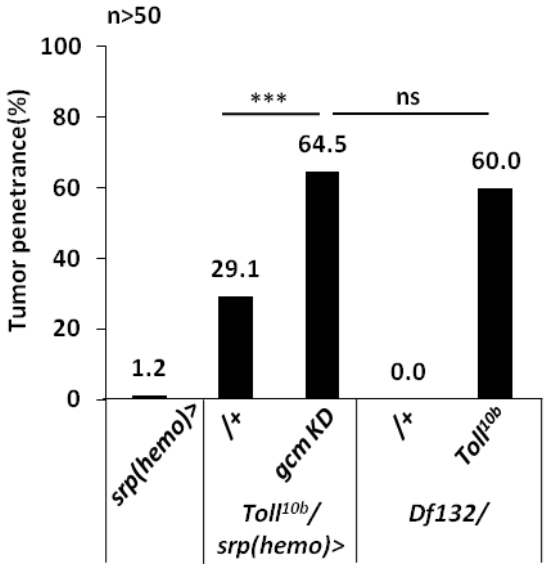

Figure 22: Gcm inhibits Toll-mediated melanotic tumor formation in 3rd instar larvae. Tumor penetrance in $Toll^{10b}$/*srp(hemo)>gcm KD* (column 3) and *Df132/+;*$Toll^{10b}$/+ (column 5) as compared to controls (n>50).

Impact of Gcm on definitive hematopoiesis

Similar to our analysis on the interaction between Gcm and the JAK/STAT pathway, we asked whether the interaction between Gcm and the Toll cascade also impacts the definitive hematopoietic organ, the lymph gland. For that, I assessed the phenotype in terms of precociously histolysed lymph glands in $Toll^{10b}$/+ and $Toll^{10b}$/*gcm>gcm KD*. In both cases, the

lymph gland loses its integrity and displays only part of the primary and/or secondary lobes as compared to the complete lymph glands present in the control larvae at a comparable developmental stage (**Figure 23**). Because of the fully penetrant precocious histolysis phenotype, I decided to also analyze the expression profile of the L4 lamellocyte marker. Comparing the number of L4 expressing cells in *Toll^{10b}/+* and *Toll^{10b}/gcm>gcm KD* lymph glands may not provide accurate information because the L4 marker is cytoplasmic and lamellocytes form aggregates. For this reason, I performed a semi-quantitative analysis by measuring the intensity of GFP signal as a reporter of (L4 expression) in Z-stack confocal projection images. The higher GFP intensity observed in *Toll^{10b}/gcm>gcm KD* (**Figure 23C,D, compare green color intensity and Figure 23E**) suggests a more severe lamellocyte phenotype and hence communication between the hematopoietic waves. This data might further explain the source of the increase in circulating lamellocytes in *Toll^{10b}/gcm>gcm KD* larvae (**Figure 21G, rows four and five, column three**).

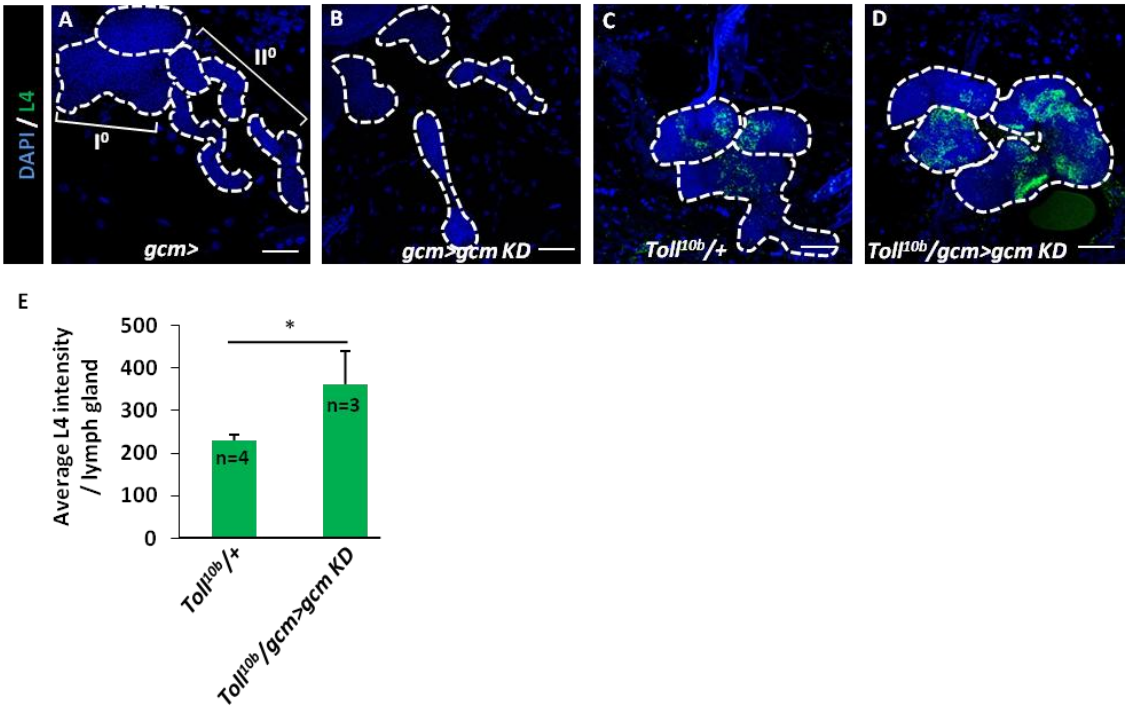

Figure 23: Effects of the *gcm KD* on the *Toll^{10b}* mediated phenotypes. (**A-D**) Lymph glands indicated by hatched lines and immunolabeled with lamellocyte marker L4 (green) and DAPI (blue), scale bar: 50µm. (**A,B**) Control lymph glands. (*gcm>*): I° and II° indicate primary and secondary lobes, respectively. (**C,D**) show hypertrophic glands, lack of lobes and L4 expression. (**E**) Semi-quantitative analysis on the lamellocyte marker L4 intensity/lymph gland in the indicated genotypes. **P*<0.0.5.

Constitutively active Toll cascade inhibits *gcm* expression

So far, our data shows that Gcm inhibits the tumorous phenotype induced by the constitutively active Toll cascade. Interestingly, LPS treatment, which induces TLR signaling, was performed on microglia cultures from *C57BL/6* mice in our laboratory and results in decreased expression levels of the *gcm* murine ortholog *mGcm2* gene (Yuasa et al., in preparation). This prompted us to assess if Toll signaling also impacts *gcm* expression in flies. To that purpose, I performed LPS treatment on S2 cells transfected with a *p6kb-gcm-gal4* plasmid that harbors the 6kb *gcm* promoter sequence (*gcm* reporter) (FLICI *et al.* 2014). This reporter contains the necessary *cis*-regulatory elements for *gcm* expression in embryonic hemocytes (Zsamboki, unpublished data) and harbors at least 2 canonical binding sites for the NF-κB transcription factor Dorsal ($GGG(W)_nCCM$) (MARKSTEIN *et al.* 2002). In addition, ChIPseq data on Dorsal reveals its binding on the *gcm* promoter within the region covered by the reporter (ZEITLINGER *et al.* 2007).

The expression of the AMP encoding gene *AttacinB* is highly induced upon LPS treatment (DE GREGORIO *et al.* 2002) (**Figure 24A**). Interestingly, *gcm* reporter expression levels decrease by 1.5x as compared to what observed in non-LPS treated samples (**Figure 24B**). LPS, however contains bacterial peptidoglycan and acts as an immunostimulant that activates several cascades in *Drosophila*, such as the IMD, JNK and Toll pathways (SLUSS *et al.* 1996; LEULIER *et al.* 2003). This suggests that *gcm* inhibition in S2 cells might not be only due to Toll signaling,

but also to other inflammatory cascades. The above data were further validated *in vivo* upon measuring the endogenous expression levels of *gcm* in $Toll^{10b}$/+ embryos. For this analysis, I used stage (5-7) embryos, when *gcm* is specifically expressed in the hemocyte anlagen (BERNARDONI *et al.* 1997). Interestingly, the levels of *gcm* transcripts decrease by 3x as compared to what observed in control animals (**Figure 24C**), suggesting an inhibitory role of the Toll cascade. In conclusion, the *in vitro* and *in vivo* data suggest that the Gcm-Toll regulatory network is subjected to cross-inhibition between Gcm and Toll signaling. Whether additional inflammatory cascades such as the IMD pathway might be also inhibiting *gcm* remains to be established.

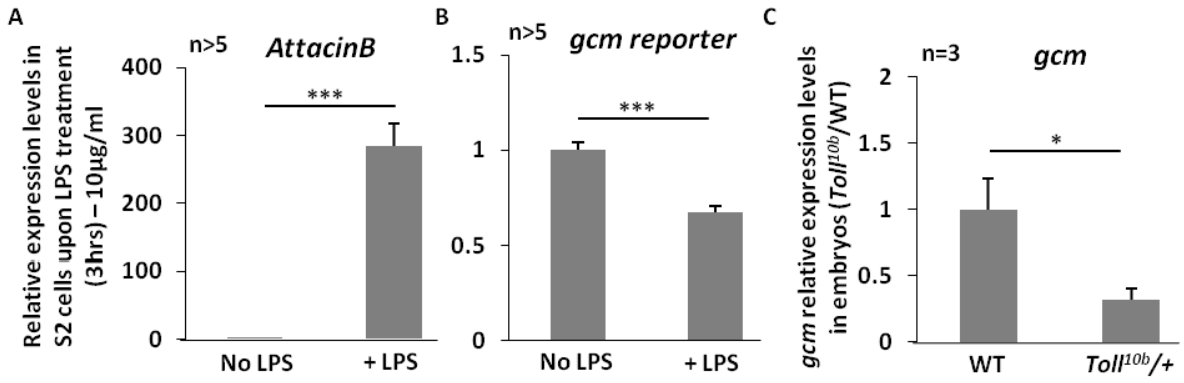

Figure 24: The Toll cascade inhibits *gcm* expression. (**A,B**) Expression levels of *AttacinB* and *gcm* reporter in S2 cells upon LPS treatment for 3hrs (10µg/mL), as compared to what observed in non-treated samples (>5 independent assays). (**C**) Endogenous *gcm* expression levels in WT and $Toll^{10b}$/+ embryos stages (5-7) (3 independent assays). **P*<0.0.5, ***P*<0.01; ****P*<0.001.

Gcm impacts the expression of genes associated with mitochondria in gcm^{26}/+;$Toll^{10b}$/+ circulating hemocytes

To further understand the interaction between Gcm and Toll signaling that contributes to the strong inflammatory response, I investigated the molecular landscape of circulating hemocytes in 3rd instar larvae. For this, high throughput sequencing analysis was performed on

hemocytes from double mutant *gcm*^{26}/+;*Toll*^{10b}/+ and single mutant *Toll*^{10b}/+ and *gcm*^{26}/+ larvae. To assess the efficiency of the hemocyte extraction protocol, the levels of the hemocyte marker *serpent* were measured in whole 3rd instar larvae and extracted hemocytes, where an enrichment of 3x is documented in the latter (**Figure 25A**). Our transcriptome analysis reveals a total of 472 differentially expressed genes in *gcm*^{26}/+;*Toll*^{10b}/+ as compared to what observed in the single mutants.

Interestingly, Go-term analysis on these genes highlights the mitochondria with the highest fold enrichments, the highest number of genes associated with each process and the most significant p-values (**Figure 25C**). The mitochondrion plays crucial roles in cellular energy production, respiration, differentiation, cellular growth, in addition to its involvement in signaling cascades, and in the induction of apoptosis and in inflammation after activating the NF-κB pathway (McBride *et al.* 2006; Lopez-Armada *et al.* 2013). Interestingly, many studies link the mitochondria with cancer, where the immortal cell resists the apoptotic cascade mediated by the mitochondria, leading to metabolic imbalances, mitochondrial respiration deficiency and consequently a deficit in Adenosine triphosphate (ATP) production (Kroemer 2006; Lopez-Armada *et al.* 2013).

Next, we analyzed the group of genes associated with each mitochondrial process. A list of 24 genes is obtained, where 19 are up-regulated and 5 are down-regulated as compared to what was observed with single mutants (**Figure 25D**). Among the up-regulated genes, the heat shock protein *Hsp60D* involved in protein targeting to mitochondria constitutes an interesting hit, due to its link to inflammation. The ortholog gene of *Hsp60D* in mammals induces a proinflammatory response in innate immune cells, and interestingly, this is associated with TLR signaling (Kol *et al.* 2000; Ohashi *et al.* 2000). In *Drosophila*, *Hsp60D* plays role in immune

system regulation and apoptosis (ARYA AND LAKHOTIA 2008). The increase in *Hsp60D* transcript levels correlates with published data on flies infected by Gram-positive and Gram-negative bacteria, where the expression levels of heat-shock proteins are up-regulated by at least 2x upon immune challenge (IRVING *et al.* 2005). The data from mammals and *Drosophila* highlights a strong link between Hsp60D, inflammation and further spots light onto a possible Gcm inhibitory/regulatory impact on Hsp60D that might be associated with the melanotic phenotype obtained in $gcm^{26}/+;Toll^{10b}/+$.

Interestingly, the list of down-regulated genes harbors a total of 5 targets that belong to the cytochrome P450 complex, located within the inner mitochondrial membrane (**Figure 25D**). This complex is encoded by 83 genes in *Drosophila* as compared to the 57 genes found in humans (TIJET *et al.* 2001; SIM AND INGELMAN-SUNDBERG 2010). The cytochrome P450 enzymes are involved in oxidation-reduction processes to metabolize endogenous and exogenous chemicals and compounds, such as hormones, vitamins and drugs (OGU AND MAXA 2000; COELHO *et al.* 2015). Studies also demonstrated a link between cytochrome P450 genes and inflammatory responses in both mammals and *Drosophila*. In line with our data, intraperitoneal acute LPS treatment (1mg/kg) in mice, which activates TLR signaling and induces an inflammatory response similar to that triggered by the $Toll^{10b}$ systemic mutation in flies, leads to a decrease in hepatic cytochrome P450 mRNA levels (THEKEN *et al.* 2011). Moreover, a microarray study performed on *Drosophila* adult males after bacterial infection (DE GREGORIO *et al.* 2002), revealed that Toll signaling represses the expression of 7 cytochrome P450 genes, among which *Cyp4ac1* and *Cyp6w1* are present in our list (**Figure 25D**). The Gcm DamID screen did not reveal any Gcm binding site within the promoter regions of the cytochrome P450 down-regulated genes. These targets might have been missed in the screen as we observed for

other known direct targets of Gcm. Although the cytochrome P450 genes may be indirect targets of Gcm, there may be several explanations to the above finding. If the number of cells in which Gcm binds to the *Cyp* promoter is low, the resulting DamID peak may be very low and be considered significant.

In conclusion, our transcriptome analysis shows that in double mutants $gcm^{26}/+;Toll^{10b}/+$, the mitochondrial molecular landscape of circulating hemocytes is affected, where *gcm* mutation impacts the expression of genes associated with mitochondria that might be linked to the strong increase obtained in the penetrance of tumors and percentage of circulating lamellocytes.

Description of gene clusters from transcriptome analysis

The two tumor-producing genotypes in our transcriptome analysis are $Toll^{10b}/+$ and $gcm^{26}/+;Toll^{10b}/+$. The $gcm^{26}/+$ animals do not show any tumor phenotype and are considered as control animals in our analysis. This suggests the activation of two clusters of genes, the pro-inflammatory cluster, which induces the tumorous phenotypes in $Toll^{10b}/+$ and $gcm^{26}/+;Toll^{10b}/+$ and the anti-inflammatory cluster that inhibits melanotic tumor formation and mainly induced in $gcm^{26}/+$ animals. In contrast, the 472 differentially expressed genes in $gcm^{26}/+;Toll^{10b}/+$ show very different profiles of expression as compared to what observed in the single mutants (**Figure 25B**). The bioinformatic analysis allowed us to classify these genes into 6 clusters according to their expression patterns. Cluster 1 harbors 11.4% of the genes and shows a progressive decrease in gene expression from $gcm^{26}/+$ to $Toll^{10b}/+$, with further decrease in $gcm^{26}/+;Toll^{10b}/+$ hemocytes. This cluster behaves oppositely to cluster 4, which harbors 5.9% of the genes and shows a progressive increase from $gcm^{26}/+$ to $Toll^{10b}/+$ to $gcm^{26}/+;Toll^{10b}/+$ (**Figure 25B**). Cluster 4 fits nicely with the tumor penetrance data, where a progressive increase is documented

from *gcm*^{26}/+ (no tumors) to *Toll*^{10b}/+ (22.2%) to *gcm*^{26}/+;*Toll*^{10b}/+ (75.5%) (**Figure 21D**). We would have expected that the majority of genes are present within these two clusters. Instead, 50% of the 472 genes belong to cluster 5, where the expression levels are very low *Toll*^{10b}/+ animals, they are higher in *gcm*^{26}/+ and further augment in the double mutants *gcm*^{26}/+;*Toll*^{10b}/+ (**Figure 25B**). Next, clusters 3 and 6 show similar gene expression levels in *gcm*^{26}/+ and *Toll*^{10b}/+ that either further decrease in *gcm*^{26}/+;*Toll*^{10b}/+ (cluster 3) or further increase as in the case of cluster 6 (**Figure 25B**). Interestingly, clusters 3 and 6 show the major impact of the double mutants on the expression levels of different genes. This suggests that Gcm and Toll signaling cooperate to further induce or repress genes. Finally, cluster 2 harbors the lowest percentage of genes (3%) with a progressive decrease from *Toll*^{10b}/+ to *gcm*^{26}/+ to *gcm*^{26}/+;*Toll*^{10b}/+. In conclusion, the changes in the expression levels of the 472 differentially expressed genes sheds light onto the impact of Gcm onto wide classes of genes that behave differently during an inflammatory state. Further investigations on each cluster will help in understanding the overall role of Gcm on each category and on inflammation.

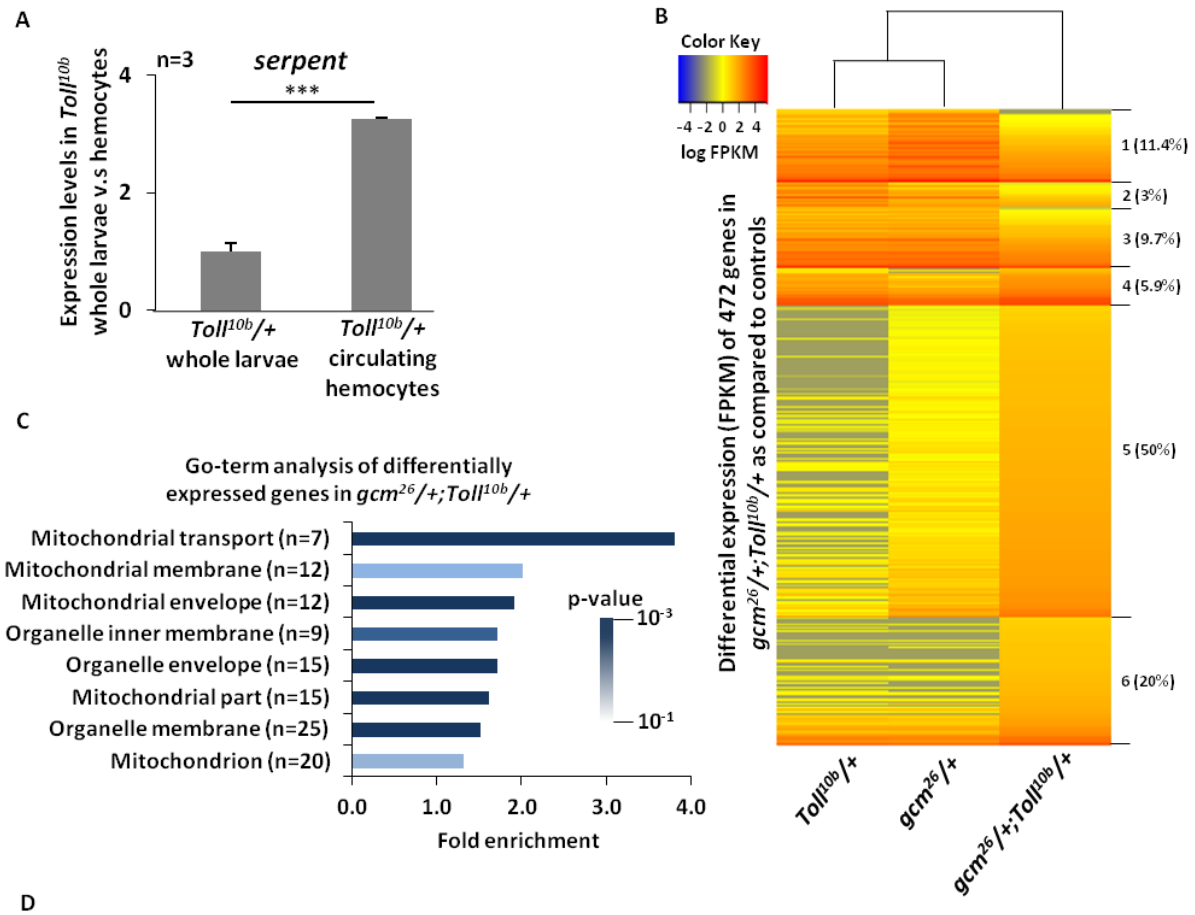

D

Drosophila gene	Gene function
ND-B14.5AL	ATP synthesis coupled electron transport
CG5265	carnitine and fatty acid metabolism
CG14740	citrate synthase activity
fzo	mitochondrial fusion
UQCR-14L	mitochondrial respiratory chain assembly
Porin2 Ucp4B CG7514	mitochondrial transport
bb8	mitochondrion organization
CG2137 P5CDh2	oxidation-reduction process
orb2	positive and negative regulation of translation
Hsc70-1	protein folding
Hsp60D Tim13 tomboy40	protein targeting to mitochondrion
SdhAL	respiratory electron transport chain
Dic2 Dic3	transmembrane transporter
Cyp28a5 Cyp4ac1 Cyp4d1 Cyp6w1 Cyp9b2	oxidation-reduction process

Up-regulated genes

Down-regulated genes

Figure 25: Gcm impacts genes associated with mitochondria in circulating hemocytes. (**A**) Endogenous *serpent* expression levels in $Toll^{10b}$/+ whole larvae and circulating hemocytes (3 independent assays). ***P<0.001 (**B**) Heatmap representing the 472 differentially expressed genes (Fragments Per Kilobase Million) in gcm^{26}/+;$Toll^{10b}$/+ as compared to what is observed in single mutants; Note the classification of genes into 6 clusters according to their expression levels in the 3 tested genotypes, and the percentage of genes associated with each cluster is indicated in parenthesis. (**C**) Go-term analysis on the differentially expressed genes in gcm^{26}/+;$Toll^{10b}$/+ showing the fold enrichment of various mitochondrial processes and the corresponding number of genes associated with each process. p-values range from 0.001 to 0.1. (**D**) List of up-regulated (pink) and down-regulated (green) genes and their respective functions.

Discussion

The Gcm DamID screen highlighted direct interaction with the Toll cascade major inhibitor *cactus*. In this chapter I show the regulatory function of Gcm on the Toll mediated inflammatory response and its effect in inhibiting melanotic tumor formation induced by the constitutive activation of the Toll cascade. I also highlight the impact of Gcm onto the production of lamellocytes in the definitive hematopoietic organ, the lymph gland, further demonstrating that the two hematopoietic waves interact during the inflammatory response. Finally, to understand the interaction between Gcm and Toll signaling, I show that the *gcm* mutation impacts the expression of a wide set of genes associated with the mitochondria.

Gcm inhibitory role on Toll signaling cascade

Gcm is a transcription factor transiently expressed and essential for the development of embryonic plasmatocytes (BERNARDONI *et al.* 1997; LEBESTKY *et al.* 2000). My data shows for the first time the effect of a developmental factor specifically expressed in the primitive wave on inflammatory cascades like the Toll and the JAK/STAT pathways, where Gcm inhibits melanotic tumor formation induced by the over-activation of the JAK/STAT and Toll cascades. Thus, Gcm

regulates the competence to respond to inflammation. In addition, my data describes for the first time the communication occurring between the primitive and the definitive hematopoietic waves.

The DamID screen highlighted the Toll cascade major inhibitor *cactus* as a Gcm downstream target (CATTENOZ *et al.* 2016b). This reveals the direct connection between Gcm and the Toll pathway. My data shows that Gcm inhibits the Toll-mediated melanotic tumor formation. In this context, it would be necessary to validate *cactus* as a potential candidate required in the cell-autonomous and non-autonomous mediated melanotic tumor formation. Studies revealed that *cactus* mutant animals develop melanotic tumors (MAKHIJANI *et al.* 2011). Although *cactus* represents an important target and is associated with melanotic tumors when mutated (LEMAITRE *et al.* 1995b; MINAKHINA AND STEWARD 2006; VALANNE *et al.* 2011), it is very likely that other Toll cascade inhibitors are also downstream to Gcm. *Spn77Ba* and *Spn27A* are indirect Toll cascade inhibitors and Gcm DamID targets. These genes code for serine protease inhibitors that repress a protease-phenoloxidase (PO) cascade and ultimately melanin synthesis, which in turn prevents melanization in normal conditions. They regulate the Toll cascade by preventing excess melanin production by lamellocytes, which are also produced upon Toll cascade activation (TANG *et al.* 2008). Interestingly, microarray studies revealed that *Spn27A* is down-regulated in larval hemocytes upon immune challenge (IRVING *et al.* 2005). In addition, *Spn27A* mutant larvae show a melanotic phenotype linked to the activation of the Toll pathway (NAPPI *et al.* 2005). This further highlights the importance of Serpins in melanotic tumor formation. In this line, investigating further the impact of Gcm on Serpins and *cactus* in the context of melanotic tumor formation will help in understanding the overall role of the developmental factor Gcm on inflammation. In other words, we ask whether Gcm inhibits lamellocyte differentiation through Serpins.

The slightly different phenotypes observed upon using the *gcm*^{26} null mutation and the *gcm KD* approach (number of lamellocytes: 2255.5 in *gcm*^{26}*/+;Toll*^{10b}*/+* as compared to 1395.3 in *Toll*^{10b}*/gcm>gcm KD*, penetrance of tumors: 75.5% in *gcm*^{26}*/+;Toll*^{10b}*/+* as compared to 40% in *Toll*^{10b}*/gcm>gcm KD*) may have several explanations that are not mutually exclusive: 1) the levels of *gcm* transcripts may differ between *gcm KD* and *gcm*^{26}*/+* animals. 2) *gcm* silencing through the *Gal4-UAS* system needs time, through the expression of the *Gal4* driver and the *UAS RNAi* reporter, whereas in the *gcm*^{26} null mutation, *gcm* expression is affected from the earliest embryonic stages. qPCR analysis at different stages will help in understanding the observed phenotypes.

Comparing the JAK/STAT and Toll phenotypes reveals an overall increase in the total number of circulating hemocytes in both *hop*$^{Tum-l}$*/+* and *hop*$^{Tum-l}$*/gcm>gcm KD* (**Results, Chapter I, Figure 1F**) as compared to what observed in *Toll*^{10b}*/+*, *Toll*^{10b}*/gcm>gcm KD* and *gcm*^{26}*/+;Toll*^{10b}*/+* (**Figure 21F, columns four to six and Figure 21G, rows three to six, column two**). The expressivity in terms of size of melanotic tumors associated with the *Toll*^{10b} systemic mutation is also higher as compared to what observed in the *hop*$^{Tum-l}$ systemic mutation and more melanized tissues are observed in *gcm*^{26}*/+;Toll*^{10b}*/+* animals as well (**Figure 21E**). This suggests that more hemocytes are recruited to the melanotic masses when a *Toll*^{10b} systemic mutation is present as compared to a *hop*$^{Tum-l}$ mutation, which in turn may lead to a decrease in the total count of circulating hemocytes in 3rd instar larvae. This likely explains the overall difference in the total number of circulating hemocytes in the *hop*$^{Tum-l}$ and *Toll*^{10b} backgrounds.

Gcm impact on mitochondria and melanotic tumors

In *Drosophila*, the mitochondria are also studied in the context of melanotic tumor formation. *Heixuedian* (*heix*) is a potential melanotic tumor suppressor gene that acts as a mitochondrial electron carrier (XIA *et al.* 2015). *heix* mutation leads to lymph gland hypertrophy, over-proliferation of hemocytes and the formation of melanotic tumors. Interestingly, this phenotype is linked to the activation of JAK/STAT, Toll and IMD pathways (XIA *et al.* 2015). We would have expected to have decreased expression levels of *heix* upon an inflammatory response. However, our transcriptome data reveals its progressive increase from gcm^{26}/+ to $Toll^{10b}$/+ to gcm^{26}/+;$Toll^{10b}$/+. This makes it belong to cluster 4, which fits nicely with the tumor penetrance data, where a progressive increase is documented from gcm^{26}/+ (no tumors) to $Toll^{10b}$/+ (22.2%) to gcm^{26}/+;$Toll^{10b}$/+ (75.5%). The importance of this gene falls in its unexpected behavior. This might be due to the following hypothesis that in gcm^{26}/+, although no penetrance of tumor is documented, but the mitochondrial machinery might be impacted, where *heix* acts as a mitochondrial electron carrier. This is a key aspect to investigate in order to understand the unexpected behavior of *heix*.

The up-regulated and/or down-regulated sets of genes reveal potential roles in inducing a proinflammatory and/or anti-inflammatory conditions. Our data highlights *Hsp60D* and the cytochrome P450 genes as interesting hits due to their link to inflammation in mammals and *Drosophila* (KOL *et al.* 2000; OHASHI *et al.* 2000; DE GREGORIO *et al.* 2002; IRVING *et al.* 2005; THEKEN *et al.* 2011). Future studies will validate potential candidates *in vitro* and *in vivo*, such as *Hsp60D* from the up-regulated list and *Cyp4ac1* from the down-regulated list. For the *in vitro* assay, assessing the expression levels of *Hsp60D* and cytochrome P450 encoding genes by qPCR on circulating hemocytes from gcm^{26}/+;$Toll^{10b}$/+ will validate the transcriptome data. For the *in*

vivo assay, assessing tumor penetrance upon knocking down *Hsp60D* (VDRC #19167), which is a Gcm DamID target in embryonic hemocytes or combining a *Cyp4ac1* mutation with a $Toll^{10b}$ background ($Toll^{10b}$/*gcm>Hsp60D KD* or $Toll^{10b}$/*Cyp4ac1*), will reveal the impact of these genes on melanotic tumor formation/inhibition, and will further elucidate the relation between Gcm, mitochondria and Toll signaling. Moreover, it is important to assess the mitochondrial distribution in hemocytes using a *UAS-mitoGFP* strain (Bloomington #8442), which expresses GFP with a mitochondrial import signal, along with an antibody against the mitochondrial ATP synthase (anti-ATP5A abcam #14748), to evaluate the efficiency of the mitochondrial machinery upon *gcm KD* in different genotypes.

It remains to be seen how the link is established between Gcm, mitochondria and Toll signaling. Future *in vivo* studies will elucidate the impact of Gcm on the mitochondrial function and efficiency in hemocytes. Moreover, these analyses will further help understanding the communication between the primitive hematopoiesis and post-embryonic organs involved in immunity.

Chapter III

Published article: An evolutionary conserved interaction between the Gcm transcription factor and the SF1 nuclear receptor in the female reproductive system

This chapter of my PhD thesis refers to a research article published in "Scientific Reports" (CATTENOZ *et al.* 2016a).

In mammals, the maturation and preservation of spermatozoids after copulation, occurs upon secretion of specific molecules by the female reproductive tract epithelium (SCOTT 2000; SUAREZ AND PACEY 2006; CATTENOZ *et al.* 2016a). Interestingly, female insects like *Drosophila* display a tissue called "spermatheca" that has similar roles in preserving the spermatozoids. Molecules involved in attracting and storing the sperms are produced by the secretory cells (SC) surrounding the spermatheca tissue (WOLFNER 2011; CATTENOZ *et al.* 2016a). Hr39 is a hormone receptor in *Drosophila* that plays role in SC generation and ensures fertility. Its mammalian orthologs are the nuclear receptor 5A1 and 5A2 (NR5A1 and NR5A2). The former is involved in cell proliferation, bile acid metabolism and steroidogenesis (LEE AND MOORE 2008), whereas the latter plays role in the development of the pituitary gland, adrenal gland and gonads (PARKER AND SCHIMMER 1997). Mutations in *NR5A2* are associated with endometriosis, the main cause of women infertility (ATTAR *et al.* 2009; NOEL *et al.* 2010; CATTENOZ *et al.* 2016a).

Here we report Gcm as a major transcriptional regulator of *Hr39* during spermatheca development. In addition, the absence of Gcm prevents the generation of SCs and results in full female sterility in flies. To transpose our results to mammals, we show that Gcm expression alters the DNA methylation profile of the *mouseNr5a1* (*mNr5a1*) locus in mouse embryonic

fibroblasts (MEF) cells. Moreover, we report that Gcm orthologs (mGcm1 and mGcm2) known to be expressed in the placenta, parathyroid gland, thymus, kidney and nervous system (SCHREIBER *et al.* 2000; HASHEMOLHOSSEINI AND WEGNER 2004; THOMEE *et al.* 2005; HITOSHI *et al.* 2011) are expressed in the uterus as well.

My contribution to this study was by performing transfection assays with *pCIG-mGcm1* and *pCIG-mGcm2* in mammalian HeLa cells followed by qPCR assays to measure the expression levels of *hNR5A1* and *hNR5A2* (**Figure 5A,D in the following manuscript**). In addition, I performed mouse dissections from *C57BL/6* females, followed by RNA extractions from the uterus and qPCR assays to assess *mGcm1*, *mGcm2* and *mNr5a1* expression levels (**Figure 5F in the following manuscript**).

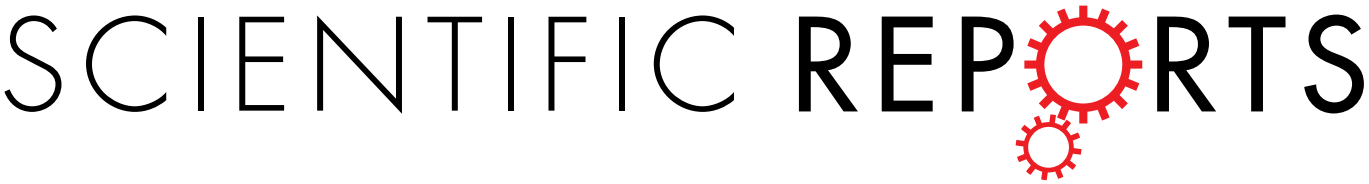

OPEN

Received: 26 August 2016
Accepted: 01 November 2016
Published: 25 November 2016

An evolutionary conserved interaction between the Gcm transcription factor and the SF1 nuclear receptor in the female reproductive system

Pierre B. Cattenoz[1,2,3,4], Claude Delaporte[1,2,3,4], Wael Bazzi[1,2,3,4] & Angela Giangrande[1,2,3,4]

NR5A1 is essential for the development and for the function of steroid producing glands of the reproductive system. Moreover, its misregulation is associated with endometriosis, which is the first cause of infertility in women. Hr39, the *Drosophila* ortholog of NR5A1, is expressed and required in the secretory cells of the spermatheca, the female exocrine gland that ensures fertility by secreting substances that attract and capacitate the spermatozoids. We here identify a direct regulator of Hr39 in the spermatheca: the Gcm transcription factor. Furthermore, lack of Gcm prevents the production of the secretory cells and leads to female sterility in *Drosophila*. Hr39 regulation by Gcm seems conserved in mammals and involves the modification of the DNA methylation profile of *mNr5a1*. This study identifies a new molecular pathway in female reproductive system development and suggests a role for hGCM in the progression of reproductive tract diseases in humans.

In mammals and insects, the process of spermatozoid maturation occurs first in the male before copulation and second after copulation where molecules secreted by the female reproductive tract epithelium preserve and capacitate the spermatozoids[1–4]. Capacitation is primordial for fertilisation and spermatozoids are viable in the female reproductive tract for several days in human[5], several years in honey bees[6,7] and several decades in ants[8]. In both mammals and insects, the inability to capacitate/store the spermatozoids has a strong impact on female fertility[9–15].

Several insect species have developed specific structures called spermathecae that preserve the spermatozoids well after copulation in the female reproductive tract. The molecules that attract, store and capacitate the spermatozoids in the spermatheca are produced by a layer of secretory cells (SC)[12]. The hormone receptor Hr39 allows the generation of the SC, hence ensuring female fertility. Two mammalian orthologs of Hr39 have been described. The nuclear receptor 5A2 (NR5A2 also known as LRH-1) was associated with pre-eclampsia in humans and is involved in cell proliferation, bile acid metabolism and steroidogenesis[16,17]. The nuclear receptor 5A1 (NR5A1 also known as SF-1) (human *NR5A1* gene is *hNR5A1* and mouse ortholog is *mNr5a1* throughout the text)[14,15] is involved in the development and in the function of the pituitary gland, of the adrenal gland and of the gonads[18,19]. Its mutation leads to severe defects in sexual organ formation and its misexpression is associated with changes in its DNA methylation profile and with endometriosis, the major cause of infertility in women[20–23].

In this study, we identify the zinc finger transcription factor Glial cells missing (Gcm also known as Glial cell deficient or Glide) as a major transcriptional regulator of *Hr39* during *Drosophila* spermatheca development. While the complete lack of Gcm leads to embryonic lethality due to the loss of glia[24], we show that its partial lack is compatible with life and leads to almost complete sterility in females. In addition, clones of cells completely lacking Gcm in the spermatheca are devoid of SC. We show that Gcm controls the differentiation of the SC by controlling the expression of Hr39 directly. Such transcriptional control seems evolutionarily conserved, as the

[1]Institut de Génétique et de Biologie Moléculaire et Cellulaire, Illkirch, France. [2]Centre National de la Recherche Scientifique, UMR7104, Illkirch, France. [3]Institut National de la Santé et de la Recherche Médicale, U964, Illkirch, France. [4]Université de Strasbourg, Illkirch, France. Correspondence and requests for materials should be addressed to A.G. (email: angela@igbmc.fr)

Gcm murine orthologs (mGCM1 and mGCM2), which were described for their expression in placenta, parathyroid, thymus, kidney and nervous system[25–29], are also expressed in the uterus. Finally, assays in cells indicate that the Gcm family promotes the expression of mNR5A1/hNR5A1 and that the mGCM proteins induce the same changes in the DNA methylation of the *hNR5a1* locus as those observed in endometriosis.

Collectively, our data reveal the regulatory pathway underlying SC differentiation in the *Drosophila* spermatheca and the conserved regulation of Hr39 and NR5A1, which represents the first evidence of the functional conservation of the Gcm transcription factors. Understanding the regulation of Hr39 expression may shed light on the physiopathological mechanisms of the major cause of infertility in women.

Results

Gcm is required for female fertility and is expressed in the *Drosophila* spermatheca. In *Drosophila*, the complete lack of the Gcm protein leads to embryonic lethality due to the transformation of glial cells into neurons[24,30,31]. Viable hypomorphic mutations, however, allow the analysis of *gcm* mutant animals at later stage[24,31–33]: the gcm^{rA87} allele is due to the insertion of a P-element containing the *LacZ* gene in the promoter of *gcm* and the *gcmGal4* allele has been produced upon replacement of the *LacZ* by the *Gal4* gene[24,31–33]. The *gcmGal4* homozygous and the transheterozygous $gcmGal4/gcm^{rA87}$ animals reach adulthood and display fertility defects. To assess whether the defects are sex specific, we crossed wild type (WT, *Oregon-R)* males with *gcmGal4* homozygous or with transheterozygous females and found a significantly reduced number of offspring compared to that obtained in control crosses (<1% and 20% of the progeny, respectively, Fig. 1a). In contrast, fertility assays on transheterozygous males showed no fertility defects (data not shown). Thus, Gcm is required in reproduction in females, in addition to its well-known role in glia and blood development[24,30,31,34–38].

To clarify the role of Gcm on fertility, we crossed the *gcmGal4* driver, which faithfully mimics the expression of Gcm[32,33], with a *UAS-RFP* reporter. RFP expression was detected in the adult spermatheca, while no labelling was observed in the ovaries nor in the oviduct (Fig. 1b). Gcm expression in the adult spermatheca was confirmed by qPCR assays (Supplemental Figure S1).

Finally, a GO-term analysis on a genome-wide screen aiming at identifying the direct targets of Gcm[39] specifically highlighted the genes involved in the reproductive system development as the most enriched class of genes after those involved in nervous system development, in line with the known role of Gcm at the glial determinant[24,30,31] (Fig. 1c). Comparison between this screen and the published transcriptome of the spermatheca[13] revealed that 387 direct targets of Gcm are expressed in this organ (Fig. 1d, list in Supplemental Table S1).

This data indicate that Gcm is necessary for female fertility and that it is expressed in the spermatheca.

The *gcm* mutation affects the secretory cells of the spermathecae. Two elegant studies[14,40] showed that the spermatheca of *Drosophila* contains a layer of lumen epithelial cells (LEC) expressing the Runt-domain transcription factor Lozenge (Lz), which is essential for the development of the whole spermatheca[14] (Fig. 2a). Surrounding the LEC is the layer of SC that express and require the transcription factor Hindsight (Hnt)[15]. Accessory cells are located basal (basal cells, BC) to the SC and apical (apical cells, AC) to the LEC. The AC are thought to secrete a cuticular canal that connects the secretory unit to the lumen of the spermatheca, which contains the spermatozoids. AC and BC undergo apoptosis during pupal spermatheca development, with some BC being still present in young adult females[14].

To assess the mode of action of Gcm, we analysed the morphology of the spermathecae in animals carrying altered levels of Gcm. The WT SC appear as a translucent layer of cells surrounding a dark cuticular structure that is produced by the LEC (Fig. 2b). In hypomorphic *gcm* conditions (*gcmGal4* homozygous animals), the SC layer is completely absent, leaving the dark cuticular structure relatively unaffected (Fig. 2c). Accordingly, immunolabelling assays show a complete lack of SC in homozygous *gcmGal4* females (Fig. 2f,h), which leads to the absence of spermatozoids in the spermathecae (Supplemental Figures S2a–d). The lack of SC in *gcm* homozygous females is also observed in other hypomorphic *gcm* conditions such as transheterozygous $gcmGal4/gcm^{rA87}$ animals and can be rescued by overexpressing Gcm (Supplemental Figures S2e–g). Of note, some spermathecae from transheterozygous $gcmGal4/gcm^{rA87}$ animals show few remaining SC (Supplemental Figure S2h'), explaining why this strain is not completely sterile. In addition, the number of SC significantly decreases when Gcm is knocked-down by RNAi (*gcm KD*) using the *gcmGal4* as a driver (Fig. 2g,h). The egg laying rate is in agreement with this data. A positive correlation was previously made between the number of SC of the spermathecae and the number of eggs laid[15] and indeed the number of SC as well as the egg laying rate decrease in *gcm* hypomorphs (Fig. 2h,i). The reduction in SC number no longer persists in *gcm KD* spermathecae that also carry the *UAS-gcm* transgene. Indeed, these spermathecae carry supernumerary SC (Fig. 2h), suggesting that Gcm expression may be sufficient to induce the differentiation of the SC.

Finally, to analyse the phenotype of a null *gcm* allele, MARCM clones were produced using the *Df(2L)132* strain in which the *gcm* gene is completely deleted[33,41] (Supplemental Figure S2i). Similar clonal analyses were also performed using a *gcm* hypomorphic but lethal mutation induced by P-element mutagenesis, gcm^{3424} (Fig. 2j–k'''). Recombination was induced at the 3rd instar larval stage prior to spermatheca differentiation. WT clones contain both cell types (SC and LEC), whereas *Df(2L)132* and gcm^{34} mutant clones contain LEC but completely lack SC. Thus, Gcm is necessary for the differentiation of SC. Given the strong phenotype observed in loss of function *gcm* alleles, we assessed the consequences of overexpressing Gcm in its own territory of expression in WT animals (*gcm > gcm GOF*). In these gain of function (GOF) animals, the dark cuticular structure and the LEC are present but the morphology of the spermatheca is altered (Fig. 2d, Supplemental Figures S2j-j"). In addition, these spermathecae display a very high number of SC (Fig. 2h).

Altogether, this data clearly indicate that Gcm is expressed and required in the spermatheca to control SC differentiation.

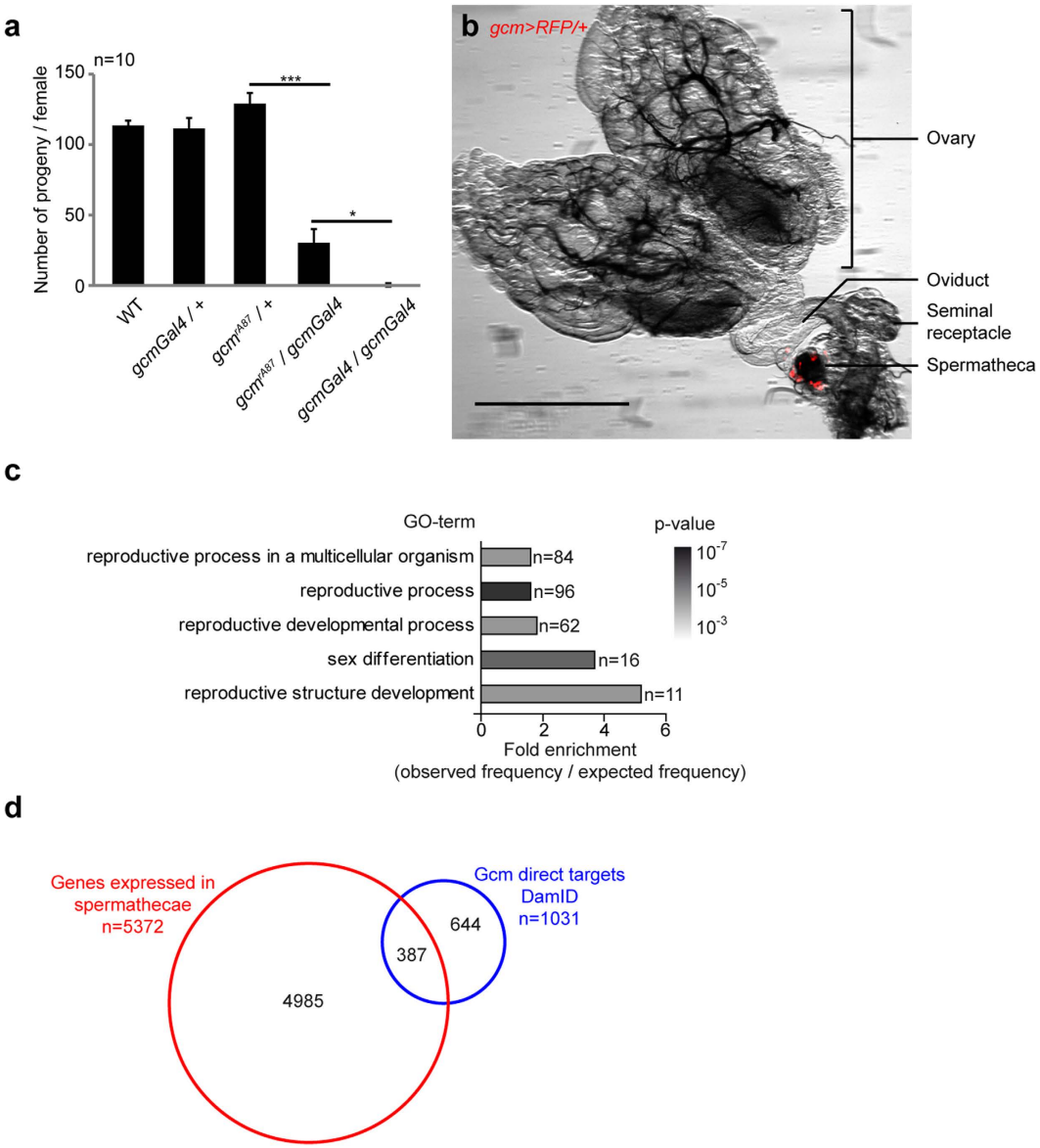

Figure 1. Gcm is expressed in the spermatheca and controls fertility. (**a**) Fertility assays carried out on *gcm* hypomorphs. The histogram shows the average number of progenies per female of the following genotypes: wild type (WT), *gcmGal4/+* and $gcm^{rA87}/+$, which represent the control strains, as well as *gcmGal4/*gcm^{rA87} and *gcmGal4/gcmGal4*, which represent *gcm* hypomorphic conditions. Ten crosses were made per genotype (n = 10). The error bars represent standard errors of the mean (s.e.m.). Student test was used to calculate the p-values: >0.05 = ns; <0.05–0.01 <= *; <0.01–0.001 <= **; <0.001 = ***. (**b**) Reproductive system of an adult control female (*gcmGal4/+;UAS-RFP*). Overlay of the images taken with white light and by epifluorescence (561nm). The scale bar represents 500 μm. (**c**) GO-term enrichment analysis of the genes directly targeted by Gcm according to a DamID screen[39]. The histogram represents the fold enrichments obtained for GO-terms linked to reproduction (enrichment >1.5, FDR <2%, p-value < 10^{-3}), n = number of genes. (**d**) Overlap between the direct targets of Gcm according to a DamID screen (blue) and the genes expressed in spermatheca according to a spermatheca transcriptome[13].

Gcm is expressed in the precursors of the secretory cells. The mutant phenotype prompted us to assess the role and the mode of action of Gcm. Given the early and transient expression of Gcm in glial cells[24,30,31], we analysed the mutant spermathecae and the profile of Gcm expression during development. Spermathecae develop during the pupal stage and the different cell types arise from multipotent precursors (MP) that express Lz and divide to produce the lumen epithelium precursors (LEP) also expressing Lz as well as the secondary precursors called Secretory Unit Precursors (SUP), which do not express Lz[14]. Each SUP divides and produces the AC and a tertiary precursor, which in turn divides and produces the SC as well as the BC that undergoes apoptosis at the adult stage (Fig. 3h)[14].

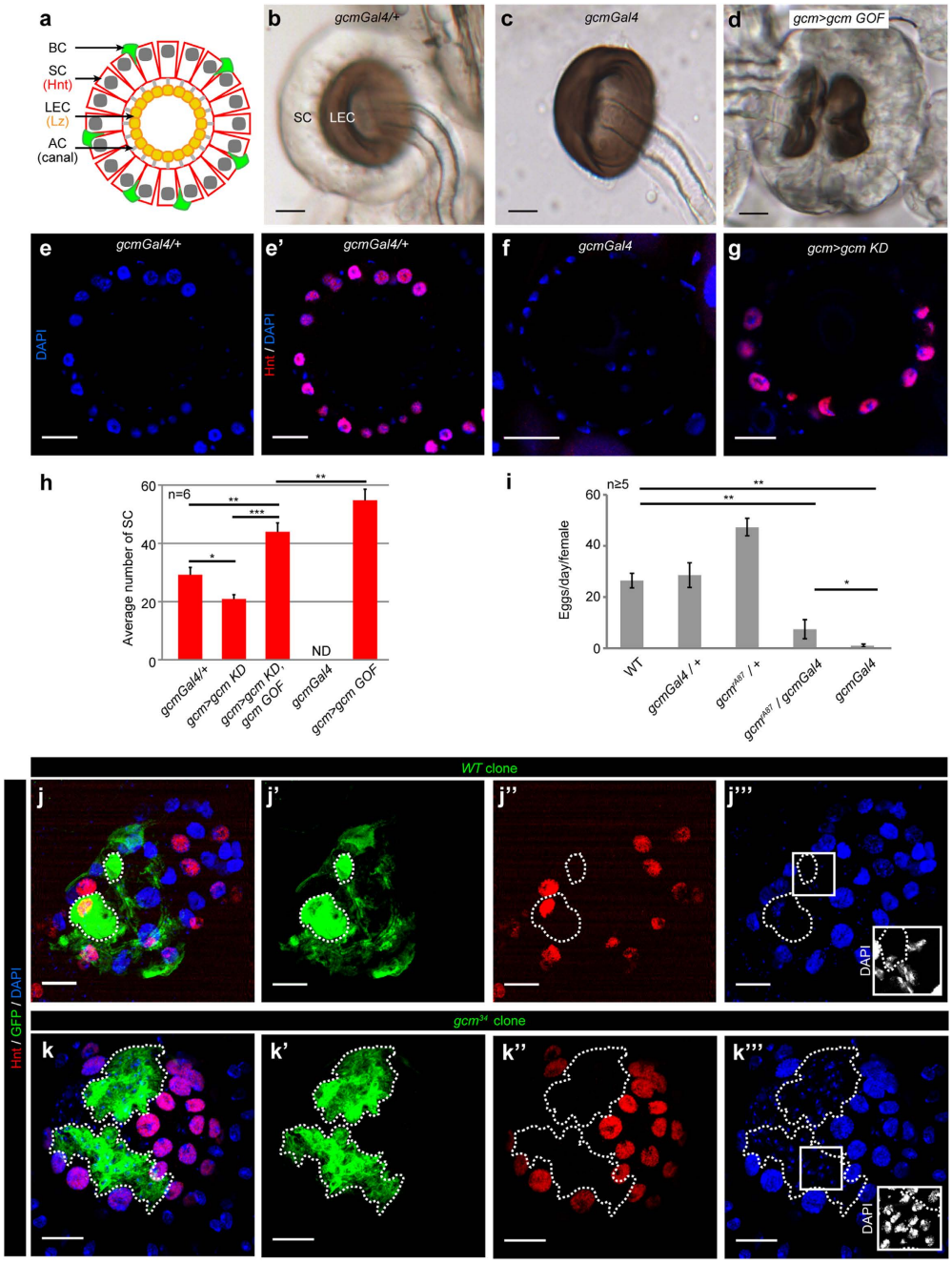

Figure 2. Gcm is involved in the development of the secretory cells of the spermatheca. (**a**) Schematic representation of an adult spermatheca cross-section. The SC express Hindsight (Hnt) and the LEC Lozenge (Lz). (**b–d**) Spermathecae analysed by bright-field microscopy. The spermathecae were dissected from adult females (1 to 3-day-old) *gcmGal4/+* (control) (**b**), *gcmGal4* (**c**), and *gcmGal4/+;UAS-gcm/+* (*gcm > gcm GOF*) (**d**). Unless otherwise specified, all scale bars here and in the following figures represent 20 μm. (**e–g**) Single optical sections of spermathecae analysed by confocal microscopy from adult females of the following genotypes: *gcmGal4/+* (**e,e'**), *gcmGal4* (**f**) and *gcmGal4/+;UAS-gcmRNAi/+* (*gcm > gcm KD*) (**g**) labelled with anti-Hnt (Hnt, in red) and DAPI (blue). (**e**) and (**e'**) represent the DAPI and the overlap of DAPI and anti-Hnt labelling of the *gcmGal4/+* spermatheca, respectively. (**h**) Average number of secretory cells counted in cross-sections of adult spermathecae of the indicated genotypes (see materials and methods). At least 6 spermathecae were analysed per genotype, the error bars and p-values are as described for Fig. 1a. (**i**) Number of eggs laid per female and per day for the indicated genotypes. At least five replicates were made per genotype. (**j–k'''**) MARCM clonal analysis in a *gcm* mutant background. The images represent full projections of spermathecae analysed by confocal microscopy from adult females showing WT (**j–j'''**) or gcm^{34} mutant (**k–k'''**) clones. The spermathecae were labelled with anti-GFP (the clones express GFP, in green), anti-Hnt (Hnt, in red) and DAPI (blue) (**j,k**), the clones are indicated by dashed lines. Each marker is shown individually in (**j'** and **k'**) for anti-GFP, (**j''** and **k''**) for anti-Hnt and (**j'''** and **k'''**) for DAPI. The insets in (**j'''** and **k'''**) show a higher magnification of the nuclei with the DAPI in grey. See also Supplemental Figures S2 and S4.

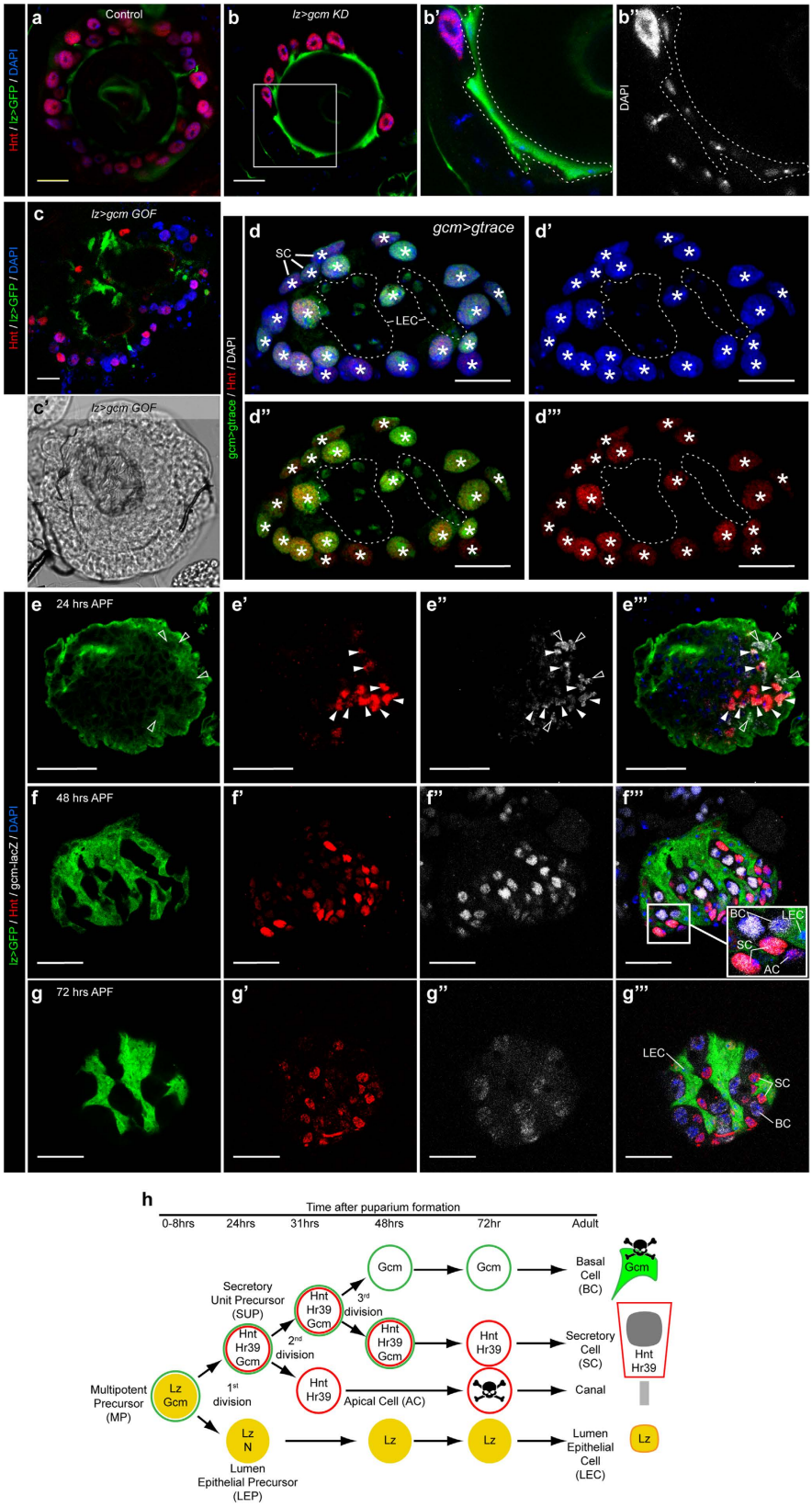

Figure 3. Gcm is expressed early in the secretory cell precursor to initiate the differentiation of the secretory cell. (**a–c**) Single confocal sections of spermathecae from adult females (1 to 3-day-old) *lzGal4,UAS-mCD8GFP/+* (control) (**a**), *lzGal4,UAS-mCD8GFP/+;UAS-gcmRNAi* (*lz > gcm KD*) (**b**) and *lzGal4,UAS-mCD8GFP/+;UAS-gcm* (*lz > gcm GOF*) **(c)** labelled with anti-GFP (*lz > GFP*, in green), anti-Hnt (Hnt, in red) and DAPI (blue). The region indicated by the white square in (**b**) is magnified in (**b'**) and (**b"**), in which the LEC are indicated by a dashed line. DAPI is in grey in (**b"**). (**c'**) Bright-field image of a *lz > gcm GOF* spermatheca. (**d–d"'**) Confocal projection of a *gcmGal4/+;g-trace/+* (*gcm > g-trace*) adult spermatheca labelled with anti-Hnt

(Hnt, in red), anti-GFP (*gcm > g-trace*, in green) and DAPI (blue). (**d**) represents the overlay of anti-Hnt, anti-GFP and DAPI, (**d'**) shows the DAPI labelling, (**d"**) Gcm lineage and Hnt and (**d"'**) anti-Hnt. The white asterisks indicate the SC and the LEC are indicated by a dashed line. (**e–g"'**) Confocal projections of *lzGal4,UAS-mCD8GFP/+;gcm^{rA87}/+* pupal spermathecae labelled with anti-βgal (*gcm-lacZ*, in grey), anti-Hnt (Hnt, in red), anti-GFP (*lz > GFP*, in green) and DAPI (blue). The images were taken at 28 hrs after puparium formation (APF) (**e–e"'**), 48 hrs APF (**f–f"'**) and 72 hrs APF (**g–g"'**). Each marker is shown individually in (**e**–**g**) for anti-GFP, (**e',f',g'**) for anti-Hnt, (**e",f",g"**) for anti-βgal and the overlay of the three channels and DAPI is shown in (**e"',f"',g"'**). The white arrowheads indicate cells expressing Gcm and Hnt, which correspond to the SUP, the empty arrowheads indicate cells expressing Lz and Gcm, which correspond to the MP (**e–e"'**). The inset **(in f"')** shows SC expressing Hnt and low levels of Gcm, BC expressing high levels of Gcm, an AC expressing Hnt only and an LEC expressing Lz. (**h**) Schematic representation of spermatheca development (modified from ref. 15). The time scale is indicated above the schematic in hours APF. The yellow circles indicate Lz expression, the red circles Hnt and the green circles Gcm expression. The skull pictograms indicate the cells undergoing apoptosis. See also Figure S3.

First, we knocked down Gcm expression using the *lzGal4* driver (*lz > gcm KD*), which is active in the MP. Like in hypomorphic conditions and in *gcm > gcm KD* animals, RNAi-mediated down-regulation of Gcm in the MP leads to the decrease of the number of SC in the adult spermatheca (Fig. 3a,b) and the LEC are not impacted (Fig. 3b–b"). The similar phenotypes obtained with *gcm>* and *lz>*, a driver that is not active in the SUP[14], suggest that the *gcm* promoter is already active in the MP that generates all cell types of the spermatheca (including SC and LEC). We then proceeded to overexpress Gcm under the control of the *lzGal4* driver (*lz > gcm GOF*) and found that this leads to severe spermatheca defects including a deformed and almost absent cuticular structure. This phenotype is stronger than the overexpression of Gcm using the *gcmGal4* driver (*gcm > gcm GOF*) in which the cuticular structure can still be observed (compare Fig. 3c' and Supplemental Figures S2j–j"). This indicates that premature Gcm expression prevents LEC development and suggests that Gcm is expressed below threshold levels in the MP.

Following this, we tracked the lineage of the Gcm expressing cells by crossing the *g-trace* flies[42] with the *gcm-Gal4* flies and found that both SC and LEC originate from cells expressing Gcm (white asterisks and dashed line, respectively, in Fig. 3d–d"'). In addition, we tracked Gcm expression during spermatheca development using the *gcm^{rA87}* βGal reporter in heterozygous conditions. By 24hrs after puparium formation (APF), after the division of the MP, the SUP co-expresses Gcm and Hnt (full arrowheads in Fig. 3e–e"', h)[15] and some MP can still be seen co-expressing Lz and βGal (empty arrowheads in Fig. 3e–e"'). At 48 hrs and 72 hrs APF, three types of cells can be identified: the LEC expressing exclusively Lz, the cells expressing Hnt and low levels of Gcm, which comprise the SC (Fig. 3f"'), and the BC expressing Gcm and almost no Hnt (Fig. 3f,g). Few apoptotic AC can also be detected, expressing Hnt (Fig. 3f"'). This confirms that Gcm and Lz are transcribed in the MP and that Gcm remains expressed in the SUP and its offspring.

Finally, in the adult spermatheca, cell-specific immunolabelling on animals carrying the *gcmGal4* driver and the *UAS-mCD8GFP* reporter (*gcm > GFP*, Supplemental Figures S3a, S3c–c") and anti-βgal labelling on the enhancer trap line *gcm^{rA87}* in heterozygous conditions (Supplemental Figure S3b) indicate that Gcm is expressed exclusively in the adult BC. These are the cells that undergo apoptosis[14] (Supplemental Figures S3c–c"), as shown by the decreased number of labelled cells in old *gcm > GFP* spermathecae compared to young ones (Supplemental Figures S3d–e'). Of note, the number of BC decreases in the *gcm > gcm GOF* spermathecae that instead present a very high number of SC (Fig. 2h, Supplemental Figure S3f), suggesting that the BC may convert into SC in *gcm > gcm GOF* spermathecae.

Collectively, our data show that Gcm starts to be expressed in the MP, specifies SUP differentiation and triggers the differentiation of the SC.

Gcm induces the expression of Hr39 and triggers secretory cell differentiation. Hr39 and Hnt are two transcription factors involved in the development of the spermatheca: knock out as well as *KD* of *hnt* and *Hr39* lead to defective production of SC in the spermatheca[13–15]. In addition, they both contain canonical Gcm binding sites (GBS)[43,44] and were identified as direct targets of Gcm by the genome-wide screen using the DNA adenine methyltransferase identification (DamID) procedure[39,45] (Fig. 4a,d). To validate our data functionally, we analysed the regulation of Hnt and Hr39 by Gcm in S2 cells transfected with a Gcm expression vector. The levels of *Hr39* transcripts are significantly induced by Gcm (Fig. 4b). Next, we built luciferase reporters carrying the two GBS present in the *Hr39* locus where Gcm is binding according to the DamID screen and reporters carrying the mutated GBS. Upon co-transfection with the Gcm expression vector, both GBS present in the *Hr39* locus induce luciferase activity and mutations of either GBS reduces the luciferase expression levels (Fig. 4c), indicating that Gcm induces Hr39 expression through these two GBS (Fig. 4a–c). The endogenous levels of Hnt are not significantly induced by Gcm in S2 cells (Fig. 4e), however, the *hnt* locus possesses one GBS in the promoter region (Fig. 4d) and a luciferase assay similar to that performed on Hr39 indicates a significant induction of *hnt* reporter expression by Gcm, which decreases upon GBS mutagenesis (Fig. 4f). Thus, Gcm is also able to induce the expression of Hnt through the GBS. The lack of induction of the endogenous Hnt in S2 cells is likely due to the absence of cofactors or to the unavailability of the enhancer region targeted by Gcm. In all cases, the mutation of the GBS does not abolish the induction of the luciferase activity completely. This may be due to an indirect effect of Gcm on these promoters or to the presence of non-canonical GBS. Overall, this data indicate that Gcm promotes Hr39 expression and likely contributes to the induction of Hnt expression as well.

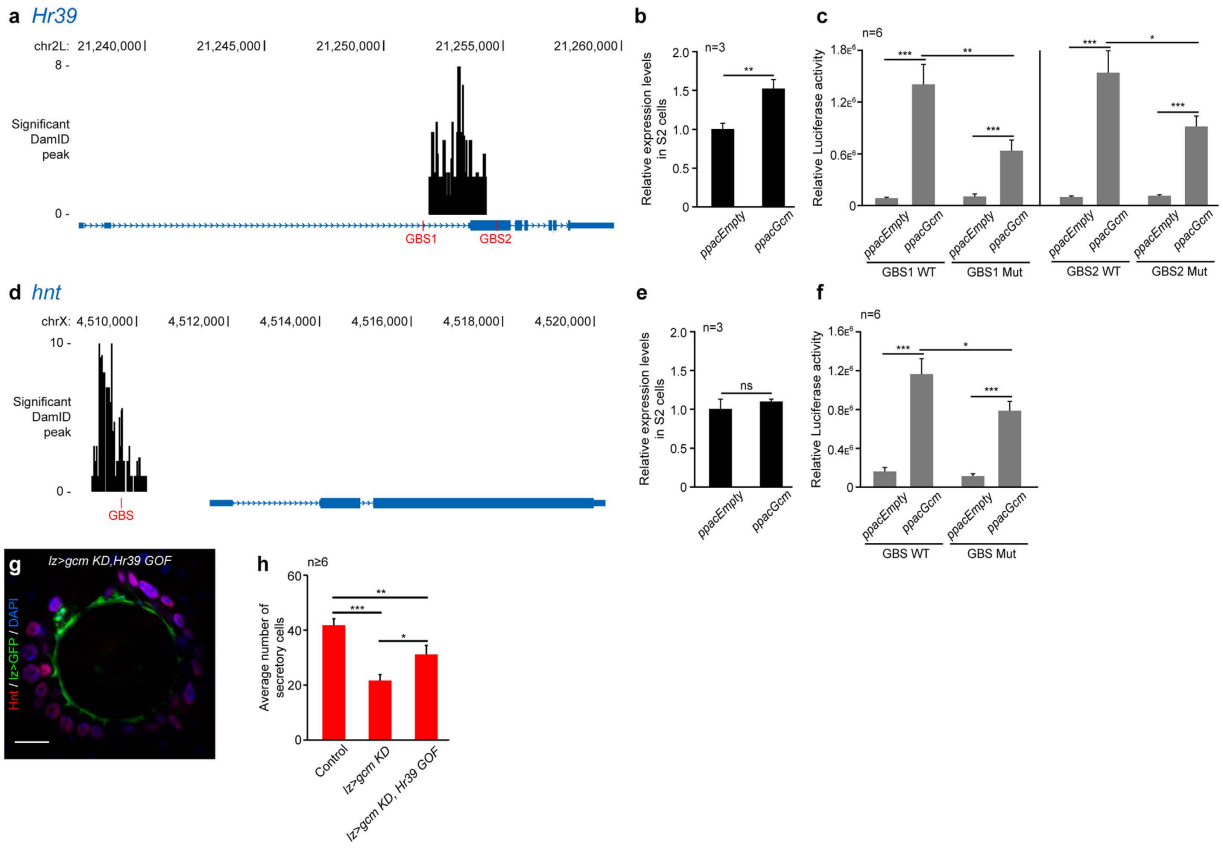

Figure 4. Gcm induces the expression of Hr39 and Hnt. (**a,d**) *Hr39* (**a**) and *hnt* (**d**) loci in the *Drosophila* genome (blue rectangles for exons, blue lines for the introns, the arrowheads indicate the orientation). The canonical Gcm binding sites (GBS) are indicated in red and the black histograms indicate the regions targeted by Gcm[39]. (**b,e**) Expression levels of *Hr39* (**b**) and *hnt* (**e**) measured by qPCR assays in S2 cells transfected with an empty vector (*ppacEmpty*) or with a vector expressing Gcm (*ppacGcm*). The levels are relative to those observed upon transfecting the *ppacEmpty* vector. (**c,f**) Luciferase assays carried out in S2 cells transfected with *ppacEmpty* or with *ppacGcm* and with luciferase vectors carrying the regions covering WT (GBS1 WT and GBS2 WT) or mutated GBS (GBS1 Mut and GBS2 Mut) at the *Hr39* locus (**c**) and the WT or mutated GBS present at the *hnt* locus (**f**). (**g**) Single confocal section of *lzGal4,UAS-mCD8GFP/+;UAS-gcmRNAi,UAS-Hr39* (*lz > gcm KD,Hr39 GOF*) spermatheca from adult female labelled with anti-GFP (*lz > GFP*, green), anti-Hnt (Hnt, in red) and DAPI (blue). (**h**) Average number of SC counted in cross-sections of spermathecae of the indicated genotypes. The *gcm KD* and the *gcm KD,Hr39 GOF* were driven by *lzGal4*. The error bars and p-values (**b**,**c**,**e**,**f and h**) are as described for Fig. 1a. n indicates the number of assays.

Finally, we complemented this data by assessing the biological relevance of the interaction between Gcm and Hr39. Since *gcm KD* in the MP (*lzGal4* driver) leads to a decrease in SC number at adult stage (Fig. 3a,b), we overexpressed Hr39 in *lz > gcm KD* spermathecae and found rescue of the mutant phenotype (Fig. 4g,h). The increased number of SC in the adult compared to that observed in animals that only express low levels of Gcm strongly suggests that Hr39 is indeed a major target of Gcm in the development of the female reproductive system. Of note, Hr39 is already detected in the genital discs of the late 3rd instar larvae[13,14] suggesting that the role of Gcm is not to initiate Hr39 expression but to maintain or increase Hr39 expression during the first division of the MP after pupal formation.

The orthologs of Gcm regulate mNR5A1 expression and are expressed in the mouse uterus. The closest mammalian orthologs of the *Hr39* gene are *Nr5a1* and *Nr5a2,* which code respectively for SF-1[13] and LRH-1[14] and are both involved in the formation and function of mammalian reproductive tissues[46–48]. We hence assessed whether the functional conservation includes the regulation of *Nr5a1* and *Nr5a2* by the orthologs of Gcm: mGCM1 and mGCM2. First, we measured the endogenous levels of *hNR5A1* and *hNR5A2* in HeLa cells (human) and those of *mNR5A1* and *mNR5A2* in mouse embryonic fibroblasts (MEF) upon transfection of mGCM1 and mGCM2 expression vectors. While the levels of expression of *hNR5A2/mNr5a2* are not modulated by the mGCM proteins, the expression levels of the *hNR5A1/mNr5a1* transcripts significantly increase when either mGCM proteins are expressed (Fig. 5a–e). In HeLa cells, both mGCM1 and mGCM2 induce hNR5A1 expression at similar levels (Fig. 5a) and in MEF, mGCM2 induces mNR5A1 expression at higher levels than mGCM1 (9-fold increase compared to WT with mGCM1 versus 6E5-fold increase with

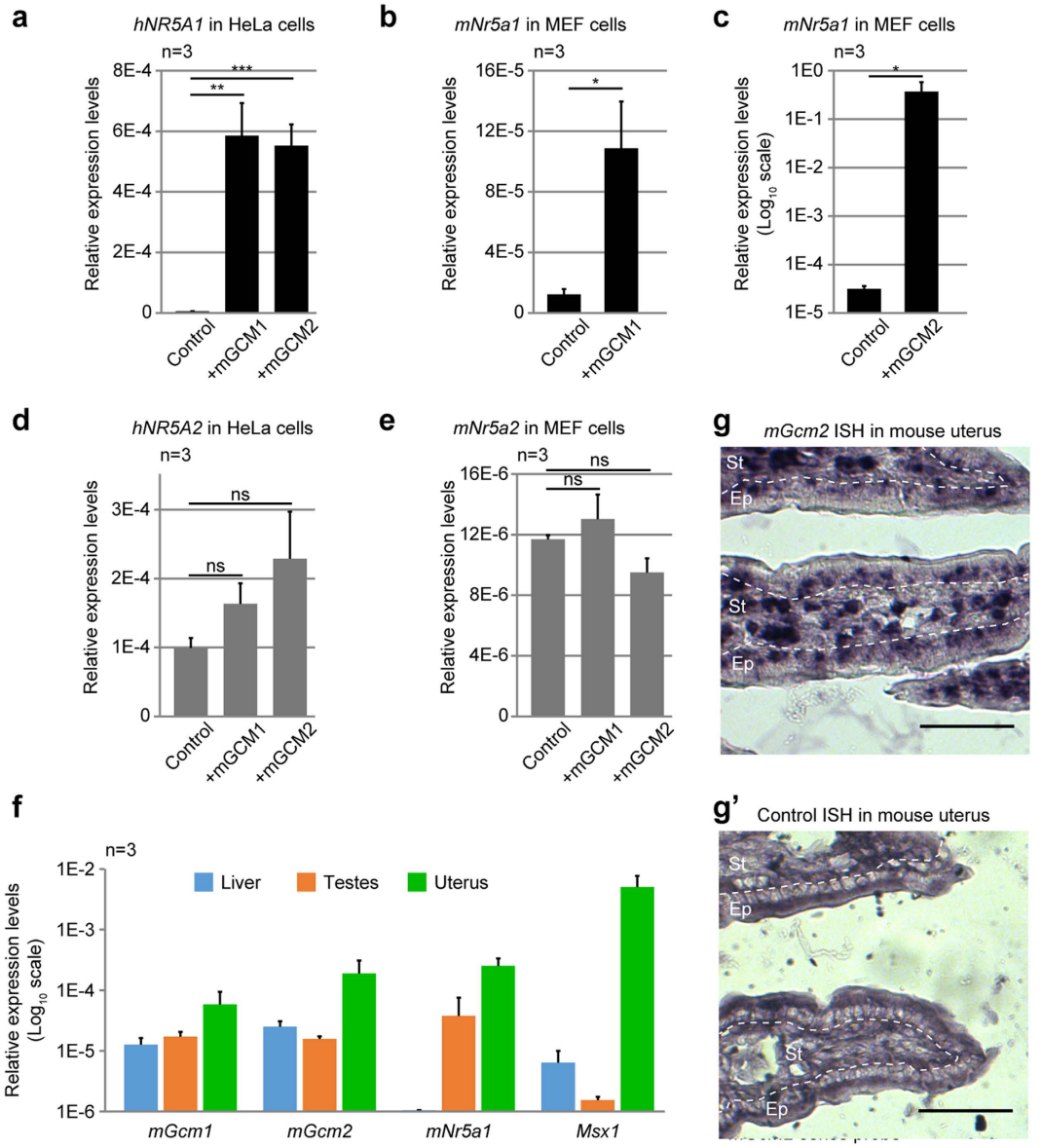

Figure 5. The mGCM proteins induce the expression of the *Hr39* ortholog in mammals. (**a**,**d**) Expression levels of *hNR5A1* (in black (**a**)) and *hNR5A2* (in grey (**d**)) in HeLa cells transfected with an empty vector (Control), an expression vector for mGCM1 (+mGCM1) or an expression vector for mGCM2 (+mGCM2), measured by qPCR. (**b**,**c**,**e**) Expression levels of *mNr5a1* (in black, (**b**,**c**) and *mNr5a2* (in grey, (**e**)) in MEF cells transfected with an empty vector (Control) or with an expression vectors for mGCM1 or mGCM2, measured by qPCR. The y-axis is in $\log_{10}$ scale in (**c**) and the error bars and p-values are as described for Fig. 1a. n indicates the number of assays. (**f**) Expression levels of *mGcm1*, *mGcm2*, *mNr5a1* and that of the transcription factor *Msx1* in mouse liver, testes and uterus measured by qPCR. The levels are relative to the house-keeping genes *Actb* and *Gapdh*. Each experiment was carried out on three mice. The error bars represent s.e.m. and the y-axis is in $\log_{10}$ scale. (**g**,**g'**) *In situ* hybridisation on adult mouse uterus section targeting *mGcm2* using anti-sense *mGcm2* probe (**g**) and negative control using the sense *mGcm2* probe (**g'**). Scale bar represents 50 μm, the stroma (St) of the endometrium corresponds to the area indicated by a dashed line and Ep indicates the columnar epithelium.

mGCM2) (Fig. 5b,c). Then, quantitative PCR (qPCR) analyses indicate that *mGcm1*, *mGcm2* and *mNr5a1* are expressed in the adult mouse uterus and that their levels of expression in this tissue are higher than those found in liver and testes (Fig. 5f). It is important to note, however, that their levels are one order of magnitude lower than the transcription factor *Msx1*, which is known to be strongly active in the uterus[49] (Fig. 5f). *In situ* hybridisation assays confirm the expression of *mGcm2* mostly in the stroma of the endometrium (Fig. 5g). No signal could be detected using the *mGcm1* probe, likely due to the low levels of *mGcm1* expression it that tissue. This suggests that the regulation of Hr39 expression by Gcm observed in *Drosophila* is conserved in evolution and that mGCM proteins might regulate the expression of mNR5A1 in the mouse uterus.

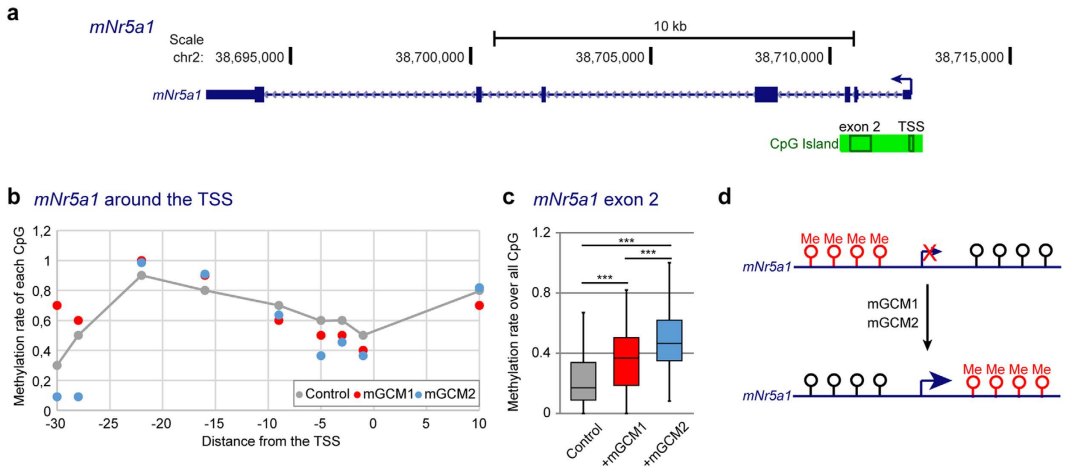

Figure 6. mGCM1 and mGCM2 regulate the methylation profile of *mNr5a1*. (**a**) Schematic representation of the *mNr5a1* locus in the mouse genome. The gene is represented as in Fig. 4a. The genomic coordinates of the locus (genome version mm10) are indicated above the gene. The CpG island is highlighted in green, the rectangles within the CpG island indicate the analysed regions in exon 2 and at TSS. (**b**) Methylation rate for each CpG 30 nucleotides before the TSS and 10 nucleotides after the TSS. The methylation rate in MEF transfected with an empty vector (Control) is indicated in grey, the methylation rate in MEF transfected with an expression vector for mGCM1 is in red and for mGCM2 in blue. Dots above the grey line indicate CpG hypermethylation and dots below indicate CpG hypo-methylation compared to the control cells. (**c**) Box plot representing the distribution of the methylation rate in the CpG island of *mNr5a1* in MEF cells transfected with an empty vector (Control), an expression vector for mGCM1 (+mGCM1) or for mGCM2 (+mGCM2)). The methylation rates were measured for the 51 CpG contained in the exon 2 area highlighted in (**a**) using bisulfite sequencing. The p-values were estimated using paired student test (see materials and methods) and are represented as described in Fig. 1a. (**d**) Schematic representation of the impact of the mGCM protein family on the DNA methylation profile of *mNr5a1*.

Mammalian GCM proteins have been associated with DNA demethylation at the promoter of their target genes: hGCM1 affects *Syncytin 2* demethylation in human placenta[50] and mGCM1 and mGCM2 affect *Hes5* demethylation in the mouse embryo[29]. For this reason, it was proposed that mGCM proteins trigger DNA demethylation, even though the molecular mode of action was not understood. To further characterize the impact of the *mGcm* genes, we asked whether mNR5A1 regulation by mGCM1 and mGCM2 is associated with changes in the DNA methylation profile of the *mNr5a1* gene using transfected cells. In human and mouse, the *Nr5a1* genes contain a CpG island that covers the transcription start site (TSS) until the 3rd exon (Fig. 6a). The methylation rate of each CpG within the regions covering the 2nd exon and the TSS was estimated by bisulfite sequencing in MEF transfected with an empty vector (Control) or with expression vectors of mGCM1 or mGCM2. The three CpG located around the TSS are demethylated in the presence of mGCM1 or mGCM2 proteins compared to that observed upon transfecting the control plasmid (Fig. 6b). In addition, a significant increase in CpG methylation is observed in the exon 2 region upon mGCM1 or mGCM2 transfection (Fig. 6c). The highest levels of methylation are observed when the cells are transfected with mGCM2 (Fig. 6c), in agreement with the strong increase in *mNr5a1* expression levels observed in MEF cells overexpressing mGCM2 (Fig. 5e). These data show that the mGCM proteins are not specifically involved in DNA demethylation and fit with the emerging view that gene expression is linked to DNA demethylation at the promoter and to DNA hypermethylation in the gene body[51] (Fig. 6d). Our data are also in line with the recent hypothesis that transcription factors can bind demethylated as well as methylated DNA[52]. Finally, the high levels of expression of hNR5A1/mNR5A1 observed in endometriotic tissues are also linked to high levels of CpG methylation around exon 2 and low levels around the TSS[53–56].

Overall, this data suggest that the *mGcm* genes induce the transcription of *mNr5a1* and this is associated with important changes in the DNA methylation profile at the *mNr5a1* locus.

Discussion

In this study, we discover a molecular cascade required in the *Drosophila* female reproductive system that may be conserved in mammals. The *Drosophila* transcription factor Gcm is expressed during the development of the SC of the spermatheca and mutations or knock-down of Gcm inhibit the development of these cells, leading to female sterility. Gcm acts by targeting the ortholog of the *hNR5A1/mNR5A1* hormone receptor *Hr39*. Finally, the orthologous genes *mGcm1* and *mGcm2* are expressed in the mouse uterus, induce the expression of hNR5A1/mNR5A1 in human and murine cell lines, respectively and modify the DNA methylation profile of *mNr5a1*. This suggest that defects in the hGCM pathway may be associated with pathologies affecting women reproductive system.

Common and tissue-specific features of the Gcm pathways. Gcm is required in the nervous, in the immune and in the reproductive systems. These Gcm dependent pathways display a common feature as, in all

cases, a multipotent precursor gives rise to cells with different identities. In the nervous system, the neuroblast can produce glia or neurons, in the immune system the prohemocyte can produce plasmatocytes or crystal cells and in the spermatheca the MP can produce SC or LEC. Gcm is absolutely required to induce one fate over the other as *gcm* mutant animals lack glia and display supernumerary neurons[24,30,31] and the number of plasmatocyte decreases whereas that of the crystal cells increases[36,38]. In the spermatheca, the absence of SC in homozygous *gcmGal4* animals is accompanied by an increase in LEC number (Fig. 2h, Supplemental Figure S4), suggesting that Gcm induces the differentiation of the SC at the expense of the LEC.

A second common feature between the three developmental events is the transient and early expression of Gcm. In the spermatheca, Gcm is expressed during the differentiation of the SC but no longer present in the adult SC. Similarly, Gcm is expressed early in the glial and in the hemocyte lineages but its transcripts are not detected in the mature cells[34,36,57,58]. Thus, the Gcm fate determinant provides a trigger that needs to be erased to allow terminal differentiation. In the nervous system, Gcm activates the transcription of its target gene *repo*, which remains expressed in glial cells until adulthood[59]. The Repo homeobox containing protein constitutes the pan-glial specific transcription factor that induces the expression of late glial genes, maintains the glial fate and actually contributes to Gcm degradation[57,59] (Trebuchet, unpublished results). In the spermatheca, Gcm induces the expression of the Hr39 transcription factor that is required for SC formation and that remains expressed in those cells until adulthood[13–15], Hr39 may hence play a maintenance role similar to that played by Repo in the glial cells. Recent data suggest that early and transient expression of fate determinants may be a general rule that allows stable and terminal cell differentiation. Interestingly, the *Drosophila* proneural transcription factor Atonal (Ato) is expressed early during photoreceptor differentiation but needs to be switched off for normal eye development[60].

A third common feature between the three systems is the participation of the Notch pathway. In the spermatheca, the production of the SC from the initial MP encompasses three cells divisions. The first and third divisions involve the Notch pathway and trigger the differentiation of the LEP and the SC respectively[14,15]. In these two divisions, Notch is activate only in the cells that do not express Gcm suggesting that Notch and Gcm may interact negatively. Such negative interaction was previously reported during the differentiation of the adult sensory organ precursors (SOP). Constitutive activation of the Notch pathway in the SOP represses *gcm* expression and prevents the production of glial cells; accordingly, lack of Notch induces gcm expression and the production of glia at the expense of neurons[61,62]. Finally, during the development of the embryonic hemocytes, there is no report of interaction between Gcm and the Notch pathway, however Gcm is involved in plasmatocyte development and Notch in crystal cell development[34,36,63]. Importantly, several members of the Notch pathway are directly regulated by Gcm including the two ligands Serrate and Delta[39], which suggests a strong interaction between Gcm and Notch that remains to be investigated.

Our work also highlights the cell-specific nature of the Gcm differentiation pathways: while the Gcm transcription factor is required to induce several cell identities, its downstream factors are cell-specific. Repo expression is absent in the spermatheca and Hr39 expression is absent in glial cells. Moreover, the overexpression of Gcm in the spermatheca does not activate Repo expression in those cells nor does Gcm overexpression in the embryonic nervous system activate Hr39 expression in that territory (data not shown). Thus, although 'master regulators' are considered as simple molecular switches, this represents an oversimplified view of cell differentiation. The activity of such potent transcription factors rather relies on the history of a given cell, that is, its specific transcriptional and epigenetic asset. For example, the ectopic expression of the famous *eyeless* master gene induces the formation of ectopic eyes on wings, legs and antennae[64], while in the embryonic nervous system its ectopic expression alters the axonal wiring of the ventral nerve cord[65].

Finally, the expression profile of Gcm gives an important insight on spermatheca differentiation. Our study shows that Gcm and Lz are co-expressed in the MP and that Gcm remains expressed exclusively in the SUP following the asymmetrical division of the MP whereas Lz is repressed in the SUP[14]. A comparable interaction between Gcm and Lz was observed during the differentiation of the embryonic hemocytes. Gcm is required for the differentiation of the plasmatocytes and Lz for the differentiation of the crystal cells[38]. Initially, Gcm is expressed in all prohemocytes but subsequently its expression fades away in the precursors of the crystal cells, which allows for the expression of Lz[34,37,38]. Thus, Gcm induces the plasmatocyte fate and inhibits the crystal cell fate through inhibition of Lz: as mentioned above, *gcm* mutant animals display supernumerary crystal cells and in addition ectopic Gcm expression in the crystal cell precursors using the *lzGal4* driver prevents the expression of Lz and converts cells into plasmatocytes[36,38]. We propose that in the spermatheca, Gcm is expressed at low levels in the MP where it cohabits with Lz, then its expression progressively rises in the SUP until its levels become sufficient to repress Lz expression in this cell. SUP cells that express low levels of Gcm adopt the LEC fate. The absence of Gcm binding sites at the *lz* locus and the known role of Gcm as an activator of transcription prompt us to speculate that Gcm represses Lz expression indirectly. The transcriptional repressor Tramtrack (Ttk)[66,67] was already described as an inhibitor of Lz expression in the larval eye disc[68], is a downstream target of Gcm[39,69–71] and is expressed in the spermatheca[72]. Future studies will determine whether Ttk could act as the intermediary protein between Gcm and Lz inhibition.

A conserved role for the Gcm family of proteins in the regulation of Hr39/Nr5a1 and fertility. Hr39 and NR5A1 transcription factors were proposed to share similar functions and to target similar genes for the development of specific secretory glands of the reproductive system (steroidogenic glands in mammals and spermathecae in *Drosophila*)[13,14,73]. Our study suggests that the control of Hr39 and NR5A1 by the GCM protein family is also conserved. Gcm controls female fertility due to its effects on the SC in the spermathecae, and the lack of SC is explained by the lack of induction of Hr39. This regulation is conserved in mammals with the *mGcm1* and *mGcm2* genes inducing mNR5A1 expression in MEF cells and being expressed in the reproductive system. This represents the first evidence of functional conservation for GCM proteins in similar biological systems of *Drosophila* and mammals.

Endometriosis[20–23,54,74] is an oestrogen-dependent disorder defined by the ectopic growth of endometrium-like tissue (reviewed in ref. 75), which represents the leading cause of women infertility[76–78]. A major feature of endometriotic tissues is the overexpression of hNR5A1 and the modification of the *hNR5A1* DNA methylation profile in that tissue: the *hNR5A1* TSS is demethylated and the CpG island covering exon 2 is hypermethylated[22,53–55]; the present study shows that *mNr5a1* expression and its DNA methylation profile are regulated by the two mGCM proteins (Fig. 6d). This suggests that the GCM protein family could be involved in the pathogenesis of endometriosis. Over the past ten years, several studies aimed at identifying the molecular basis of endometriosis by comparing the transcriptomes of healthy endometrium to endometriotic tissue[56,79–84]. hGCM1 and hGCM2 did not come out in any of these studies. The large majority of these reports used micro-array to profile gene expression and both *hGCM1* and *hGCM2* were below the detection range in all studies even in healthy tissues whereas we detected *mGcm1* expression by qPCR and *mGcm2* expression by qPCR and *in situ* hybridisation. Several factors may explain the difficulty to identify the *hGCM* genes in those analyses, among them the known instability of their RNA and their potential transient expression (reviewed in ref. 85). This indicates that the study of GCM1 and GCM2 in endometriosis should be carried out using highly sensitive methods and possibly during the development of the disease to catch the transient presence of their transcripts.

Overall, our study suggests that the GCM regulatory network is robustly conserved and that *Drosophila* represents a model of choice to decipher this pathway in the reproductive system. Finally, this study indicates that the Gcm transcription factor has a much broader role than initially thought. We foresee that the deep analysis of its regulatory network will allow us to understand pleiotropic differentiation pathways and hence the role and mode of action of potent fate determinants.

Materials and Methods

Fly strain. Flies were raised on standard medium at 25 °C. The genotype and provenance of the strains are detailed in Supplemental experimental procedures.

Fertility and egg laying assays. Fertility and egg laying assays are detailed in Supplemental experimental procedures. For fertility assays, the progeny produced in 12 days by 3 virgins of the indicated genotypes crossed with one male WT were counted and reported to number of progeny/female. For the egg laying assays, the number of eggs laid in 48 hrs by five females of the indicated genotypes crossed with ten males WT were counted and reported to number of eggs/females/days. The p-values were estimated after variance analysis using bilateral student test with equal variance.

Immunolabelling. The spermathecae were labelled using standard immunolabelling protocol as described in ref. 39. The list of antibodies and the labelling protocol are detailed in in Supplemental experimental procedures.

Secretory cell and basal cell counts. For each spermatheca, the Hnt/DAPI positive cells (SC) were counted from the stack of six focal plans taken at 3 μm interval in the middle of the spermatheca (the plan giving the largest cross-section of the spermatheca). This was repeated in at least six independent spermathecae for each genotype. The average number of SC and the s.e.m. are represented in Figs 2h and 4h. The p-values were estimated as described for the fertility assays.

qPCR and luciferase assay in S2 cells. The transfection of S2 cells, the quantitative PCR (qPCR) and the luciferase assay were performed as described in Cattenoz *et al.*[39] and detailed in Supplemental experimental procedures. Each experiment was carried out in triplicates.

***In situ* hybridisation and RNA extraction from mouse uterus.** RNA *in situ* hybridisation with digoxigenin-labelled probes for *mGcm2* transcripts was performed as described in Vernet *et al.*[86] with slight modifications detailed in Supplemental experimental procedures. The qPCR were carried out on *C57BL/6* mouse uterus RNA extracted from 3 different animals with TRI reagent.

Transfection and qPCR in mammalian cells. HeLa cells transfection was performed as described in Cattenoz *et al.*[39] and MEF cells transfection was performed as detailed in Supplemental experimental procedures. 48 hrs after transfection, the cells were sorted according to GFP expression before RNA extraction. Reverse transcription and qPCR were carried out as described for the S2 cells with the primer pairs listed in Supplemental experimental procedures.

Bisulfite sequencing in MEF cells. MEF cells transfected and sorted as described above were used to analyse the methylation profile of *mNr5a1* locus. The procedure is detailed in Supplemental experimental procedures. The loci of interest were then amplified by PCR, cloned and sequenced. At least 10 clones were sequenced per condition. The p-values were estimated after variance analysis using bilateral student test for paired samples.

References

1. Suarez, S. S. & Pacey, A. A. Sperm transport in the female reproductive tract. *Hum Reprod Update* **12,** 23–37, doi: 10.1093/humupd/dmi047 (2006).
2. Scott, M. A. A glimpse at sperm function *in vivo*: sperm transport and epithelial interaction in the female reproductive tract. *Anim Reprod Sci* **60,** 337–348, doi: 10.1016/S0378-4320(00)00130-5 (2000).
3. Varner, D. D. Odyssey of the spermatozoon. *Asian J Androl* **17,** 522–528, doi: 10.4103/1008-682x.153544 (2015).
4. Suarez, S. S. Mammalian sperm interactions with the female reproductive tract. *Cell Tissue Res* **363,** 185–194, doi: 10.1007/s00441-015-2244-2 (2016).
5. Wilcox, A. J., Weinberg, C. R. & Baird, D. D. Timing of sexual intercourse in relation to ovulation. Effects on the probability of conception, survival of the pregnancy, and sex of the baby. *N Engl J Med* **333,** 1517–1521, doi: 10.1056/NEJM199512073332301 (1995).

6. Al-Lawati, H., Kamp, G. & Bienefeld, K. Characteristics of the spermathecal contents of old and young honeybee queens. *J Insect Physiol* **55,** 116–121, doi: 10.1016/j.jinsphys.2008.10.010 (2009).
7. Locke, S. J. & Peng, Y. S. The Effects of Drone Age, Semen Storage and Contamination on Semen Quality in the Honey-Bee (Apis-Mellifera). *Physiol Entomol* **18,** 144–148, doi: 10.1111/j.1365-3032.1993.tb00461.x (1993).
8. Pamilo, P. Life-Span of Queens in the Ant Formica-Exsecta. *Insect Soc* **38,** 111–119, doi: 10.1007/Bf01240961 (1991).
9. Ashrafzadeh, A., Karsani, S. A. & Nathan, S. Mammalian sperm fertility related proteins. *Int J Med Sci* **10,** 1649–1657, doi: 10.7150/ijms.6395 (2013).
10. O'Flaherty, C. Redox regulation of mammalian sperm capacitation. *Asian J Androl* **17,** 583–590, doi: 10.4103/1008-682x.153303 (2015).
11. Wolfner, M. F. "S.P.E.R.M." (seminal proteins (are) essential reproductive modulators): the view from Drosophila. *Soc Reprod Fertil Suppl* **65,** 183–199 (2007).
12. Wolfner, M. F. Precious essences: female secretions promote sperm storage in Drosophila. *PLoS Biol* **9,** e1001191, doi: 10.1371/journal.pbio.1001191 (2011).
13. Allen, A. K. & Spradling, A. C. The Sf1-related nuclear hormone receptor Hr39 regulates Drosophila female reproductive tract development and function. *Development* **135,** 311–321, doi: 10.1242/dev.015156 (2008).
14. Sun, J. & Spradling, A. C. NR5A nuclear receptor Hr39 controls three-cell secretory unit formation in Drosophila female reproductive glands. *Curr Biol* **22,** 862–871, doi: 10.1016/j.cub.2012.03.059 (2012).
15. Sun, J. & Spradling, A. C. Ovulation in Drosophila is controlled by secretory cells of the female reproductive tract. *Elife* **2,** e00415, doi: 10.7554/eLife.00415 (2013).
16. Lee, Y. K. & Moore, D. D. Liver receptor homolog-1, an emerging metabolic modulator. *Front Biosci* **13,** 5950–5958 (2008).
17. Zhang, D. *et al.* Dysfunction of Liver Receptor Homolog-1 in Decidua: Possible Relevance to the Pathogenesis of Preeclampsia. *PLoS One* **10,** e0145968, doi: 10.1371/journal.pone.0145968 (2015).
18. El-Khairi, R. & Achermann, J. C. Steroidogenic factor-1 and human disease. *Semin Reprod Med* **30,** 374–381, doi: 10.1055/s-0032-1324720 (2012).
19. Parker, K. L. & Schimmer, B. P. Steroidogenic factor 1: a key determinant of endocrine development and function. *Endocr Rev* **18,** 361–377, doi: 10.1210/edrv.18.3.0301 (1997).
20. Attar, E. *et al.* Prostaglandin E2 via steroidogenic factor-1 coordinately regulates transcription of steroidogenic genes necessary for estrogen synthesis in endometriosis. *J Clin Endocrinol Metab* **94,** 623–631, doi: 10.1210/jc.2008-1180 (2009).
21. Noel, J. C. *et al.* Steroidogenic factor-1 expression in ovarian endometriosis. *Appl Immunohistochem Mol Morphol* **18,** 258–261, doi: 10.1097/PAI.0b013e3181c06948 (2010).
22. Xue, Q. *et al.* Transcriptional activation of steroidogenic factor-1 by hypomethylation of the 5′ CpG island in endometriosis. *J Clin Endocrinol Metab* **92,** 3261–3267, doi: 10.1210/jc.2007-0494 (2007).
23. Zeitoun, K., Takayama, K., Michael, M. D. & Bulun, S. E. Stimulation of aromatase P450 promoter (II) activity in endometriosis and its inhibition in endometrium are regulated by competitive binding of steroidogenic factor-1 and chicken ovalbumin upstream promoter transcription factor to the same cis-acting element. *Mol Endocrinol* **13,** 239–253, doi: 10.1210/mend.13.2.0229 (1999).
24. Vincent, S., Vonesch, J. L. & Giangrande, A. Glide directs glial fate commitment and cell fate switch between neurones and glia. *Development* **122,** 131–139 (1996).
25. Hashemothosseini, S. & Wegner, M. Impacts of a new transcription factor family: mammalian GCM proteins in health and disease. *J Cell Biol* **166,** 765–768, doi: 10.1083/jcb.200406097 (2004).
26. Schreiber, J. *et al.* Placental failure in mice lacking the mammalian homolog of glial cells missing, GCMa. *Molecular and Cellular Biology* **20,** 2466–2474, doi: 10.1128/Mcb.20.7.2466-2474.2000 (2000).
27. Thomee, C. *et al.* GCMB mutation in familial isolated hypoparathyroidism with residual secretion of parathyroid hormone. *J Clin Endocr Metab* **90,** 2487–2492, doi: 10.1210/jc.2004-2450 (2005).
28. Hashemolhosseini, S. *et al.* Restricted expression of mouse GCMa/Gcm1 in kidney and thymus. *Mech Develop* **118,** 175–178, doi: 10.1016/S0925-4773(02)00239-3 (2002).
29. Hitoshi, S. *et al.* Mammalian Gcm genes induce Hes5 expression by active DNA demethylation and induce neural stem cells. *Nat Neurosci* **14,** 957–964, doi: 10.1038/nn.2875 (2011).
30. Hosoya, T., Takizawa, K., Nitta, K. & Hotta, Y. glial cells missing: a binary switch between neuronal and glial determination in Drosophila. *Cell* **82,** 1025–1036 (1995).
31. Jones, B. W., Fetter, R. D., Tear, G. & Goodman, C. S. glial cells missing: a genetic switch that controls glial versus neuronal fate. *Cell* **82,** 1013–1023 (1995).
32. Paladi, M. & Tepass, U. Function of Rho GTPases in embryonic blood cell migration in Drosophila. *J Cell Sci* **117,** 6313–6326, doi: 10.1242/jcs.01552 (2004).
33. Soustelle, L. & Giangrande, A. Novel gcm-dependent lineages in the postembryonic nervous system of Drosophila melanogaster. *Developmental dynamics: an official publication of the American Association of Anatomists* **236,** 2101–2108, doi: 10.1002/dvdy.21232 (2007).
34. Bernardoni, R., Vivancos, V. & Giangrande, A. glide/gcm is expressed and required in the scavenger cell lineage. *Dev Biol* **191,** 118–130 (1997).
35. Jacques, C., Soustelle, L., Nagy, I., Diebold, C. & Giangrande, A. A novel role of the glial fate determinant glial cells missing in hematopoiesis. *Int J Dev Biol* **53,** 1013–1022, doi: 10.1387/ijdb.082726cj (2009).
36. Bataille, L., Auge, B., Ferjoux, G., Haenlin, M. & Waltzer, L. Resolving embryonic blood cell fate choice in Drosophila: interplay of GCM and RUNX factors. *Development* **132,** 4635–4644, doi: 10.1242/dev.02034 (2005).
37. Alfonso, T. B. & Jones, B. W. gcm2 promotes glial cell differentiation and is required with glial cells missing for macrophage development in Drosophila. *Developmental Biology* **248,** 369–383, doi: 10.1006/dbio.2002.0740 (2002).
38. Lebestky, T., Chang, T., Hartenstein, V. & Banerjee, U. Specification of Drosophila hematopoietic lineage by conserved transcription factors. *Science* **288,** 146–149 (2000).
39. Cattenoz, P. B. *et al.* Functional Conservation of the Glide/Gcm Regulatory Network Controlling Glia, Hemocyte, and Tendon Cell Differentiation in Drosophila. *Genetics* **202,** 191–219, doi: 10.1534/genetics.115.182154 (2016).
40. Mayhew, M. L. & Merritt, D. J. The morphogenesis of spermathecae and spermathecal glands in Drosophila melanogaster. *Arthropod Struct Dev* **42,** 385–393, doi: 10.1016/j.asd.2013.07.002 (2013).
41. Lane, M. E. & Kalderon, D. Genetic investigation of cAMP-dependent protein kinase function in Drosophila development. *Genes Dev* **7,** 1229–1243 (1993).
42. Evans, C. J. *et al.* G-TRACE: rapid Gal4-based cell lineage analysis in Drosophila. *Nat Methods* **6,** 603–605, doi: 10.1038/nmeth.1356 (2009).
43. Miller, A. A., Bernardoni, R. & Giangrande, A. Positive autoregulation of the glial promoting factor glide/gcm. *The EMBO journal* **17,** 6316–6326, doi: 10.1093/emboj/17.21.6316 (1998).
44. Ragone, G. *et al.* Transcriptional regulation of glial cell specification. *Dev Biol* **255,** 138–150 (2003).
45. van Steensel, B. & Henikoff, S. Identification of *in vivo* DNA targets of chromatin proteins using tethered dam methyltransferase. *Nature biotechnology* **18,** 424–428, doi: 10.1038/74487 (2000).
46. Luo, X. R., Ikeda, Y. Y. & Parker, K. L. A Cell-Specific Nuclear Receptor Is Essential for Adrenal and Gonadal Development and Sexual-Differentiation. *Cell* **77,** 481–490, doi: 10.1016/0092-8674(94)90211-9 (1994).

47. Ozisik, G., Achermann, J. C. & Jameson, J. L. The role of SF1 in adrenal and reproductive function: insight from naturally occurring mutations in humans. *Mol Genet Metab* **76,** 85–91, doi: 10.1016/S1096-7192(02)00032-X (2002).
48. Duggavathi, R. *et al.* Liver receptor homolog 1 is essential for ovulation. *Gene Dev* **22,** 1871–1876, doi: 10.1101/gad.472008 (2008).
49. Pavlova, A., Boutin, E., Cunha, G. & Sassoon, D. Msx1 (Hox-7.1) in the adult mouse uterus: cellular interactions underlying regulation of expression. *Development* **120,** 335–345 (1994).
50. Liang, C. Y. *et al.* GCM1 Regulation of the Expression of Syncytin 2 and Its Cognate Receptor MFSD2A in Human Placenta. *Biol Reprod* **83,** 387–395, doi: 10.1095/biolreprod.110.083915 (2010).
51. Jones, P. A. The DNA methylation paradox. *Trends Genet* **15,** 34–37, doi: 10.1016/S0168-9525(98)01636-9 (1999).
52. Zhu, H., Wang, G. & Qian, J. Transcription factors as readers and effectors of DNA methylation. *Nature reviews. Genetics*, doi: 10.1038/nrg.2016.83 (2016).
53. Xue, Q., Zhou, Y. F., Zhu, S. N. & Bulun, S. E. Hypermethylation of the CpG Island Spanning From Exon II to Intron III is Associated With Steroidogenic Factor 1 Expression in Stromal Cells of Endometriosis. *Reprod Sci* **18,** 1080–1084, doi: 10.1177/1933719111404614 (2011).
54. Dyson, M. T. *et al.* Genome-wide DNA methylation analysis predicts an epigenetic switch for GATA factor expression in endometriosis. *PLoS Genet* **10,** e1004158, doi: 10.1371/journal.pgen.1004158 (2014).
55. Xue, Q. *et al.* Methylation of a Novel CpG Island of Intron 1 Is Associated With Steroidogenic Factor 1 Expression in Endometriotic Stromal Cells. *Reprod Sci* **21,** 395–400, doi: 10.1177/1933719113497283 (2014).
56. Yamagata, Y. *et al.* Genome-wide DNA methylation profiling in cultured eutopic and ectopic endometrial stromal cells. *PLoS One* **9,** e83612, doi: 10.1371/journal.pone.0083612 (2014).
57. Flici, H. *et al.* Interlocked loops trigger lineage specification and stable fates in the Drosophila nervous system. *Nat Commun* **5,** 4484, doi: 10.1038/ncomms5484 (2014).
58. Laneve, P. *et al.* The Gcm/Glide molecular and cellular pathway: new actors and new lineages. *Dev Biol* **375,** 65–78, doi: 10.1016/j.ydbio.2012.12.014 (2013).
59. Halter, D. A. *et al.* The Homeobox Gene Repo Is Required for the Differentiation and Maintenance of Glia Function in the Embryonic Nervous-System of Drosophila-Melanogaster. *Development* **121,** 317–332 (1995).
60. Quan, X. J. *et al.* Post-translational Control of the Temporal Dynamics of Transcription Factor Activity Regulates Neurogenesis. *Cell* **164,** 460–475, doi: 10.1016/j.cell.2015.12.048 (2016).
61. Umesono, Y., Hiromi, Y. & Hotta, Y. Context-dependent utilization of Notch activity in Drosophila glial determination. *Development* **129,** 2391–2399 (2002).
62. Van de Bor, V. & Giangrande, A. Notch signaling represses the glial fate in fly PNS. *Development* **128,** 1381–1390 (2001).
63. Lebestky, T., Jung, S. H. & Banerjee, U. A Serrate-expressing signaling center controls Drosophila hematopoiesis. *Genes Dev* **17,** 348–353, doi: 10.1101/gad.1052803 (2003).
64. Halder, G., Callaerts, P. & Gehring, W. J. Induction of ectopic eyes by targeted expression of the eyeless gene in Drosophila. *Science* **267,** 1788–1792 (1995).
65. Kammermeier, L. *et al.* Differential expression and function of the Drosophila Pax6 genes eyeless and twin of eyeless in embryonic central nervous system development. *Mech Dev* **103,** 71–78 (2001).
66. Read, D. & Manley, J. L. Alternatively spliced transcripts of the Drosophila tramtrack gene encode zinc finger proteins with distinct DNA binding specificities. *The EMBO journal* **11,** 1035–1044 (1992).
67. Tang, A. H., Neufeld, T. P., Kwan, E. & Rubin, G. M. PHYL acts to down-regulate TTK88, a transcriptional repressor of neuronal cell fates, by a SINA-dependent mechanism. *Cell* **90,** 459–467 (1997).
68. Siddall, N. A., Hime, G. R., Pollock, J. A. & Batterham, P. Ttk69-dependent repression of lozenge prevents the ectopic development of R7 cells in the Drosophila larval eye disc. *BMC Dev Biol* **9,** 64, doi: 10.1186/1471-213X-9-64 (2009).
69. Egger, B. *et al.* Gliogenesis in Drosophila: genome-wide analysis of downstream genes of glial cells missing in the embryonic nervous system. *Development* **129,** 3295–3309 (2002).
70. Freeman, M. R., Delrow, J., Kim, J., Johnson, E. & Doe, C. Q. Unwrapping glial biology: Gcm target genes regulating glial development, diversification, and function. *Neuron* **38,** 567–580 (2003).
71. Altenhein, B. *et al.* Expression profiling of glial genes during Drosophila embryogenesis. *Dev Biol* **296,** 545–560 (2006).
72. Chintapalli, V. R., Wang, J. & Dow, J. A. T. Using FlyAtlas to identify better Drosophila melanogaster models of human disease. *Nature genetics* **39,** 715–720, doi: 10.1038/ng2049 (2007).
73. Val, P., Lefrancois-Martinez, A. M., Veyssiere, G. & Martinez, A. SF-1 a key player in the development and differentiation of steroidogenic tissues. *Nucl Recept* **1,** 8, doi: 10.1186/1478-1336-1-8 (2003).
74. Chen, P., Wang, D. B. & Liang, Y. M. Evaluation of estrogen in endometriosis patients: Regulation of GATA-3 in endometrial cells and effects on Th2 cytokines. *J Obstet Gynaecol Res*, doi: 10.1111/jog.12957 (2016).
75. Bulun, S. E. Mechanisms of Disease Endometriosis. *New Engl J Med* **360,** 268–279, doi: 10.1056/NEJMra0804690 (2009).
76. Lessey, B. A., Lebovic, D. I. & Taylor, R. N. Eutopic endometrium in women with endometriosis: ground zero for the study of implantation defects. *Semin Reprod Med* **31,** 109–124, doi: 10.1055/s-0032-1333476 (2013).
77. Missmer, S. A. *et al.* Incidence of laparoscopically confirmed endometriosis by demographic, anthropometric, and lifestyle factors. *Am J Epidemiol* **160,** 784–796, doi: 10.1093/aje/kwh275 (2004).
78. Practice Committee of the American Society for Reproductive, M. Endometriosis and infertility: a committee opinion. *Fertil Steril* **98,** 591–598, doi: 10.1016/j.fertnstert.2012.05.031 (2012).
79. Kopelman, A. *et al.* Analysis of Gene Expression in the Endocervical Epithelium of Women With Deep Endometriosis. *Reprod Sci*, doi: 10.1177/1933719116638179 (2016).
80. Yamagata, Y. *et al.* Retinoic acid has the potential to suppress endometriosis development. *J Ovarian Res* **8,** 49, doi: 10.1186/s13048-015-0179-6 (2015).
81. Aghajanova, L. & Giudice, L. C. Molecular evidence for differences in endometrium in severe versus mild endometriosis. *Reprod Sci* **18,** 229–251, doi: 10.1177/1933719110386241 (2011).
82. Borghese, B. *et al.* Gene expression profile for ectopic versus eutopic endometrium provides new insights into endometriosis oncogenic potential. *Mol Endocrinol* **22,** 2557–2562, doi: 10.1210/me.2008-0322 (2008).
83. Sherwin, J. R. *et al.* Global gene analysis of late secretory phase, eutopic endometrium does not provide the basis for a minimally invasive test of endometriosis. *Hum Reprod* **23,** 1063–1068, doi: 10.1093/humrep/den078 (2008).
84. Burney, R. O. *et al.* Gene expression analysis of endometrium reveals progesterone resistance and candidate susceptibility genes in women with endometriosis. *Endocrinology* **148,** 3814–3826, doi: 10.1210/en.2006-1692 (2007).
85. Cattenoz, P. B. & Giangrande, A. New Insights in the Clockwork Mechanism Regulating Lineage Specification: Lessons From the Drosophila Nervous System. *Dev Dynam* **244,** 332–341, doi: 10.1002/dvdy.24228 (2015).
86. Vernet, N. *et al.* Retinoic acid metabolism and signaling pathways in the adult and developing mouse testis. *Endocrinology* **147,** 96–110, doi: 10.1210/en.2005-0953 (2006).

Acknowledgements

We thank C. Papin, I. Stoll, N. Vernet, Y. Yuasa, G. Aiello, R. Sakr, C. Albrecht, N. Di Iacovo and the Imaging Center of the IGBMC for technical assistance and Y. Yuasa, V. Dasari and N. Di Iacovo for critical reading of

the manuscript. Stocks obtained from the Bloomington Drosophila Stock Center (NIH P40OD018537) and FlyORF as well as antibodies obtained from the Developmental Studies Hybridoma Bank were used in this study. This work was supported by INSERM, CNRS, UDS, Hôpital de Strasbourg, ARC, INCA and ANR grants. P. Cattenoz was funded by the ANR and W. Bazzi by the USIAS and FRM (FDT20160435111). The IGBMC was also supported by a French state fund through the ANR labex. This study was supported by the grant ANR-10-LABX-0030-INRT, a French State fund managed by the Agence Nationale de la Recherche under the frame program Investissements d'Avenir ANR-10-IDEX-0002-02.

Author Contributions

A.G. and P.B.C. conceived and designed the experiments. P.B.C., C.D. and W.B. performed the experiments. A.G. and P.B.C. analysed the data. A.G. and P.B.C. wrote the paper.

Additional Information

Supplementary information accompanies this paper at http://www.nature.com/srep

Competing financial interests: The authors declare no competing financial interests.

How to cite this article: Cattenoz, P. B. *et al.* An evolutionary conserved interaction between the Gcm transcription factor and the SF1 nuclear receptor in the female reproductive system. *Sci. Rep.* **6**, 37792; doi: 10.1038/srep37792 (2016).

Publisher's note: Springer Nature remains neutral with regard to jurisdictional claims in published maps and institutional affiliations.

Supplementary Information for:

An evolutionary conserved interaction between the Gcm transcription factor and the SF1 nuclear receptor in the female reproductive system

Pierre B. Cattenoz, Claude Delaporte, Wael Bazzi and Angela Giangrande*

Institut de Génétique et de Biologie Moléculaire et Cellulaire, IGBMC/CNRS/INSERM/UDS, BP 10142**,** 67404 ILLKIRCH, CU de Strasbourg, France.

***Corresponding author :**

Angela Giangrande,
Institut de Génétique et de Biologie Moléculaire et Cellulaire,
CNRS/INSERM/UDS, BP 10142,
67404 Illkirch Cedex,
CU de Strasbourg,
France.
angela@igbmc.fr

List of files:

Supplemental Figure S1, related to Figure 1

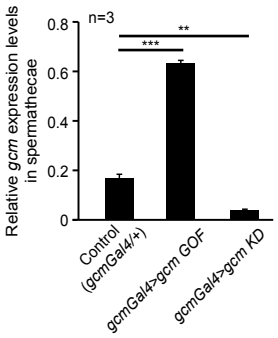

Supplemental Figure S1: Expression levels of Gcm in *gcm KD* and *gcm GOF* spermatheca

Expression levels of gcm in adult spermathecae measured by qPCR in *gcmGal4/+* (Control), *gcmGal4/+;UAS-gcm/+* (*gcm>gcm GOF*) and *gcmGal4/+;UAS-gcmRNAi/+* (*gcm>gcm KD*) animals. Each measurement was carried out in triplicate, normalised to the housekeeping genes *Gapdh* and *Act5C* and represented as described for **Figure 1a**. Each sample was prepared using at least 15 spermathecae.

Supplemental Figure S2, related to Figure 2

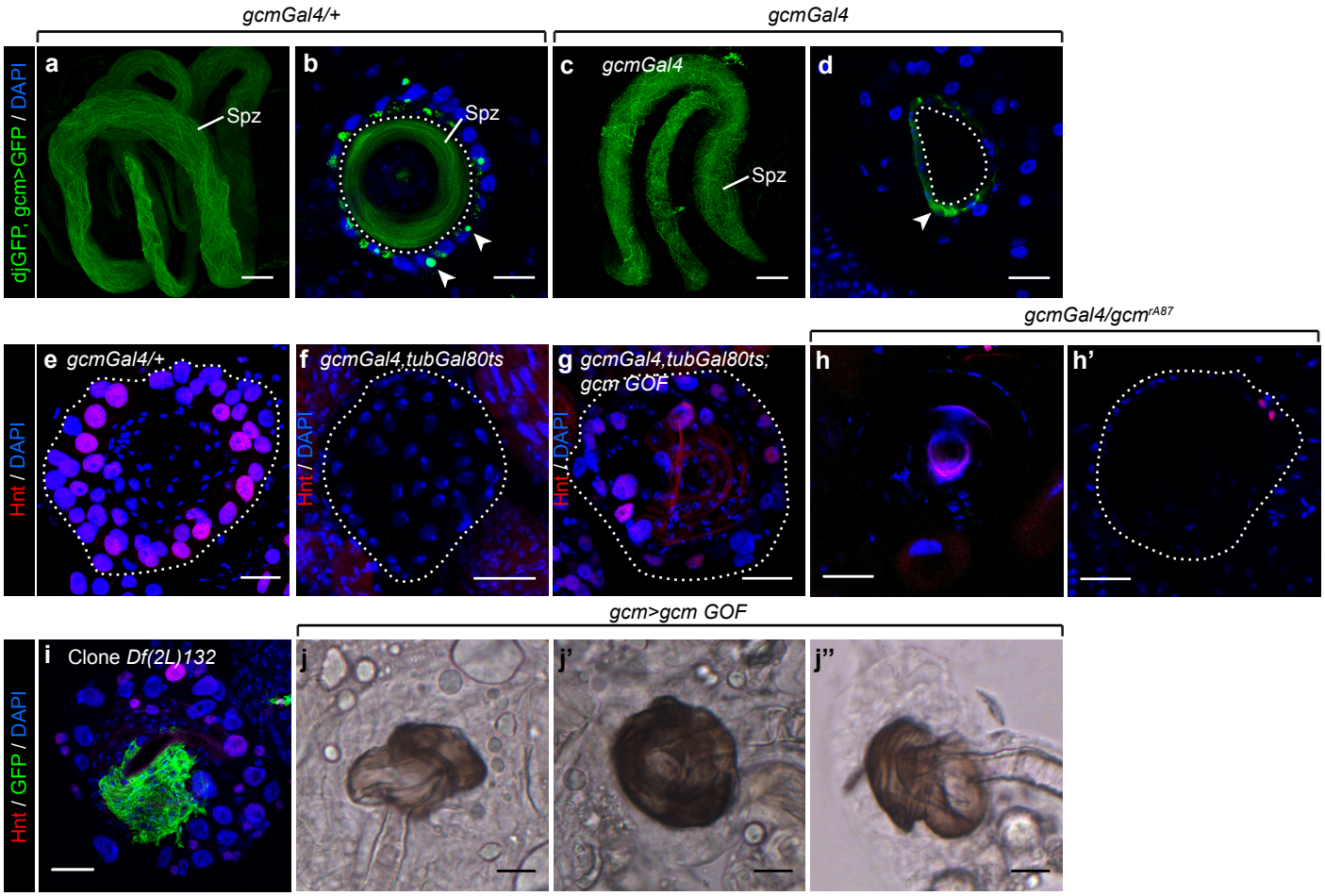

Supplemental Figure S2: Expression and role of Gcm in the spermatheca
a, c) Full confocal projections of *gcmGal4>GFP/+* **(a)** and *gcmGal4>GFP* homozygous **(c)** adult female seminal receptacles, carrying GFP positive spermatozoids (Spz) from *donjuanGFP* males (*djGFP*), labelled with anti-GFP (in green). The presence of the GFP signal in the seminal receptacles indicates that the females were inseminated. **b, d)** show single sections of the spermathecae that are attached to the seminal receptacles **(a, c)** labelled with anti-GFP (green) and DAPI (blue). The lumen of the spermatheca is outlined by a dashed line. Note the presence of GFP labelled spermatozoids in the *gcmGal4>GFP/+* spermatheca **(b)** and the absence of spermatozoids in the *gcmGal4>GFP* homozygous spermatheca **(d)**. The GFP positive cells (white arrowheads in **b and d**) indicate cells in which *gcm* promoter is activated (see **Supplemental Figure S3**). **e-g)** Full confocal projections of 1-day-old *gcmGal4/+* **(e)**, *gcmGal4/gcmGal4,tubGal80ts* (*gcmGal4,tubGal80ts*)**(f)** and *gcmGal4/gcmGal4,tubGal80ts;UAS-gcm* (*gcmGal4,tubGal80ts;gcm GOF*) **(g)** adult spermathecae from animals put at 29°C for 24 hrs after puparium formation to induce Gcm expression and labelled with anti-Hnt (Hnt, in red) and DAPI (blue). The dashed line outline the spermatheca. There are no SC in **(f)** whereas there are several SC (in red) in **(g)**. **h, h')** Single confocal sections of *gcmGal4/gcmrA87* adult spermathecae labelled with anti-Hnt (Hnt, in red) and DAPI (blue). The spermatheca is outlined with a dashed line in **(h')**. **i)** MARCM clone analysis of a null *gcm* mutation (*Df(2L)132*). The image represents the full projection of an adult spermatheca analysed by confocal microscopy. The clones are labelled with anti-GFP (green), anti-Hnt labelling is in red and DAPI in blue. **j-j")** Images of spermathecae analysed by bright-field microscopy. The spermathecae were dissected from *gcmGal4/+;UAS-gcm/+* (*gcm>gcm GOF*) adult females (1 to 3-day-old).

Supplemental Figure S3, related to Figure 3

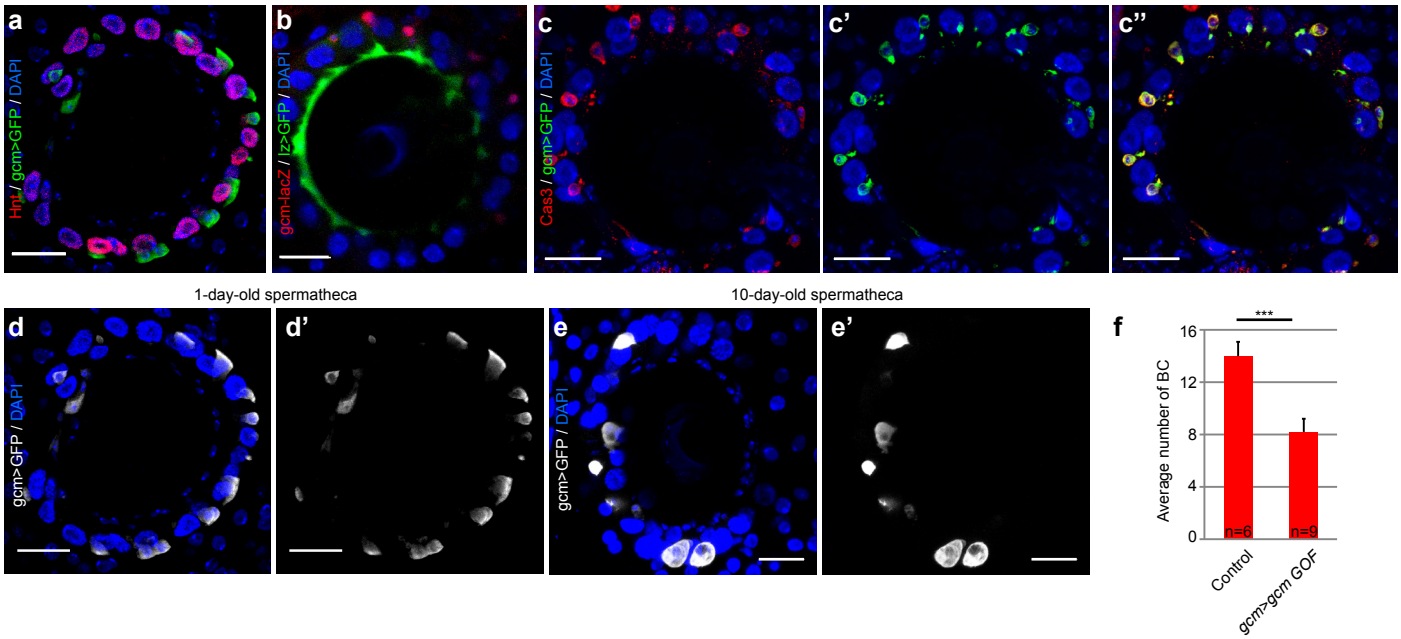

Supplemental Figure S3: Expression and role of Gcm in the spermatheca
a-c'') Single sections of adult spermathecae taken by confocal microscopy from adult control females (1 to 3-day-old). A gcmGal4,UAS-mCD8GFP/+ spermatheca **(a)** was labelled with DAPI (blue), anti-Hnt (Hnt, in red, secretory cell labelling) and anti-GFP (gcm>GFP, in green). A lzGal4,UAS-mCD8GFP/+;gcmrA87/+ adult spermatheca **(b)** was labelled with DAPI (blue), anti-βgal (gcm-lacZ, in red) and anti-GFP (lz>GFP, in green). A gcmGal4,UAS-mCD8GFP/+ adult spermatheca **(c-c'')** was labelled with anti-Caspase 3 (Cas3, in red), anti-GFP (gcm>GFP, in green) and DAPI (blue). **(c)** represents the overlay between anti-Cas3 and DAPI labelling, **(c')** between anti-GFP and DAPI labelling and **(c'')** between anti-Cas3, anti-GFP and DAPI labelling. **d-e')** Confocal projection of 1-day-old **(d, d')** and 10-day-old **(e, e')** gcmGal4,UAS-mCD8GFP/+ (gcm>GFP) adult spermathecae labelled with anti-GFP (gcm>GFP in grey) and DAPI (blue). **(d)** and **(e)** represent the overlay of DAPI and anti-GFP, **(d')** and **(e')** represent anti-GFP alone. **f)** Average number of basal cells (BC) counted in cross-sections of adult spermathecae of the indicated genotypes: gcmGal4/+ (Control) and gcmGal4/+;UAS-gcm/+ (gcm>gcm GOF). At least 6 spermathecae were analysed per genotype, the error bars and p-values are as described for **Figure 1a**.

Supplemental Figure S4, related to Figure 2

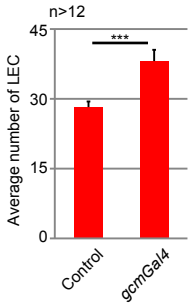

Supplemental Figure S4: lumen epithelial cells in gcm hypomorph spermatheca

Average number of lumen epithelial cells (LEC) counted in cross-sections of adult spermathecae of the indicated genotypes: *gcmGal4/+* (Control) and *gcmGal4* homozygous. At least 13 spermathecae were analysed per genotype, the error bars and p-values are as described for **Figure 1a**.

Supplemental experimental procedures

Fly strain

Flies were raised on standard medium at 25˚C. The following strains were used: the WT strain was *Oregon-R* (Bloomington #109612), *gcmGal4,UAS-mCD8GFP/CyO* [1] and *gcm^{rA87}/CyO* (Bloomington #5445) [2,3] were crossed with *sna^{Sco}/CyO,Tb^{1}* (Bloomington # 36335) to generate *gcmGal4,UAS-mCD8GFP/CyO,Tb^{1}* and *gcm^{rA87}/CyO,Tb^{1}* to identify homozygous and transheterozygous animals; the *gcm KD* was *P(TRiP.JF01075)attP2* (Bloomington #31519) and the *gcm GOF* was *UAS-gcmF18A* [4]; the efficiency of *gcm KD* and *gcm GOF* were verified by measuring the levels of Gcm expression in spermatheca using the driver *gcmGal4* **(Figure S1)**. Other strains used are *P[UAS-RedStinger]6* (*UAS-RFP* in the text, Bloomington #8547), *lzGal4,UAS-mCD8GFP* (Bloomington #6314), *UAS-Hr39* (FlyORF F00605) [5], *UAS-FLP:ubiFRT stop stinger III* (*g-trace* in the text) (Bloomington #28282). For the presence of spermatozoids in *gcmGal4/+* and *gcmGal4* homozygous spermathecae, 10 virgins of each genotype were mated for 3 days before dissection with 20 males *donjuanGFP* (*djGFP*, B# 5417) that express GFP in the spermatozoids [6] **(Figures S2a-d)**. For the rescue of the hypomorphic condition *gcmGal4* homozygous **(Figures S2e-g)**, *gcmGal4,UAS-mCD8GFP/CyO,Tb^{1}* animals were crossed with *Oregon-R*, *gcmGal4,tubGal80^{ts}/CyO,Tb^{1}* or *gcmGal4,tubGal80^{ts}/CyO,Tb^{1};UAS-gcmF18A* [1]. Animals *gcmGal4,UAS-mCD8GFP/+*, *gcmGal4,tubGal80^{ts}/gcmGal4,UAS-mCD8GFP* and *gcmGal4,tubGal80^{ts}/gcmGal4,UAS-mCD8GFP;UAS-gcmF18A* were collected and incubated at 29°C for 24hrs APF and then put at 25°C until adulthood. For the MARCM clones, the strain *Df(2L)132/CyO* [7] was recombined with *FRT40A* (Bloomington #8212) to generate *FRT40A,Df(2L)132/CyO*; the strain *gcm^{34}*, produced by imprecise excision obtained upon mutagenesis [2,8], was recombined with *FRT40A* (Bloomington #8212) to generate *FRT40A,gcm^{34}/CyO*. The clones were generated as follow: the three strains *FRT40A, FRT40A,Df(2L)132/CyO* and *FRT40A,gcm^{34}/CyO* were crossed with *hsFLP,UAS-mCD8GFP;tubGal80,FRT40A;tubGal4* (Bloomington #42725), the progeny was then heat shocked at larval stage L3 at 37˚C for 3 hrs and the spermathecae were dissected in 1 to 3-day-old adults.

Fertility and egg laying assays

For fertility assays, three 1-day-old virgins of a given genotype were crossed with one 1-day-old male *Oregon-R* on standard medium at 25˚C. The cross was flipped every three days for twelve days. The progeny issued from the four bottles is counted at the adult stage. Each cross was replicated at least ten times and paired with a control (*Oregon-R* females). The average number of progeny per female of the ten replicates and standard error of the mean are represented in **Figure 1a**. For the egg laying assays, five 1-day-old females of the indicated genotypes were crossed with ten 1-day-old males *Oregon-R* for 3 days, then the flies were transferred to a cage to count the number of eggs laid over 48 hrs. The number of eggs was then reported to the number of females and the number of days in **Figure 2i**. The p-values were estimated after variance analysis using bilateral student test with equal variance (ns for not significant; "*" for p-value < 0.05, 0.01 <; "**" for p-value < 0.01, 0.001 <; "***" for p-value < 0.001)).

Immunolabelling

The spermathecae were dissected from 1 to 3-day-old females in PBS, fixed 20 min in 4% paraformaldehyde/PBS at room temperature (RT), rinsed 15 min in PTX (PBS, 0.3% triton-x100), incubated with blocking reagent (Roche) for 1 hr at RT, incubated overnight at 4˚C with primary antibodies diluted in blocking reagent, washed three times 10 min with PTX, incubated 1 hr at RT with the secondary antibodies, rinsed three times 10 min with PTX, incubated 30 min with DAPI (Sigma) diluted to 10^{-3} g/L in blocking reagent and mounted on slide in vectashield (Vector Laboratories). For immunolabelling of the pupal spermatheca, white pupae (0 hr after puparium formation (APF)) were collected and fixed at 24 hrs, 48 hrs or 72 hrs APF overnight in 4% paraformaldehyde at 4˚C. Then, the spermathecae were dissected and treated as the adult spermathecae. The slides were analysed by confocal microscopy (Leica, SP5) and the images treated with Fiji [9]. The following antibodies were used: rabbit anti-RFP 1/500 (abcam #ab62341), chicken anti-GFP 1/1000 (abcam #ab13970), mouse anti-Hnt 1/100 (DSHB 1G9), rabbit anti-βgal 1/500 (Cappel # 55976) and rabbit anti-Caspase 3 1/100 (abcam #13847). Secondary antibodies were: donkey anti-chicken coupled with FITC 1/400 (Jackson #703-095-155), donkey anti-rabbit coupled with Cy3 1/600 (Jackson #711-165-152), goat anti-mouse coupled with Alexa Fluor 647 1/400 (Jackson #115-605-166).

Secretory cell and basal cell counts

The spermatheca were dissected and labelled with anti-Hnt antibody and DAPI as described above. For each spermatheca, the Hnt/DAPI positive cells (secretory cells) were counted from the stack of six focal plans taken at 3µm interval in the middle of the spermatheca (the plan giving the largest cross-section of the spermatheca). This was repeated in at least six independent spermathecae for each genotype. The average number of secretory cells and the standard error of the mean are represented in **Figure 2h** and **Figure 4h**. The p-values were estimated after

variance analysis using bilateral student test with equal variance (ns for not significant; "*" for p-value <0.05, 0.01<, "**" for p-value <0.01, 0.001<, "***" for p-value < 0.001).

qPCR and luciferase assay in S2 cells

The transfection of S2 cells, the quantitative PCR (qPCR) and the luciferase assay were performed as described in Cattenoz et al. [10]. For the qPCR, 6 million S2 cells were plated per well in 6-well plates in 1.5 mL of Schneider medium complemented with 10% Fetal Calf Serum (FCS) and 0.5% penicillin and 0.5% streptomycin (PS). Cells were transfected 12 hrs after plating using the Effectene transfection reagent (Qiagen) using 2 µg of *pPac-gal4* vector and 1 µg of *pUAS-GFP* for the negative control (*ppacEmpty*) and 2 µg of *pPac-gcm* [11] and 1 µg of *4.3kb repo-GFP* (*repoGFP*) [12] for the *gcm* GOF assays (*ppacGcm*). After 48 hrs of transfection, the cells were sorted on a BD FACSAria according to GFP expression to obtain more than 80% of transfected cells in the sample. The RNA was then extracted using TRI reagent (Sigma), 1 µg of RNA per sample was DNAse treated with RNAse free DNAse 1 (Thermo Fisher) and reverse transcribed with Superscript II (Invitrogen). Quantitative PCR (qPCR) assays were performed on a lightcycler LC480 (Roche) with SYBR master (Roche) on the equivalent of 5 ng of reverse transcribed RNA with the primer pairs targeting *Hr39*, *hnt*, *Gapdh1* and *Act5c* listed below. Each PCR was carried out in triplicates on at least three biological replicates. The quantity of each transcript was normalized to the quantity of *Gapdh1* and *Act5c*. The p-values were measured comparing the control with the transfected cells using student test, the bars represent the standard error of the mean.

For the luciferase assay, WT and mutant reporters were built for each GBS at *Hr39* and *hnt* loci. Sense and anti-sense oligonucleotides covering the GBS in each gene were synthesized using flanking restriction sites for KpnI at the 5' extremity and NheI at the 3' extremity. Each pair of oligonucleotides was designed with the WT GBS and with a mutated GBS that is not bound by Gcm (mutated for nucleotides 2, 3, 6 and/or 7: list below, the restriction sites are indicated in capital letters). For each WT and mutant GBS, 2 µg of annealed oligonucleotide were digested with 20 U of KpnI (NEB # R3142S) and 20 U of NheI (NEB # R3131S) in Cutsmart buffer (NEB # B7204S) for 1 h 30 min at 37ºC. The digested double stranded probes were then cleaned and ligated in *pGL4.23* (Promega #E841A) (ratio plasmid:probe = 1:6). Transfections of *Drosophila* S2 cells were carried out in 12-well plates using Effectene transfection reagent (Qiagen #301427) according to manufacturer's instructions. Cells were transfected with 0.5 µg *pPac-lacZ*, 0.5 µg *pGL4.23* carrying the indicated GBS, 0.5 µg *pPac-gcm* [11] or 0.5 µg *pPac* [13]. 48 hrs after transfection, cells were collected, washed once in cold PBS and resuspended in 100 µL of lysis buffer (25 mM Tris-phosphate pH7.8, 2 mM EDTA, 1 mM DTT, 10% glycerol, 1% Triton X-100). The suspensions were frozen / thawed four times in liquid nitrogen and centrifuged 30 min at 4ºC at 13000 g. The Luciferase and βgal activities were measured in triplicates for each sample. For βgal measurements, 20 µL of lysate were mixed with 50 µL of β-galactosidase assay buffer (60 mM Na2PO4, 40 mM NaH2PO4, 10 mM KCl, 1 mM MgCl2, 50 mM β-mercaptoethanol) and 20 µL ONPG (4mg / mL) and incubated at 37ºC for 20 min. The reaction was stopped by adding 50 µL 1M Na2CO3 and the DO at 415 nm was measured. For Luciferase activity, 10 µL of protein lysate were analysed on an opaque 96-well plate (Packard instrument # 6005290) with a Berthold Microluminat LB96P Luminometer by injecting 50 µL of luciferase buffer (20 mM Tris-phosphate pH 7.8, 1 mM MgCl2, 2.5 mM MgSO4, 0.1 mM EDTA, 0.5 mM ATP, 0.5 mM luciferine, 0.3 mM coenzyme A, 30 mM DTT). For both βgal and Luciferase assays, background levels were estimated using lysate from not transfected S2 cells. The relative Luciferase activities were calculated as follow: first the background was subtracted from each value, then the average values of the technical triplicate were calculated. From there, the Luciferase activity of each sample was normalized to the βgal activity (Luciferase activity / βgal activity) to correct for transfection efficiency variability and the ratio (Luciferase with Gcm / Luciferase without Gcm) was calculated. For each WT and mutant GBS, biological triplicates were carried out.

In situ hybridisation and RNA extraction from mouse uterus

RNA *in situ* hybridisation with digoxigenin-labelled probes for *mGcm2* transcripts was performed as described in Vernet et *al.* [14] with slight modifications. Cryosections (10 µm sections) of mouse (*C57BL/6*) uterus were labelled with sense or anti-sense probes targeting *mGcm2* (only the anti-sense probe is shown). The probes were synthesized from the clone 40054293 inserted into *pCR-BluntII-TOPO* using the Ribo-probe *in vitro* transcription system (Promega).

To assess *mGcm1*, *mGcm2* and *mNr5a1* levels of expression in uterus (**Figure 5f)**, the RNA was extracted from the uterus of *C57BL/6* using TRI reagent (Sigma) and the qPCR were carried out as described below for mammalian cells. The levels were estimated from 3 different animals.

Transfection and qPCR in mammalian cells

HeLa cells were plated in 6-well plates, 400,000 cells per well, in 1.6 mL of DMEM medium complemented with 5% FCS and gentamycin. Cells were transfected 12 hrs after plating using Effectene transfection reagent (Qiagen). Briefly, 1 µg of *pCIG* vector, 1 µg of *pCIG* vector expressing mGCM1 (*pCIG-mGcm1)* [15] or 1 µg of *pCIG* vector

expressing mGCM2 (*pCIG-mGcm2)* were mixed with 100 µL of EC buffer and 8 µL of enhancer, incubated 5 min at room temperature, then 10 µL of Effectene were added and the mix was incubated at room temperature for 20 min. 200 µL of DMEM medium + 5% FCS + gentamycin were added to the mix before spreading it on the cells. 48 hrs after transfection, the RNA was extracted using TRI reagent (Sigma).

MEF cells were plated in 6-well plates, 400,000 cells per well, in 1.6 mL of DMEM medium (4.5g/L glucose) complemented with 10% FCS, 1% sodium pyruvate and 0.5% penicillin and 0.5% streptomycin. Cells were transfected 12 hrs after plating using Effectene transfection reagent (Qiagen). Briefly, 1 µg of *pCIG* vector, 1 µg of *pCIG* vector expressing mGCM1 (*pCIG-mGcm1)* [15] or 1 µg of *pCIG* vector expressing mGCM2 (*pCIG-mGcm2)* were mixed with 100 µL of EC buffer and 8 µL of enhancer, incubated 5 min at room temperature, then 10 µL of Effectene were added and the mix was incubated at room temperature for 20 min. 200 µL of DMEM medium + 5% FCS + gentamycin were added to the mix before spreading it on the cells. After 48 hrs of transfection, the cells were sorted on a BD FACSAria according to GFP expression (the *pCIG* vectors express GFP constitutively) to obtain more than 80% of transfected cells in the sample. The RNA was then extracted using TRI reagent (Sigma).

Reverse transcription and qPCR were carried out as described for the S2 cells with the primer pairs listed below. The quantity of each transcript was normalized to the quantity of the housekeeping genes *Glyceraldehyde 3 phosphate dehydrogenase* (*Gapdh*) and *Actin Beta (ActnB).*

Bisulfite sequencing in MEF cells

MEF cells transfected and sorted as described above were used to analyse the methylation profile of *mNr5a1* locus. After sorting, the cells were incubated 1.5 hrs at 37°C in 20 mM EDTA, 10 mM Tris pH 8.0, 200 mM NaCl, 0.2% Triton X-100 and 100 mg/mL proteinase K and centrifuged at room temperature for 5 min at 14000 rpm. The DNA was precipitated from the supernatant by adding 1 vol. of isopropanol and 1/20 vol. of 4M NaCl, incubating the sample overnight at -20°C and centrifugation at 4°C for 25 min at 14000 rpm. The DNA pellet was suspended in demineralized water and treated with RNAse A for 1 hr at 37°C. Then 500 ng of DNA was digested with BamH1 restriction enzyme and converted with bisulfite using EZ DNA methylation Direct Kit (ZYMO #D5020) according to the manufacturer instruction. The loci of interest were then amplified by PCR using the ZymoTaq DNA polymerase (ZYMO #E2001) and the primers indicated below. The PCR products were cloned in pGEM-T Easy vector and sequenced by Sanger sequencing (GATC Biotech). At least 10 clones were sequenced per condition. The p-values were estimated after variance analysis using bilateral student test for paired samples (ns for not significant; "*" for p-value <0.05, 0.01<, "**" for p-value <0.01, 0.001<, "***" for p-value < 0.001).

List of primers:

specie	gene	Forward	Reverse
drosophila	Act5c	GCCAGCAGTCGTCTAATCCA	GACCATCACACCCTGGTGAC
drosophila	Gapdh1	CCCAATGTCTCCGTTGTGGA	TGGGTGTCGCTGAAGAAGTC
drosophila	Hr39	CCCAACTGGCTTTTGGGTAAC	AGAGGTGTCGTTGATGCAGTT
drosophila	hnt	TTTCAACGGGAACCAAGCCT	AGCATTTTTCCAACGGCTAGTT
drosophila	lz	CACCTATGTCACCATCCGGG	ACCTTGATGGCTTTGGCGTA
human	ACTNB	ATGATGATATCGCCGCGCTC	TCGATGGGGTACTTCAGGGT
human	GAPDH	GAGAAGGCTGGGGCTCATTT	AGTGATGGCATGGACTGTGG
human	NR5A1	AGCTGCAAGGGCTTCTTCAA	GCTTGTACATCGGCCCAAAC
human	NR5A2	GAGTCCAGGGAAAGACTTGCT	GCCTTGGGAAGGACACATCA
drosophila	Hr39GBS1mut	gagaGGTACCatattcttgtaattaaaaagttagtcgttgcttatgcatgcttatcttccGCTAGCgaga	tctcGCTAGCggaagataagcatgcataagcaacgactaacttttttaattacaagaatatGGTACCtctc
drosophila	Hr39GBS1wt	gagaGGTACCatattcttgtaattaaaaagttatgcgggacttatgcatgcttatcttccGCTAGCgaga	tctcGCTAGCggaagataagcatgcataagtcccgcataacttttttaattacaagaatatGGTACCtctc
drosophila	Hr39GBS2mut	gagaGGTACCagtgggcttaggatcttcgcacaacgactctccggcgggcatatcacgtcGCTAGCgaga	tctcGCTAGCgacgtgatatgcccgccggagagtcgttgtgcgaagatcctaagcccactGGTACCtctc
drosophila	Hr39GBS2wt	gagaGGTACCagtgggcttaggatcttcgcaccccgcatctccggcgggcatatcacgtcGCTAGCgaga	tctcGCTAGCgacgtgatatgcccgccggagatgcggggtgcgaagatcctaagcccactGGTACCtctc
drosophila	hntGBSmut	gagaGGTACCctggcttttaatgtatatttacaacgacttgccattaccatcattatattGCTAGCgaga	tctcGCTAGCaatataatgatggtaatggcaagtcgttgtaaatatacattaaaagccagGGTACCtctc
drosophila	hntGBSwt	gagaGGTACCctggcttttaatgtatatttaacacgcattgccattaccatcattatattGCTAGCgaga	tctcGCTAGCaatataatgatggtaatggcaatgcgtgttaaatatacattaaaagccagGGTACCtctc
mouse	ActnB	TACCAACTGGGACGACATGGAGAA	GCTCGAAGTCTAGAGCAACATAGC
mouse	Gapdh	TGAACGGGAAGCTCACTGG	TCCACCACCCTGTTGCTGTA
mouse	Gcm1	AAAGCCAGACAGAAGCAGCA	GCTCGCCTTTGGACTGGAAA

mouse	Gcm2	CACAGCGGATACCCTGTCAC	CAGCCGTGCTATTGAGGTGT
mouse	Nr5a1	CCGAGAGTCAGAGCTGCAAA	CATTCGATCAGCACGCACAG
mouse	Nr5a2	CAGTTCGATCAGCGGGAGTT	TGGGTAGTTGCAAACCGTGT
mouse	Msx1	CCGAAAGCCCCGAGAAACTA	CGCTCGGCAATAGACAGGTA
mouse bisulfite	Nr5a1 CpG exon 2	GTTTTGTTTTAGAGGAAGGGAATGA	CCCCCAAAACAATCCAACTATATAC
mouse bisulfite	Nr5a1 CpG TSS	GGTATTTTTAAATTGGATTAGTAAA	ATACAAAAAATAAAAAACAAACTAC

Supplemental bibliography

1 Soustelle, L. & Giangrande, A. Novel gcm-dependent lineages in the postembryonic nervous system of Drosophila melanogaster. *Developmental dynamics : an official publication of the American Association of Anatomists* **236**, 2101-2108, doi:10.1002/dvdy.21232 (2007).

2 Vincent, S., Vonesch, J. L. & Giangrande, A. Glide directs glial fate commitment and cell fate switch between neurones and glia. *Development* **122**, 131-139 (1996).

3 Jones, B. W., Fetter, R. D., Tear, G. & Goodman, C. S. glial cells missing: a genetic switch that controls glial versus neuronal fate. *Cell* **82**, 1013-1023 (1995).

4 Bernardoni, R., Miller, A. A. & Giangrande, A. Glial differentiation does not require a neural ground state. *Development* **125**, 3189-3200 (1998).

5 Bischof, J. *et al.* A versatile platform for creating a comprehensive UAS-ORFeome library in Drosophila. *Development* **140**, 2434-2442, doi:10.1242/dev.088757 (2013).

6 Santel, A., Winhauer, T., Blumer, N. & Renkawitz-Pohl, R. The Drosophila don juan (dj) gene encodes a novel sperm specific protein component characterized by an unusual domain of a repetitive amino acid motif. *Mech Dev* **64**, 19-30 (1997).

7 Lane, M. E. & Kalderon, D. Genetic investigation of cAMP-dependent protein kinase function in Drosophila development. *Genes Dev* **7**, 1229-1243 (1993).

8 Bernardoni, R., Vivancos, V. & Giangrande, A. glide/gcm is expressed and required in the scavenger cell lineage. *Developmental biology* **191**, 118-130 (1997).

9 Schindelin, J. *et al.* Fiji: an open-source platform for biological-image analysis. *Nat Methods* **9**, 676-682, doi:10.1038/nmeth.2019 (2012).

10 Cattenoz, P. B. *et al.* Functional Conservation of the Glide/Gcm Regulatory Network Controlling Glia, Hemocyte, and Tendon Cell Differentiation in Drosophila. *Genetics* **202**, 191-219, doi:10.1534/genetics.115.182154 (2016).

11 Miller, A. A., Bernardoni, R. & Giangrande, A. Positive autoregulation of the glial promoting factor glide/gcm. *The EMBO journal* **17**, 6316-6326, doi:10.1093/emboj/17.21.6316 (1998).

12 Laneve, P. *et al.* The Gcm/Glide molecular and cellular pathway: new actors and new lineages. *Dev Biol* **375**, 65-78, doi:10.1016/j.ydbio.2012.12.014 (2013).

13 Krasnow, M. A., Saffman, E. E., Kornfeld, K. & Hogness, D. S. Transcriptional activation and repression by Ultrabithorax proteins in cultured Drosophila cells. *Cell* **57**, 1031-1043 (1989).

14 Vernet, N. *et al.* Retinoic acid metabolism and signaling pathways in the adult and developing mouse testis. *Endocrinology* **147**, 96-110, doi:10.1210/en.2005-0953 (2006).

15 Soustelle, L. *et al.* Neurogenic role of Gcm transcription factors is conserved in chicken spinal cord. *Development* **134**, 625-634, doi:10.1242/dev.02750 (2007).

Table S1: list of genes directly targeted by Gcm and expressed in spermatheca

Genes directly targeted by Gcm (DamID screen, Cattenoz et al., 2016)	FBgn ID	Expression level in wild type spermatheca (average of two replicates, Allen and Spradling, 2008)
abd-A	FBgn0000014	1829,095
Abd-B	FBgn0000015	677,4245
ago	FBgn0041171	322,1235
AGO1	FBgn0262739	285,8825
Alh	FBgn0261238	131,733
Amun	FBgn0030328	238,319
aop	FBgn0000097	253,3475
apt	FBgn0015903	80,7979
Asph	FBgn0034075	154,041
Atet	FBgn0020762	395,57
Atg18a	FBgn0035850	1107,745
Atg5	FBgn0029943	148,614
Atg9	FBgn0034110	425,416
Atpalpha	FBgn0002921	1462,565
att-ORFB	FBgn0067782	88,1157
aux	FBgn0037218	594,9015
Axn	FBgn0026597	157,274
B52	FBgn0004587	1488,09
babos	FBgn0034724	135,052
bbg	FBgn0087007	2010,615
ben	FBgn0000173	2030,455
Best1	FBgn0040238	455,301
beta-Man	FBgn0037215	450,122
brat	FBgn0010300	99,5663
bt	FBgn0005666	697,293
bur	FBgn0000239	285,802
caps	FBgn0023095	253,692
CASK	FBgn0013759	316,754
cbt	FBgn0043364	1183,14
cbx	FBgn0011241	243,0905
CenG1A	FBgn0028509	469,813
CG10055	FBgn0037482	169,1075
CG10098	FBgn0037472	572,0075
CG10178	FBgn0032684	167,13
CG10195	FBgn0032787	93,28125
CG10311	FBgn0038420	2515,81
CG10465	FBgn0033017	1077,596
CG10939	FBgn0010620	1299,975
CG1103	FBgn0037235	218,371
CG1109	FBgn0046222	125,185
CG1124	FBgn0037290	1162,495
CG11279	FBgn0036342	393,922

CG11537	FBgn0035400	875,004
CG11576	FBgn0039882	353,8115
CG11920	FBgn0039274	167,485
CG11961	FBgn0034436	910,8705
CG12007	FBgn0037293	373,9425
CG12054	FBgn0039831	158,3635
CG12547	FBgn0250830	192,1735
CG12948	FBgn0037739	103,7605
CG12991	FBgn0030847	3409,88
CG13096	FBgn0032050	149,327
CG13366	FBgn0025633	156,689
CG13384	FBgn0032036	190,9485
CG13506	FBgn0034723	558,174
CG13728	FBgn0036716	108,20965
CG13907	FBgn0035173	398,4595
CG14040	FBgn0031676	348,458
CG14442	FBgn0029893	146,667
CG14478	FBgn0028953	278,568
CG14687	FBgn0037835	151,309
CG14764	FBgn0033236	191
CG14995	FBgn0035497	259,762
CG15523	FBgn0039727	220,99
CG1598	FBgn0033191	502,09
CG1677	FBgn0029941	365,829
CG17002	FBgn0033122	167,88
CG17266	FBgn0033089	87,80935
CG2145	FBgn0030251	1066,94
CG2162	FBgn0035388	258,393
CG2182	FBgn0037360	527,9685
CG2201	FBgn0032955	355,782
Cg25C	FBgn0000299	277,816
CG2617	FBgn0032877	136,6545
CG2811	FBgn0035082	307,318
CG30015	FBgn0050015	209,106
CG30069	FBgn0050069	413,4735
CG30080	FBgn0050080	126,7545
CG30159	FBgn0050159	541,558
CG30344	FBgn0050344	1228,855
CG3036	FBgn0031645	986,6955
CG30463	FBgn0050463	279,3715
CG30497	FBgn0050497	1359,405
CG31365	FBgn0051365	152,792
CG31368	FBgn0051368	103,878
CG31457	FBgn0051457	101,66915
CG31637	FBgn0051637	670,041
CG31650	FBgn0031673	186,0595
CG32264	FBgn0052264	555,1535
CG32344	FBgn0052344	155,0555

CG32486	FBgn0266918	493,772
CG32521	FBgn0052521	535,1485
CG32640	FBgn0052640	923,0625
CG33158	FBgn0053158	87,4974
CG3402	FBgn0035148	208,413
CG34317	FBgn0085346	87,7564
CG3558	FBgn0025681	252,7325
CG3702	FBgn0031590	652,7435
CG3760	FBgn0022343	781,8275
CG3781	FBgn0029853	214,034
CG3792	FBgn0031662	549,183
CG3857	FBgn0023520	127,3298
CG40006	FBgn0058006	139,7875
CG42238	FBgn0250867	93,85015
CG42389	FBgn0259735	342,392
CG43658	FBgn0263706	207,06
CG43675	FBgn0263750	1012,1355
CG4452	FBgn0035981	1170,395
CG45186	FBgn0266696	1132,88
CG4747	FBgn0043456	501,1685
CG5087	FBgn0035953	159,6335
CG5270	FBgn0037897	112,0487
CG5346	FBgn0038981	600,2225
CG5445	FBgn0030838	220,76
CG5789	FBgn0039207	121,699
CG5867	FBgn0027586	4016,45
CG6023	FBgn0030912	81,5793
CG6040	FBgn0038679	267,17
CG6145	FBgn0033853	1071,365
CG6276	FBgn0038316	302,3585
CG6398	FBgn0030870	568,0415
CG7009	FBgn0038861	102,41315
CG7029	FBgn0039026	257,271
CG7139	FBgn0027532	682,843
CG7337	FBgn0031374	583,441
CG7378	FBgn0030976	140,6595
CG7806	FBgn0032018	303,3565
CG7987	FBgn0038244	143,767
CG8188	FBgn0030863	81,53025
CG8507	FBgn0037756	467,826
CG9281	FBgn0030672	1409,69
CG9300	FBgn0036886	109,11155
CG9650	FBgn0029939	383,3235
CG9701	FBgn0036659	4153,89
CG9780	FBgn0037230	80,07805
CG9799	FBgn0038146	113,65085
CG9801	FBgn0037623	238,3685
cindr	FBgn0027598	146,3195

CkIalpha	FBgn0015024	922,2765
coro	FBgn0265935	1181,195
Cortactin	FBgn0025865	131,3395
corto	FBgn0010313	1077,61
COX7C	FBgn0040773	4380,115
cpo	FBgn0263995	1444,055
Crag	FBgn0025864	349,2645
crb	FBgn0259685	351,172
CrebA	FBgn0004396	1595,61
CREG	FBgn0025456	303,495
crq	FBgn0015924	404,3545
Cy	FBgn0283531	296,1175
D2hgdh	FBgn0023507	271,794
dally	FBgn0263930	584,2865
dap	FBgn0010316	271,126
DCTN1-p150	FBgn0001108	324,751
Den1	FBgn0033716	157,937
Diap1	FBgn0260635	2749,735
dj-1beta	FBgn0039802	431,59
Dl	FBgn0000463	171,823
DMAP1	FBgn0034537	115,33905
Dmtn	FBgn0037443	557,328
DnaJ-1	FBgn0263106	6758,065
dnr1	FBgn0260866	222,918
dnt	FBgn0024245	97,99755
DOR	FBgn0035542	486,865
dos	FBgn0016794	339,02
dpy	FBgn0053196	1570,855
drk	FBgn0004638	1060,39
drongo	FBgn0020304	672,84
Dscam1	FBgn0033159	84,1407
Dys	FBgn0260003	3099,89
E2f1	FBgn0011766	2029,85
Edem1	FBgn0023511	323,928
edl	FBgn0023214	291,1635
eIF-2gamma	FBgn0263740	942,966
eIF-3p40	FBgn0022023	1929,29
eIF-4a	FBgn0001942	6124,24
eIF5B	FBgn0026259	685,0165
Eip63E	FBgn0005640	1166,54
Eip74EF	FBgn0000567	447,344
Elal	FBgn0013949	157,7995
EloA	FBgn0039066	187,6915
Ent1	FBgn0031250	799,01
Epac	FBgn0085421	963,4245
Esp	FBgn0013953	314,4645
ex	FBgn0004583	299,0635
Fas2	FBgn0000635	526,6475

Fas3	FBgn0000636	852,5175
FER	FBgn0000723	131,925
fwd	FBgn0004373	609,5835
fz2	FBgn0016797	433,395
g	FBgn0001087	131,3705
Gale	FBgn0035147	1014,0025
GalT1	FBgn0053145	84,23735
Gcn5	FBgn0020388	250,3245
glec	FBgn0015229	511,565
Glut4EF	FBgn0267336	164,9285
Gmd	FBgn0031661	485,4145
Gug	FBgn0010825	512,232
gw	FBgn0051992	895,2145
h	FBgn0001168	5930,74
hang	FBgn0026575	152,127
hdly	FBgn0038842	3544,44
heph	FBgn0011224	213,0225
hh	FBgn0004644	477,587
Hmgcr	FBgn0263782	95,68645
hng2	FBgn0037634	94,9183
HnRNP-K	FBgn0267791	340,9705
hppy	FBgn0263395	298,003
Hr39	FBgn0261239	772,797
Hrb87F	FBgn0004237	1038,851
Hs6st	FBgn0038755	153,8465
Hsc70-4	FBgn0266599	12644,75
Hsc70Cb	FBgn0026418	641,0515
hth	FBgn0001235	726,5975
Idh	FBgn0001248	3326,935
if	FBgn0001250	275,283
ImpL2	FBgn0001257	131,3735
InR	FBgn0283499	144,56
Inx3	FBgn0265274	594,4525
jar	FBgn0011225	1007,4675
jbug	FBgn0028371	732,383
jigr1	FBgn0039350	157,6645
jumu	FBgn0015396	144,6845
Kap-alpha1	FBgn0024889	484,8155
KLHL18	FBgn0037978	107,88
ko	FBgn0020294	707,648
koi	FBgn0265003	595,6345
ksh	FBgn0040890	669,6045
l(1)10Bb	FBgn0001491	420,4975
l(2)k12914	FBgn0263852	3145,32
l(3)neo38	FBgn0265276	196,739
l(3)psg2	FBgn0035617	113,9855
Lac	FBgn0010238	1923,46
lama	FBgn0016031	1087,34

lbl	FBgn0008651	1484,115
loco	FBgn0020278	455,156
lola	FBgn0283521	828,4015
lsn	FBgn0260940	280,314
luna	FBgn0040765	94,43645
mbc	FBgn0015513	1122,725
mei-P26	FBgn0026206	91,289
Meltrin	FBgn0265140	103,1934
Mes2	FBgn0037207	275,719
Mes-4	FBgn0039559	84,78605
mew	FBgn0004456	866,7745
mfas	FBgn0260745	581,6975
mgl	FBgn0261260	716,8855
mib1	FBgn0263601	303,742
mino	FBgn0027579	219,214
Mlp84B	FBgn0014863	606,092
mrj	FBgn0034091	1724,175
mRpL53	FBgn0050481	196,9175
msi	FBgn0011666	148,8165
msps	FBgn0027948	463,6045
mtd	FBgn0013576	865,4615
Mvl	FBgn0011672	354,929
nahoda	FBgn0034797	106,39835
Ndae1	FBgn0259111	103,5275
Ndfip	FBgn0052177	1977,31
ND-MNLL	FBgn0029971	1807,635
neur	FBgn0002932	96,80635
NKAIN	FBgn0085442	152,775
nkd	FBgn0002945	104,84615
noc	FBgn0005771	422,5045
osp	FBgn0003016	405,4145
oys	FBgn0033476	922,7415
p130CAS	FBgn0035101	165,78
par-1	FBgn0260934	93,9153
par-6	FBgn0026192	488,499
Pdk1	FBgn0020386	1056,35
peb	FBgn0003053	842,197
Pep	FBgn0004401	1102,5555
Pfrx	FBgn0027621	180,896
PGAP3	FBgn0033088	217,1185
Pgd	FBgn0004654	541,2645
PH4alphaEFB	FBgn0039776	8051,64
pho	FBgn0002521	549,4505
ph-p	FBgn0004861	171,9425
Pino	FBgn0016926	1174,95
pio	FBgn0020521	496,5205
Pka-C1	FBgn0000273	84,73255
Pli	FBgn0025574	137,3795

pnr	FBgn0003117	1827,98
pnt	FBgn0003118	2030,275
pnut	FBgn0013726	579,796
Pp2C1	FBgn0022768	194,47
Ppa	FBgn0020257	585,5515
prtp	FBgn0030329	530,5815
psq	FBgn0263102	152,468
Ptp61F	FBgn0267487	1716,745
Ptp99A	FBgn0004369	251,6575
Pu	FBgn0003162	933,49
Pura	FBgn0035802	1020,345
px	FBgn0003175	273,0125
pyd	FBgn0262614	1562,895
Pym	FBgn0034918	149,3055
qsm	FBgn0028622	359,591
r	FBgn0003189	116,765
Rab5	FBgn0014010	1099,214
Rab7	FBgn0015795	3783,915
Rac2	FBgn0014011	607,2435
RanBP3	FBgn0039110	406,878
RapGAP1	FBgn0264895	448,128
Ras85D	FBgn0003205	545,923
Rbcn-3B	FBgn0023510	367,62
Rcd4	FBgn0032034	188,79
rdx	FBgn0264493	516,5365
retn	FBgn0004795	3303,91
rho	FBgn0004635	442,029
rho-7	FBgn0033672	257,817
RhoGEF3	FBgn0264707	141,212
rin	FBgn0015778	215,582
RnrS	FBgn0011704	222,299
robl	FBgn0024196	1104,58
Roc2	FBgn0044020	706,575
RpL17	FBgn0029897	8210,895
Rpn9	FBgn0028691	497,4765
S	FBgn0003310	166,3285
S6k	FBgn0283472	926,1285
scaf	FBgn0033033	689,6155
schlank	FBgn0040918	459,5625
scny	FBgn0260936	356,0485
Sdc	FBgn0010415	700,8805
Sema-5c	FBgn0250876	104,0513
Sh3beta	FBgn0035772	2314,405
shot	FBgn0013733	2537,105
Shroom	FBgn0085408	774,104
sip3	FBgn0039875	491,6555
Sirup	FBgn0031971	101,1519
siz	FBgn0026179	817,2835

Slip1	FBgn0024728	406,9095
slv	FBgn0025469	462,7635
smid	FBgn0016983	178,432
smo	FBgn0003444	197,764
Snx3	FBgn0038065	1012,6165
Socs36E	FBgn0041184	586,758
Socs44A	FBgn0033266	195,805
SoxN	FBgn0029123	254,3775
Spn	FBgn0010905	145,3065
SPoCk	FBgn0052451	138,0055
Spps	FBgn0039169	95,9651
spri	FBgn0085443	85,04325
sqd	FBgn0263396	607,8055
Srp19	FBgn0015298	952,216
Ssadh	FBgn0039349	257,847
Ssdp	FBgn0011481	422,85
ssp3	FBgn0032723	85,136
Stat92E	FBgn0016917	1965,775
sty	FBgn0014388	153,1655
Su(Tpl)	FBgn0014037	1132,55
Sur-8	FBgn0038504	123,2645
sws	FBgn0003656	428,5395
Taf4	FBgn0010280	609,292
Tango11	FBgn0050404	511,76
TBCB	FBgn0034451	295,5295
Ten-m	FBgn0004449	243,6385
TER94	FBgn0261014	1483,58
Tina-1	FBgn0035083	3143,01
Tis11	FBgn0011837	453,957
tmod	FBgn0082582	247,0415
tna	FBgn0026160	921,1385
toc	FBgn0015600	207,3655
TRAM	FBgn0040340	9577,845
trbl	FBgn0028978	287,3145
Trim9	FBgn0051721	132,807
trn	FBgn0010452	127,328
Tsp42Ea	FBgn0029508	2371,83
Tsp66E	FBgn0035936	528,7745
twin	FBgn0011725	371,3215
ush	FBgn0003963	536,773
Usp10	FBgn0052479	847,299
Usp47	FBgn0016756	809,1385
Usp8	FBgn0038862	137,4285
uzip	FBgn0004055	270,623
vih	FBgn0264848	235,558
vimar	FBgn0022960	159,4325
wake	FBgn0266418	251,123
wgn	FBgn0030941	111,2778

wun	FBgn0016078	293,285
Wwox	FBgn0031972	128,813
X11L	FBgn0026313	118,71785
yin	FBgn0265575	128,719
Zasp52	FBgn0265991	750,3135
ZIPIC	FBgn0039740	81,0034
Zir	FBgn0031216	265,127
Zn72D	FBgn0263603	227,223
Zpr1	FBgn0030096	220,2635

4. DISCUSSION AND PERSPECTIVES

Discussion and Perspectives

Gcm is a transcription factor necessary for embryonic plasmatocyte differentiation in *Drosophila* (BERNARDONI *et al.* 1997; ALFONSO AND JONES 2002) and a link between Gcm and inflammation has been suggested by a previous study in the lab (JACQUES *et al.* 2009). Gcm interact biochemically with the JAK/STAT regulator dPIAS and a recent Gcm DamID screen has identified direct interactions with key inhibitors of the JAK/STAT pathway (*Ptp61F*, *Socs36E*, *Socs44A*, *ken and barbie* (*ken*) and *Su(var)3-9*), and of the Toll cascade (*cactus*) (JACQUES *et al.* 2009; CATTENOZ *et al.* 2016b). This has raised an important question as to whether Gcm is necessary to control the inflammatory response. To that purpose, for my PhD thesis I have proposed to decipher the impact of Gcm on the innate immune response and inflammation, by focusing on the JAK/STAT and Toll signaling cascades *in vivo*. Both pathways are highly conserved in evolution and activated upon infections to induce the immune response (AGGARWAL AND SILVERMAN 2008; HETRU AND HOFFMANN 2009; YANG *et al.* 2015).

Gcm is expressed during embryonic hematopoiesis (BERNARDONI *et al.* 1997; ALFONSO AND JONES 2002) but not in definitive hematopoietic organ, the lymph gland. Given the presence of distinct hematopoietic waves, the current challenge at the time I started my PhD was to assess the relative contribution of the two waves to the inflammatory response. To that purpose, the second aim of my PhD work was to assess the specific impact of an embryonic factor in immune response, a process thought to rely on the lymph gland.

Concerning the role of Gcm in the immune response, I have shown that this factor inhibits the formation of melanotic tumors induced by the over-activation of the JAK/STAT and Toll cascades. This formally demonstrates the importance of primitive hematopoiesis in the inflammatory response. Moreover, I have shown that Gcm inhibits the secretion of the

proinflammatory cytokines Upd2 and Upd3 from embryonic hemocytes, which impacts the JAK/STAT pathway non-autonomously in post-embryonic immune tissues and the definitive hematopoietic organ, the lymph gland and shows that the Gcm developmental factor is necessary to regulate the competence to respond to inflammation. My data demonstrate for the first time the communication occurring between the primitive and the definitive hematopoietic waves. Finally, to further understand the interaction between Gcm and the inflammatory cascades, I have performed high throughput sequencing analyses and showed the impact of Gcm on genes associated with the mitochondria.

During my PhD, I have also contributed to a study that aimed to further understand the role of the Gcm transcription factor in the development of the spermatheca (CATTENOZ *et al.* 2016a).

Gcm affects several inflammatory cascades and immune responses

My data shows that Gcm inhibits the formation of melanotic tumors induced by the over-activation of the JAK/STAT and Toll cascades. Interestingly for the JAK/STAT pathway, I demonstrate that inhibiting melanotic tumor formation is mediated by over-expressing the Gcm DamID target *Ptp61F*. Given that Gcm has direct interactions with other inhibitors including *Socs36E, Socs44A, ken and barbie* (*ken*) and *Su(var)3-9* of the JAK/STAT pathway, it would be interesting to assess the competence of other inhibitors in rescuing the melanotic phenotype upon their specific over-expression in the primitive wave.

Furthermore, the Toll cascade inhibitors *cactus*, *Spn77Ba* and *Spn27A* are also Gcm direct targets. Studies revealed that *cactus* mutant animals develop melanotic tumors (MAKHIJANI *et al.* 2011). However, it would be interesting to investigative further the impact of

Gcm on Serpins in the context of melanotic tumor formation, which will help in understanding the overall role of the developmental factor Gcm on inflammation.

The impact of Gcm on inflammatory responses is not restricted to chronic conditions such as the JAK/STAT and Toll cascades. My data reveals that acute inflammatory responses induced by wasp infestation are also inhibited by Gcm (**Results, Chapter I, Figure 4K,L**). Given the broad impact of Gcm on chronic and acute inflammatory responses, it is important to ask whether other inflammatory cascades are also impacted by Gcm. One important cascade would be the IMD pathway. The importance of focusing on the IMD cascade is also based on the fact that the Toll and IMD pathways can cross-talk to induce increased effects against pathogens (TANJI *et al.* 2007). Interestingly, the Gcm DamID screen identifies *dnr1* (defense repressor 1) as a direct target. *dnr1* negatively regulates the activation of the NF-κB transcription factor Relish and consequently inhibits IMD signaling (FOLEY AND O'FARRELL 2004; TANJI AND IP 2005). Thus, it would be interesting to investigative the impact of Gcm on *dnr1* in the primitive wave and on the formation of melanotic tumors. This would open novel perspectives onto Gcm-IMD interaction.

Gcm and the inflammatory cytokines

My data shows that communication between the hematopoietic waves is crucial for a proper immune response and that Gcm controls the secretion of Upd2 and Upd3 proinflammatory cytokines from embryonic hemocytes. The following schematic summarizes my data and proposes a model for Gcm role and mode of action on the JAK/STAT pathway that also takes into account published data (**Figure 26**).

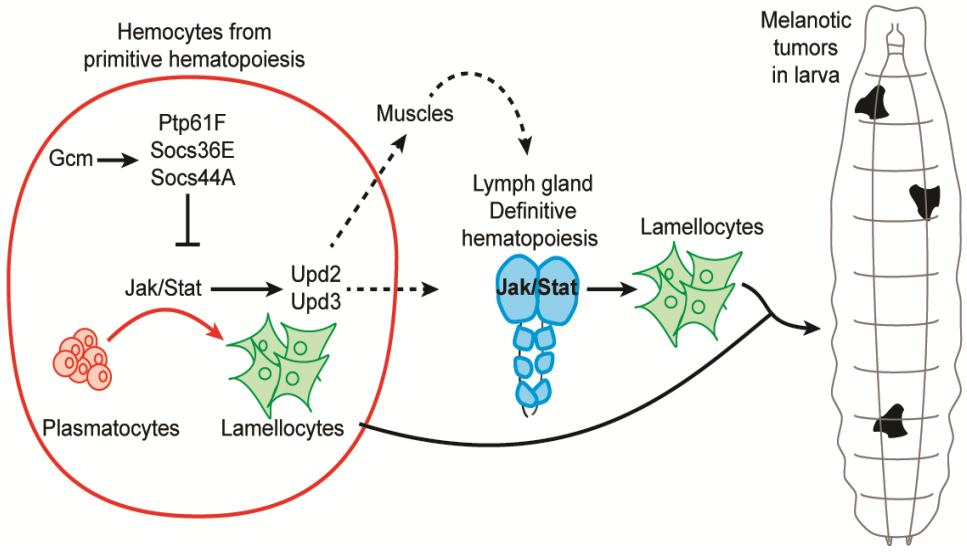

Figure 26: Schematic of Gcm regulatory role and the communication between both waves. Gcm induces the expression of JAK/STAT inhibitors in embryonic hemocytes that in turn regulate JAK/STAT signaling. In the absence of Gcm (*gcm KD*), JAK/STAT signaling induces the trans-differentiation of plasmatocytes into lamellocytes and the secretion of proinflammatory cytokines (Upd2 and Upd3). Upd2 and Upd3 induce subsequent JAK/STAT activation in post-embryonic tissues, such as the somatic muscles and the lymph gland. This leads to over-proliferation of hemocytes and differentiation of lamellocytes that aggregate and form melanotic masses on 3rd instar larvae.

In addition to JAK/STAT signaling, inflammatory cascades include Toll, JNK and IMD pathways. The cytokines/ligands acting as activators of these cascades include Spatzle (Spz) in the case of the Toll cascade (SHIA *et al.* 2009) and Eiger (TNF-α) in the case of the JNK pathway (IGAKI AND MIURA 2014). The IMD pathway involves PGRPs, which are innate immune molecules present in short (S) or long (L) forms. Short forms can also activate the Toll cascade and are located within the hemolymph, fat body cells, hemocytes and cuticle, whereas long forms are mainly present in hemocytes (DZIARSKI AND GUPTA 2006). Given the wide impact of Gcm on the inflammatory response (chronic/acute), it will be important to assess whether this factor also controls other cytokines/ligands such as Spz, Eiger and PGRPs. To further address this aspect, it will be necessary to measure the expression levels of the above cytokines in *gcm*

KD hemocytes. This analysis could spot additional Gcm regulatory roles on the secretion of proinflammatory cytokines in response to inflammatory conditions.

Gcm and the mitochondria

My transcriptome data on circulating hemocytes from gcm^{26}/+;$Toll^{10b}$/+ shows the impact of Gcm on the mitochondria, which highlights a novel interaction. Interestingly, many studies link the mitochondria with cancer, where the immortal cell resists the apoptotic cascade mediated by the mitochondria, leading to a deficit in Adenosine triphosphate (ATP) production (KROEMER 2006; LOPEZ-ARMADA *et al.* 2013). The differentially expressed genes in the double mutants reveal potential roles in inducing a proinflammatory and/or anti-inflammatory conditions. These genes include *Hsp60D* and the cytochrome P450 genes due to their link to inflammation (KOL *et al.* 2000; OHASHI *et al.* 2000; DE GREGORIO *et al.* 2002; IRVING *et al.* 2005; THEKEN *et al.* 2011). Thus, it is necessary to validate those candidates *in vivo* for melanotic tumor formation/inhibition. This will further elucidate the relation between Gcm, mitochondria and Toll signaling.

Gcm affects definitive hematopoiesis

Gcm is a developmental factor necessary in the primitive wave only (BERNARDONI *et al.* 1997; ALFONSO AND JONES 2002). Upon wasp infestation in 3rd instar larvae, Gcm is no longer expressed in hemocytes. Interestingly, my data shows that acute inflammatory responses induced by wasp infestation are also inhibited by Gcm (**Results, Chapter I, Figure 4K,L**). This reveals that a developmental transcription factor is necessary to regulate the competence to respond to inflammation. Thus, looking into the molecular landscape of hemocytes upon and inflammatory response will elucidate the impact of Gcm in this process.

Moreover, my data demonstrate the communication occurring between distinct hematopoietic waves. The embryonic hemocytes signal to the lymph gland through cytokine secretion, a process regulated by Gcm. In this context, several questions arise. 1) What is the specific contribution of embryonic hemocytes to the inflammatory response of the definitive hematopoietic wave? To address this issue, we are planning to assess the lymph gland phenotype upon embryonic hemocytes ablation. This can be achieved by over-expressing pro-apoptotic encoding genes such as *reaper* and *hid* in the primitive wave and assessing the definitive hematopoietic organ in terms of proliferating and differentiating of hemocytes. 2) Can the lymph gland signal to the embryonic hemocytes during an immune response? Studies reveal that over-expressing the JAK/STAT pathway specifically in the lymph gland induces melanotic tumor formation and over-proliferation of hemocytes in circulation (KIMBRELL *et al.* 2002). In order to assess the aspect, it would be necessary to G-trace the circulating hemocytes upon JAK/STAT over-expression in the lymph gland. This will elucidate the proportion of hemocytes coming from embryonic origin and contributing to melanotic tumor formation. Answering these questions will help understanding the homeostatic interactions occurring between hematopoietic waves.

Gcm affects homing/mobilization

My work on the Gcm-JAK/STAT interaction suggests that Gcm has an impact on hemocyte homing/mobilization. The majority of the plasmatocytes during the larval stage migrates and gets attached to the cuticular epidermis, forming the sessile compartment. These cells mobilize into circulation upon infection (LANOT *et al.* 2001; KURUCZ *et al.* 2007; MAKHIJANI *et al.* 2011). Several studies highlighted two important proteins involved in

determining the circulating and sessile status of hemocytes: Eater and Edin. Eater is a phagocytic receptor present on plasmatocyte membranes (KOCKS *et al.* 2005) that is also required in normal conditions for the attachment of plasmatocytes to the sessile compartment (BRETSCHER *et al.* 2015) (**Figure 27A**). I have found that *eater* expression levels decrease in *gcm KD* circulating hemocytes (**Results, Chapter I, Figure S7A**), which further explain the observed recruitment of sessile cells in *repoGal80,gcm>gcm KD,UAS-hop*$^{Tum\text{-}l}$ (**Results, Chapter I, Figure 4A-F**). Edin (Elevated during infection) in contrast, is a small peptide secreted by the fat body upon infections and it plays role in the recruitment of sessile blood cells into circulation (VANHA-AHO *et al.* 2015) (**Figure 27A**). This shows that Eater and Edin play antagonistic roles in the attachment/recruitment of hemocytes. *edin* expression is also inhibited by WntD: a secreted protein of the *Drosophila* Wnt family, and *wntD* mutant flies show high *edin* expression levels with a consequent recruitment of sessile cells into circulation (GORDON *et al.* 2005; GORDON *et al.* 2008). Our DamID screen identified *wntD* as a Gcm direct target (CATTENOZ *et al.* 2016b), suggesting that Gcm regulates *wntD* at the transcriptional level (**Figure 27B**). Thus, Gcm may act on hemocytes by, on the one hand, increasing their attachment (through *eater*) and on the other hand by decreasing their mobilization (upon decreasing *edin* levels) (**Figure 27C**). Future studies will clarify the role of Gcm: one important experiment will be to measure *edin* expression levels in the fat body upon *gcm KD* and to determine *wntD* expression levels in *gcm KD* hemocytes.

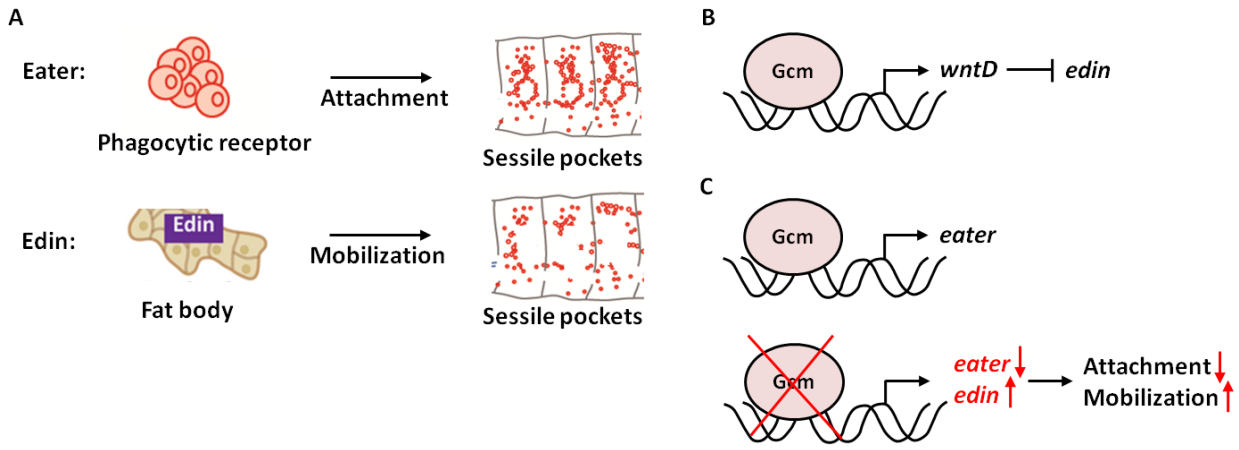

Figure 27: Schematic for Gcm potential regulatory role on sessile hemocytes. (**A**) Eater is expressed on plasmatocytes and prevents mobilization of sessile hemocytes. Edin is a small peptide secreted by the fat body and induces mobilization of hemocytes. (**B**) Gcm induces its DamID target *wntD*, which in turn regulates *edin*. (**C**) *gcm KD* leads to decreased *eater* expression levels in circulating hemocytes and induces mobilization of sessile hemocytes.

Functional conservation of Gcm in evolution

The two *Drosophila gcm* genes are conserved in evolution. *Drosophila* and mammalian Gcm proteins have a conserved DNA-binding domain (DBD) "(A/G)CCCGCAT" (AKIYAMA *et al.* 1996; WEGNER AND RIETHMACHER 2001). In mammals, the two Gcm homologs *GCMa/GCM1* and *GCMb/GCM2* were shown to be involved in placental development from embryonic day 7.5 (E7.5) until (E17.5) (ALTSHULLER *et al.* 1996; BASYUK *et al.* 1999; NAIT-OUMESMAR *et al.* 2000) and in the development of the parathyroid gland, respectively (KIM *et al.* 1998; GORDON *et al.* 2001). My data shows that mGcm2 induces JAK/STAT inhibitors *SOCS1*, *SOCS3* and *PTPN2* in a human leukemia cell line (K562) highlighting a possible conserved role of the Gcm genes in mammalian immunity (**Results, Chapter I, Figure S13A**). Our laboratory has found that *mGcm2* is expressed in adult murine immune cells from bone marrow, spleen and thymus, such as B-cells, T-cells (involved in adaptive immunity) and Plasmacytoid dendritic cells (pDCs) (involved in innate immunity) (Yuasa et al., in preparation). To

complement this data, it would be necessary to characterize the molecular landscape of B-cells, T-cells and Plasmacytoid dendritic cells (pDCs) in the conditional knockout mice for *mGcm2* (cKO *mGcm2*). This analysis will give an insight as to whether the role of Gcm in the immune system response is conserved in evolution. Interestingly, the *mGcm1* gene does not seem to be expressed in the adult immune system. If this is confirmed, it would be interesting to analyze the profile of expression of *mGcm1* in immune cells during mouse development as well.

Conclusive remarks

Given the known impact of immunity in tumor development, future studies in *Drosophila* will provide a better characterization for Gcm role in inhibiting melanotic tumor formation. Furthermore, focusing on Gcm orthologs in mammals will provide additional evidence for a possible conserved function in immunity. Given the evolutionary conservation of the basic biological processes, I believe that my work will shed light on the immune response in higher organisms as well. In the long term, this may help understanding the physio-pathological mechanisms underlying human diseases linked to the immune system, which represent a heavy burden to our societies.

5. BIBLIOGRAPHY

Bibliography

Agaisse, H., and N. Perrimon, 2004 The roles of JAK/STAT signaling in Drosophila immune responses. Immunol Rev 198**:** 72-82.

Aggarwal, K., and N. Silverman, 2008 Positive and negative regulation of the Drosophila immune response. BMB Rep 41**:** 267-277.

Akira, S., and K. Takeda, 2004 Toll-like receptor signalling. Nat Rev Immunol 4**:** 499-511.

Akira, S., S. Uematsu and O. Takeuchi, 2006 Pathogen recognition and innate immunity. Cell 124**:** 783-801.

Akiyama, Y., T. Hosoya, A. M. Poole and Y. Hotta, 1996 The gcm-motif: a novel DNA-binding motif conserved in Drosophila and mammals. Proc Natl Acad Sci U S A 93**:** 14912-14916.

Alfonso, T. B., and B. W. Jones, 2002 gcm2 promotes glial cell differentiation and is required with glial cells missing for macrophage development in Drosophila. Dev Biol 248**:** 369-383.

Altshuller, Y., N. G. Copeland, D. J. Gilbert, N. A. Jenkins and M. A. Frohman, 1996 Gcm1, a mammalian homolog of Drosophila glial cells missing. FEBS Lett 393**:** 201-204.

Amoyel, M., A. M. Anderson and E. A. Bach, 2014 JAK/STAT pathway dysregulation in tumors: a Drosophila perspective. Semin Cell Dev Biol 28**:** 96-103.

Arbouzova, N. I., and M. P. Zeidler, 2006 JAK/STAT signalling in Drosophila: insights into conserved regulatory and cellular functions. Development 133**:** 2605-2616.

Arnot, C. J., N. J. Gay and M. Gangloff, 2010 Molecular mechanism that induces activation of Spatzle, the ligand for the Drosophila Toll receptor. J Biol Chem 285**:** 19502-19509.

Arya, R., and S. C. Lakhotia, 2008 Hsp60D is essential for caspase-mediated induced apoptosis in Drosophila melanogaster. Cell Stress Chaperones 13**:** 509-526.

Attar, E., H. Tokunaga, G. Imir, M. B. Yilmaz, D. Redwine *et al.*, 2009 Prostaglandin E2 via steroidogenic factor-1 coordinately regulates transcription of steroidogenic genes necessary for estrogen synthesis in endometriosis. J Clin Endocrinol Metab 94**:** 623-631.

Baeg, G. H., R. Zhou and N. Perrimon, 2005 Genome-wide RNAi analysis of JAK/STAT signaling components in Drosophila. Genes Dev 19**:** 1861-1870.

Balkwill, F., and A. Mantovani, 2001 Inflammation and cancer: back to Virchow? Lancet 357**:** 539-545.

Baron, M. H., 2013 Concise Review: early embryonic erythropoiesis: not so primitive after all. Stem Cells 31**:** 849-856.

Basyuk, E., J. C. Cross, J. Corbin, H. Nakayama, P. Hunter *et al.*, 1999 Murine Gcm1 gene is expressed in a subset of placental trophoblast cells. Dev Dyn 214**:** 303-311.

Bataille, L., B. Auge, G. Ferjoux, M. Haenlin and L. Waltzer, 2005 Resolving embryonic blood cell fate choice in Drosophila: interplay of GCM and RUNX factors. Development 132**:** 4635-4644.

Baxter, E. J., L. M. Scott, P. J. Campbell, C. East, N. Fourouclas *et al.*, 2005 Acquired mutation of the tyrosine kinase JAK2 in human myeloproliferative disorders. Lancet 365**:** 1054-1061.

Belvin, M. P., and K. V. Anderson, 1996 A conserved signaling pathway: the Drosophila toll-dorsal pathway. Annu Rev Cell Dev Biol 12**:** 393-416.

Bernardoni, R., V. Vivancos and A. Giangrande, 1997 glide/gcm is expressed and required in the scavenger cell lineage. Dev Biol 191**:** 118-130.

Betz, A., N. Lampen, S. Martinek, M. W. Young and J. E. Darnell, Jr., 2001 A Drosophila PIAS homologue negatively regulates stat92E. Proc Natl Acad Sci U S A 98**:** 9563-9568.

Bina, S., V. M. Wright, K. H. Fisher, M. Milo and M. P. Zeidler, 2010 Transcriptional targets of Drosophila JAK/STAT pathway signalling as effectors of haematopoietic tumour formation. EMBO Rep 11**:** 201-207.

Binari, R., and N. Perrimon, 1994 Stripe-specific regulation of pair-rule genes by hopscotch, a putative Jak family tyrosine kinase in Drosophila. Genes Dev 8**:** 300-312.

Binggeli, O., C. Neyen, M. Poidevin and B. Lemaitre, 2014 Prophenoloxidase activation is required for survival to microbial infections in Drosophila. PLoS Pathog 10**:** e1004067.

Brand, A. H., and N. Perrimon, 1993 Targeted gene expression as a means of altering cell fates and generating dominant phenotypes. Development 118**:** 401-415.

Bretscher, A. J., V. Honti, O. Binggeli, O. Burri, M. Poidevin *et al.*, 2015 The Nimrod transmembrane receptor Eater is required for hemocyte attachment to the sessile compartment in Drosophila melanogaster. Biol Open 4**:** 355-363.

Brightbill, H. D., and R. L. Modlin, 2000 Toll-like receptors: molecular mechanisms of the mammalian immune response. Immunology 101**:** 1-10.

Brooks, A. J., W. Dai, M. L. O'Mara, D. Abankwa, Y. Chhabra *et al.*, 2014 Mechanism of activation of protein kinase JAK2 by the growth hormone receptor. Science 344**:** 1249783.

Brown, S., N. Hu and J. C. Hombria, 2001 Identification of the first invertebrate interleukin JAK/STAT receptor, the Drosophila gene domeless. Curr Biol 11**:** 1700-1705.

Bruckner, K., L. Kockel, P. Duchek, C. M. Luque, P. Rorth *et al.*, 2004 The PDGF/VEGF receptor controls blood cell survival in Drosophila. Dev Cell 7**:** 73-84.

Callus, B. A., and B. Mathey-Prevot, 2002 SOCS36E, a novel Drosophila SOCS protein, suppresses JAK/STAT and EGF-R signalling in the imaginal wing disc. Oncogene 21**:** 4812-4821.

Cattenoz, P. B., C. Delaporte, W. Bazzi and A. Giangrande, 2016a An evolutionary conserved interaction between the Gcm transcription factor and the SF1 nuclear receptor in the female reproductive system. Sci Rep 6**:** 37792.

Cattenoz, P. B., and A. Giangrande, 2013 Lineage specification in the fly nervous system and evolutionary implications. Cell Cycle 12**:** 2753-2759.

Cattenoz, P. B., A. Popkova, T. D. Southall, G. Aiello, A. H. Brand *et al.*, 2016b Functional Conservation of the Glide/Gcm Regulatory Network Controlling Glia, Hemocyte, and Tendon Cell Differentiation in Drosophila. Genetics 202**:** 191-219.

Chang, A. N., A. B. Cantor, Y. Fujiwara, M. B. Lodish, S. Droho *et al.*, 2002 GATA-factor dependence of the multitype zinc-finger protein FOG-1 for its essential role in megakaryopoiesis. Proc Natl Acad Sci U S A 99**:** 9237-9242.

Chen, E., L. M. Staudt and A. R. Green, 2012 Janus kinase deregulation in leukemia and lymphoma. Immunity 36**:** 529-541.

Chen, H. W., X. Chen, S. W. Oh, M. J. Marinissen, J. S. Gutkind *et al.*, 2002 mom identifies a receptor for the Drosophila JAK/STAT signal transduction pathway and encodes a protein distantly related to the mammalian cytokine receptor family. Genes Dev 16**:** 388-398.

Cherry, S., and N. Silverman, 2006 Host-pathogen interactions in drosophila: new tricks from an old friend. Nat Immunol 7**:** 911-917.

Coelho, A., S. Fraichard, G. Le Goff, P. Faure, Y. Artur *et al.*, 2015 Cytochrome P450-dependent metabolism of caffeine in Drosophila melanogaster. PLoS One 10**:** e0117328.

Colotta, F., S. K. Dower, J. E. Sims and A. Mantovani, 1994 The type II 'decoy' receptor: a novel regulatory pathway for interleukin 1. Immunol Today 15**:** 562-566.

Coussens, L. M., and Z. Werb, 2002 Inflammation and cancer. Nature 420**:** 860-867.

Crozatier, M., J. M. Ubeda, A. Vincent and M. Meister, 2004 Cellular immune response to parasitization in Drosophila requires the EBF orthologue collier. PLoS Biol 2**:** E196.

Daga, A., C. A. Karlovich, K. Dumstrei and U. Banerjee, 1996 Patterning of cells in the Drosophila eye by Lozenge, which shares homologous domains with AML1. Genes Dev 10**:** 1194-1205.

De Gregorio, E., P. T. Spellman, P. Tzou, G. M. Rubin and B. Lemaitre, 2002 The Toll and Imd pathways are the major regulators of the immune response in Drosophila. EMBO J 21**:** 2568-2579.

de Groot, R. P., J. A. Raaijmakers, J. W. Lammers, R. Jove and L. Koenderman, 1999 STAT5 activation by BCR-Abl contributes to transformation of K562 leukemia cells. Blood 94**:** 1108-1112.

Du, W., J. Hong, Y. C. Wang, Y. J. Zhang, P. Wang *et al.*, 2012 Inhibition of JAK2/STAT3 signalling induces colorectal cancer cell apoptosis via mitochondrial pathway. J Cell Mol Med 16**:** 1878-1888.

Dushay, M. S., and E. D. Eldon, 1998 Drosophila immune responses as models for human immunity. Am J Hum Genet 62**:** 10-14.

Dziarski, R., and D. Gupta, 2006 The peptidoglycan recognition proteins (PGRPs). Genome Biol 7**:** 232.

Earl, T. M., I. B. Nicoud, J. M. Pierce, J. P. Wright, N. E. Majoras *et al.*, 2009 Silencing of TLR4 decreases liver tumor burden in a murine model of colorectal metastasis and hepatic steatosis. Ann Surg Oncol 16**:** 1043-1050.

Elrod-Erickson, M., S. Mishra and D. Schneider, 2000 Interactions between the cellular and humoral immune responses in Drosophila. Curr Biol 10**:** 781-784.

Evans, C. J., V. Hartenstein and U. Banerjee, 2003 Thicker than blood: conserved mechanisms in Drosophila and vertebrate hematopoiesis. Dev Cell 5**:** 673-690.

Fernandez, N. Q., J. Grosshans, J. S. Goltz and D. Stein, 2001 Separable and redundant regulatory determinants in Cactus mediate its dorsal group dependent degradation. Development 128**:** 2963-2974.

Fischer, J. A., E. Giniger, T. Maniatis and M. Ptashne, 1988 GAL4 activates transcription in Drosophila. Nature 332**:** 853-856.

Flici, H., P. B. Cattenoz, O. Komonyi, P. Laneve, B. Erkosar *et al.*, 2014 Interlocked loops trigger lineage specification and stable fates in the Drosophila nervous system. Nat Commun 5**:** 4484.

Foley, E., and P. H. O'Farrell, 2004 Functional dissection of an innate immune response by a genome-wide RNAi screen. PLoS Biol 2**:** E203.

Fossett, N., K. Hyman, K. Gajewski, S. H. Orkin and R. A. Schulz, 2003 Combinatorial interactions of serpent, lozenge, and U-shaped regulate crystal cell lineage commitment during Drosophila hematopoiesis. Proc Natl Acad Sci U S A 100**:** 11451-11456.

Fossett, N., S. G. Tevosian, K. Gajewski, Q. Zhang, S. H. Orkin *et al.*, 2001 The Friend of GATA proteins U-shaped, FOG-1, and FOG-2 function as negative regulators of blood, heart, and eye development in Drosophila. Proc Natl Acad Sci U S A 98**:** 7342-7347.

Franc, N. C., K. White and R. A. Ezekowitz, 1999 Phagocytosis and development: back to the future. Curr Opin Immunol 11**:** 47-52.

Furqan, M., N. Mukhi, B. Lee and D. Liu, 2013 Dysregulation of JAK-STAT pathway in hematological malignancies and JAK inhibitors for clinical application. Biomark Res 1**:** 5.

Gay, N. J., M. Gangloff and A. N. Weber, 2006 Toll-like receptors as molecular switches. Nat Rev Immunol 6**:** 693-698.

Geissler, K., and O. Zach, 2012 Pathways involved in Drosophila and human cancer development: the Notch, Hedgehog, Wingless, Runt, and Trithorax pathway. Ann Hematol 91**:** 645-669.

Ghosh, S., A. Singh, S. Mandal and L. Mandal, 2015 Active hematopoietic hubs in Drosophila adults generate hemocytes and contribute to immune response. Dev Cell 33**:** 478-488.

Gordon, J., A. R. Bennett, C. C. Blackburn and N. R. Manley, 2001 Gcm2 and Foxn1 mark early parathyroid- and thymus-specific domains in the developing third pharyngeal pouch. Mech Dev 103**:** 141-143.

Gordon, M. D., J. S. Ayres, D. S. Schneider and R. Nusse, 2008 Pathogenesis of listeria-infected Drosophila wntD mutants is associated with elevated levels of the novel immunity gene edin. PLoS Pathog 4**:** e1000111.

Gordon, M. D., M. S. Dionne, D. S. Schneider and R. Nusse, 2005 WntD is a feedback inhibitor of Dorsal/NF-kappaB in Drosophila development and immunity. Nature 437**:** 746-749.

Granger, D. N., and E. Senchenkova, 2010 *Inflammation and the Microcirculation*. 2010 by Morgan & Claypool Life Sciences., San Rafael CA.

Greenhalgh, C. J., and D. J. Hilton, 2001 Negative regulation of cytokine signaling. J Leukoc Biol 70**:** 348-356.

Haddad, B. R., L. Gu, T. Mirtti, A. Dagvadorj, P. Vogiatzi *et al.*, 2013 STAT5A/B gene locus undergoes amplification during human prostate cancer progression. Am J Pathol 182**:** 2264-2275.

Hanratty, W. P., and C. R. Dearolf, 1993 The Drosophila Tumorous-lethal hematopoietic oncogene is a dominant mutation in the hopscotch locus. Mol Gen Genet 238**:** 33-37.

Hari, K. L., K. R. Cook and G. H. Karpen, 2001 The Drosophila Su(var)2-10 locus regulates chromosome structure and function and encodes a member of the PIAS protein family. Genes Dev 15**:** 1334-1348.

Harrison, D. A., R. Binari, T. S. Nahreini, M. Gilman and N. Perrimon, 1995 Activation of a Drosophila Janus kinase (JAK) causes hematopoietic neoplasia and developmental defects. EMBO J 14**:** 2857-2865.

Harrison, D. A., P. E. McCoon, R. Binari, M. Gilman and N. Perrimon, 1998 Drosophila unpaired encodes a secreted protein that activates the JAK signaling pathway. Genes Dev 12**:** 3252-3263.

Hartenstein, V., 2006 Blood cells and blood cell development in the animal kingdom. Annu Rev Cell Dev Biol 22**:** 677-712.

Harvey, K. F., X. Zhang and D. M. Thomas, 2013 The Hippo pathway and human cancer. Nat Rev Cancer 13**:** 246-257.

Hashemolhosseini, S., and M. Wegner, 2004 Impacts of a new transcription factor family: mammalian GCM proteins in health and disease. J Cell Biol 166**:** 765-768.

He, R., B. Liu, C. Yang, R. C. Yang, G. Tobelem *et al.*, 2003 Inhibition of K562 leukemia angiogenesis and growth by expression of antisense vascular endothelial growth factor (VEGF) sequence. Cancer Gene Ther 10**:** 879-886.

Hemmi, H., O. Takeuchi, T. Kawai, T. Kaisho, S. Sato *et al.*, 2000 A Toll-like receptor recognizes bacterial DNA. Nature 408**:** 740-745.

Hetru, C., and J. A. Hoffmann, 2009 NF-kappaB in the immune response of Drosophila. Cold Spring Harb Perspect Biol 1**:** a000232.

Hitoshi, S., Y. Ishino, A. Kumar, S. Jasmine, K. F. Tanaka *et al.*, 2011 Mammalian Gcm genes induce Hes5 expression by active DNA demethylation and induce neural stem cells. Nat Neurosci 14**:** 957-964.

Holz, A., B. Bossinger, T. Strasser, W. Janning and R. Klapper, 2003 The two origins of hemocytes in Drosophila. Development 130**:** 4955-4962.

Hombria, J. C., and S. Sotillos, 2013 JAK-STAT pathway in Drosophila morphogenesis: From organ selector to cell behavior regulator. JAKSTAT 2**:** e26089.

Honti, V., G. Csordas, R. Markus, E. Kurucz, F. Jankovics *et al.*, 2010 Cell lineage tracing reveals the plasticity of the hemocyte lineages and of the hematopoietic compartments in Drosophila melanogaster. Mol Immunol 47**:** 1997-2004.

Hosoya, T., K. Takizawa, K. Nitta and Y. Hotta, 1995 glial cells missing: a binary switch between neuronal and glial determination in Drosophila. Cell 82**:** 1025-1036.

Hou, X. S., M. B. Melnick and N. Perrimon, 1996 Marelle acts downstream of the Drosophila HOP/JAK kinase and encodes a protein similar to the mammalian STATs. Cell 84**:** 411-419.

Hultmark, D., 2003 Drosophila immunity: paths and patterns. Curr Opin Immunol 15**:** 12-19.

Igaki, T., and M. Miura, 2014 The Drosophila TNF ortholog Eiger: emerging physiological roles and evolution of the TNF system. Semin Immunol 26**:** 267-274.

Ikebe, M., Y. Kitaura, M. Nakamura, H. Tanaka, A. Yamasaki *et al.*, 2009 Lipopolysaccharide (LPS) increases the invasive ability of pancreatic cancer cells through the TLR4/MyD88 signaling pathway. J Surg Oncol 100**:** 725-731.

Imler, J. L., and J. A. Hoffmann, 2001 Toll receptors in innate immunity. Trends Cell Biol 11**:** 304-311.

Irving, P., J. M. Ubeda, D. Doucet, L. Troxler, M. Lagueux *et al.*, 2005 New insights into Drosophila larval haemocyte functions through genome-wide analysis. Cell Microbiol 7**:** 335-350.

Iwasaki, A., and R. Medzhitov, 2004 Toll-like receptor control of the adaptive immune responses. Nat Immunol 5**:** 987-995.

Jacques, C., L. Soustelle, I. Nagy, C. Diebold and A. Giangrande, 2009 A novel role of the glial fate determinant glial cells missing in hematopoiesis. Int J Dev Biol 53**:** 1013-1022.

Jang, I. H., N. Chosa, S. H. Kim, H. J. Nam, B. Lemaitre *et al.*, 2006 A Spatzle-processing enzyme required for toll signaling activation in Drosophila innate immunity. Dev Cell 10**:** 45-55.

Jiang, H., P. H. Patel, A. Kohlmaier, M. O. Grenley, D. G. McEwen *et al.*, 2009 Cytokine/Jak/Stat signaling mediates regeneration and homeostasis in the Drosophila midgut. Cell 137**:** 1343-1355.

Jiravanichpaisal, P., S. Roos, L. Edsman, H. Liu and K. Soderhall, 2009 A highly virulent pathogen, Aeromonas hydrophila, from the freshwater crayfish Pacifastacus leniusculus. J Invertebr Pathol 101**:** 56-66.

Jones, A. V., S. Kreil, K. Zoi, K. Waghorn, C. Curtis *et al.*, 2005 Widespread occurrence of the JAK2 V617F mutation in chronic myeloproliferative disorders. Blood 106**:** 2162-2168.

Jones, B. W., R. D. Fetter, G. Tear and C. S. Goodman, 1995 glial cells missing: a genetic switch that controls glial versus neuronal fate. Cell 82**:** 1013-1023.

Jung, S. H., C. J. Evans, C. Uemura and U. Banerjee, 2005 The Drosophila lymph gland as a developmental model of hematopoiesis. Development 132**:** 2521-2533.

Kacsoh, B. Z., and T. A. Schlenke, 2012 High hemocyte load is associated with increased resistance against parasitoids in Drosophila suzukii, a relative of D. melanogaster. PLoS One 7**:** e34721.

Kallio, J., H. Myllymaki, J. Gronholm, M. Armstrong, L. M. Vanha-aho *et al.*, 2010 Eye transformer is a negative regulator of Drosophila JAK/STAT signaling. FASEB J 24**:** 4467-4479.

Kammerer, M., and A. Giangrande, 2001 Glide2, a second glial promoting factor in Drosophila melanogaster. EMBO J 20**:** 4664-4673.

Kaplan, M. H., 2013 STAT signaling in inflammation. JAKSTAT 2**:** e24198.

Kari, B., G. Csordas, V. Honti, G. Cinege, M. J. Williams *et al.*, 2016 The raspberry Gene Is Involved in the Regulation of the Cellular Immune Response in Drosophila melanogaster. PLoS One 11**:** e0150910.

Karsten, P., I. Plischke, N. Perrimon and M. P. Zeidler, 2006 Mutational analysis reveals separable DNA binding and trans-activation of Drosophila STAT92E. Cell Signal 18**:** 819-829.

Kawai, T., and S. Akira, 2010 The role of pattern-recognition receptors in innate immunity: update on Toll-like receptors. Nat Immunol 11**:** 373-384.

Kelsh, R. M., and P. J. McKeown-Longo, 2013 Topographical changes in extracellular matrix: Activation of TLR4 signaling and solid tumor progression. Trends Cancer Res 9**:** 1-13.

Kiladjian, J. J., 2012 The spectrum of JAK2-positive myeloproliferative neoplasms. Hematology Am Soc Hematol Educ Program 2012**:** 561-566.

Kim, J., B. W. Jones, C. Zock, Z. Chen, H. Wang *et al.*, 1998 Isolation and characterization of mammalian homologs of the Drosophila gene glial cells missing. Proc Natl Acad Sci U S A 95**:** 12364-12369.

Kimbrell, D. A., C. Hice, C. Bolduc, K. Kleinhesselink and K. Beckingham, 2002 The Dorothy enhancer has Tinman binding sites and drives hopscotch-induced tumor formation. Genesis 34**:** 23-28.

Kocks, C., J. H. Cho, N. Nehme, J. Ulvila, A. M. Pearson *et al.*, 2005 Eater, a transmembrane protein mediating phagocytosis of bacterial pathogens in Drosophila. Cell 123**:** 335-346.

Kol, A., A. H. Lichtman, R. W. Finberg, P. Libby and E. A. Kurt-Jones, 2000 Cutting edge: heat shock protein (HSP) 60 activates the innate immune response: CD14 is an essential receptor for HSP60 activation of mononuclear cells. J Immunol 164**:** 13-17.

Kopp, E. B., and R. Medzhitov, 1999 The Toll-receptor family and control of innate immunity. Curr Opin Immunol 11**:** 13-18.

Kotaja, N., U. Karvonen, O. A. Janne and J. J. Palvimo, 2002 PIAS proteins modulate transcription factors by functioning as SUMO-1 ligases. Mol Cell Biol 22**:** 5222-5234.

Kounatidis, I., and P. Ligoxygakis, 2012 Drosophila as a model system to unravel the layers of innate immunity to infection. Open Biol 2**:** 120075.

Kroemer, G., 2006 Mitochondria in cancer. Oncogene 25**:** 4630-4632.

Krzemien, J., M. Crozatier and A. Vincent, 2010 Ontogeny of the Drosophila larval hematopoietic organ, hemocyte homeostasis and the dedicated cellular immune response to parasitism. Int J Dev Biol 54**:** 1117-1125.

Krzemien, J., L. Dubois, R. Makki, M. Meister, A. Vincent *et al.*, 2007 Control of blood cell homeostasis in Drosophila larvae by the posterior signalling centre. Nature 446**:** 325-328.

Kuper, H., H. O. Adami and D. Trichopoulos, 2000 Infections as a major preventable cause of human cancer. J Intern Med 248**:** 171-183.

Kurucz, E., B. Vaczi, R. Markus, B. Laurinyecz, P. Vilmos *et al.*, 2007 Definition of Drosophila hemocyte subsets by cell-type specific antigens. Acta Biol Hung 58 Suppl**:** 95-111.

Kurucz, E., C. J. Zettervall, R. Sinka, P. Vilmos, A. Pivarcsi *et al.*, 2003 Hemese, a hemocyte-specific transmembrane protein, affects the cellular immune response in Drosophila. Proc Natl Acad Sci U S A 100**:** 2622-2627.

Laneve, P., C. Delaporte, G. Trebuchet, O. Komonyi, H. Flici *et al.*, 2013 The Gcm/Glide molecular and cellular pathway: new actors and new lineages. Dev Biol 375**:** 65-78.

Langer, J. A., E. C. Cutrone and S. Kotenko, 2004 The Class II cytokine receptor (CRF2) family: overview and patterns of receptor-ligand interactions. Cytokine Growth Factor Rev 15**:** 33-48.

Lanot, R., D. Zachary, F. Holder and M. Meister, 2001 Postembryonic hematopoiesis in Drosophila. Dev Biol 230**:** 243-257.

Lebestky, T., T. Chang, V. Hartenstein and U. Banerjee, 2000 Specification of Drosophila hematopoietic lineage by conserved transcription factors. Science 288**:** 146-149.

Lebestky, T., S. H. Jung and U. Banerjee, 2003 A Serrate-expressing signaling center controls Drosophila hematopoiesis. Genes Dev 17**:** 348-353.

Lee, M. J., M. E. Kalamarz, I. Paddibhatla, C. Small, R. Rajwani *et al.*, 2009 Virulence factors and strategies of Leptopilina spp.: selective responses in Drosophila hosts. Adv Parasitol 70**:** 123-145.

Lee, Y. K., and D. D. Moore, 2008 Liver receptor homolog-1, an emerging metabolic modulator. Front Biosci 13**:** 5950-5958.

Lemaitre, B., and J. Hoffmann, 2007 The host defense of Drosophila melanogaster. Annu Rev Immunol 25**:** 697-743.

Lemaitre, B., E. Kromer-Metzger, L. Michaut, E. Nicolas, M. Meister *et al.*, 1995a A recessive mutation, immune deficiency (imd), defines two distinct control pathways in the Drosophila host defense. Proc Natl Acad Sci U S A 92**:** 9465-9469.

Lemaitre, B., M. Meister, S. Govind, P. Georgel, R. Steward *et al.*, 1995b Functional analysis and regulation of nuclear import of dorsal during the immune response in Drosophila. EMBO J 14**:** 536-545.

Lerner, A. B., and T. B. Fitzpatrick, 1950 Biochemistry of melanin formation. Physiol Rev 30**:** 91-126.

Leulier, F., C. Parquet, S. Pili-Floury, J. H. Ryu, M. Caroff *et al.*, 2003 The Drosophila immune system detects bacteria through specific peptidoglycan recognition. Nat Immunol 4**:** 478-484.

Levine, R. L., M. Loriaux, B. J. Huntly, M. L. Loh, M. Beran *et al.*, 2005 The JAK2V617F activating mutation occurs in chronic myelomonocytic leukemia and acute myeloid leukemia, but not in acute lymphoblastic leukemia or chronic lymphocytic leukemia. Blood 106**:** 3377-3379.

Levy, D. E., and J. E. Darnell, Jr., 2002 Stats: transcriptional control and biological impact. Nat Rev Mol Cell Biol 3**:** 651-662.

Libby, P., P. M. Ridker and G. K. Hansson, 2009 Inflammation in atherosclerosis: from pathophysiology to practice. J Am Coll Cardiol 54**:** 2129-2138.

Liew, F. Y., H. Liu and D. Xu, 2005a A novel negative regulator for IL-1 receptor and Toll-like receptor 4. Immunol Lett 96**:** 27-31.

Liew, F. Y., D. Xu, E. K. Brint and L. A. O'Neill, 2005b Negative regulation of toll-like receptor-mediated immune responses. Nat Rev Immunol 5**:** 446-458.

Lin, T. S., S. Mahajan and D. A. Frank, 2000 STAT signaling in the pathogenesis and treatment of leukemias. Oncogene 19**:** 2496-2504.

Lindsay, S. A., and S. A. Wasserman, 2014 Conventional and non-conventional Drosophila Toll signaling. Dev Comp Immunol 42**:** 16-24.

Lopez-Armada, M. J., R. R. Riveiro-Naveira, C. Vaamonde-Garcia and M. N. Valcarcel-Ares, 2013 Mitochondrial dysfunction and the inflammatory response. Mitochondrion 13**:** 106-118.

Luo, C., B. Shen, J. L. Manley and L. Zheng, 2001 Tehao functions in the Toll pathway in Drosophila melanogaster: possible roles in development and innate immunity. Insect Mol Biol 10**:** 457-464.

Luo, H., W. P. Hanratty and C. R. Dearolf, 1995 An amino acid substitution in the Drosophila hopTum-l Jak kinase causes leukemia-like hematopoietic defects. EMBO J 14**:** 1412-1420.

Luo, H., P. Rose, D. Barber, W. P. Hanratty, S. Lee *et al.*, 1997 Mutation in the Jak kinase JH2 domain hyperactivates Drosophila and mammalian Jak-Stat pathways. Mol Cell Biol 17**:** 1562-1571.

Luo, H., P. E. Rose, T. M. Roberts and C. R. Dearolf, 2002 The Hopscotch Jak kinase requires the Raf pathway to promote blood cell activation and differentiation in Drosophila. Mol Genet Genomics 267**:** 57-63.

Maeda, H., and T. Akaike, 1998 Nitric oxide and oxygen radicals in infection, inflammation, and cancer. Biochemistry (Mosc) 63**:** 854-865.

Mahla, R. S., M. C. Reddy, D. V. Prasad and H. Kumar, 2013 Sweeten PAMPs: Role of Sugar Complexed PAMPs in Innate Immunity and Vaccine Biology. Front Immunol 4**:** 248.

Mai, C. W., Y. B. Kang and M. R. Pichika, 2013 Should a Toll-like receptor 4 (TLR-4) agonist or antagonist be designed to treat cancer? TLR-4: its expression and effects in the ten most common cancers. Onco Targets Ther 6**:** 1573-1587.

Makhijani, K., B. Alexander, T. Tanaka, E. Rulifson and K. Bruckner, 2011 The peripheral nervous system supports blood cell homing and survival in the Drosophila larva. Development 138**:** 5379-5391.

Makki, R., M. Meister, D. Pennetier, J. M. Ubeda, A. Braun *et al.*, 2010 A short receptor downregulates JAK/STAT signalling to control the Drosophila cellular immune response. PLoS Biol 8**:** e1000441.

Mandal, L., J. A. Martinez-Agosto, C. J. Evans, V. Hartenstein and U. Banerjee, 2007 A Hedgehog- and Antennapedia-dependent niche maintains Drosophila haematopoietic precursors. Nature 446**:** 320-324.

Mao, H., Z. Lv and M. S. Ho, 2012 Gcm proteins function in the developing nervous system. Dev Biol 370**:** 63-70.

Markstein, M., P. Markstein, V. Markstein and M. S. Levine, 2002 Genome-wide analysis of clustered Dorsal binding sites identifies putative target genes in the Drosophila embryo. Proc Natl Acad Sci U S A 99**:** 763-768.

McBride, H. M., M. Neuspiel and S. Wasiak, 2006 Mitochondria: more than just a powerhouse. Curr Biol 16**:** R551-560.

McDowell, J. M., M. Dhandaydham, T. A. Long, M. G. Aarts, S. Goff *et al.*, 1998 Intragenic recombination and diversifying selection contribute to the evolution of downy mildew resistance at the RPP8 locus of Arabidopsis. Plant Cell 10**:** 1861-1874.

McLornan, D., M. Percy and M. F. McMullin, 2006 JAK2 V617F: a single mutation in the myeloproliferative group of disorders. Ulster Med J 75**:** 112-119.

Medzhitov, R., 2008 Origin and physiological roles of inflammation. Nature 454**:** 428-435.

Medzhitov, R., and C. Janeway, Jr., 2000 Innate immunity. N Engl J Med 343**:** 338-344.

Mikkola, H. K., and S. H. Orkin, 2006 The journey of developing hematopoietic stem cells. Development 133**:** 3733-3744.

Miller, A. A., R. Bernardoni and A. Giangrande, 1998 Positive autoregulation of the glial promoting factor glide/gcm. EMBO J 17**:** 6316-6326.

Minakhina, S., and R. Steward, 2006 Melanotic mutants in Drosophila: pathways and phenotypes. Genetics 174**:** 253-263.

Mogensen, T. H., 2009 Pathogen recognition and inflammatory signaling in innate immune defenses. Clin Microbiol Rev 22**:** 240-273, Table of Contents.

Moncrieffe, M. C., J. G. Grossmann and N. J. Gay, 2008 Assembly of oligomeric death domain complexes during Toll receptor signaling. J Biol Chem 283**:** 33447-33454.

Muller, P., D. Kuttenkeuler, V. Gesellchen, M. P. Zeidler and M. Boutros, 2005 Identification of JAK/STAT signalling components by genome-wide RNA interference. Nature 436**:** 871-875.

Nait-Oumesmar, B., A. B. Copperman and R. A. Lazzarini, 2000 Placental expression and chromosomal localization of the human Gcm 1 gene. J Histochem Cytochem 48**:** 915-922.

Nam, H. J., I. H. Jang, H. You, K. A. Lee and W. J. Lee, 2012 Genetic evidence of a redox-dependent systemic wound response via Hayan protease-phenoloxidase system in Drosophila. EMBO J 31**:** 1253-1265.

Nappi, A. J., F. Frey and Y. Carton, 2005 Drosophila serpin 27A is a likely target for immune suppression of the blood cell-mediated melanotic encapsulation response. J Insect Physiol 51**:** 197-205.

Nielsen, C., H. S. Birgens, B. G. Nordestgaard, L. Kjaer and S. E. Bojesen, 2011 The JAK2 V617F somatic mutation, mortality and cancer risk in the general population. Haematologica 96**:** 450-453.

Noel, J. C., B. Borghese, D. Vaiman, I. Fayt, V. Anaf *et al.*, 2010 Steroidogenic factor-1 expression in ovarian endometriosis. Appl Immunohistochem Mol Morphol 18**:** 258-261.

Nusslein-Volhard, C., and E. Wieschaus, 1980 Mutations affecting segment number and polarity in Drosophila. Nature 287**:** 795-801.

O'Neill, L. A., D. Golenbock and A. G. Bowie, 2013 The history of Toll-like receptors - redefining innate immunity. Nat Rev Immunol 13**:** 453-460.

O'Shea, J. J., M. Gadina and R. D. Schreiber, 2002 Cytokine signaling in 2002: new surprises in the Jak/Stat pathway. Cell 109 Suppl**:** S121-131.

Oblak, A., and R. Jerala, 2011 Toll-like receptor 4 activation in cancer progression and therapy. Clin Dev Immunol 2011**:** 609579.

Ogu, C. C., and J. L. Maxa, 2000 Drug interactions due to cytochrome P450. Proc (Bayl Univ Med Cent) 13**:** 421-423.

Ohashi, K., V. Burkart, S. Flohe and H. Kolb, 2000 Cutting edge: heat shock protein 60 is a putative endogenous ligand of the toll-like receptor-4 complex. J Immunol 164**:** 558-561.

Ooi, J. Y., Y. Yagi, X. Hu and Y. T. Ip, 2002 The Drosophila Toll-9 activates a constitutive antimicrobial defense. EMBO Rep 3**:** 82-87.

Ornitz, D. M., R. W. Moreadith and P. Leder, 1991 Binary system for regulating transgene expression in mice: targeting int-2 gene expression with yeast GAL4/UAS control elements. Proc Natl Acad Sci U S A 88**:** 698-702.

Owusu-Ansah, E., and U. Banerjee, 2009 Reactive oxygen species prime Drosophila haematopoietic progenitors for differentiation. Nature 461**:** 537-541.

Oyallon, J., N. Vanzo, J. Krzemien, I. Morin-Poulard, A. Vincent *et al.*, 2016 Two Independent Functions of Collier/Early B Cell Factor in the Control of Drosophila Blood Cell Homeostasis. PLoS One 11**:** e0148978.

Palis, J., J. Malik, K. E. McGrath and P. D. Kingsley, 2010 Primitive erythropoiesis in the mammalian embryo. Int J Dev Biol 54**:** 1011-1018.

Park, J. M., H. Brady, M. G. Ruocco, H. Sun, D. Williams *et al.*, 2004 Targeting of TAK1 by the NF-kappa B protein Relish regulates the JNK-mediated immune response in Drosophila. Genes Dev 18**:** 584-594.

Parker, K. L., and B. P. Schimmer, 1997 Steroidogenic factor 1: a key determinant of endocrine development and function. Endocr Rev 18**:** 361-377.

Patient, R. K., and J. D. McGhee, 2002 The GATA family (vertebrates and invertebrates). Curr Opin Genet Dev 12**:** 416-422.

Pencik, J., H. T. Pham, J. Schmoellerl, T. Javaheri, M. Schlederer *et al.*, 2016 JAK-STAT signaling in cancer: From cytokines to non-coding genome. Cytokine 87**:** 26-36.

Peter, M. E., A. V. Kubarenko, A. N. Weber and A. H. Dalpke, 2009 Identification of an N-terminal recognition site in TLR9 that contributes to CpG-DNA-mediated receptor activation. J Immunol 182**:** 7690-7697.

Petraki, S., B. Alexander and K. Bruckner, 2015 Assaying Blood Cell Populations of the Drosophila melanogaster Larva. J Vis Exp.

Pietra, D., S. Li, A. Brisci, F. Passamonti, E. Rumi *et al.*, 2008 Somatic mutations of JAK2 exon 12 in patients with JAK2 (V617F)-negative myeloproliferative disorders. Blood 111**:** 1686-1689.

Popkova, A., R. Bernardoni, C. Diebold, V. Van de Bor, B. Schuettengruber *et al.*, 2012 Polycomb controls gliogenesis by regulating the transient expression of the Gcm/Glide fate determinant. PLoS Genet 8**:** e1003159.

Querfurth, H. W., and F. M. LaFerla, 2010 Alzheimer's disease. N Engl J Med 362**:** 329-344.

Rawlings, J. S., K. M. Rosler and D. A. Harrison, 2004 The JAK/STAT signaling pathway. J Cell Sci 117**:** 1281-1283.

Rehorn, K. P., H. Thelen, A. M. Michelson and R. Reuter, 1996 A molecular aspect of hematopoiesis and endoderm development common to vertebrates and Drosophila. Development 122**:** 4023-4031.

Rizki, T. M., and R. M. Rizki, 1992 Lamellocyte differentiation in Drosophila larvae parasitized by Leptopilina. Dev Comp Immunol 16**:** 103-110.

Rizki, T. M., R. M. Rizki and E. H. Grell, 1980 A mutant affecting the crystal cells inDrosophila melanogaster. Wilhelm Roux's archives of developmental biology 188**:** 91-99.

Rock, F. L., G. Hardiman, J. C. Timans, R. A. Kastelein and J. F. Bazan, 1998 A family of human receptors structurally related to Drosophila Toll. Proc Natl Acad Sci U S A 95**:** 588-593.

Rock, K. L., and H. Kono, 2008 The inflammatory response to cell death. Annu Rev Pathol 3**:** 99-126.

Rogler, G., 2014 Chronic ulcerative colitis and colorectal cancer. Cancer Lett 345**:** 235-241.

Rosetto, M., Y. Engstrom, C. T. Baldari, J. L. Telford and D. Hultmark, 1995 Signals from the IL-1 receptor homolog, Toll, can activate an immune response in a Drosophila hemocyte cell line. Biochem Biophys Res Commun 209**:** 111-116.

Roth, J., and C. M. Blatteis, 2014 Mechanisms of fever production and lysis: lessons from experimental LPS fever. Compr Physiol 4**:** 1563-1604.

Rugendorff, A., A. Younossi-Hartenstein and V. Hartenstein, 1994 Embryonic origin and differentiation of the Drosophila heart. Roux's archives of developmental biology 203**:** 266-280.

Schindelin, J., I. Arganda-Carreras, E. Frise, V. Kaynig, M. Longair *et al.*, 2012 Fiji: an open-source platform for biological-image analysis. Nat Methods 9**:** 676-682.

Schmid, M. R., I. Anderl, L. Vesala, L. M. Vanha-aho, X. J. Deng *et al.*, 2014 Control of Drosophila blood cell activation via Toll signaling in the fat body. PLoS One 9**:** e102568.

Schreiber, J., E. Riethmacher-Sonnenberg, D. Riethmacher, E. E. Tuerk, J. Enderich *et al.*, 2000 Placental failure in mice lacking the mammalian homolog of glial cells missing, GCMa. Mol Cell Biol 20**:** 2466-2474.

Scott, L. M., P. J. Campbell, E. J. Baxter, T. Todd, P. Stephens *et al.*, 2005 The V617F JAK2 mutation is uncommon in cancers and in myeloid malignancies other than the classic myeloproliferative disorders. Blood 106**:** 2920-2921.

Scott, M. A., 2000 A glimpse at sperm function in vivo: sperm transport and epithelial interaction in the female reproductive tract. Anim Reprod Sci 60-61**:** 337-348.

Shia, A. K., M. Glittenberg, G. Thompson, A. N. Weber, J. M. Reichhart *et al.*, 2009 Toll-dependent antimicrobial responses in Drosophila larval fat body require Spatzle secreted by haemocytes. J Cell Sci 122**:** 4505-4515.

Silverman, N., R. Zhou, S. Stoven, N. Pandey, D. Hultmark *et al.*, 2000 A Drosophila IkappaB kinase complex required for Relish cleavage and antibacterial immunity. Genes Dev 14**:** 2461-2471.

Silvers, M., and W. P. Hanratty, 1984 Alterations in the production of hemocytes due to a neoplastic mutation of Drosophila melanogaster. J Invertebr Pathol 44**:** 324-328.

Sim, S. C., and M. Ingelman-Sundberg, 2010 The Human Cytochrome P450 (CYP) Allele Nomenclature website: a peer-reviewed database of CYP variants and their associated effects. Hum Genomics 4**:** 278-281.

Sinenko, S. A., T. Hung, T. Moroz, Q. M. Tran, S. Sidhu *et al.*, 2010 Genetic manipulation of AML1-ETO-induced expansion of hematopoietic precursors in a Drosophila model. Blood 116**:** 4612-4620.

Sluss, H. K., Z. Han, T. Barrett, D. C. Goberdhan, C. Wilson *et al.*, 1996 A JNK signal transduction pathway that mediates morphogenesis and an immune response in Drosophila. Genes Dev 10**:** 2745-2758.

Small, C., I. Paddibhatla, R. Rajwani and S. Govind, 2012 An introduction to parasitic wasps of Drosophila and the antiparasite immune response. J Vis Exp**:** e3347.

Sorrentino, R. P., Y. Carton and S. Govind, 2002 Cellular immune response to parasite infection in the Drosophila lymph gland is developmentally regulated. Dev Biol 243**:** 65-80.

Soustelle, L., and A. Giangrande, 2007 Novel gcm-dependent lineages in the postembryonic nervous system of Drosophila melanogaster. Dev Dyn 236**:** 2101-2108.

Soustelle, L., C. Jacques, B. Altenhein, G. M. Technau, T. Volk *et al.*, 2004 Terminal tendon cell differentiation requires the glide/gcm complex. Development 131**:** 4521-4532.

Soustelle, L., F. Trousse, C. Jacques, J. Ceron, P. Cochard *et al.*, 2007 Neurogenic role of Gcm transcription factors is conserved in chicken spinal cord. Development 134**:** 625-634.

Srivastava, G. K., R. Reinoso, A. K. Singh, I. Fernandez-Bueno, D. Hileeto *et al.*, 2011 Trypan Blue staining method for quenching the autofluorescence of RPE cells for improving protein expression analysis. Exp Eye Res 93**:** 956-962.

St Johnston, D., 2002 The art and design of genetic screens: Drosophila melanogaster. Nat Rev Genet 3**:** 176-188.

Stofanko, M., S. Y. Kwon and P. Badenhorst, 2010 Lineage tracing of lamellocytes demonstrates Drosophila macrophage plasticity. PLoS One 5**:** e14051.

Suarez, S. S., and A. A. Pacey, 2006 Sperm transport in the female reproductive tract. Hum Reprod Update 12**:** 23-37.

Sun, H., B. N. Bristow, G. Qu and S. A. Wasserman, 2002 A heterotrimeric death domain complex in Toll signaling. Proc Natl Acad Sci U S A 99**:** 12871-12876.

Tan, K. L., S. C. Goh and S. Minakhina, 2012 Genetic screen for regulators of lymph gland homeostasis and hemocyte maturation in Drosophila. G3 (Bethesda) 2**:** 393-405.

Tang, H., Z. Kambris, B. Lemaitre and C. Hashimoto, 2008 A serpin that regulates immune melanization in the respiratory system of Drosophila. Dev Cell 15**:** 617-626.

Tanji, T., X. Hu, A. N. Weber and Y. T. Ip, 2007 Toll and IMD pathways synergistically activate an innate immune response in Drosophila melanogaster. Mol Cell Biol 27**:** 4578-4588.

Tanji, T., and Y. T. Ip, 2005 Regulators of the Toll and Imd pathways in the Drosophila innate immune response. Trends Immunol 26**:** 193-198.

Tauszig, S., E. Jouanguy, J. A. Hoffmann and J. L. Imler, 2000 Toll-related receptors and the control of antimicrobial peptide expression in Drosophila. Proc Natl Acad Sci U S A 97**:** 10520-10525.

Tavian, M., and B. Peault, 2005 Embryonic development of the human hematopoietic system. Int J Dev Biol 49**:** 243-250.

Tepass, U., L. I. Fessler, A. Aziz and V. Hartenstein, 1994 Embryonic origin of hemocytes and their relationship to cell death in Drosophila. Development 120**:** 1829-1837.

Tevosian, S. G., A. E. Deconinck, A. B. Cantor, H. I. Rieff, Y. Fujiwara *et al.*, 1999 FOG-2: A novel GATA-family cofactor related to multitype zinc-finger proteins Friend of GATA-1 and U-shaped. Proc Natl Acad Sci U S A 96**:** 950-955.

Theken, K. N., Y. Deng, M. A. Kannon, T. M. Miller, S. M. Poloyac *et al.*, 2011 Activation of the acute inflammatory response alters cytochrome P450 expression and eicosanoid metabolism. Drug Metab Dispos 39**:** 22-29.

Thomas, S. J., J. A. Snowden, M. P. Zeidler and S. J. Danson, 2015 The role of JAK/STAT signalling in the pathogenesis, prognosis and treatment of solid tumours. Br J Cancer 113**:** 365-371.

Thomee, C., S. W. Schubert, J. Parma, P. Q. Le, S. Hashemolhosseini *et al.*, 2005 GCMB mutation in familial isolated hypoparathyroidism with residual secretion of parathyroid hormone. J Clin Endocrinol Metab 90**:** 2487-2492.

Tijet, N., C. Helvig and R. Feyereisen, 2001 The cytochrome P450 gene superfamily in Drosophila melanogaster: annotation, intron-exon organization and phylogeny. Gene 262**:** 189-198.

Vainchenker, W., and S. N. Constantinescu, 2013 JAK/STAT signaling in hematological malignancies. Oncogene 32**:** 2601-2613.

Valanne, S., J. H. Wang and M. Ramet, 2011 The Drosophila Toll signaling pathway. J Immunol 186**:** 649-656.

Van De Bor, V., and A. Giangrande, 2002 glide/gcm: at the crossroads between neurons and glia. Curr Opin Genet Dev 12**:** 465-472.

van Steensel, B., J. Delrow and S. Henikoff, 2001 Chromatin profiling using targeted DNA adenine methyltransferase. Nat Genet 27**:** 304-308.

van Steensel, B., and S. Henikoff, 2000 Identification of in vivo DNA targets of chromatin proteins using tethered dam methyltransferase. Nat Biotechnol 18**:** 424-428.

Vanha-Aho, L. M., I. Anderl, L. Vesala, D. Hultmark, S. Valanne *et al.*, 2015 Edin Expression in the Fat Body Is Required in the Defense Against Parasitic Wasps in Drosophila melanogaster. PLoS Pathog 11**:** e1004895.

Villarino, A. V., Y. Kanno, J. R. Ferdinand and J. J. O'Shea, 2015 Mechanisms of Jak/STAT signaling in immunity and disease. J Immunol 194**:** 21-27.

Vincent, S., J. L. Vonesch and A. Giangrande, 1996 Glide directs glial fate commitment and cell fate switch between neurones and glia. Development 122**:** 131-139.

Virchow, R., 1881 An Address on the Value of Pathological Experiments. Br Med J 2**:** 198-203.

Virchow, R., 1989 Cellular pathology. As based upon physiological and pathological histology. Lecture XVI--Atheromatous affection of arteries. 1858. Nutr Rev 47**:** 23-25.

Vlisidou, I., and W. Wood, 2015 Drosophila blood cells and their role in immune responses. FEBS J 282**:** 1368-1382.

Waltzer, L., L. Bataille, S. Peyrefitte and M. Haenlin, 2002 Two isoforms of Serpent containing either one or two GATA zinc fingers have different roles in Drosophila haematopoiesis. EMBO J 21**:** 5477-5486.

Wang, F., W. Meng, B. Wang and L. Qiao, 2014a Helicobacter pylori-induced gastric inflammation and gastric cancer. Cancer Lett 345**:** 196-202.

Wang, L., I. Kounatidis and P. Ligoxygakis, 2014b Drosophila as a model to study the role of blood cells in inflammation, innate immunity and cancer. Front Cell Infect Microbiol 3**:** 113.

Webster, N., J. R. Jin, S. Green, M. Hollis and P. Chambon, 1988 The yeast UASG is a transcriptional enhancer in human HeLa cells in the presence of the GAL4 trans-activator. Cell 52**:** 169-178.

Wegner, M., and D. Riethmacher, 2001 Chronicles of a switch hunt: gcm genes in development. Trends Genet 17**:** 286-290.

Wolfner, M. F., 2011 Precious essences: female secretions promote sperm storage in Drosophila. PLoS Biol 9**:** e1001191.

Wolska, A., E. Lech-Maranda and T. Robak, 2009 Toll-like receptors and their role in hematologic malignancies. Curr Mol Med 9**:** 324-335.

Wood, W., and A. Jacinto, 2007 Drosophila melanogaster embryonic haemocytes: masters of multitasking. Nat Rev Mol Cell Biol 8**:** 542-551.

Wood, W., and P. Martin, 2017 Macrophage Functions in Tissue Patterning and Disease: New Insights from the Fly. Dev Cell 40**:** 221-233.

Xia, Y., S. Z. Midoun, Z. Xu and L. Hong, 2015 Heixuedian (heix), a potential melanotic tumor suppressor gene, exhibits specific spatial and temporal expression pattern during Drosophila hematopoiesis. Dev Biol 398**:** 218-230.

Xu, J. H., J. J. Fu, X. L. Wang, J. Y. Zhu, X. H. Ye *et al.*, 2013 Hepatitis B or C viral infection and risk of pancreatic cancer: a meta-analysis of observational studies. World J Gastroenterol 19**:** 4234-4241.

Yan, R., S. Small, C. Desplan, C. R. Dearolf and J. E. Darnell, Jr., 1996 Identification of a Stat gene that functions in Drosophila development. Cell 84**:** 421-430.

Yang, C. X., C. Y. Li and W. Feng, 2013 Toll-like receptor 4 genetic variants and prognosis of breast cancer. Tissue Antigens 81**:** 221-226.

Yang, H., and D. Hultmark, 2016 Tissue communication in a systemic immune response of Drosophila. Fly (Austin) 10**:** 115-122.

Yang, H., J. Kronhamn, J. O. Ekstrom, G. G. Korkut and D. Hultmark, 2015 JAK/STAT signaling in Drosophila muscles controls the cellular immune response against parasitoid infection. EMBO Rep 16**:** 1664-1672.

Yuan, X., Y. Zhou, W. Wang, J. Li, G. Xie *et al.*, 2013 Activation of TLR4 signaling promotes gastric cancer progression by inducing mitochondrial ROS production. Cell Death Dis 4**:** e794.

Zambon, R. A., M. Nandakumar, V. N. Vakharia and L. P. Wu, 2005 The Toll pathway is important for an antiviral response in Drosophila. Proc Natl Acad Sci U S A 102**:** 7257-7262.

Zanet, J., A. Jayo, S. Plaza, T. Millard, M. Parsons *et al.*, 2012 Fascin promotes filopodia formation independent of its role in actin bundling. J Cell Biol 197**:** 477-486.

Zeitlinger, J., R. P. Zinzen, A. Stark, M. Kellis, H. Zhang *et al.*, 2007 Whole-genome ChIP-chip analysis of Dorsal, Twist, and Snail suggests integration of diverse patterning processes in the Drosophila embryo. Genes Dev 21**:** 385-390.

Zettervall, C. J., I. Anderl, M. J. Williams, R. Palmer, E. Kurucz *et al.*, 2004 A directed screen for genes involved in Drosophila blood cell activation. Proc Natl Acad Sci U S A 101**:** 14192-14197.

Zeyda, M., and T. M. Stulnig, 2009 Obesity, inflammation, and insulin resistance--a mini-review. Gerontology 55**:** 379-386.

UNIVERSITÉ DE STRASBOURG

igbmc institut de génétique et de biologie moléculaire et cellulaire

École Doctorale des Sciences de la Vie et de la Santé STRASBOURG

Wael BAZZI

Une nouvelle cascade régulant l'hématopoïèse et la réponse inflammatoire chez la drosophile

Résumé

Les cellules immunitaires provenant des deux vagues hématopoïétiques jouent des rôles distincts dans la réponse immunitaire, ce qui pose la question d'une potentielle communication entre les deux vagues d'hématopoïèse. De plus, la réponse immunitaire joue un rôle primordial dans la progression des tumeurs. Les cascades inflammatoires telles que la voie JAK/STAT et la voie Toll régulent l'hématopoïèse et les mutations affectant ces voies sont associées à des défauts hématopoïétiques et au développement de cancer du sang chez l'humain. Les deux voies de signalisation sont conservées au cours de l'évolution. La voie Toll a notamment été découverte chez la drosophile. Comme chez les mammifères, les mutations dans ces cascades produisent chez la larve des tumeurs des cellules du « sang » appelées tumeurs mélanotiques qui sont dues à la prolifération et à la présence d'hémocytes à l'état inflammatoire qui s'agrègent et forment des masses noires mélanisées. Au cours de mon doctorat, j'ai caractérisé l'impact de Gcm, le seul facteur de transcription spécifique de l'hématopoïèse primitive, sur la réponse immunitaire innée et l'activation de l'inflammation. Je me suis concentré sur les voies Toll et JAK/STAT en utilisant le modèle de la drosophile. J'ai pu montrer que Gcm inhibe la formation des tumeurs mélanotiques provoquées par l'activation constitutive de l'une ou l'autre voie. Gcm agit en activant l'expression d'inhibiteurs de chacune des deux voies. De plus, mes données montrent pour la première fois l'interaction entre les vagues d'hématopoïèses primitive et définitive, une interaction qui est nécessaire pour monter une réponse inflammatoire efficace. Dans ce système, Gcm inhibe la sécrétion de cytokines pro-inflammatoire Upd2 et Upd3 des hémocytes embryonnaires. Mes résultats indiquent également que Gcm a un impact sur l'expression de gènes mitochondriaux dans un fond génétique qui conduit au développement de tumeurs mélanotiques et à un état inflammatoire. Enfin, j'ai transposé mes résultats à un système mammifère en montrant que chez la souris, Gcm induit l'expression d'inhibiteur de la voie JAK/STAT dans une lignée cellulaire leucémique humaine. Pour conclure, mes données mettent en évidence l'importance de la communication entre les deux vagues d'hématopoïèse dans le système immunitaire et montrent qu'une voie de régulation développementale régule la capacité du système à répondre à l'inflammation.

Summary

Immune cells originating from different hematopoietic waves play role in mounting an efficient immune response, which raises the aspect of communication between distinct waves. In addition, immune responses have pivotal roles in modulating tumor progression. Inflammatory cascades, such as the JAK/STAT and Toll pathways are also known to regulate hematopoiesis and mutations in either of them are associated with hematopoietic defects and blood cancers in humans. Both pathways are highly conserved in evolution and interestingly, the Toll cascade was initially discovered in *Drosophila*. Like in mammals, mutations within these cascades produce the so called "melanotic tumors" in *Drosophila* larvae, which are due to blood cell proliferation and to the presence of hemocytes in an inflammatory state that aggregate and form black melanized masses. During my PhD, I proposed to decipher the impact of Gcm, the only known transcription factor specific to embryonic hematopoiesis on innate immune response and inflammation, by focusing on the JAK/STAT and Toll signaling cascades *in vivo* using the simple *Drosophila* model. I was able to show that Gcm inhibits melanotic tumors formation induced by the over-activation of both the JAK/STAT and Toll cascades. This is mediated by inducing the expression of JAK/STAT and Toll cascades inhibitors. In addition, my data describes for the first time the interaction occurring between the primitive and definitive hematopoietic waves and necessary to trigger an appropriate inflammatory response, where Gcm inhibits the secretion of the proinflammatory cytokines Upd2 and Upd3 from embryonic hemocytes. Moreover, I show that Gcm impacts the molecular landscape of mitochondrial genes in genetic backgrounds that lead to melanotic tumors and to an inflammatory state. Interestingly, I transpose my findings to vertebrates by showing that a GCM murine gene induces the expression of JAK/STAT inhibitors in a human leukemia cell line. In conclusion, my data highlights the importance of hematopoietic wave communication in the immune response and show that a developmental pathway regulates the competence to respond to inflammation.